Vol. 57 MARCH, 1953 No. 3

THE JOURNAL OF PHYSICAL CHEMISTRY

(Registered in U. S. Patent Office)

Founded by Wilder D. Bancroft

Symposium on Electrode Chemistry, September, 1952, Atlantic City, N. J.

(*Continued inside*)

Founded by Wilder D. Bancroft

THE JOURNAL OF PHYSICAL CHEMISTRY

(Registered in U. S. Patent Office)

Published monthly (except July, August and September) by the American Chemical Society at 20th and Northampton Sts., Easton, Pa.

Entered as second-class matter at the Post Office at Easton, Pennsylvania.

The *Journal of Physical Chemistry* is devoted to the publication of selected symposia in the broad field of physical chemistry and to other contributed papers.

Manuscripts originating in the British Isles, Europe and Africa should be sent to F. C. Tompkins, The Faraday Society, 6 Gray's Inn Square, London W. C. 1, England.

Manuscripts originating elsewhere should be sent to W. Albert Noyes, Jr., Department of Chemistry, University of Rochester, Rochester 3, N. Y.

Correspondence regarding accepted copy, proofs and reprints should be directed to Assistant Editor, Allen D. Bliss, Department of Chemistry, Simmons College, 300 The Fenway, Boston 15, Mass.

Business Office: American Chemical Society, 1155 Sixteenth St., N. W., Washington 6, D. C.

Advertising Office: American Chemical Society, 332 West 42nd St., New York 36, N. Y.

Articles must be submitted in duplicate, typed and double spaced. They should have at the beginning a brief Abstract, in no case exceeding 300 words. Original drawings should accompany the manuscript. Lettering at the sides of graphs (black on white or blue) may be pencilled in, and will be typeset. Figures and tables should be held to a minimum consistent with adequate presentation of information. Photographs will not be printed on glossy paper except by special arrangement. All footnotes and references to the literature should be numbered consecutively and placed on the manuscript at the proper places. Initials of authors referred to in citations should be given. Nomenclature should conform to that used in *Chemical Abstracts*, mathematical characters marked for italic, Greek letters carefully made or annotated, and subscripts and superscripts clearly shown. Articles should be written as briefly as possible consistent with clarity and should avoid historical background unnecessary for specialists.

Symposium papers should be sent in all cases to Secretaries of Divisions sponsoring the symposium, who will be responsible for their transmittal to the Editor. The Secretary of the Division by agreement with the Editor will specify a time after which symposium papers cannot be accepted. The Editor reserves the right to refuse to publish symposium articles, for valid scientific reasons. Each symposium paper may not exceed four printed pages (about sixteen double spaced typewritten pages) in length except by prior arrangement with the Editor.

Remittances and orders for subscriptions and for single copies, notices of changes of address and new professional connections, and claims for missing numbers should be sent to the American Chemical Society, 1155 Sixteenth St., N. W., Washington 6, D. C. Changes of address for the *Journal of Physical Chemistry* must be received on or before the 30th of the preceding month.

Claims for missing numbers will not be allowed (1) if received more than sixty days from date of issue (because of delivery hazards, no claims can be honored from subscribers in Central Europe, Asia, or Pacific Islands other than Hawaii), (2) if loss was due to failure of notice of change of address to be received before the date specified in the preceding paragraph, or (3) if the reason for the claim is "missing from files."

Subscription Rates: to members of the American Chemical Society, $8.00 for 1 year, $15.00 for 2 years, $22.00 for 3 years; to nonmembers, $10.00 for 1 year, $18.00 for 2 years, $26.00 for 3 years. Postage free to countries in the Pan American Union; Canada, $0.40; all other countries, $1.20. Single copies, $1.25; foreign postage, $0.15; Canadian postage $0.05.

The American Chemical Society and the Editors of the *Journal of Physical Chemistry* assume no responsibility for the statements and opinions advanced by contributors to THIS JOURNAL.

The American Chemical Society also publishes *Journal of the American Chemical Society, Chemical Abstracts, Industrial and Engineering Chemistry, Chemical and Engineering News* and *Analytical Chemistry*. Rates on request.

(Continued from first page of cover)

THE JOURNAL OF
PHYSICAL CHEMISTRY

Founded by Wilder D. Bancroft

VOLUME 57 MARCH 18, 1953 NUMBER 3

THEORY OF THE FARADAIC ADMITTANCE. II. ANALYSIS OF THE CURRENT-INTERRUPTER METHOD

BY DAVID C. GRAHAME

Department of Chemistry, Amherst College, Amherst, Massachusetts

Received November 17, 1952

The theory of the current-interrupter method of studying the impedance of metal-solution interfaces is examined. It is found that an exact solution to the problem of predicting the results of an experiment, given all the determining parameters, is too complicated to be useful. The reverse problem, that of deducing the parameters from the results of experiment, is still more difficult. With the aid of certain simplifying assumptions it is possible to obtain approximate solutions which reveal the major characteristics of the problem. Four quantities can be evaluated in favorable cases. These are: (1) the iR drop through the solution before the current interruption, (2) the capacity of the electrical double layer, (3) a weighted average of the forward and backward components of the current, i_{av}, and (4) a lower limit to w_1k_1, the product of the concentration of the major reactant and its specific reaction rate constant. A method is outlined which should make it possible to present the results of current-interrupter studies in compact form. The present practice of calculating the capacity from the initial current and a value of dE/dt not corresponding to the moment of interruption is shown to account for the belief that the interrupter method measures pseudo-capacity.

In a previous paper[1] (hereafter referred to as part I) it was shown how the results of impedance measurements on a smooth homogeneous electrode could be predicted from a knowledge of diffusion coefficients, reaction rate constants, surface layer concentrations, transfer coefficients and transference numbers of the ions making up the solution. The reverse problem, that of deducing certain of these parameters from independent knowledge of some of the others together with the results of sufficiently precise impedance measurements, was not discussed in detail, although it was pointed out that not all of the parameters could be evaluated by impedance measurements alone.

An entirely analogous problem exists with respect to what we may call the current-interrupter method of measuring the properties of a metal-solution interface. In this method a constant current is passed across the interface to be investigated until a steady state has been attained, and the current is then interrupted as abruptly as possible. The potential of the electrode is measured relative to any convenient secondary electrode, and this measurement is made just prior to the interruption and also as soon thereafter as possible. The potential is also measured for a further period, which may be made as long as desired.

In the present paper, equations will be derived which relate the potential, measured as a function of time after the interruption, to some of the parameters enumerated above. It should be understood that our object is not necessarily to produce equations with a practical application, but rather to examine the mathematical theory, independent of any of the very specialized assumptions which have heretofore been made implicitly in studies of this problem. In other words our primary objective is that of understanding clearly what are the factors which influence the potential decay and what mathematical steps would be necessary to evaluate it.

The converse problem of evaluating the parameters from measurements made by the current-interrupter method will be discussed only incidentally. This is a far more difficult problem and is regarded by the present author as essentially insoluble, apart from the measurement of the iR drop in the solution, the capacity of the electrical double layer in the absence of pseudo-capacity, and perhaps the estimation of what we shall call i_{av} in the treatment to follow. These are also the

(1) D. C. Grahame, *J. Electrochem. Soc.*, **99**, 370 C (1952).

quantities most readily obtained by the impedance method, it may be remarked. In fact it has been observed that any circumstance which renders a given parameter more difficult to observe by the impedance method also renders the measurement of that same parameter more difficult in the current-interrupter method. This is certainly no accident, since the current-interrupter is, in fact, a rather specialized tool for measuring a function of the impedance.

It will be assumed that the current density at the electrode is everywhere the same. This requires that the electrode be smooth and homogeneous and that the disposition of the electrodes be of an appropriate symmetry. The current which flows under steady-state conditions will be called the faradaic current and will be assumed to be a function of (among other things) the potential difference across the interface, E, measured from the interior of the metallic phase to a point just beyond the electrical double layer. The absolute value of this potential need not be known, since only relative values enter into the final calculation. Thus E may be regarded as the potential of the electrode when measured relative to the equilibrium potential (potential of zero current), after correction has been made for the iR drop in the solution occasioned by the flow of current in that part of the solution through which the potential E happens to be measured. The paramount advantage of the current-interrupter method is that after interruption the potential is measured with no external current flowing, so that this correction vanishes.

The current which flows under steady-state conditions is assumed to be also a function of the concentrations w_i of the substances present close to the interface. By this we do *not* mean their concentrations within the electrical double layer. This latter would be a defensible definition, but it would not be convenient. For substances in solution we shall mean the concentration at a point just outside the double layer or, more precisely, an extrapolated concentration representing what the concentration at the interface would be if any concentration gradients existing just outside the double layer (and not caused by it) were extrapolated to the interface.

For many purposes it is convenient to regard some of the substances whose concentrations determine the faradaic current as ions. This can be done in the absence of an excess of an inert electrolyte only if diffusion theory does not enter into the calculation. If it is desired to introduce diffusion theory, neutral salt molecules (*e.g.*, NaCl) must be taken as the substances whose concentrations control the current. How this may be done was discussed in part I, but concerns us less in the present paper.

The Basic Equation for di/dt

The assumptions just introduced may be written as

$$i = f(E, w_1, w_2, w_3, \text{etc.}) \qquad (1)$$

where i is the steady-state current. It will now be assumed further that this equation gives the magnitude of the *faradaic* current even in the absence of a steady state. It does not give the magnitude of the non-faradaic or double-layer current, since this latter depends also upon dE/dt. Indeed, this is the most satisfactory way of distinguishing in principle between the two kinds of current, and equation (1) will now be taken as the definition of a faradaic current. A discussion of this point and an alternative definition are given in part I.

The flow of faradaic current is always accompanied by the occurrence of an electrochemical reaction. For the sake of generality it will be considered for the moment that more than one faradaic process occurs or may occur at the interface. The current corresponding to each of these processes will be distinguished with a literal superscript, i^a, i^b, i^c, etc., and thus the total faradaic current will be

$$i = i^a + i^b + i^c + \ldots \qquad (2)$$

and therefore

$$di/dt = di^a/dt + di^b/dt + di^c/dt + \ldots \qquad (3)$$

It is necessary at this point to introduce a restriction upon the generality of the results to be obtained. It will be assumed that the substances whose concentrations control the partial current i^a do not affect the partial currents i^b, i^c, and so on. This restriction means that the equations which follow do not apply to the so-called "electrochemical mechanism" of hydrogen ion discharge, since both the primary and secondary discharge reactions involve the hydrogen atom, the first as a product and the second as a reactant.

According to the above assumption, each partial current is a function of its own set of variables, the potential E being the only common variable

$$i^a = f^a(E, w_1^a, w_2^a, w_3^a, \text{etc.})$$
$$i^b = f^b(E, w_1^b, w_2^b, w_3^b, \text{etc.})$$
$$\text{etc.}$$

The derivative of i^a with respect to time is given by

$$di^a/dt = \xi^a dE/dt + f_1^a\, dw_1^a/dt + f_2^a\, dw_2^a/dt + f_3^a\, dw_3^a/dt + \ldots \qquad (4)$$

where

$$\xi^a = (\partial i^a/\partial E)_{w_1^a}; \quad f_1^a = (\partial i^a/\partial w_1^a)_{E^a, w_2^a, w_3^a};$$
$$f_2^a = (\partial i^a/\partial w_2^a)_{E^a, w_1^a, w_3^a}; \quad f_3^a = (\partial i^a/\partial w_3^a)_{E^a, w_1^a, w_2^a} \qquad (5)$$

An entirely similar set of equations can be written for di^b/dt, di^c/dt, etc., the only difference being in the superscripts. Then

$$di/dt = (\xi^a + \xi^b + \xi^c + \ldots)dE/dt + f_1^a\, dw_1^a/dt + f_1^b\, dw_1^b/dt + f_1^c\, dw_1^c/dt + f_2^a\, dw_2^a/dt + f_2^b\, dw_2^b/dt + f_2^c\, dw_2^c/dt + f_3^a\, dw_3^a/dt + f_3^b\, dw_3^b/dt + f_3^c\, dw_3^c/dt + \ldots \qquad (6)$$

This equation may be regarded as the fundamental equation governing the rate of change of the current with time after the current interruption. It will be shown below how one may also obtain the rate of change of *potential* with time from this equation.

Outline of the Exact Method of Solution

In this and the following sections the superscripts a, b, etc., will be omitted, because only a single faradaic current will be under consideration. The net current i (really i^a) can be thought of as

composed of two parts, a forward component $\vec{i}$ and a backward component $\overleftarrow{i}$.

$$i = \vec{i} - \overleftarrow{i} \tag{7}$$

The minus sign is used because it is convenient to think of each component of the current as a positive quantity.

It is customary and essentially correct to assert that each component of the current is given by an exponential expression of the form

$$\vec{i} = n\mathfrak{F}w_1k_1 \exp [\alpha n\mathfrak{F}E/RT] \tag{8}$$

$$\overleftarrow{i} = n\mathfrak{F}w_2k_2 \exp [-(1-\alpha)n\mathfrak{F}E/RT] \tag{9}$$

where α is the fraction of the potential acting to assist the forward reaction and $1 - \alpha$ is the fraction of the potential acting to hinder the back reaction. k_1 and k_2 are reaction rate constants whose magnitudes depend upon the choice of reference potential with respect to which E is measured. Under some circumstances (but notably not in polarographic techniques) there is a natural potential of zero current, and if the potential is computed relative to this potential, E will be what is ordinarily called the overvoltage or overpotential. It will be assumed that this method of reckoning the potential has been chosen whenever it is possible to do so. Otherwise an arbitrary potential of reference must be chosen.

In equations (8) and (9) n is an integer representing the number of electrons transferred in one act of the faradaic process under consideration. The process is not necessarily a slow process in the ordinary sense, but it must not be so fast that k_1 and k_2 must be reckoned infinite, in which case equations (8) and (9) would have no meaning and the components to which w_1 and w_2 refer would have to be regarded as components of the electrical double layer.

The quantity n is necessarily the same in equations (8) and (9), since the same faradaic process is under consideration. It must be emphasized that the equations apply to one and only one such process; it would be an error to apply them to a pair of consecutive faradaic processes.

Implicit in equations (8) and (9) is the assumption that the currents $\vec{i}$ and $\overleftarrow{i}$ are functions *only* of the parameters included in the equations. This cannot be rigorously true. The current $\vec{i}$ depends upon the potential energy of the reduction product (we are thinking now of the faradaic process as a reduction process), which is why k_1 depends upon the chemical nature of the surface upon which the reaction takes place for instance. A deposit of a foreign substance (the product of the reduction) may well change the potential energy of that substance on the surface, which is to say it changes the nature of the surface and thereby changes k_1. Therefore the use of equation (8) assumes either that the deposited substance is present in quantities much less than a monolayer or in sufficient thickness so that further deposits do not change the nature of the surface. The intermediate case, namely that in which the substance is present in amounts ranging from perhaps a tenth of a monolayer to three or four monolayers, is not considered here.

Because of the large effect of the exponential term relative to the effect of concomitant changes in the coefficient k, equations (8) and (9) are nevertheless likely to remain very nearly valid over large ranges of potential, as is indeed rendered likely from the fact that the Tafel equation seems to apply in most instances from moderate to very large current densities, where the possibility of experimental errors ultimately obscures the comparison with experiment.

From equations (5), (7), (8) and (9)

$$\xi = (\partial i/\partial E)_{w_i} = (n\mathfrak{F}/RT)(\alpha\vec{i} + [1-\alpha]\overleftarrow{i}) = (n\mathfrak{F}/RT)i_{av} \tag{10}$$

where we have let

$$i_{av} = \alpha\vec{i} + (1-\alpha)\overleftarrow{i} \tag{11}$$

At the equilibrium potential (potential of zero current) $\vec{i} = \overleftarrow{i}$ and

$$i_{av} = i_{eq}$$

where i_{eq} is the exchange current at the equilibrium potential. From equations (8) and (9) it is possible (given all the needed parameters) to calculate i_{av} and therefore ξ.

At the moment of current interruption all of the dw/dt's equal zero (as will be proved in a sequel to this paper by W. T. Scott), so that equation (6) provides a relation between the two unknown rates $(di/dt)_{t=0}$ and $(dE/dt)_{t=0}$. A second relation is found from the differential capacity of the electrical double layer, assumed known like the other parameters of the problem. At the moment of current interruption, $t = 0$, the electrical double layer is charged to a certain potential E, and a certain faradaic current i_0 flows. Neither the potential nor the concentrations of the active substances can change discontinuously at the moment of interruption, so that the current at the first instant after interruption is the same as it was in the steady state before interruption. Since the double layer behaves electrically like a capacitor (non-linear with respect to potential), its rate of discharge is given by the equation

$$dE/dt = -i/C \tag{12}$$

This equation is valid not only at the moment of discharge but any time thereafter. It provides a means of measuring C at the moment of interruption, subject to a practical limitation to be discussed below. Differentiation with respect to time gives

$$di/dt = -(d/dt)(C\,dE/dt) = -C(d^2E/dt^2) - (dC/dE)(dE/dt)^2 \tag{13}$$

Elimination of di/dt through equation (6) gives (for one faradaic current)

$$-(d/dt)(C\,dE/dt) = -C(d^2E/dt^2) - (dC/dE)(dE/dt)^2 = \xi\,dE/dt + f_1\,dw_1/dt + f_2\,dw_2/dt + \ldots \tag{13a}$$

At the moment of current interruption all of the dw/dt's are zero, as stated above. Since $(dE/dt)_{t=0}$ is known from equation (12), equation (13a)

permits the calculation of $(d^2E/dt^2)_{t=0}$. After the moment of interruption the dw/dt's are no longer zero and their evaluation can be done in principle through the application of Fick's laws of diffusion. The boundary conditions are functions of the current, which is in turn a function of the concentrations of the reactants and of the potential E. Therefore the boundary conditions must be established through the simultaneous solution of equation 13a and Fick's laws as applied to each component. The f's in equation 13a are functions of the w's and of the potential, thus making it necessary to consider equations (5), (7), (8) and (9) simultaneously with the above. As a mathematical proposition the problem is determinate, but no serious attempt has been made to achieve an explicit formulation of the solution because it is clear that it would be too complicated to be of any real use. The purpose of this discussion has been to show what an accurate solution would involve and also to show that the much simpler solutions which have sometimes been proposed rest upon assumptions which have not always been pointed out.

It is concluded therefore that the only rigorously correct use which can be made of this formulation of the problem at the present time is the evaluation of the characteristics of the potential decay at the moment of interruption.

Alternative Approximate Method of Solution

There is an alternative procedure which is not rigorous because it cannot be carried to completion without the introduction of an inexact assumption, but which is nevertheless of interest as the nearest approach to an exact solution which now seems possible for times later than $t = 0$.

From equations (12) and (7)

$$\int \frac{dE}{\overrightarrow{i} - \overleftarrow{i}} = -\int \frac{1}{C}\,dt \qquad (14)$$

and from equations (8) and (9)

$$\int \frac{dE}{w_1k_1 \exp(\alpha n\mathfrak{F}E/RT) - w_2k_2 \exp[-(1-\alpha)n\mathfrak{F}E/RT]} = -n\mathfrak{F}\int \frac{1}{C}\,dt \qquad (15)$$

This equation cannot be integrated further without assumption because the w's are functions not only of E but also of t and of the other w. Nevertheless it is at least worthwhile to consider the consequences of equation (15) when w_1 and w_2 are constant after the interruption. In order to make the computations as simple as possible, and also because it is the most likely situation, we shall let $\alpha = 1/2$. Further we shall compute the potential E relative to the equilibrium potential which would prevail if the concentrations w_1 and w_2 were the same in the interior of the phases as at the interface, just outside the double layer. This has the effect of giving somewhat fictitious values to k_1 and k_2, but it is easy to translate one set of values to another if the actual concentrations are known. With this understanding one can write $w_1k_1 = w_2k_2$ (from equations (7), (8) and (9)). For simplicity we shall assume C independent of potential. Then equation (15) becomes

$$\int \operatorname{csch}(n\mathfrak{F}E/2RT)\,dE = -2n\mathfrak{F}w_1k_1t/C \qquad (16)$$

The hyperbolic cosecant can be integrated through the identity

$$\int \operatorname{csch}\theta\,d\theta = \ln \tanh|\theta/2| + \text{constant} \qquad (17)$$

so that

$$\ln \tanh|n\mathfrak{F}E/4RT| = -n^2\mathfrak{F}^2w_1k_1(t+t')/RTC \qquad (18)$$

where t' has been introduced as a constant of integration. The time t is measured from the moment of current interruption. t' has the meaning that *if equation (18) had been valid before the current interruption*, the potential would have been infinite at $t = -t'$.

Because of the identity

$$\tanh^{-1}x = \tfrac{1}{2}\ln\frac{1+x}{1-x} \qquad (19)$$

equation (18) can be written

$$|E| = \frac{2RT}{n\mathfrak{F}}\ln\frac{1+\exp[-n^2\mathfrak{F}^2w_1k_1(t+t')/RTC]}{1-\exp[-n^2\mathfrak{F}^2w_1k_1(t+t')/RTC]} \qquad (20)$$

When t is large this becomes

$$|E| = (2RT/n\mathfrak{F})\exp[-n^2\mathfrak{F}^2w_1k_1(t+t')/RTC] \qquad (21)$$

which is the equation for the decay of the potential of a condenser of capacity C through a resistor of resistance $RT/n^2\mathfrak{F}^2w_1k_1$. This result applies only when t is so large that the forward and back reactions are of nearly equal magnitude. It is also required that w_1 and w_2 be constant, as stated above.

It has been observed experimentally by S. Schuldiner[2] that the decay curves of such substances as cadmium ion in the presence of an excess of an inert electrolyte and on a mercury surface are substantially flat for long periods after the current interruption. This would seem to mean that the effects of diffusion are negligible in the time intervals involved, beginning perhaps 10^{-6} second after current interruption and continuing for perhaps 10^{-3} second thereafter. If diffusion caused any considerable changes in w_1 and w_2, that fact should show up as a decay of the potential during the time of observation, because the electrode is essentially at equilibrium with respect to the reaction $Cd^{++} + 2e \rightleftarrows Cd$ during the whole period of observation. (If it were not, *that* fact would also cause the curve to have a detectable finite slope.) So it appears that changes in the w's may turn out to be unimportant in the time intervals commonly used in the current-interrupter technique, *i.e.*, greater than 10^{-6} and less than 10^{-3} sec. This conclusion must be regarded as tentative pending further experimental evidence.

In Fig. 1 there are shown a number of potential-time curves calculated from equation (20) and representing the expected behavior (in the absence of changes of w_1 and w_2) of substances with different rate constants k_1. The significant parameter is $k_1w_1n^2\mathfrak{F}^2/CRT$, and this is marked on the various curves. For the lowermost curve the equilibrium potential is 0.118 v. below the steady-state potential, and for each curve going up that difference is half as much as for the curve beneath it. The steady-state current i_0 is the same for all, 10^{-3} ampere. Thus the lowermost curve corresponds to the reaction which is intrinsically the slowest, and consecutive curves involve approximately successive doubling of the quantity k_1w_1. Since w_1 is decreasing,[3] k is more than doubling from curve to curve. The potential is arbitrarily set at zero corresponding to the moment of interruption. Actually E is larger, relative to the equilibrium potential, the slower the reaction. All of the curves are computed to represent an initial current, i_0, of 10^{-3} amp. and a C of 20 microfarads. The area is immaterial. Thus the slope at $t = 0$ is the same for all, namely, 50 v./sec.

It needs to be borne in mind that the slope of the decay curve cannot be measured experimentally at $t = 0$. There is always a time interval t^* during which readings of potential are unreliable because of imperfections in the apparatus. If $t^* = 2.5 \times 10^{-4}$ sec. in the example given, the earliest measured slope will be in error (if it is called the initial slope) by from 15% to a factor of 5, going from the slowest to the fastest reaction considered. If the current density is 100 times as great, the value of t^* will need to be 1/100 as much to maintain the same accuracy. Thus it appears, as one would expect, that the accuracy is greater the slower the reaction and the smaller the value of t^*. For extremely fast reactions, such as the reduction of Cd^{++}, it is probably quite impossible even to estimate the initial value of the slope from the decay curve, even at low current densities. This fact has given rise to the mistaken idea that the initial slope is much less than it really is, and if the capacity C is calculated from that value of the slope, much too large a capacity value is obtained. It is presumably in this way that

(2) S. Schuldiner, private communication.

(3) Since the initial current is by hypothesis constant, the initial concentration decreases as the rate constant increases

too-large values of the capacity of the electrical double layer have been found in the presence of reversibly reducible ions. The error has led to the belief that the interrupter method measures pseudo-capacity, but in reality it is no more than the result of using non-corresponding values of i and dE/dt in the equation $C = -i/(dE/dt)$.

When the current is limited by diffusion, as under polarographic conditions above the half-wave potential, then equation (20) can no longer be valid since w_1 and w_2 must certainly change rapidly with time. The initial slope is still $-i_0/C$ but the potential does not level off as fast as it otherwise would. Qualitatively the effect will be to make the reaction appear slower than it is, since each observed curve will be very nearly like one of those calculated for a lower value of k_1w_1. Thus it should be possible to set a lower limit to the value of $w_1k_1n^2\mathfrak{F}^2/CRT$ by finding which one of the appropriate curves it most nearly resembles. For that purpose it is necessary to compute a set of curves for each appropriate value of i_0. This would appear to be one way, and perhaps the only way at present, to give quantitative significance to decay curves obtained by the interrupter method.

Regardless of the validity of the theory upon which the treatment rests, a plot of the apparent value of $w_1k_1n^2\mathfrak{F}^2/CRT$ against potential, for instance, would provide an acceptable way of reporting results of current-interrupter studies. This would take the place of the present practice of reporting a fictitious value of C obtained by dividing the initial current by a value of dE/dt which does not properly reflect the value of that slope at the moment of current interruption.

If i is negligible, as it will be at sufficiently large values of E, and if w_1 is either held constant or assumed constant, then the integration of equation (15) gives

$$\exp(-\alpha n\mathfrak{F}E/RT) - \exp(-\alpha n\mathfrak{F}E_0/RT) = (\alpha n^2\mathfrak{F}^2w_1k_1/RT)\int_0^t (1/C)dt \quad (22)$$

If the capacity of the electrical double layer C is also constant or assumed so, equation (22) reduces to the more convenient form

$$E_0 - E = (RT/\alpha n\mathfrak{F}) \ln\left(1 + \frac{\alpha n\mathfrak{F}i_0t}{RTC}\right) \quad (23)$$

which is identical with a result derived in essentially the same manner by Frumkin in 1943.[4] Busing and Kauzmann[5] have given a similar derivation, apparently without knowledge of Frumkin's prior work. It is also possible to derive equation (23) from equation (13a), but the method is circuitous and not particularly helpful.

Although the above results cannot be applied indiscriminately to the hydrogen overvoltage problem, they may be considered to be valid (subject to the stated limitations) provided the observed current is not a function of the concentration of hydrogen atoms on the surface. This restriction is necessary in order that equation (8) may give the rate of the reaction correctly. If there is a slow secondary discharge reaction (sometimes called the electrochemical reaction) depending upon the concentration of hydrogen atoms on the interface, then the above treatment is not valid.

When all the w's are constant, or more generally when all the f dw/dt terms in equation (13a) are zero or negligible,

(4) A. Frumkin, *Acta Physicochim. U.S.S.R.*, **18**, 30 (1943).

(5) W. R. Busing and W. Kauzmann, *J. Chem. Phys.*, **20**, 1129 (1952).

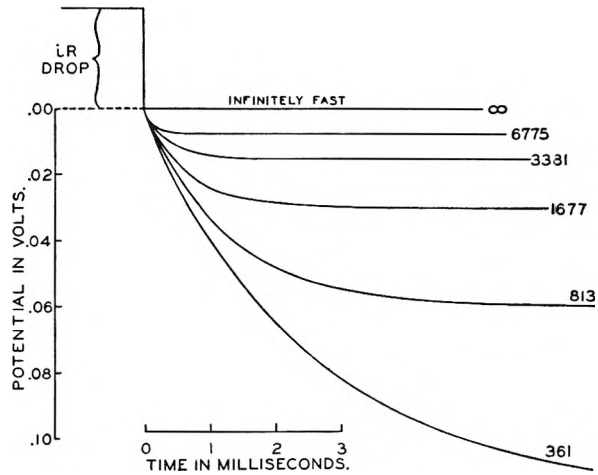

Fig. 1.—Calculated potential decay curves for reactions of several intrinsic speeds. Initial current 10^{-3} amp., $C = 20$ microfarads, $k_1w_1n^2\mathfrak{F}^2/CRT$ as marked.

equation (13a) can be written

$$-C(d^2E/dt^2) - (dC/dE)(dE/dt)^2 = \xi\, dE/dt \quad (24)$$

or when C is independent of E

$$-C(d^2E/dt^2) = \xi\, dE/dt \quad (25)$$

If one were now to assume, quite erroneously, that ξ is a constant, independent of potential, then equation (25) could be integrated to give

$$E = E_0 \exp(-\xi t/C) \quad (26)$$

which is the equation for the decay of the potential of a condenser of capacity C through a resistor of resistance $1/\xi$. According to this equation the slope of the decay curve is given by

$$\frac{dE}{dt} = \frac{n\mathfrak{F}E}{RT}\frac{i_{av}}{C} \quad (27)$$

whereas in fact it is given by i/C. These facts are mentioned because of the claim rather frequently made that one can represent the decay of the potential of an electrode by an "equivalent circuit" consisting of a capacitor equal to the capacity of the electrical double layer and a resistor of more or less vaguely specified magnitude. Equations (26) and (27) are approximately valid very close to the equilibrium potential, but not elsewhere. No equivalent circuit is known which possesses the properties of an electrode after current interruption, and it appears futile to attempt to consider the problem in this manner.

At the moment of interruption, the dw/dt terms are all zero and equation (24) is valid. Then since C, dE/dt, d^2E/dt^2 and dC/dE are all experimentally ascertainable quantities, that equation can be used to find ξ. This is tantamount to an evaluation of i_{av} (*cf.* eq. (10)).

Therefore the quantities which can be measured by the interrupter method are (1) an iR drop before current interruption, (2) the capacity of the electrical double layer (if the faradaic current is not too large or if the intrinsic speed of the reaction is not too great), (3) i_{av}, a weighed average of the forward and backward reactions, and (4) a lower limit to w_1k_1 before current interruption.

The author is grateful to the Office of Naval Research for financial support of this work.

CHARGING PROCESSES ON ANODIC POLARIZATION OF TITANIUM

BY COLBY D. HALL, JR., AND NORMAN HACKERMAN

Department of Chemistry, The University of Texas, Austin, Texas

Received November 17, 1952

Anodic charging curves for titanium in neutral NaCl solutions show a linear potential increase to the oxygen evolution potential. The charge passed is sufficient to deposit three oxygens on each titanium surface atom based on area as determined by measurement of polarization capacity. This corresponds to a monolayer if the oxygen is present as atoms having the same size as covalently bonded oxygen. Potential *vs.* log time curves for the decay of oxygen overvoltage show that discharge of the double layer capacitance occurs both by a continuation of the oxygen evolution reaction and by flow of current through a resistance. For the latter process, the resistance–capacitance product increases with increasing total time of oxygen evolution. This effect is attributed to the formation of a TiO_2 film. After several hours of continuous oxygen evolution at current densities greater than 10^{-3} amp./cm.^{2}, oxygen evolution ceases and the potential rises to +10 v. These effects are attributed to thickening of the TiO_2 film, which grows by outward migration of titanium ions. The space charge of these excess positive ions in the film can account for most of the measured electrode potential, so that the film-to-solution potential is not sufficient for oxygen evolution. At 10 v., the film breaks down and pitting occurs.

Introduction

The anodic polarization of metals has been studied largely with respect to oxygen overvoltage and the mechanism of oxygen evolution. It is generally accepted that a complete film of oxygen is present on an electrode from which oxygen is being evolved,[1] but there is no general agreement as to whether the film is composed of chemisorbed oxygen or of metal oxide. It is recognized, of course, that the mechanism may not be the same for all metals and for all experimental conditions.

Bowden[2] measured the charge required to change a platinum electrode from the reversible hydrogen potential to the reversible oxygen potential, and *vice versa*. The potential–time curves showed arrests whose length depended on the duration of previous hydrogen or oxygen evolution. Except for the charge passed during the arrests, a definite quantity of 3×10^{-3} coulomb/cm.^{2} was required for the change. The arrests during cathodic polarization were considered to represent removal of an oxide of platinum. The potentials of the arrests were the same as those measured for a PtO_2-coated platinum wire in the corresponding solutions.

Armstrong, Himsworth and Butler[3] do not agree that an oxide is formed on platinum during oxygen evolution. They attribute the arrest to a high local concentration of oxygen, since they found the potential to be affected considerably by stirring. They say, however, that an oxide is formed on gold.

Pearson and Butler[4] found that the potential–time curve for the anodic polarization of platinum from the hydrogen evolution potential to the oxygen evolution potential contains two linear regions, for which the charges passed are sufficient to remove a monolayer of hydrogen atoms and to deposit a monolayer of oxygen atoms.

Hickling and co-workers[5] studied the anodic behavior of Pt, Au, Ni, Ag, Cu and Co by an oscillographic method, and observed potential–time curves having linear portions. Hickling attributes rapid increases of potential to charging of a double layer, and the slower linear increases to formation of films of metal oxides of definite composition. He found that changes of slope occur at the reversible potentials of metal/oxide or lower oxide/higher oxide electrodes. El Wakkad and Emara,[6] using Hickling's method and also a direct method found evidence for the consecutive formation of PtO and PtO_2.

Titanium offers an example of a metal quite active in the e.m.f. series which, nevertheless, exhibits a marked degree of passivity toward dissolution and toward anodic dissolution. The present authors have measured the cathodic and anodic polarization of titanium.[7] Further investigations have now provided additional information on the processes involved in the anodic polarization of titanium.

Experimental Procedure

Apparatus.—Polarization measurements were made by the direct method, in a circular path apparatus, using saturated calomel half-cells as the reference electrodes. The titanium coupons were polished on No. 2/0 metallographic paper and cleaned by rubbing with filter paper moistened with ethyl alcohol, then with dry lens tissue. For most of the measurements, the coupons were 5.0 cm.^{2} in projected area and were cast in a plastic wafer which was inserted into a machined plastic holder so that the coupon was flush with the face of the holder. These are designated as "flush coupons." One series of measurements was made with a coupon of 4.0 cm.^{2} projected area, mounted in a machined plastic holder in such a way that the exposed face of the coupon was recessed $^3/_{32}$ inch behind the face of the holder. This is designated as a "recessed coupon." Further details of the apparatus are described elsewhere.[7]

Materials.—The titanium was made by the Remington Arms Company. Spectrographic analysis showed that it contained over 99% Ti, with 0.725% C, 0.25% Fe, and traces of other elements. All measurements were made in 0.50 *M* NaCl solution, made up from analytical reagent grade NaCl and distilled water. The solutions were kept saturated with air and were held at 30°.

Surface Area.—The surface area of the titanium coupons was determined by a capacitance method based on that of Wagner.[8] The roughness factor, or ratio of real to projected area, was found to be 10 ± 3. A measurement of surface area by krypton adsorption, obtained quite recently, gives the roughness factor as 2.2 ± 0.2. It is not entirely clear at this time which of these values is correct. The interpretation of the results has been made on the basis of the earlier measurement.

(1) N. K. Adam, "The Physics and Chemistry of Surfaces," 3rd ed., John Wiley and Sons, Inc., New York, N. Y., p. 326.

(2) F. P. Bowden, *Proc. Roy. Soc. (London)*, **A125**, 446 (1929).

(3) G. Armstrong, F. R. Himsworth and J. A. V. Butler, *ibid.*, **A143**, 89 (1933).

(4) J. D. Pearson and J. A. V. Butler, *Trans. Faraday Soc.*, **34**, 1163 (1938).

(5) A. Hickling, *ibid.*, **41**, 333 (1945); *ibid.*, **42**, 518 (1946); A. Hickling and J. E. Spice, *ibid.*, **43**, 762 (1947); A. Hickling and D. Taylor, *Discussions Faraday Soc.*, **1**, 277 (1947); *Trans. Faraday Soc.*, **44**, 262 (1948); S. E. S. El Wakkad and A. Hickling, *ibid.*, **46**, 820 (1950).

(6) S. E. S. El Wakkad and S. H. Emara, *J. Chem. Soc.*, 461 (1952).

(7) C. D. Hall, Jr., and N. Hackerman, to be published.

(8) C. Wagner, *J. Electrochem. Soc.*, **97**, 71 (1950).

Quantities which involve area are given in terms of *projected* area unless designated otherwise. Where *real* area, based on a roughness factor of 10, is meant, the abbreviation $cm.^2_{real}$ is used.

Results

All potentials are given on the saturated calomel electrode scale and are good to 0.01 v. in all cases unless otherwise noted.

Anodic Charging Curves.—Charging curves for the anodic polarization of titanium at constant current densities are shown in Fig. 1. Curve 1 is a potential–time curve for a coupon which was left on open circuit. Curve 2 is referred to both the time and the charge density scales. Except at the lowest current density, the charge required to reach a constant oxygen evolution potential is approximately the same at all current densities shown. The average is 1.45×10^{-2} coulomb/cm.^{2}. The potential increase is linear for current densities of 2×10^{-7} amp./cm.^{2} and larger, and the rates of increase are about equal, as may be seen in curves 4 through 7. At the smaller current densities of curves 2 and 3, the initial rate of increase is greater than that of the later portions of the curves.

Polarization at Higher Current Densities.—Figure 2 shows potential–time curves for flush coupons polarized at 2×10^{-3} amp./cm.^{2} and at 6×10^{-3} amp./cm.^{2}, and for a recessed coupon polarized at 6×10^{-3} amp./cm.^{2}. At these current densities, the initial linear rise of potential is too rapid to show up on the figure. After reaching the oxygen evolution value, the potential remains constant for one to several hours, then begins a constantly accelerating increase which continues to +9 to +10.5 v. It then fluctuates erratically over a range of ±0.4 v., but maintains a fairly constant average value. At the beginning of the rapid potential rise, visible evolution of oxygen ceases. Shortly thereafter, the surface of the titanium develops a thin, transparent brown film. At +10 v., this film changes to a dark blue, and pits develop on the coupon surface. As the pits grow, a white, gelatinous precipitate of hydrous titanium oxide is formed in the solution.

Anodic Polarization Decay and Repolarization.—A coupon which had reached a constant potential of +0.19 v. on open circuit was then polarized anodically at 2×10^{-7} amp./cm.^{2}. The potential increased rapidly to +0.55 v., where it remained constant for about 40 minutes, then increased linearly with time at a rate equal to that of a freshly prepared coupon polarized at the same current density, and finally became constant at the oxygen evolution potential, +0.97 v. Another coupon which had been polarized cathodically at $2 + 10^{-8}$ amp./cm.^{2} to a constant potential of +0.12 v. was made anodic at the same current density. The potential increased fairly rapidly to +0.25 v., remained constant for about 3 hours, and then increased again at a rate about equal to that of a fresh coupon at the same current density.

These effects were further investigated in a series of measurements in which a coupon was alternately polarized anodically and left on open circuit. The sequence of steps of polarization and decay of polarization may be followed in the potential–time curve of Fig. 3. The current was started at the times designated by odd-numbered points, and was stopped at times designated by even-numbered points. The potential–time curves for polarization and for polarization decay are shown on a larger scale in Figs. 4 and 5, respectively, in which the time scales start at the instant of starting or stopping the current. These curves are numbered to correspond to the sections of Fig. 3 beginning with the indicated number, *e.g.*, curve 2 extends from point 2 to point 3. Figure 6 shows the data for polarization decay, plotted as potential *vs.* log time.

The anodic current density was 6×10^{-6} amp./cm.^{2} in the original polarization of curve 1, and in the repolarizations of curves 3, 5, 7 and 9. In the repolarizations of curves 11 and 15, the current density was 2×10^{-7} amp./cm.^{2}. At point 13, *cathodic* polarization was started at 2×10^{-7} amp./cm.^{2}, and the current density was increased in steps to 2×10^{-4} amp./cm.^{2}, where it was held for 45 minutes. At this current density, hydrogen was evolved slowly at a potential of −1.20 v. After the cathodic current was stopped, the potential increased, finally becoming constant as shown in the last part of curve 14, Fig. 3.

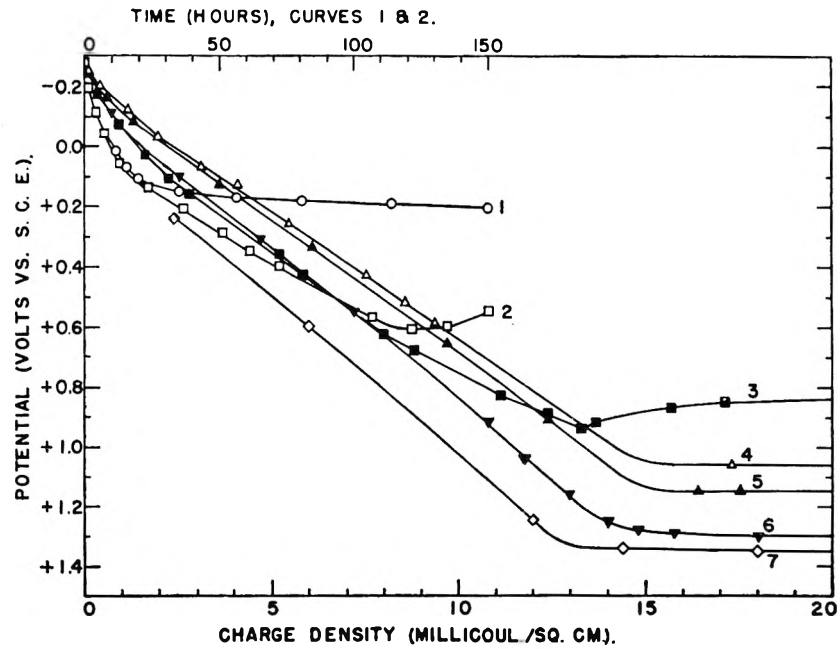

Fig. 1.—Anodic charging curves for titanium in aerated 0.5 *M* NaCl at 30°: 1, 0.0 amp./cm.^{2}; 2, 2.0×10^{-8} amp./cm.^{2}; 3, 6.0×10^{-3} amp./cm.^{2}; 4, 2.0×10^{-7} amp./cm.^{2}; 5, 6.0×10^{-7} amp./cm.^{2}; 6, 6.0×10^{-6} amp./cm.^{2}; 7, 2.0×10^{-5} amp./cm.^{2}.

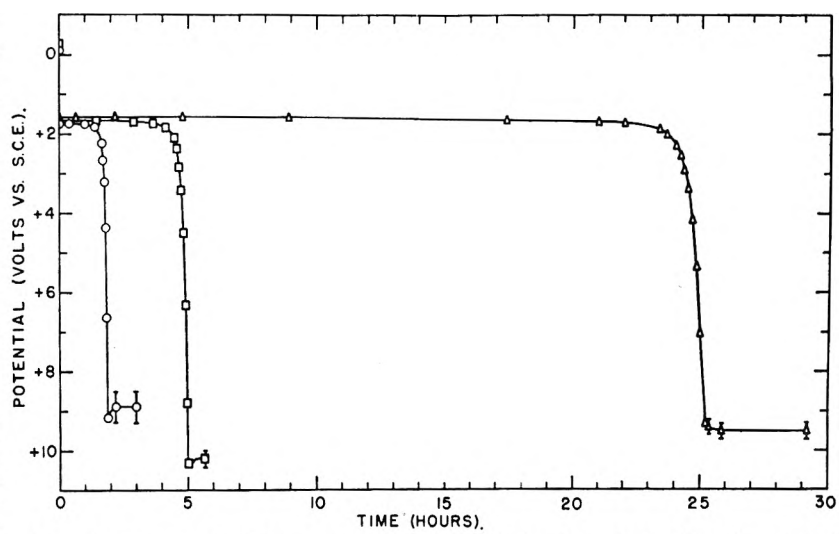

Fig. 2.—Time–potential curves for anodic polarization of titanium in aerated 0.5 *M* NaCl at 30°: Δ, 2.0×10^{-3} amp./cm.^{2}, flush coupon; ○, 6.0×10^{-3} amp./cm.^{2}, flush coupon; □, 6.0×10^{-3} amp./cm.^{2}, recessed coupon.

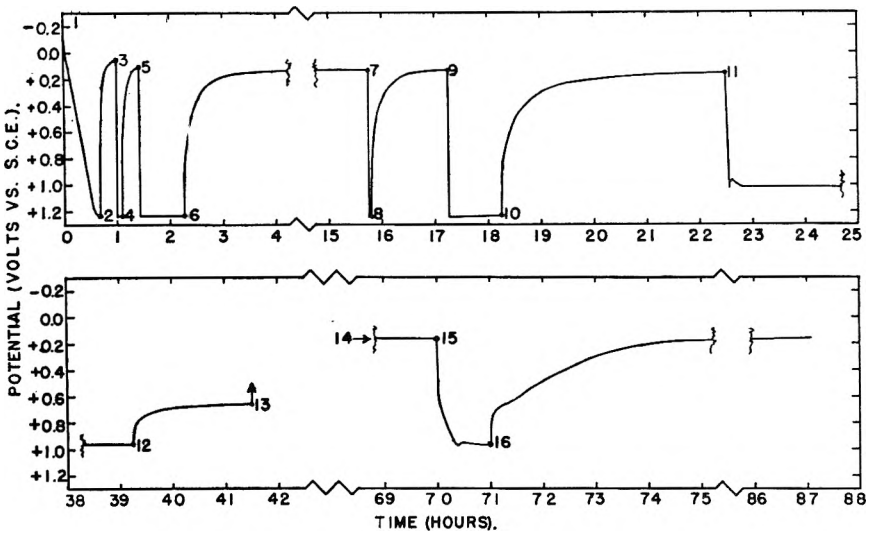

Fig. 3.—Time–potential curves for anodic polarization, depolarization and repolarization of titanium in aerated 0.5 *M* NaCl at 30°. The odd numbers indicate time at which current was started and the even numbered points show times at which current stopped.

The rate of increase of potential for the original polarization, curve 1 of Fig. 4, is the same as that for the polarization at the same current density shown in curve 6 of Fig. 1. In each subsequent repolarization at 6×10^{-6} amp./cm.^{2}, the potential reached the oxygen evolution potential, +1.23 v., in less than the 30 seconds required to make the first reading. By repolarizing at 2×10^{-7} amp./cm.^{2}, it was possible to follow the potential increase as shown in curves 11 and 15. From curve 11, it is calculated that the capacitance of the titanium surface is 3 μfd./cm.$^2{}_{real}$, and the charge required to repolarize to the oxygen evolution potential is 4×10^{-6} coulomb/cm.$^2{}_{real}$.

Discussion

Anodic Charging Process.—The increase of potential in the original polarization of a freshly prepared titanium coupon is proportional to the quantity of electricity that has passed, and therefore presumably to the amount of oxygen that has been deposited on the surface. However, the measurements on polarization decay and repolarization show quite clearly that the phenomenon is more complex, and that the potential is not, under all conditions, simply a function of the quantity of oxygen present on the surface. The results indicate that two distinct processes occur simultaneously: anodic deposition of oxygen on the titanium surface, and charging of an electrical double layer.

The original polarization to the oxygen evolution potential requires a charge 360 times as great as that required for repolarization after the polarization has been allowed to decay on open circuit. It is obvious that the original polarization produces a change on the surface which is not reversed by standing on open circuit. This irreversible change may be best explained as the deposition of a layer of chemisorbed oxygen. The charge used in depositing oxygen is essentially equal to the total charge of the original polarization. It is equal to 9.0×10^{15} electrons/cm.^{2}. The area occupied by each atom in the titanium surface may be calculated to be 7.4×10^{-16} cm.^{2}. Thus, the polarizing charge is equivalent to 6.6 electrons for each titanium atom in the surface, and can deposit, on the area occupied by each titanium atom, about 3.3 atoms or ions of oxygen.

It is not possible to determine with certainty whether the oxygen in the chemisorbed layer is present as $O^=$ ions, or whether the ions have given up their electrons to the metal and remain as O atoms. However, this question may be considered from the standpoint of the sizes of the two types of particles. The radius of an oxide ion in ionic crystals is 1.40×10^{-8} cm. Taking this as an approximation of the radius of a chemisorbed oxide ion, the area occupied by each ion in a hexagonally close-packed layer is 6.8×10^{-16} cm.^{2}, and there are 1.5×10^{15} $O^=$/cm.^{2} in a monolayer. The charge passed in polarizing to the oxygen evolution potential is equivalent to 4.5×10^{15} O^-/cm.$^2{}_{real}$, or three layers of oxide ions. It does not seem likely that the electrostatic repulsion of these closely packed negative particles would permit a film three layers deep to have the degree of stability observed for the chemisorbed oxygen. In the strong electric field present at the oxygen evolution potential, dipole attraction between the highly polarizable oxide ions would assist in stabilizing the film, but this effect would largely disappear on open circuit, and repolarization would then require a larger charge than is observed.

The radius of covalently bonded oxygen, 0.74×10^{-8} cm., may be used as an approximation of the radius of a chemisorbed neutral oxygen atom. The area for each atom in a hexagonally closed-packed layer is then 1.9×10^{-16} cm.^{2}, and there are 5.3×10^{15} O/cm.^{2} in a monolayer. The original polarizing charge can thus deposit 4.5/5.3, or 85%, of a monolayer. The difference between this and a complete monolayer may be accounted for either by the uncertainty in the value for the roughness factor, or by assuming that some hydroxyl radicals are included in the layer. This approximation of a monolayer and the lack of repulsion between the neutral particles, provide good arguments for assuming that the chemisorbed oxygen is present as neutral atoms.

The increase of potential with time at zero applied current density is obviously caused by some process which occurs spontaneously on the titanium surface. This process is assumed to be the chemisorption of oxygen from the aerated solution. According to the electron configuration theory of passivity,[9] such a chemisorbed film causes the potential of the metal to become more noble by satisfying the residual valence forces of the metal atoms in the surface. Uhlig[10] considers this "chemical passivity" to be "the important factor in explaining

(9) H. H. Uhlig and J. Wulff, *Trans. Am. Inst. Mining Met. Engrs.*, **135**, 494 (1939); H. H. Uhlig, *Trans. Electrochem. Soc.*, **85**, 307 (1944).
(10) H. H. Uhlig, *J. Electrochem. Soc.*, **97**, 215C (1950).

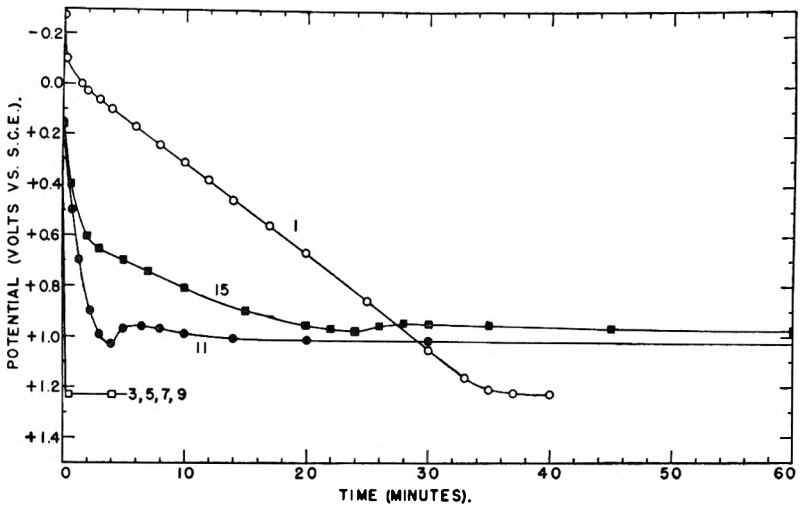

Fig. 4.—Time–potential curves for anodic polarization and repolarization of titanium in aerated 0.5 *M* NaCl at 30°. (For explanation of curve numbers, see Fig. 3.) ○, 6×10^{-6} amp./cm.^{2}; ●, 2×10^{-7} amp./cm.^{2}

corrosion resistance of metals . . . such as . . . titanium . . ." The process of spontaneous passivation approaches its limit as the potential approaches +0.2 v. This potential, attained by a fresh coupon when left on open circuit is approximately the same as that attained in the decay of the oxygen overvoltage. It apparently represents the zero-current potential of titanium on which oxygen is chemisorbed, either spontaneously or by anodic deposition.

The adsorption of oxygen, increasing the potential in proportion to the number of atoms adsorbed, can account for only a part of the potential increase during the original polarization, since the potential after open-circuit decay of polarization is only +0.2 v., even though all of the adsorbed oxygen is known to be still present. The major portion of the increase to the oxygen evolution potential must occur in the diffuse double layer. The capacitance of this double layer, as determined from the initial rate of increase of potential in repolarization, is about 3 μfd./cm.^{2}real. This is smaller than the capacitance usually measured on an anode or cathode surface.

At very low applied current densities, the charging curves (Fig. 1) are non-linear in their early portions. This is because the initial rate of chemisorption of dissolved oxygen is greater than the rate of deposition of oxygen from OH^- by the applied current. At potentials higher than +0.2 v., the spontaneous chemisorption does not occur, and the potential increase is then linear at the rate determined by the applied current density. The total charge passed by the applied current in reaching a constant potential is less than at higher current densities, since a part of the oxygen in the adsorbed layer originates as O_2, and does not require current for its adsorption.

Decay of Anodic Polarization.—When the current to an anode is stopped during oxygen evolution, the reaction must continue at a rate determined by the potential. The double layer is discharged, and the potential decreases. Armstrong and Butler[11] show that, for an electrode reaction whose rate is $I = ke^{aE}$, the potential during decay of overvoltage follows the equation $E = K - 0.12 \log t$, where K is a constant and t is time after stopping of the current. The present results for titanium show partial agreement with this equation, as may be seen in Fig. 6. Curves 6, 8 and 10 have short arrests of slope about −0.12 in the region of +0.8 v. Curve 12 and curve 16 down to +0.65 v., are almost linear, and have slopes of −0.10 and −0.12, respectively. At lower potentials, all of the curves except curve 12 have slopes of about −0.5, until they level off at +0.05 to +0.16 v. The length of the arrest having a slope of −0.12 is greater with longer time of previous oxygen evolution. Comparison of curves 6 and 8 shows that the arrest is shortened slightly by prolonged standing on open circuit during the step of curve 6. The arrest is shortened also by cathodic treatment preceding an anodic polarization and polarization decay, as shown by curves 12 and 16.

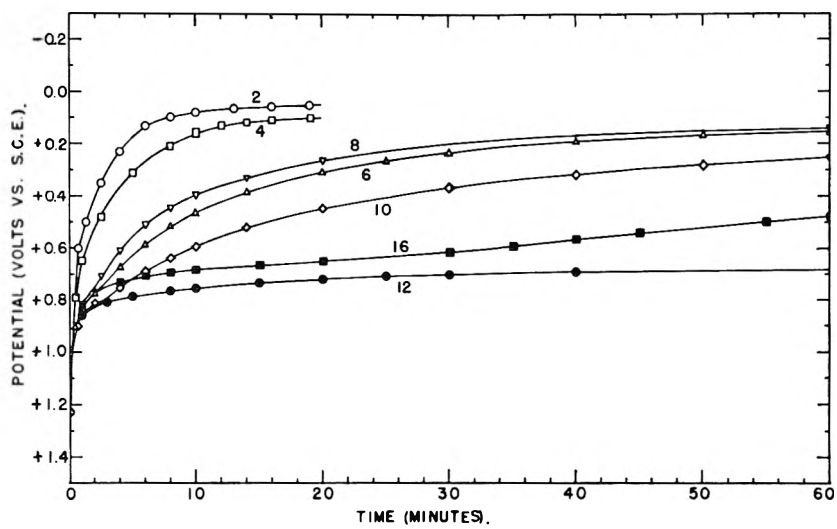

Fig. 5.—Time–potential curves for open-circuit depolarization of titanium, following anodic polarization, in aerated 0.5 *M* NaCl at 30°. (For explanation of curve numbers, see Fig. 3.) ○, following 6×10^{-6} amp./cm.^{2}; ●, following 2×10^{-7} amp./cm.^{2}.

If a capacitance C is charged to a potential E'_0, and discharged through a resistance R, the potential E' during discharge is $E' = E'_0 e^{-t'/RC}$, where t' is in seconds, R is in ohms, and C is in farads. This

(11) G. Armstrong and J. A. V. Butler, *Trans. Faraday Soc.*, **29**, 1261 (1933).

function may be written

$$t' = -2.3RC \log E'/E_0', \text{ or}$$
$$\log t' = 0.36 + \log RC + \log (-\log E'/E_0')$$

A plot of E' *vs.* log t' is a sigmoid curve asymptotic to $E' = E_0'$ and to $E' = 0$. Its middle portion is nearly linear. The maximum slope, which occurs at $E' = E_0'/e = 0.37\ E_0'$, is

$$dE'/d \log t' = -2.3E_0'/e = -0.85E_0'$$

The slope thus depends only on E_0'. A change in RC shifts the entire curve along the log t' axis. A family of such curves having different values of RC strongly resembles the curves of Fig. 6 at potentials below the arrest. This suggests that the potential below the arrest is controlled by the discharge of the double-layer capacitance through a leakage resistance, and that the effect of increasing the time of oxygen evolution is to increase the value of the product RC.

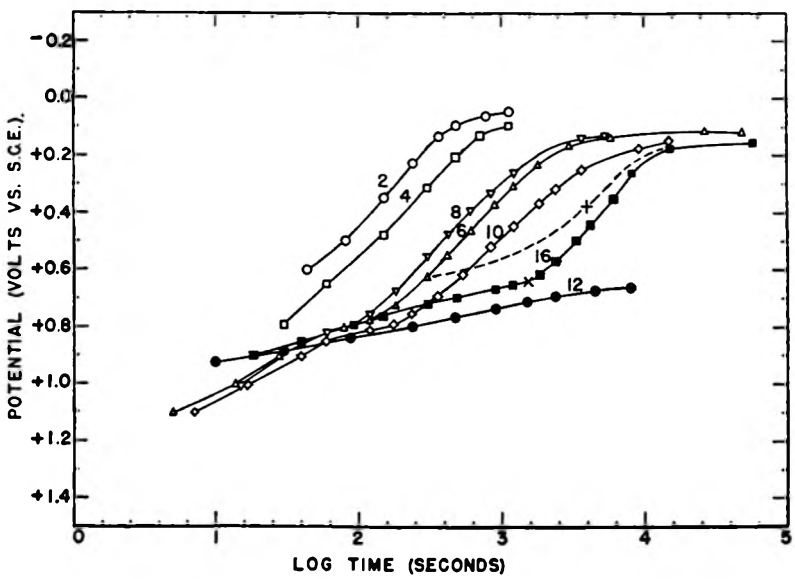

Fig. 6.—Potential *vs.* log time for open-circuit depolarization of titanium, following anodic polarization, in aerated 0.5 *M* NaCl at 30°: ○, following 6×10^{-6} amp./cm.²; ●, following 2×10^{-7} amp./cm.².

Since the length of the arrest in Fig. 6 depends on the total time of previous oxygen evolution, rather than on the duration of the immediately preceding polarization step, it is obvious that whatever causes the lengthening of the arrest is not substantially lost during polarization decay. It is known that a visible TiO_2 film is formed on the surface after oxygen evolution ceases at high current densities, and it is likely that some TiO_2 forms during oxygen evolution. It is, therefore, probable that TiO_2 also forms, although very slowly, at low current densities. The gradual accumulation of TiO_2 could quite conceivably cause an increase of RC, and thereby lengthen the arrest. Cathodic polarization would be expected to remove some TiO_2 and shorten the arrest.

All of the curves of Fig. 6 are in accord with an assumption that the double layer is discharged by two processes, one a logarithmic function, the other an exponential function of time. The first process is oxygen evolution, which requires the passage of electrons through the double layer boundary at the metal surface. The second process is leakage of current around the double layer boundary through an external resistance. The two discharge paths are electrically in parallel, so that the currents are additive. In the early part of each discharge, the oxygen evolution current is the larger, and the potential follows the logarithmic equation, giving a linear E *vs.* log t plot. As E approaches the reversible oxygen potential, the current for oxygen evolution approaches zero. When it becomes smaller than the leakage current, the potential obeys the exponential decay law, giving a sigmoid E *vs.* log t curve. In successive steps of polarization decay, following longer oxygen evolution, the amount of TiO_2 on the surface becomes larger. Thus RC is larger and the leakage current is smaller. The arrest, *i.e.*, the logarithmic decay, is lengthened, since it continues so long as the oxygen evolution current is larger than the leakage current. In curves 2 and 4, the arrest apparently ended before the first reading was made.

The sigmoid portions of the experimental curves do not have exactly the same shape and slope as the theoretical E' *vs.* log t' curves, because the time scale is not based on the start of the exponential decay. Since the exponential equation applies only after the oxygen evolution current becomes negligible, the proper initial values, *i.e.*, $E' = E_0'$ at $t' = 0$, are those existing at the time of changeover of control from logarithmic to exponential. Since the currents for the two types of discharge are comparable near the changeover, it is not very sharp, but it may be taken to be the end of the linear arrest. If the potential and time at this point are designated as E_c and t_c, and the final constant potential as E_f, then $E_0' = E_c - E_f$, and $t' = t - t_c$. In Fig. 6, the apparent changeover point on curve 16 is marked with an X, at $t_c = 1500$ seconds, and E *vs.* log t' is plotted as a broken line. Similar curves for the earlier polarization decay steps would lie closer to the log t curves. A value for E_0' may be obtained from each curve as $-(dE/d \log t')_{max}/0.85$.

These values probably are more reliable than those calculated as $E_c - E_f$, because of the indefiniteness of the changeover point. The exponential decay equation shows that when $t' = RC$, $E' = E_0' e^{-1} = 0.37E_0'$. Thus, RC may be obtained from the experimental curves at t' when $E = E_f + 0.37\ E_0'$. For curve 16, this point is marked with a + on the broken curve. The values of RC are: curve 2, 210 sec.; curve 4, 310 sec.; curve 6, 1200 sec.; curve 8, 930 sec.; curve 10, 2400 sec.; and curve 16, 4000 sec. From curves 2 and 10 it is seen that RC increases more than 10 times in 2 hours of oxygen evolution.

Anodic Processes at High Current Densities.—The TiO_2 film which forms on the metal surface during oxygen evolution is considered to be dis-

tinct from the layer of chemisorbed oxygen which is deposited during the linear potential rise in the original polarization. The basis for the distinction is that the titanium atoms on which oxygen is chemisorbed are not removed from the metal lattice, whereas this removal is required for the formation of the metal oxide. It is probable that titanium atoms are removed from the metal lattice only at the rather high positive potential which exists on the electrode during oxygen evolution. The higher oxygen overvoltage at larger current densities thus accelerates the formation of TiO_2. However, even at high current densities only a small fraction of the total current is used in forming TiO_2 during oxygen evolution. This is shown not only by the active evolution of oxygen bubbles, but also by the lack of a visible oxide film until after oxygen evolution has stopped.

The appearance of a visible surface film shortly after the cessation of oxygen evolution suggests that the cessation is caused by some degree of completion of a TiO_2 film. It is not likely that just a uniform monolayer is formed, since this would require that TiO_2 be formed more easily where the metal is covered by chemisorbed oxygen than where some oxide is already present. According to Uhlig's theory of passivity, the adsorption of oxygen on a metal atom decreases the tendency for that atom to react, whereas the removal of the atom from the metal lattice to form an oxide molecule exposes the underlying atoms and permits it to react. Thus there should be a preference for further reaction where some oxide is already present. After a spot becomes several layers thick, further thickening requires a higher potential, and there is then an increasing tendency for spreading of the spot by formation of TiO_2 at the edges. Thus the spots of oxide film can grow both by thickening and by spreading laterally over the surface.

It is seen in Fig. 2 that there is no sharp break in the curves at the beginning of the second potential rise. The cessation of oxygen evolution, which occurs at about +2 v., may be taken as the dividing point between the constant or slowly rising potential and the rapid potential increase. For reasons presented later, it is presumed that oxygen evolution is diminished where an oxide film is present, and is prevented where the film is sufficiently thick. Thus, as the area of the uncoated surface decreases, the current density for oxygen evolution, and the oxygen overvoltage, must increase. This can account for the slow increase of potential during oxygen evolution which is seen in Fig. 2. As the area of the uncoated surface becomes smaller, a given increase in the coated area constitutes a larger percentage decrease in the uncoated area. Also, as the potential becomes higher, the rate of formation of TiO_2 increases, until, just before the film is completed, this process uses almost all of the applied current. Both of these effects tend to cause the acceleration in the potential increase which occurs shortly before oxygen evolution stops.

After the cessation of oxygen evolution, all of the current is available to form TiO_2, and the film thickens rapidly. The formation of TiO_2 requires the movement of either titanium or oxide ions through the TiO_2 film. The positive titanium ions are much smaller than the oxide ions, and, therefore, are almost certainly the ones involved in the migration. They leave the surface as a result of the applied potential, pass through interstitial positions in the TiO_2 film, and combine with oxide ions at the film–solution interface.

In a recent paper,[12] Haring has proposed a mechanism for the formation of an oxide film on a tantalum anode, and for the rectifying properties exhibited by this film. Although there are marked differences between the behavior of tantalum and that of titanium, Haring's mechanism for film growth and film breakdown seem to apply to the behavior of titanium during the second anodic potential rise. Haring proposes that the positive metal ions in transit through the oxide film constitute a space charge which is balanced by oxide ions adsorbed on the outer surface of the film. The concentration of excess positive ions is greatest near the metal surface and falls off toward the solution. This unsymmetrical charge distribution constitutes a potential gradient which is maintained by the applied potential. A certain minimum potential gradient is required for movement of the metal ions through the oxide. An applied potential gradient in excess of the minimum accelerates the removal of metal ions from the metal surface and their migration through the oxide film, so that the actual potential gradient during film growth is maintained at a value only a little above the minimum. The total potential difference through the film thus is proportional to the thickness of the film. The measured potential of the electrode consists of this potential difference plus the potentials across the metal/oxide and the oxide/solution interfaces. The oxide/solution potential is the only part of the total potential which is available for the oxidation of OH^- to O_2, and during film growth, prior to film breakdown, this potential is not large enough to cause oxygen evolution. This can explain the lack of oxygen evolution on titanium during the second potential rise. The same considerations apply to the oxide-coated spots during oxygen evolution. At these sites, most of the electrode potential lies within the field of the space charge in the oxide, while on the uncoated areas the full potential is available to produce oxygen evolution.

Haring's mechanism for film growth requires an approximately linear increase of potential at constant current, at a rate proportional to current density. Figure 2 shows that the rate of increase on titanium increases with time and is not proportional to current density. The discrepancy probably is caused by the necessity for completing the coverage of the surface and by film defects where impurities are present in the metal surface. Also, non-uniform current distribution on the coupon surface may play a part. This effect shows up in the different behavior of the flush-mounted and the recessed coupons at the same current density. The sharp edge of the flush coupon was not in close contact with the plastic mounting and so was exposed to the solution. There was thus a concentration of current at and near this edge. The re-

(12) H. E. Haring, *J. Electrochem. Soc.*, **99**, 30 (1952).

cessed coupon was bounded by a plastic gasket pressed against its face, so that only a plane surface was exposed, giving a more uniform current distribution.

According to Haring, the total charge carried by the excess positive ions within the film increases as the oxide film thickens. This requires a corresponding increase in the number of oxide ions adsorbed on the outer surface of the oxide film, and causes an increase in the potential across the oxide/solution interface. When this latter potential becomes large enough, oxygen evolution begins again. This reaction, unlike the reaction of metal ions with oxide ions involved in film growth, yields electrons at the solution side of the film. These electrons, in moving through the film toward the metal, neutralize some of the positive metal ions, thereby decreasing the space charge and permitting the movement of more positive ions from the metal into the film. These ions tend to follow the path of best conductance established by the inward-moving electrons. The result is a sporadic pattern of film growth and local breakdown of the film.

The local film breakdown would be expected to occur at the areas of highest current density, *i.e.*, at the edges of the flush coupons. This is where pits were found after the potential had been at +10 v. for a while. Film breakdown at points along the sharp edge would cause further concentration of the current at these points. In these pits, titanium ions are removed from the metal so rapidly that they move some distance away from the surface before combining with oxide or hydroxyl ions, so that a hydrous oxide precipitate forms, instead of an adherent oxide film. It should be noted that while the pits are enlarging, the growth of the compact film continues on the rest of the surface, at a potential of about 10 v. This very high potential at the pits probably cannot be attributed to a potential through a remaining oxide film, but instead is probably caused by large ohmic resistance and concentration polarization effects in the electrolyte within the pits, where the current density is very high.

There is no experimental evidence that oxygen evolution begins on titanium at the end of the second potential rise, *i.e.*, at 10 v. Some bubbles were observed at the edges of the coupons, but these could be due to the aeration of the solution, or to the earlier oxygen evolution. However, the evolution of a visible quantity of oxygen probably would not be required to initiate film breakdown by Haring's mechanism. After breakdown has occurred at a few points, the electrode reaction at these points may change to the direct anodic oxidation of titanium, followed by precipitation of the ions as a hydrous oxide.

Acknowledgment.—The authors are pleased to acknowledge some financial assistance under Office of Naval Research Contract 375(02). This research is being continued under this same contract.

THE EFFECT OF ULTRASONIC WAVES ON HYDROGEN OVERVOLTAGE[1,2]

BY ERNEST YEAGER, T. S. OEY AND FRANK HOVORKA

Department of Chemistry, Western Reserve University, Cleveland, Ohio

Received November 17, 1952

The effects of ultrasonic waves on hydrogen overvoltage have been investigated at 300 kc./sec. in terms of a bright platinum surface. Polarization measurements have been made by the indirect method with an electronic commutator and gated potentiometer. The acoustical amplitude has been determined with a calibrated barium titanate hydrophone. In the absence of ultrasonic waves, the overvoltage has been found to follow the Tafel equation in both sulfuric and hydrochloric acid solutions at current densities from 0.2 to 30 ma./cm.^{2} with a Tafel slope of 0.03 and an intercept constant of 0.12. The decay of the overvoltage with time has been observed to be as low as 1 mv. during a period of 0.001 sec. following the interruption of the polarizing current. These results support the theory that the atomic combination step is responsible for hydrogen overvoltage on platinum. The Tafel slope has been found to depend to a minor extent on the type and the concentration of electrolyte. Ultrasonic waves at cavitation levels produce a decrease in the overvoltage without modifying the Tafel slope. Approximately two-thirds of this depolarization persists after the radiations have ceased. The initial values for the polarization before irradiation are recovered if the polarizing current is turned off for a matter of minutes. The instantaneous component of the depolarization is explained on the basis that the ultrasonic waves greatly reduce the concentration gradient with respect to dissolved molecular hydrogen at the electrode surface. The residual depolarization is interpreted in terms of the stripping off of irreversibly adsorbed species on the surface. The latter probably are adsorbed at the lower potential of the electrode prior to passage of polarizing current and are not readily readsorbed at the more cathodic potential of the polarized electrode.

Introduction

Ultrasonic waves are capable of producing a.c. as well as d.c. changes in the potential of a polarized gas electrode such as the hydrogen electrode. The former effect[3] appears to depend primarily on the modulation of the *IR* drop in the immediate vicinity of the electrode as a result of the periodic variations produced in the bubble size by the ultrasonic waves. The d.c. effect is more interesting in terms of fundamental information concerning polarization. Ultrasonic waves would be expected to produce a decrease in the polarization associated with a hydrogen electrode for the following two reasons.

(1) Presented at the symposium on Electrode Processes at the national meeting of the American Chemical Society in Atlantic City in September, 1952.

(2) Work partially supported by the Office of Naval Research under Contract No. N7 onr 47002, Project No. NR 051 162.

(3) *E.g.*, E. Yeager and F. Hovorka, *J. Electrochem. Soc.*, **98**, 14 (1951); E. Yeager, J. Bugosh, H. Dietrick and F. Hovorka, *J. Acoust. Soc. Am.*, **22**, 686 (1950).

First, the cavitation associated with the ultrasonic waves is capable of stripping off adsorbed materials on the electrode surface. Such a stripping action is reasonable in view of the ability of high intensity ultrasonic waves to erode a metal surface in a liquid. The second basis upon which depolarization is to be expected involves the micro-agitation associated with the impingement of ultrasonic waves on a phase discontinuity. Ultrasonic waves of even moderate intensity are very effective in reducing any concentration gradients at the electrode interfaces.

The effect of ultrasonic waves on hydrogen overvoltage was noted in 1934 by Moriguchi[4] in Japan. In 1937 Schmid and Ehret in Germany[5] and Piontelli[6] in Italy studied the effects of ultrasonic waves on hydrogen overvoltage for several metal surfaces. These workers reported that marked decreases in hydrogen overvoltage were produced by moderately intense ultrasonic waves, *i.e.*, above cavitation levels. Quantitative information concerning the acoustical amplitude was not obtained. Furthermore, the circumstances under which these experiments were conducted were far short of the requirements generally acknowledged to be a prerequisite for hydrogen overvoltage measurements. The overvoltage data obtained by these workers without ultrasonic waves are at some variance with the values now generally accepted.

It is interesting to note that Polotskii and Filippov[7] have been able to produce decreases in hydrogen overvoltage by inducing cavitation in the vicinity of the electrode with superheated steam.

In the present investigation an attempt has been made to study the effect of ultrasonic waves on hydrogen overvoltage under controlled electrochemical and acoustical conditions. Smooth platinum has been chosen as the surface upon which to initiate this study since there is some agreement[8-10] as to the nature of hydrogen overvoltage on this surface. For platinum in acid medium the discharge of the hydrogen ion to yield adsorbed atomic hydrogen is believed to be essentially reversible at moderate current densities while the combination of atomic hydrogen to form molecular hydrogen is rate determining.

Experimental Procedure

Of the various techniques for the measurement of polarization, the commutator or indirect method is particularly promising because it affords information concerning the build-up and decay of overvoltage as well as the steady-state polarization when adequate electronic instrumentation is used. With this technique the polarizing current is periodically interrupted and the potential of the polarized electrode determined relative to a reference electrode as a function of time following either the initiation or interruption of the current. In electrochemical studies involving ultrasonic waves the commutator method has additional advantages for it permits the use of small electrodes without complicated solution bridge arrangements in the immediate vicinity of the electrode. The latter would scatter the sound waves and greatly restrict quantitative acoustical measurements.

A special electronic commutator and gated potentiometer unit has been developed for these measurements. This apparatus is similar to that described previously[11] with the exception that a double potentiometer arrangement[12] is used with the gated bridge detector. With this unit the potential of a polarized electrode can be determined relative to a reference electrode with an accuracy of ±1 mv. during any 2-microsec. period following either the interruption or initiation of the polarizing current. The polarizing current can be varied from 10^{-5} through 0.4 amp. with interruption frequencies variable from 2 through 5000 per sec. and interruption periods from 3 microsec. through 0.1 sec. or one-half the repetition period depending on whichever is shorter.

The hydrogen overvoltage measurements have been carried out in an all-glass cell of the type shown in Fig. 1.

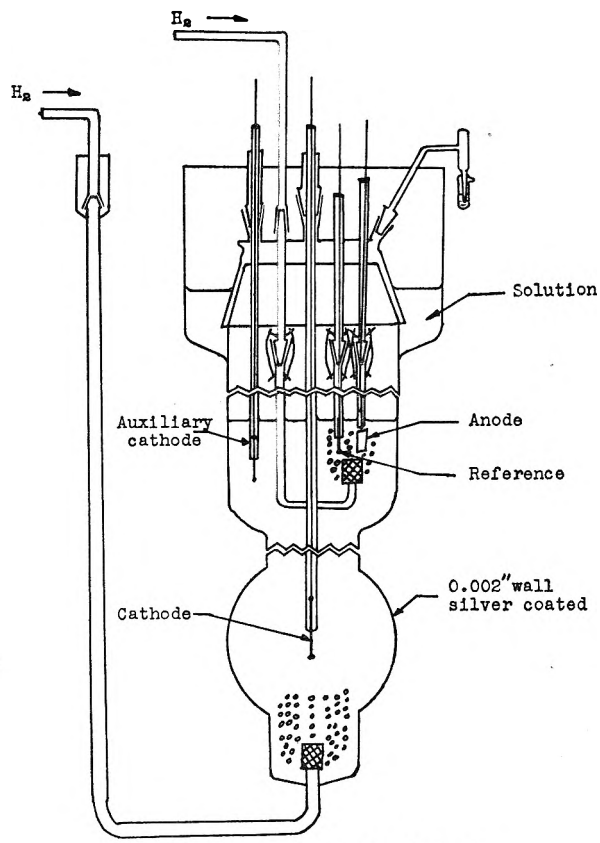

Fig. 1.—Acousto-electrochemical cell.

This cell, referred to as the acousto-electrochemical cell, is positioned within a large glass tank in such a fashion that ultrasonic waves are propagated directly through the extremely thin walls (0.002 in.) of the glass bulb (Fig. 2). The outside wall of the cell is coated with a thin film of silver conducting paint in order to minimize any electromagnetic pick-up which might interfere with the potential measurements. The tank is 2 ft. in width, 2 ft. in depth and 2.5 ft. in length. The temperature of the water in the tank has been maintained at 25 ± 0.05°. The source of the ultrasonic waves is a circular, x-cut, quartz transducer with a diameter of 2.5 in. A 800-watt, radio-frequency generator has been used to drive this transducer at its fundamental frequency of 300 kc./sec. Acoustical intensities of the order of 15 watts/cm.^{2} are available directly in front of the transducer provided the d.c. flow of water associated with

(4) N. Moriguchi, *J. Chem. Soc. Japan.*, **55**, 751 (1934).

(5) G. Schmid and L. Ehret, *Z. Elektrochem.*, **43**, 597 (1937).

(6) R. Piontelli, *Atti accad. Lincei, Classe sci. fis. mat. nat.*, **27**, 357, 581 (1938).

(7) I. Polotskii and T. Filippov, *J. Gen. Chem.* (*U.S.S.R.*), **17**, 193 (1947).

(8) L. Hammett, *Trans. Faraday Soc.*, **29**, 770 (1933).

(9) P. Dolin, B. Ershler and A. Frumkin, *Acta Physicochim.* (*U.R.S.S.*), **13**, 779 (1940).

(10) J. O'M. Bockris and A. Azzam, *Trans. Faraday Soc.*, **48**, 145 (1952).

(11) D. Staicopoulos, E. Yeager and F. Hovorka, *J. Electrochem. Soc.*, **98**, 68 (1951).

(12) ONR Technical Report No. 6, "An Improved Electronic Commutator for Polarization Measurements," Ultrasonic Research Laboratory, Western Reserve University, Contract No. N7 onr 47002, Project No. NR 051 162, December, 1951.

the sound field is not impeded and the water is relatively air free.

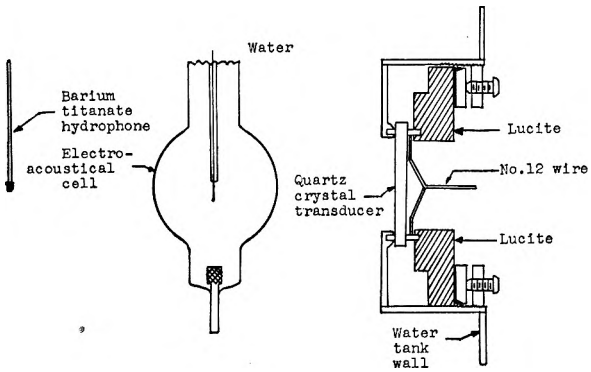

Fig. 2.—Arrangement for ultrasonic irradiation.

Acoustical pressure amplitudes have been determined with an accuracy of the order of ±10% by means of a hydrophone[13] in which the acoustically sensitive element is a polarized barium titanate cylinder with a diameter of 1/8 in., a length of 1/8 in., and a wall thickness of 0.01 in. The calibration of this hydrophone has been accomplished at 300 kc./sec. by comparison with a primary laboratory standard which had been previously calibrated by radiation pressure measurements and also checked by the U. S. Navy Underwater Sound Reference Laboratory at Orlando, Florida. The barium titanate hydrophone could not be introduced directly into the acousto-electrochemical cell during the overvoltage measurements without contaminating the solutions. Hence, it was necessary to determine the transmission characteristics of the glass cell and then to estimate the pressure amplitude within the cell from amplitude measurements in the water outside of the cell. For most of the research, the platinum cathode was located approximately 5 in. from the quartz transducer. At this distance diffraction effects associated with the finite dimensions of the transducer were evident. The diffraction effects as well as the formation of cavitation bubbles in the hydrogen-gas-saturated solution within the cell and the acoustical mismatch between the solution inside the cell and the water in the outer tank limited the accuracy of the estimated value of the acoustical pressure amplitude at the cathode to approximately 30%. The relative accuracy for a given solution, however, was probably ±10%. The sound field within the cell in the vicinity of the cathode was essentially progressive. Gas-type cavitation in the gas-saturated solution within the cell made it difficult to obtain acoustical intensities much greater than a few watts per cm.² at the cathode surface.

Provisions have been incorporated in the cell (Fig. 1) for continuously saturating the solution with hydrogen gas and for excluding oxygen gas which would otherwise act as a depolarizing agent. The hydrogen gas from a cylinder was purified by passing it through a conventional purification train (platinum at 450°) to remove primarily oxygen and then through an adsorption trap filled with activated carbon at liquid nitrogen temperature to remove any remaining trace impurities. The fritted-glass plug at the bottom of the cell permitted hydrogen gas to be bubbled over the surface of the working cathode during the polarization measurements if desired.

(13) ONR Technical Report No. 2, "Apparatus for Acoustical Measurements with Pulse-Modulated Ultrasonic Waves," *ibid.*, December, 1949.

A platinized-platinum wire with hydrogen gas bubbling around it was used as the reference electrode (Fig. 1). A reversible hydrogen electrode was also used as the anode. The latter consisted of a platinized-platinum foil, 10 cm.² in area, with hydrogen gas bubbling over the surface. At the anode molecular hydrogen was oxidized to hydrogen ions, and hence, free oxygen was not produced. The success of this technique, *i.e.*, a reversible hydrogen anode, is reflected by the fact that the potential of the anode differed by less than 5 mv. from the potential of the reversible hydrogen reference electrode for polarizing currents as high as 20 ma. The surfaces of both the reference electrode and the anode were prepared according to standard platinizing procedures.

An auxiliary cathode and a working cathode were incorporated in the cell as shown in Fig. 1. The auxiliary cathode was used for electrolytically purifying the solutions. In each case the platinum wire was sealed into soft glass tubing and electrical connection made through a copper wire which was joined to the platinum wire with silver solder. The working cathode was 14-gage (B and S) platinum wire with an exposed area of 0.4 cm.². In order to minimize the abnormally high current densities associated with sharp edges, the end of each cathode was fused to form a sphere of curvature comparable to that of the bulk of the wire.

The cathode surfaces were pretreated in the following fashion. First, the electrodes were exposed for five minutes to a solution consisting of equal volumes of concentrated nitric acid and concentrated sulfuric acid. After a rinse with distilled water, the electrodes were placed in boiling nitric acid for five minutes. The electrodes were then rinsed thoroughly with conductivity water and annealed for 10 minutes in a hydrogen flame. After preparation the cathodes were stored in a hydrogen-gas-saturated solution which was of the same composition as that involved in the subsequent overvoltage measurements. The active area of the platinum surface prepared by this procedure was very small compared to that associated with platinized-platinum electrodes of comparable apparent surface area.

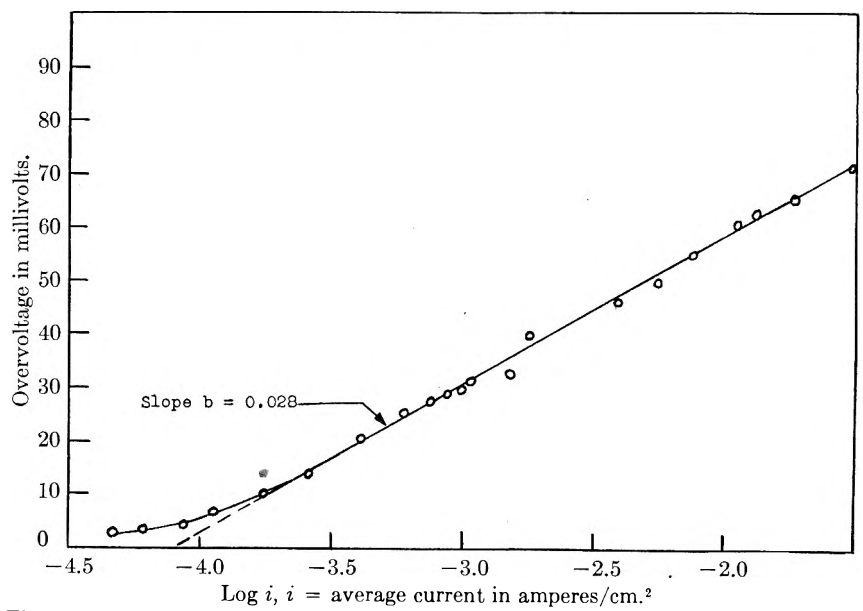

Fig. 3.—Hydrogen overvoltage on platinum: temp., 25°; electrolyte, 0.107 N H_2SO_4; current-on, 1800 microsec.; current-off, 200 microsec.

Reasonably extensive precautions have been taken to minimize impurities in the solutions used for the overvoltage measurements. Conductivity water was prepared from ordinary distilled water by two redistillations, the first of which was from an alkaline permanganate solution. Sulfuric acid (C.P. du Pont) was used in preparing the decinormal and normal sulfuric acid solutions. The hydrochloric acid solutions were obtained by diluting azeotropic solutions of hydrochloric acid which were in turn prepared by distillation. In the study of the effect of salt concentration on hydrogen overvoltage in sulfuric and hydrochloric acid solutions, reagent grade crystals of potassium sulfate or chloride were used.

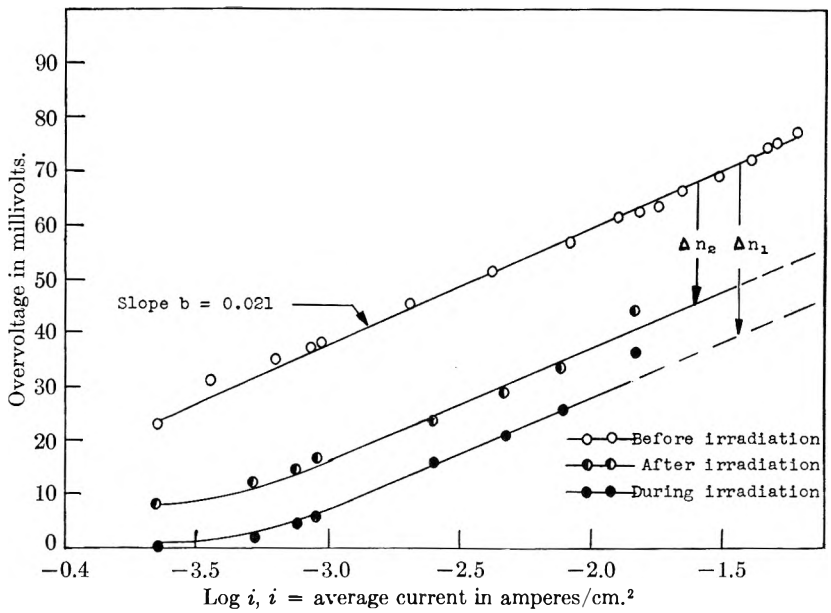

Fig. 4.—The effect of ultrasonic waves on hydrogen overvoltage on platinum in sulfuric acid: temp., 25°; electrolyte, 1.07 N H_2SO_4; current-on, 1800 microsec.; current-off, 200 microsec. —○—○—, before irradiation; —◐—◐—, after irradiation; —●—●—, during irradiation.

Prior to the actual measurements, pre-electrolysis techniques were used to eliminate or at least to minimize minute traces of impurities in the solution which might otherwise be deposited on the working cathode during the measurements. During pre-electrolysis, the potential of the auxiliary electrode was maintained more negative than the most negative value reached by the working cathode during the overvoltage measurements. Pre-electrolysis times ranged from 10 to 20 hours.

Experimental Results without Ultrasonic Waves

The curve in Fig. 3 indicates the dependence of the hydrogen overvoltage on current density in the absence of ultrasonic waves for decinormal sulfuric acid while the upper curves in Figs. 4 and 5 represent similar data for normal sulfuric and hydrochloric acid solutions, respectively. These potential measurements were made during a period of 3 microsec. following the interruption of the polarizing current with a current-on period of 1800 microsec. and a current-off period of 200 microsec. In each graph the abscissa represents the logarithm of the time-average values for the polarizing current. Data were usually recorded with increasing current density although the results obtained by subsequently decreasing the current deviated by less than 2 mv. and in many cases 1 mv. from those obtained with increasing current provided the polarizing current was never increased above 50 ma./cm.² during the run. The total time required for a run ranged from 20 to 60 min. The solutions were quiescent during these determinations.

According to Figs. 3–5, the hydrogen overvoltage on smooth or low-surface-area platinum is linearly dependent on the current density for polarizing currents from approximately 0.2 through 50 ma./cm.². For this range the hydrogen overvoltage may be represented by the Tafel equation

$$\eta = a + b \log i \qquad (1)$$

where η is the overvoltage, i is the current density and a and b are constants characteristic of the rate-determining processes and the surface. Values for the intercept constant a and the slope constant b are tabulated for various solutions in the columns marked "before irradiation" in Table I. These data have been obtained from graphs similar to those in Figs. 3–5. On the basis of duplicate determinations, the precision for the a constants before ultrasonic irradiation is estimated to be ±0.01 and for the b constants ±0.001. The values for the slope constant b are generally 0.03 which is in agreement with the work of Hammett,[8] Dolin and his co-workers,[9] and Bockris and Azzam.[10]

It is noteworthy that there are significant differences in the slope constants for the various electrolytic solutions according to the present measurements. The variations in the a constants, however, are less significant since they may represent changes in the true surface area which may be attributable to impurities specific to the electrolytes.

In Fig. 6 are shown graphs of the overvoltage in decinormal sulfuric acid as a function of current density in quiescent solution and in agitated solution. Agitation was accomplished through the passage of hydrogen bubbles over the electrode surface from a fritted glass member below the electrode as shown in Fig. 2. The polarization was depressed by approximately 6 mv., an amount which was independent of the polarizing current in the range for which eq. (1) is applicable. Similar results have been noted in normal sulfuric acid with an average value for the decrease of 5 mv.

The decay of the hydrogen overvoltage with time has been examined both with the gated potentiometers as well as with the oscillograph. On a clean platinum surface the decay has been found to be less than 1 mv. during a period as long as 0.001 sec. following the interruption of the polarizing current[14]

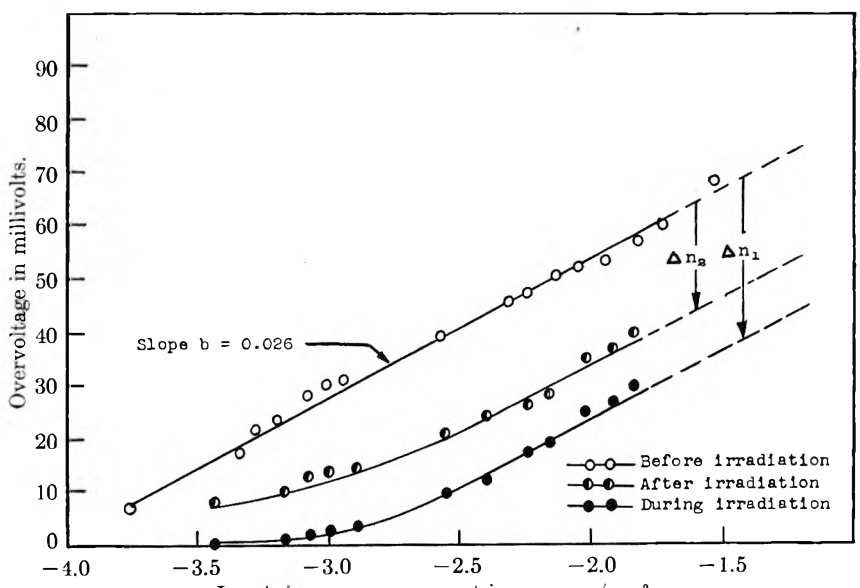

Fig. 5.—The effect of ultrasonic waves on hydrogen overvoltage on platinum in hydrochloric acid; temp., 25°; electrolyte, 1.00 N HCl; current-on, 1800 microsec.; current-off, 200 microsec.; —○—○—, before irradiation; —◐—◐—, after irradiation; —●—●—, during irradiation.

(14) Similar results were reported by S. Schuldiner at the Philadelphia meeting of the Electrochemical Society, May, 1952.

TABLE I

AVERAGE VALUES FOR THE CONSTANTS OF THE TAFEL EQUATION WITH AND WITHOUT ULTRASONIC WAVES

Electrolyte	Before irradiation		During irradiation			After irradiation		
	a_1	b	a_2	b	$\Delta\eta_1 = a_2 - a_1$ mv.	a_3	b	$\Delta\eta_2 = a_3 - a_1$ mv.
0.107 N H_2SO_4	0.12	0.028	0.09_7	0.03	-2_3	0.10_5	0.03	-1_5
1.07 N H_2SO_4	.10	.021	$.06_8$	.02	-3_2	$.07_8$	.02	-2_2
0.107 N H_2SO_4 + 0.010 N K_2SO_4	.11	.028	$.08_3$	.03	-2_7	$.09_3$	.03	-1_7
0.107 N H_2SO_4 + 1.0 N K_2SO_4	.15	.035	$.11_2$	.035	-3_8	$.12_6$	.035	-2_4
0.100 N HCl	.12	.029	$.09_7$	.03	-2_3	$.10_5$	.03	-1_5
1.00 N HCl	.11	.026	$.08_0$	.03	-3_0	$.09_0$	.03	-2_0
5.00 N HCl	.12	.031	$.08_3$	.03	-3_7	$.09_5$	.03	-2_5

for current densities below 10 ma./cm.^{2}. The build-up portion of the polarization curve is also flat within these limits.

In most cases when the polarizing current was increased about 100 ma./cm.^{2}, the results were no longer reproducible and the decay curve for the polarization showed appreciable slope (> 10 mv. in 0.001 sec.). Furthermore, when the current density was subsequently lowered, the polarization measurements were higher than before and erratic from run to run. The decay curves also retained appreciable slope. This phenomenon may be similar to the hysteresis found by Bockris and Azzam[10] in their hydrogen overvoltage measurements on platinum at current densities above 1 amp./cm.^{2}.

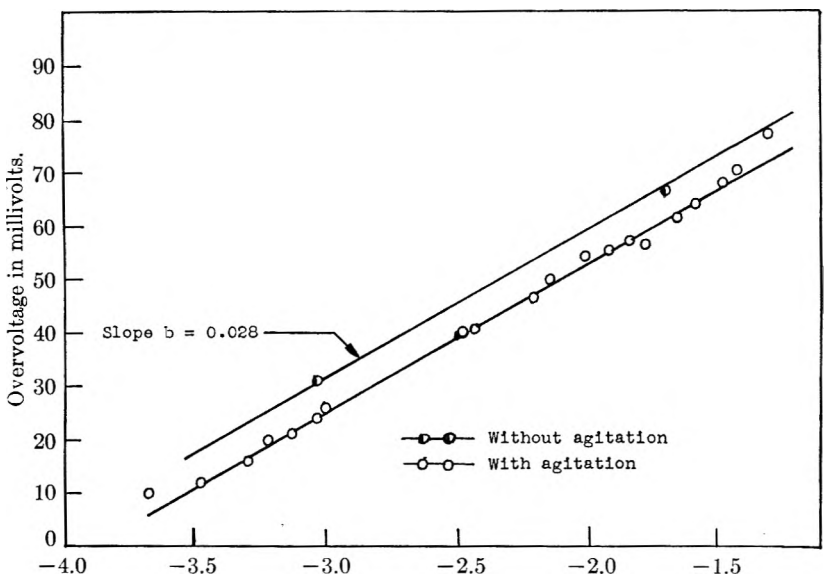

Fig. 6.—The effect of agitation on hydrogen overvoltage on platinum: temp., 25°; electrolyte, 0.107 N H_2SO_4; current-on, 1800 microsec.; current-off, 200 microsec.; —●—●—, without agitation; —○—○—, with agitation.

Experimental Results with Ultrasonic Waves

The graphs in Figs. 4 and 5 represent the effect of ultrasonic waves on hydrogen overvoltage in normal sulfuric acid and hydrochloric acid solutions. The upper curve in each figure indicates the dependence of the overvoltage on the current density prior to irradiation while the lowest curve represents the overvoltage during irradiation. Each point on the latter was obtained within 2 min. after the ultrasonic generator was turned on. The intensity of the acoustical waves was of the order of 1 watt/cm.^{2} and the frequency 300 kc./sec. Changes of as much as 30% may have occurred in the acoustical amplitude between measurements in the various electrolytes because of differences in the acoustical impedances of the solutions. From these curves it is apparent that ultrasonic waves produce a marked decrease in the overvoltage without substantially modifying the Tafel slope.

When the ultrasonic waves were stopped, only part of the initial decrease in polarization was recovered as is shown by the middle curves in Figs. 4 and 5. If the polarizing current was turned off for a substantial time, *e.g.*, two minutes, the polarization increased to the original values as represented by the upper curves in each figure. Similar results have been obtained in other electrolytic solutions and are summarized in Table I. The values listed under the heading $\Delta\eta_1$ represent the initial depolarizing action of the acoustical waves and are associated with changes in the Tafel a constant while the values under the heading $\Delta\eta_2$ represent the residual depolarization after the ultrasonic radiations have ceased. The variations in the values for $\Delta\eta_1$ can be partially accounted for in terms of variations in acoustical intensity with various electrolytes. The ratio of $\Delta\eta_2$ to $\Delta\eta_1$ is approximately $^2/_3$ in every case.

No change has been noted in the decay or build-up curve for the polarization in the presence of ultrasonic waves at current densities for which the Tafel equation has been found applicable.

In Fig. 7 is a graph which represents the dependence of overvoltage on acoustical pressure amplitude (r.m.s.) with 1.07 N sulfuric acid as the electrolyte at a time-average current density of 12.8 ma./cm.^{2}. The effect of the acoustical waves was only minor until a pressure amplitude of approximately 0.35 atm. was reached. The latter corresponded to approximately 0.08 watt/cm.^{2}. At such intensities gas-type cavitation became evident visually.

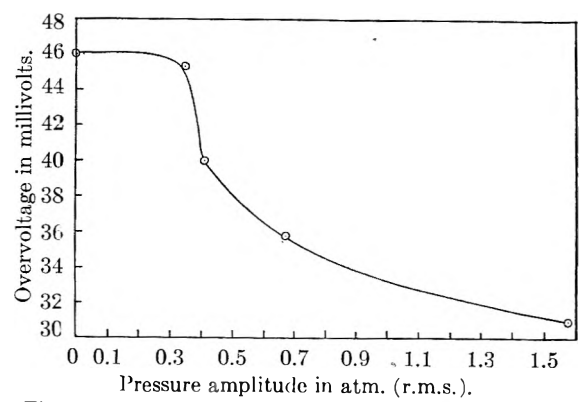

Fig. 7.—The dependence of the depolarizing effect of ultrasonic waves on acoustical pressure amplitude: temp., 25°; electrolyte, 1.066 N H_2SO_4; current density (av.), 12.8 ma./cm.^{2}; current-on, 1800 microsec.; current-off, 200 microsec.

When the cathode was exposed to ultrasonic waves of even moderate intensities (0.1 watt/cm.^{2}), a marked change occurred in the nature of the gas evolution. For a given current density, the bubble size was greatly increased. This phenomenon is not unique for electrolysis. If a liquid filled with suspended gas bubbles is placed in an ultrasonic field, the bubbles also grow larger in size and rise rapidly to the surface.

Interpretation of Results

Both the Tafel constant b value of 0.03 as well as the relatively flat decay curves support the atomic combination theory of hydrogen overvoltage which may be represented by the following steps

$$(\mathrm{H}\cdot x\mathrm{H_2O})^+ + (\mathrm{e}^- - \mathrm{Pt}) \rightleftarrows (\mathrm{H-Pt}) + x\mathrm{H_2O} \quad (1)$$

$$2(\mathrm{H-Pt}) \rightleftarrows \mathrm{H_2} + 2\mathrm{Pt} \quad (2)$$

with step 1 essentially reversible and step 2 irreversible.

The small variations of the Tafel slope constant b with the type and concentration of electrolyte may be rationalized in terms of the effects of various species present at the solution–electrode interface or the reaction rates. Ordinarily in the derivation of the simple Tafel equation by a kinetic or quasi-kinetic treatment, the various reactions associated with steps 1 and 2 are assumed to be either simply first or second order with respect to the various reactants. In the more general case, however, the forward and reverse reactions associated with step 1 may be represented as

$$[i_1^f] = [k_1^f](N - n)^Q(a_+) \exp [-\alpha(E - \psi)f/RT] \quad (2)$$

$$[i_1^r] = [k_1^r](n)^S \exp [\beta(E - \psi)f/RT] \quad (3)$$

where $[i_1^f]$ and $[i_1^r]$ represent the cathodic and the anodic currents, respectively, associated with step 1, $[k_1^f]$ and $[k_1^r]$ are constants which are dependent on the temperature, n is the surface concentration of adsorbed hydrogen in moles per unit area, N is the total number of active sites available for the adsorption of atomic hydrogen in terms of moles per unit area, (a_+) is the reaction or kinetic activity[15] of the hydrogen ions in some ill-defined portion of the solution adjacent to the electrode surface (perhaps the double layer), E is the potential of the electrode relative to the bulk of the solution, and ψ is the potential of the point at which (a_+) is specified relative to the bulk of the solution. In a sense the quantity $(N - n)$ represents the surface concentration of the species $(\mathrm{e}^- - \mathrm{Pt})$, *i.e.*, the unoccupied active sites. The quantities α and β in equations (2) and (3) are constants relating the potential difference at the solution–metal interface $(E - \psi)$ to the free energies of activation associated with the forward and reverse reactions for step 1. The quantities Q and S are constants which are close to unity and which are intended to represent the effects of various particles such as ions and solvent molecules at the electrode–solution interface. Thus, $(n)^S$ is analogous to a reaction activity. The use of the exponents Q and S is partially supported by the Freundlich isotherm particularly when the latter is expressed in the form $(n)^\rho = \kappa c$ where n is the surface concentration, of the adsorbed species, c is the bulk concentration, and ρ and κ are constants with ρ close to unity in many cases.

For step 2, the rates of the forward and reverse reactions may be expressed as

$$[i_2^f] = [k_2^f](n)^{2V} \quad (4)$$

and

$$[i_2^r] = [k_2^r](N - n)^{2W}(P)^Y \quad (5)$$

where $[i_2^f]$ and $[i_2^r]$ are the current densities to which the forward and the reverse reactions are equivalent. The term P represents the effective concentration of molecular hydrogen dissolved in the solution in terms of the partial pressure it would exert if in equilibrium with the gas phase. The terms V, W and Y are close to unity and are introduced for purposes similar to those involving Q and S in equations (2) and (3). If equations 2–5 are applied to a reversible system and compared with the thermodynamic results, it can be shown that $\alpha + \beta = 1$, $YS = V$, $YQ = W$ and the activity of the hydrogen ions in the bulk of the solution (a'_+) is assumed to be related to (a_+) by a constant factor which is a function of ψ.

If equations 2–5 are used to derive a modified Tafel equation, the overvoltage η is given by the equation

$$\eta = A + B \log (I + [k_2^r](P)^Y(N)^{2W}) \quad (6)$$

where

$$A = (2.3RT/2Yf) \log [(P)^Y/[k_2^r]] + (2.3QRT/f) \log N \quad (7)$$

$$B = -(2.3RT/2f)(S/V) \quad (8)$$

The assumptions involved in this development are that step 1 is reversible, step 2 is irreversible, and $n << N$. The form of equation (6) simplifies to that of equation (1) if the reverse reaction associated with step 2 is neglected. The factor B in equation (6) differs from that of the simple Tafel equation by the factor (S/V) or Y. Variations in the Tafel slope as reported in Table I for various solutions can be considered to reflect the dependence of this factor on the type and concentration of the electrolyte.

If equations 2–5 are applied to transient conditions and Q, S, V, W and Y are assumed to be unity, the overvoltage η_t at time t following the interruption of the polarizing current is given by the equation

$$\eta_t = \eta_0 - (2.3RT/f) \log (n_t/n_0) \quad (9)$$

where

$$(1/n_t) = \frac{-1 + [1 + (2CRT/f^2)(G)]^{1/2}}{CRT/f^2} \quad (10)$$

and

$$G = (1/n_0) + (CRT/2f^2n_0^2) + ([k_2^r]t/f) \quad (11)$$

where n_0 and n_t represent the concentration of adsorbed hydrogen at the instant of interruption and time t, respectively, and C is the capacity associated with the double layer. Equations 9–11 are applicable only when $n << N$ and $[i_2^r]$ is negligible compared to $[i_2^f]$ or when the overvoltage η_t at time t is at a value corresponding to a voltage within the linear region of the Tafel plot. This effectively limits the application of equations 9–11 to relatively small values of t.

(15) The reaction activity of the hydrogen ions may be related to the concentration by an expression of the form $a_+ = (\gamma_+)(c_+)$ where (γ_+) takes into account such effects as ionic interaction and changes in ionic solvation. The similarity to thermodynamic activity is apparent.

Unfortunately specific information is not available as to the values for the quantities N and C. In the present work experimental results at current densities above 100 ma./cm.^{2} seem to indicate that the limiting current density associated with the reaction mechanism represented by steps 1 and 2 is of the order of 1 amp./cm.^{2}. If the number of available active sites is assumed to be 10^{15} per cm.^{2} or $N = 10^{-9}$ moles/cm.^{2}, the reaction constant $[k_2^f]$ from equation (4) is then 10^{18} amp./mole. If the capacity term is assumed to be 10^{-5} to 10^{-4} μf./cm.^{2}, the decay of the overvoltage in 1 millisec. following the interruption of a polarizing current of 10^{-3} amp./cm.^{2} is of the order of 10^{-3} volt or less according to equations 9–11. This is in agreement with the experimental results. If the polarizing current is of the order of 10^{-1} amp./cm.^{2}, however, the decay in 1 millisec. is of the order of 10^{-2} volt. Appreciable slope has been noted in the oscillograms representing the decay curves at current densities of the order of 10^{-2} amp./cm.^{2} or greater. Further quantitative measurements concerning the rates of decay at high current densities will be made in the near future in order to provide more accurate information concerning the number of available sites or N.

The depolarizing effect associated with the agitation of the solution surrounding the cathode (Fig. 6) can be explained in terms of a concentration gradient with respect to dissolved molecular hydrogen. If gas bubbles were not formed at the electrode, the concentration of dissolved molecular hydrogen would attain a very large value compared to that in the bulk of the solution. When diffusion is the only process by which molecular hydrogen is removed from the electrode interface,

$$I = (2Df/\delta)(c - c_r) \qquad (12)$$

where D is the diffusion coefficient, δ is the effective thickness of the diffusion layer,[16] and $(c - c_r)$ is the difference in the concentration of dissolved molecular hydrogen at the electrode surface and in the bulk of the solution. If D is assumed to be of the order of 10^{-5} cm.^{2}/sec. and δ is assumed to be 10^{-2} cm. in an unstirred solution, $(c - c_r)$ is of the order of 10^{-5} mole/cm.^{3} for a current density of 10^{-3} amp./cm.^{2} as compared with a value of 10^{-7} moles/cm.^{3} for c_r when the equilibrium pressure is 1 atm. The concentration of molecular hydrogen at the interface would be 10^{-5} mole/cm.^{3} or P would equal 10^2 atm. for a current density of 10^{-3} amp./cm.^{2} This situation is not fully realized because of the formation of bubbles.

Bubble formation at an electrode surface, however, is not a continuous process; hence, marked concentration gradients with respect to dissolved molecular hydrogen are to be expected locally. Furthermore, the pressure within these bubbles is much greater than the hydrostatic pressure because of the surface tension. In practice nucleation theory is required to evaluate the probability of bubble formation at the electrode surface. All things considered, it seems reasonable to assume that the effective concentration c of molecular hydrogen in the solution adjacent to the electrode surface is proportional to the current density for moderate values of the latter. Thus, over a limited range of current densities, $P = \sigma I$ where the proportionality constant σ is a function of D and δ. If this approximation is applied to equation (6) and $[i_2^r]$ is assumed to be small compared to $[i_2^f]$, then

$$\eta = A + B \log I + H \qquad (13)$$

where

$$H \cong (2.3RT/2f)[k_2^r]\sigma N^2 \qquad (14)$$

The term H is independent of current density over a limited range of current densities.

Equations (13) and (14) can be used to explain the effects of stirring on a polarized hydrogen cathode. With agitation the effective thickness of the diffusion layer δ would be greatly decreased. This in turn would reduce the value of σ and hence, the term H in equation (14). The slope of the linear section of the overvoltage–log I curve, however, would be unaffected although the polarization would be decreased. This is the case experimentally (Fig. 6).

Overvoltage, more specifically activation overvoltage, is generally defined in such a manner as to be exclusive of concentration polarization effects and concentration gradients. From the above discussion it is apparent that agitation is necessary if true values for hydrogen overvoltage are to be obtained even in concentrated electrolytic solutions where ionic concentration polarization is negligible. Agitation is provided to some extent by the evolution of the hydrogen gas itself but this agitation is apparently insufficient.

The explanation of the depolarizing effect of ultrasonic waves is probably at least twofold. First, ultrasonic waves are capable of reducing any concentration gradients with respect to dissolved molecular hydrogen. Ultrasonic waves are particularly effective because of the degassing action as well as micro-agitation associated with acoustical waves at intensities above cavitation level. Such waves might readily decrease the factor H in equation (14) to an even greater extent than was attained when hydrogen gas bubbles were passed over the electrode surface.

A second factor to be considered in accounting for the depolarizing action of ultrasonic waves involves the effect of cavitation on the number of available active sites for the adsorption of hydrogen atoms on the electrode surface. During cavitation various adsorbed materials on the cathode surface may be stripped off to provide these new sites. An increase in the quantity N would decrease the overvoltage numerically without affecting the Tafel slope constant as is evident from equations 6–8.

Cavitation might also be expected to decrease the concentration of atomic hydrogen locally. This problem does occur to some extent but is insufficient in terms of the over-all rate of desorption associated with step 2. The generation of new active sites, however, is somewhat accumulative in the sense that the number of available active sites probably increases as a result of acoustical cavitation until the rate of generation of new sites is offset

(16) See, for example, G. Kortum and J. Bockris, "Textbook of Electrochemistry," Vol. II, Elsevier Publishing Co., New York, N. Y., 1951, pp. 400–405.

by the loss of active sites by the readsorption of impurities and other species.

When the ultrasonic waves were turned off, the overvoltage did not recover its original value. This can be explained on the basis that impurities and other particles adsorbed irreversibly on the electrode surface prior to the overvoltage measurements were not readily readsorbed at the more cathodic potential of the electrode when polarizing current was being passed. This hypothesis is supported by the fact that the overvoltage regained its original value when the polarizing current was turned off for a short time. Under these circumstances the potential of the electrode decayed to a voltage approaching the original value before passage of polarizing current.

The ability of ultrasonic waves to strip off adsorbed materials on the electrode surface can be readily appreciated if consideration is given to the fact that high intensity ultrasonic waves (10 watts/cm.^{2}) have been used (in this Laboratory) to produce suspensions of metals such as copper and aluminum by direct irradiation of these metals as foils in liquids. An increase in the surface area through the erosion of the electrode surface might have been considered as a direct explanation for the decrease in polarization produced by ultrasonic waves if it were not that the original values for the polarization are obtained after the current has been interrupted for a short period.

Further attention would have also been given to the "stripping off" of adsorbed hydrogen through cavitation except that such an effect would modify the slope of the overvoltage–log I plot. The only apparent way such a mechanism could be a major factor without influencing the Tafel slope would be for the stripping action to be proportional to the square of the surface concentration which is unlikely. Explanations involving the formation of electroactive materials such as free radicals through cavitation have been given little consideration since the effect of such depolarizers would be dependent on current density. Likewise, it does not seem feasible to explain the effect in terms of changes in the average temperature at the electrode because such effects would be very small in a well thermostated system and would not persist after the radiations have ceased.

Thus, the two explanations involving the factor H in equation (14) and N in equations (6) and (7) seem most feasible in terms of the experimental results. Experimental work is in progress at the present time in an attempt to further substantiate these hypotheses.

Acknowledgments.—The authors are pleased to acknowledge the assistance of Dr. D. N. Staicopoulos who helped in the design and construction of the ultrasonic propagation system and Dr. John Yeager who helped in the design and constructed the ultrasonic generator used in this investigation.

ELECTRODE PHENOMENA AND THE THERMODYNAMICS OF IRREVERSIBLE PROCESSES[1]

BY PIERRE VAN RYSSELBERGHE

Department of Chemistry, University of Oregon, Eugene, Oregon

Received November 17, 1952

The thermodynamics of irreversible processes developed by De Donder, Prigogine, de Groot and others makes possible a systematic presentation of electrochemical thermodynamics in which reversible electrode processes, reversible cells, states of electrochemical equilibrium, etc., appear as limiting cases in a more general treatment. A rational thermodynamic theory of polarization can thus be constructed. The concepts of uncompensated heat, power of irreversibility, entropy production and affinity of irreversible chemical reactions are now extended to irreversible electrochemical processes. The concept of power of polarization is introduced and its connection with electrochemical affinity and overvoltage is developed and discussed. In addition to complete cells one treats single electrodes which are the seats of one or of several half-reactions. In the case of mixed electrode processes occurring not too far from reversibility, linear relations between reaction velocities (or currents) and electrochemical affinities (or overvoltages), with application of Onsager's reciprocity principle between "drag coefficients," are used. Prigogine's theorem concerning stationary states of minimum entropy production is extended to electrochemical processes. These theoretical considerations suggest experimental investigations, in particular in the field of corrosion.

Introduction

A rational thermodynamic treatment of electrochemical systems (galvanic and electrolytic cells, single electrodes) requires the use of the thermodynamics of irreversible processes. Although by no means new this discipline is still unfamiliar to the majority of physical chemists and electrochemists. Moreover, electrochemistry has not yet been given more than scant attention by the main contributors to the field of irreversible thermodynamics. Among these we should distinguish between the authors who are concerned with the whole range of degrees of irreversibility of chemical reactions (pressure and temperature being uniform and chemical potentials corresponding to the ordinary statistical distribution functions of the various components) and the authors who are mainly concerned with the neighborhood of equilibrium and with the linear relations between reaction velocities and affinities (or more generally between flows and forces), the phenomenological coefficients obeying Onsager's reciprocal relations.[2] The first group of authors consists chiefly of De Donder and his collaborators, often designated as constituting the "Brussels or Belgian

(1) Paper presented at the Symposium on Electrode Processes held by the Division of Physical and Inorganic Chemistry of the American Chemical Society at the Atlantic City, N. J., meeting, September 14 to 19, 1952.

(2) L. Onsager, *Phys. Rev.*, **37**, 405, 2265 (1931).

school." A first presentation of electrochemical thermodynamics was included in the 1936 monograph on affinity.[3] Prigogine[4] also devoted a chapter to electrochemistry in his monograph of 1947 in which the Onsager relations and their implications are systematically added to the De Donder type of presentation of chemical thermodynamics. In de Groot's recent book[5] will be found a very brief discussion of electrochemistry which does not go beyond the scope of Prigogine's presentation. Several other authors have made some use of irreversible thermodynamics in their electrochemical studies. Among these we wish to mention particularly Piontelli[6] and Pourbaix.[7] In a monograph now nearly completed[8] we present a detailed and systematic treatment of electrochemical systems and electrode processes by the methods of the theory of affinity of De Donder and taking into account the later developments contributed by Prigogine and others. In the present communication we wish to outline the essential steps of this treatment which we believe to be of fundamental importance to the progress of our understanding of electrode processes. Time and space limitations force us to postpone to later communications certain important aspects of the subject and in particular the discussion of thermo-electrochemistry, Peltier heats, etc.

The systems we shall be considering are cells, galvanic or electrolytic, and half-cells or single electrodes. In addition to heat and work against the external pressure a cell exchanges electrical work with its surroundings through the passage of an electrical current from one terminal to the other in an external circuit. Inside the cell this current causes electrode reactions to occur in accordance with Faraday's laws of electrolysis. At the same time electrolytic migration and various polarization phenomena will occur in the system, diffusion phenomena will occur at liquid junctions, etc. All these phenomena are irreversible. Perfect reversible behavior is exceptional and is theoretically possible only for zero current. Independently of polarization, diffusion, etc., the passage of current will result in the production of the Joule heat RI^2 which is an ever-present item in the various contributions to the total uncompensated heat. It is clear that, beyond the inequalities and qualitative statements usually found in the discussions of these irreversible phenomena, a quantitative treatment such as that available through irreversible thermodynamics appears highly desirable.

The electrical potentials we shall be dealing with are the internal ones which have been clearly defined by Lange.[9] We shall designate them by the Greek letter φ. The differences of internal potentials between two phases are *Galvani potential differences*. The external electrical potentials ψ are those taken at a distance of the order of 10^{-4} cm. of the external geometrical surface of the phase. Differences of ψ potentials are *Volta potential differences*. Between the φ and ψ potentials pertaining to the same phase we have the relationship

$$\varphi = \psi + \chi \qquad (1)$$

in which χ designates the surface potential difference.

Our electrochemical systems will be of one or another of the types represented on Figs. 1 to 4: an electrode of metal α and one of metal α' dip in the same solution $\beta - \beta'$ (Fig. 1) or in separate solutions β and β' connected by means of a siphon constituted in such a manner as to minimize liquid junction potential differences (Fig. 2). To metal α we attach a piece of metal α'' identical with α'. This precaution does away with several complications to be discussed later. One may also attach pieces of a common metal to α and α' (Fig. 3). The external circuit may consist of a simple resistance or it may include one or several generators of current (Fig. 4). Our thermodynamic "closed" system is $(\alpha''\alpha\beta\beta'\alpha')$, the external circuit being a portion of the surroundings. During the lapse of time dt we have dn_{e^-} moles of electrons transported from terminal α'' to terminal α'. The positive current I flows in the opposite direction and we have

$$I = F\frac{dn_{e^-}}{dt} \qquad (2)$$

in which F represents the Faraday. The layers of solution β and β' are taken at sufficient distances from α and α' to maintain from β to β' a composition identical with that before the passage of the current. The various phenomena resulting from the passage of the current (polarization, migration, diffusion) involve the layers between α and β or α' and β'.

If we consider dn_{e^-} as positive we have at electrode α the anodic reaction

$$X^- = X + e^-(\alpha) \qquad (3)$$

and at electrode α' the cathodic reaction

$$Y + e^-(\alpha') = Y^- \qquad (4)$$

The symbols X and Y represent one or several species corresponding to the oxidized forms, the symbols X^- and Y^- one or several species corresponding to the reduced forms of the couples (X, X^-) and (Y, Y^-). It is convenient to write all electrochemical half-reactions in terms of one single electron. In addition to the electrode processes (3) and (4) we have the transfer of electrons from α to α''

$$e^-(\alpha) = e^-(\alpha'') \qquad (5)$$

(3) Th. De Donder, "L'Affinité," new presentation by P. Van Rysselberghe, Gauthier-Villars, Paris, 1936, see Chapter XVI, pp. 123–137. Th. De Donder and P. Van Rysselberghe, "Thermodynamic Theory of Affinity." Stanford University Press, 1936, see Chapter XVI, pp. 123–137.

(4) I. Prigogine, "Etude Thermodynamique des Phénomènes Irréversibles," Dunod, Paris, and Desoer, Liége, 1947, see Chapter III, pp. 29–47.

(5) S. R. de Groot, "Thermodynamics of Irreversible Processes," Interscience Publishers, Inc., New York, N. Y., 1951, see Chapter IX, pp. 181–184.

(6) R. Piontelli, see various articles and further references in "Proceedings of the Second and of the Third Meetings of the International Committee of Electrochemical Thermodynamics and Kinetics," Tamburini, Milan, 1951; Manfredi, Milan, 1952.

(7) M. Pourbaix, "Thermodynamique des Solutions Aqueuses Diluées—Rôle du pH et du Potentiel," Meinema, Delft, and Béranger, Paris, 1946. "Thermodynamics of Dilute Aqueous Solutions—with Applications to Electrochemistry and Corrosion," Longmans-Green, New York, 1949. Articles and further references in "Proceedings, etc."[6]

(8) P. Van Rysselberghe, "Electrochemical Affinity—Studies in Electrochemical Thermodynamics and Kinetics," a monograph in preparation.

(9) E. Lange, "Elektrochemie des Phasengrenzen" in "Handbuch des Experimentalphysik," Vol. XII, Part 2; also, ref. 6, 1951, see pp. 317–343.

Adding processes (3), (4) and (5) we get the cell reaction

$$X^- + Y = X + Y^- \qquad (6)$$

which, through addition on either side of ionic species not involved in the reaction, can always be written as a reaction between neutral species. This will of course be possible only if process (5) is added to (3) and (4). We have here one of the several reasons for making the terminals of the cell chemically identical. Another reason which will be immediately apparent is that in this manner there is no work of chemical extraction of the electrons to be considered in the total work done by the system.

First Law of Thermodynamics for Electrochemical Systems.—During the time dt the energy of the system is increased by dE, the heat received is dQ, the work done is dw. We have

$$dE = dQ - dw \qquad (7)$$

The work against the external pressure is $p\,dV$ and the work corresponding to the transfer of dn_{e^-} moles of electrons from α'' to α' is

$$dw_{el} = F(\varphi^{\alpha'} - \varphi^{\alpha''})dn_{e^-} \qquad (8)$$

The energy balance of our system is thus

$$dE = dQ - p\,dV - F(\varphi^{\alpha'} - \varphi^{\alpha''})dn_{e^-} \qquad (9)$$

In the particular case of a short-circuit being established between the terminals, making $\varphi^{\alpha'} = \varphi^{\alpha''}$, we have the physical chemical change of state of the system remaining the same as in (9)

$$dE = dQ_s - p\,dV \qquad (10)$$

in which the subscript s designates the condition of short-circuit. We have also

$$dQ_s = dQ - F(\varphi^{\alpha'} - \varphi^{\alpha''})dn_{e^-} \qquad (11)$$

Second Law of Thermodynamics for Electrochemical Systems

Introducing, in accordance with De Donder's method,[2] the uncompensated heat dQ', the entropy increase dS, the affinity of the reaction A and its progress $d\xi$ during the time dt, we have in the absence of electrical work, *i.e.*, for the condition of short-circuit in the case of our electrochemical system

$$dQ_s' = T\,dS - dQ_s = A\,d\xi \geq 0 \qquad (12)$$

The affinity A is that of reaction (6) and is related to the free enthalpy $G = E - TS + pV$ of the system by the relation[3,10]

$$\left(\frac{\partial G}{\partial \xi}\right)_{pT} = -A \qquad (13)$$

Here we have $d\xi = dn_{e^-}$. The ratio dQ'_s/dt has been called the power of irreversibility,[3] while the ratio of this quantity over the temperature T is the entropy production (see particularly Prigogine[4]). We have

$$P = \frac{dQ_s'}{dt} = A\frac{d\xi}{dt} = T\frac{d_iS}{dt} \geq 0 \qquad (14)$$

The total change in entropy of the system is such that

$$\frac{dS}{dt} = \frac{d_eS}{dt} + \frac{d_iS}{dt} = \frac{1}{T} \times \frac{dQ_s}{dt} + \frac{d_iS}{dt} \qquad (15)$$

(10) P. Van Rysselberghe, *Chem. Revs.*, **16**, 29, 37 (1935); *J. Chem. Educ.*, **16**, 476 (1939).

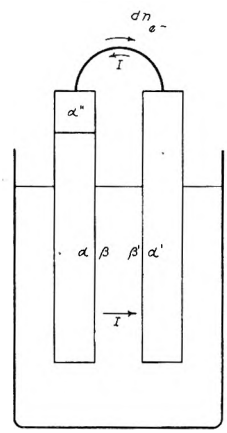

Fig. 1.

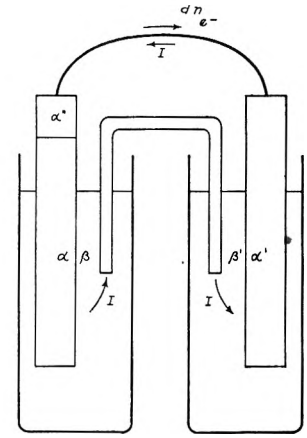

Fig. 2.

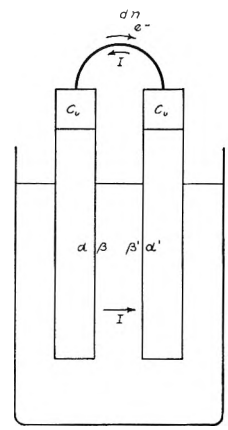

Fig. 3.

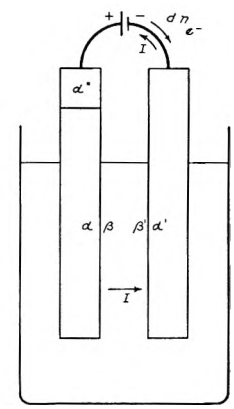

Fig. 4.

All this applies to the case of short-circuit. With performance of electrical work by the system the entropy production is decreased. The uncompensated heat, instead of being given by (12) is now given by (see (11) and (12))

$$dQ' = A\,d\xi - F(\varphi^{\alpha'} - \varphi^{\alpha''})\,dn_{e^-} \geq 0 \qquad (16)$$

or, in terms of the current defined in (2)

$$dQ' = [A/F - (\varphi^{\alpha'} - \varphi^{\alpha''})]I\,dt \geq 0 \qquad (17)$$

Introducing the corresponding value of dQ in (9) we obtain

$$dE = T\,dS - p\,dV - dQ' - F(\varphi^{\alpha'} - \varphi^{\alpha''})dn_{e^-} \qquad (18)$$

or also

$$dE = T\,dS - p\,dV - A\,d\xi \qquad (19)$$

a formula which is identical with that holding in the absence of electrical work.[3] Our reasoning is thus seen to be equivalent to that of Prigogine[4] and of de Groot[5] which is based upon the hypothesis of the validity of Gibbs' fundamental formula for the differential of entropy outside of equilibrium. Introducing the electrical power produced by the system P_{el} we see that the power of irreversibility is given by the formula

$$P = Av - P_{el} \qquad (20)$$

in which v is the reaction velocity $d\xi/dt$ or dn_{e^-}/dt.

Entropy Production Near Electrochemical Equilibrium and Entropy Production Due to the Joule Effect.—The difference $A - F(\varphi^{\alpha'} - \varphi^{\alpha''})$ being such that its product by the current is positive

can be regarded as the cause of this current and, in the range of small values of this difference, the current will be correspondingly small. The two quantities can then be regarded as proportional to each other. Representing the difference $A - F(\varphi^{\alpha'} - \varphi^{\alpha''})$ by $\bar{A}$ we have

$$v = L\bar{A} \text{ or } I = Fv = FL\bar{A} \tag{21}$$

in which L is the phenomenological coefficient[2,5] connecting reaction velocity and affinity. The power of irreversibility and the entropy production are then such that

$$P = T\frac{\mathrm{d_i}S}{\mathrm{d}t} = \frac{1}{F^2L} \times I^2 \tag{22}$$

The quantity $1/F^2L$ can be considered as a generalized resistance r and we have

$$P = rI^2 \tag{23}$$

Let us now consider the case in which the only cause of irreversibility is the internal ohmic resistance of the cell. More precisely the only resistance to be taken into account is that between layers β and β'. We have then

$$\varphi^{\beta} - \varphi^{\beta'} = RI \text{ and } \varphi^{\alpha'} - \varphi^{\alpha''} = \frac{A}{F} - RI \tag{24}$$

and

$$P = T\frac{\mathrm{d_i}S}{\mathrm{d}t} = RI^2 \tag{25}$$

The net amount of heat received during the time $\mathrm{d}t$ is

$$\mathrm{d}Q = T\,\mathrm{d}S - RI^2\,\mathrm{d}t \tag{26}$$

while the uncompensated heat is

$$\mathrm{d}Q' = RI^2\,\mathrm{d}t \tag{27}$$

Decomposition of a Cell into Pairs of Phases in Contact Case of Reversible Electrodes.—On the basis of formulas (24) we have

$$(\varphi^{\alpha'} - \varphi^{\beta'}) + (\varphi^{\beta} - \varphi^{\alpha}) + (\varphi^{\alpha} - \varphi^{\alpha''}) = A/F \tag{28}$$

when the only cause of irreversibility is the Joule effect. Decomposing A into a sum of three terms corresponding to the three processes (3), (4) and (5) and introducing the chemical potentials or sums of chemical potentials for the X, X^-, Y, Y^- species and for the electrons, we find

$$\varphi^{\alpha'} - \varphi^{\beta'} = \frac{A_c}{F} = \frac{\mu_Y + \mu_{e^-}^{\alpha'} - \mu_{Y^-}}{F} \tag{29}$$

$$\varphi^{\beta} - \varphi^{\alpha} = \frac{A_a}{F} = \frac{\mu_X - \mu_{X^-} - \mu_{e^-}^{\alpha}}{F} \tag{30}$$

$$\varphi^{\alpha} - \varphi^{\alpha''} = \frac{A_e}{F} = \frac{\mu_{e^-}^{\alpha} - \mu_{e^-}^{\alpha''}}{F} \tag{31}$$

These equations are the equilibrium conditions for the corresponding processes. Let us introduce the electrochemical potentials by adding to each chemical potential the product $z_iF\varphi$ corresponding to the molar charge z_iF of reactant or product i and the electrical potential of the phase where this species i is reacting or produced. Let

$$\tilde{\mu}_i = \mu_i + z_iF\varphi \tag{32}$$

One easily finds that the equilibrium conditions (29) to (31) can then be written

$$\tilde{A}_c = \tilde{\mu}_Y + \tilde{\mu}_{e^-}^{\alpha'} - \tilde{\mu}_{Y^-} = 0 \tag{33}$$

$$\tilde{A}_a = \tilde{\mu}_{X^-} - \tilde{\mu}_X - \tilde{\mu}_{e^-}^{\alpha} = 0 \tag{34}$$

$$\tilde{A}_e = \tilde{\mu}_{e^-}^{\alpha} - \tilde{\mu}_{e^-}^{\alpha''} = 0 \tag{35}$$

in which $\tilde{A}_c$, $\tilde{A}_a$ and $\tilde{A}_e$ are the electrochemical affinities of the three processes, $\tilde{\mu}_{X^-}$, etc., single electrochemical potentials or sums of electrochemical potentials. Intermetallic contacts are known to be unpolarizable and therefore equation (35) will always hold. On the other hand the electrochemical affinities of the cathodic and anodic processes will be different from zero whenever there is polarization.

Causes of Irreversibility Other than the Joule Effect–Polarization—Overvoltages.—When the electrodes are polarized the power of irreversibility includes, besides the RI^2 of formula (25), a term P_π which we shall call *power of polarization* and we have

$$P = \left[\frac{A_c + A_a + A_e}{F} - (\varphi^{\alpha'} - \varphi^{\alpha''})\right] I = RI^2 + P_\pi \tag{36}$$

From (24) and (31) we deduce

$$\left[\frac{A_c + A_a}{F} - (\varphi^{\alpha'} - \varphi^{\beta'}) - (\varphi^{\beta} - \varphi^{\alpha})\right] I = P_\pi \geq 0 \tag{37}$$

or, introducing separate cathodic and anodic powers of polarization

$$\varphi^{\alpha'} - \varphi^{\beta'} = \frac{A_c}{F} - \frac{P_{\pi c}}{I} \tag{38}$$

$$\varphi^{\beta} - \varphi^{\alpha} = \frac{A_a}{F} - \frac{P_{\pi a}}{I} \tag{39}$$

The ratios A_c/F and A_a/F also appear in formulas (29) and (30) which show them to be equal to the reversible values of the corresponding potential differences. Introducing again the electrochemical affinities one finds that formulas (38) and (39) can be written

$$\frac{P_{\pi c}}{I} = \frac{\tilde{A}_c}{F} = (\varphi^{\beta'} - \varphi^{\alpha'}) - (\varphi^{\beta'} - \varphi^{\alpha'})_{rev} = \eta_c > 0 \tag{40}$$

$$\frac{P_{\pi a}}{I} = \frac{\tilde{A}_a}{F} = (\varphi^{\alpha} - \varphi^{\beta}) - (\varphi^{\alpha} - \varphi^{\beta})_{rev} = \eta_a > 0 \tag{41}$$

in which the familiar *overvoltages* η_c and η_a are related with the thermodynamic concepts of power of polarization and electrochemical affinity.

Single Electrodes—Anodic and Cathodic Currents—Relative Electrical Potential Differences.—The overvoltages defined in (40) and (41) are necessarily positive because thermodynamics requires the corresponding powers of polarization or uncompensated heats or entropy productions to be positive. It is, however, convenient, whenever one studies a single electrode whose operating potential difference from metal to solution is measured by means of the method of the Haber–Luggin capillary, *i.e.*, relatively to a standard reference electrode, to give a sign to the overvoltage and to the corresponding current. Calling ϵ the metal and δ the solution one would always write, whether the electrode functions as anode or cathode

$$\eta_\epsilon = (\varphi^{\epsilon} - \varphi^{\delta}) - (\varphi^{\epsilon} - \varphi^{\delta})_{rev} \tag{42}$$

or

$$\eta_\epsilon = E_\epsilon' - E_\epsilon \tag{43}$$

in which E_ϵ' designates the relative potential difference under current and E_ϵ the reversible values of this relative difference. Both E_ϵ' and E_ϵ are so-called "reduction potentials." If one were to prefer to use "oxidation potentials" E_δ' and E_δ one would write

$$\eta_\epsilon = E_\delta - E_\delta' \tag{44}$$

with

$$E_\delta = -E_\epsilon \text{ and } E_\delta' = -E_\epsilon' \tag{45}$$

We have discussed elsewhere[11] the problem of nomenclature and conventions for these potentials. It appears preferable always to use potential differences from electrode to solution and to speak of reduction or of oxidation potentials according to whether the particular reaction under consideration occurs as a reduction or as an oxidation.

Since the second law requires that the power of polarization be positive we have

$$P_{\pi\epsilon} = \eta_\epsilon I_\epsilon \geq 0 \tag{46}$$

In the case of an anodic reaction both η_ϵ and I_ϵ are positive,

(11) P. Van Rysselberghe, ref. 6, 1951, see pp. 315–316; also, ref. 6, 1952, see pp. 409–415.

in the case of a cathodic reaction they are both negative. Introducing E_ϵ' and E_ϵ in (46) we obtain Pourbaix's formula[6]

$$(E_\epsilon' - E_\epsilon)I_\epsilon \geq 0 \qquad (47)$$

Plots of E_ϵ' against I_ϵ are *polarization curves*. It is particularly convenient to use the following system of coördinates: E_ϵ' is plotted vertically with the nobility, measured by increasing E_ϵ' values, augmenting upwards; anodic currents are plotted horizontally toward the right and cathodic currents horizontally toward the left.

Simultaneous Half-reactions at the Same Electrode.—So far we have considered the case of a single half-reaction occurring in the anodic or in the cathodic direction at the electrode ϵ or at each of the electrodes α and α' of the cells represented on Figs. 1 to 4. If several half-reactions

$$X_\rho^- = X_\rho + e^- \quad (\rho = 1, 2, \ldots) \qquad (48)$$

occur simultaneously at the same electrode (all in the same direction or some in the anodic direction and the others in the cathodic direction) the net current carried by the electrode will be

$$I_\epsilon = F\frac{dn_{e^-}}{dt} = F\Sigma\frac{d\xi_\rho}{dt} \qquad (49)$$

The power of polarization is now given by

$$P_{\pi\epsilon} = \Sigma\eta_{\rho\epsilon}I_{\rho\epsilon} = E_\epsilon'I_\epsilon - \Sigma E_{\rho\epsilon}I_{\rho\epsilon} \geq 0 \qquad (50)$$

in which $\eta_{\rho\epsilon}$ is the overvoltage of reaction ρ, $I_{\rho\epsilon}$ the partial current of that reaction, E_ϵ' the common reaction potential difference for all reactions and $E_{\rho\epsilon}$ the reversible potential difference of reaction ρ. Interesting developments into which we shall not enter here involve the introduction of mixed overvoltages for the various anodic and cathodic reactions, of average reversible potential differences, etc. Let us consider only the simple case of one anodic and one cathodic reaction. Formula (50) becomes then

$$P_{\pi\epsilon} = E_\epsilon'I_\epsilon - (E_aI_a + E_cI_c) \qquad (51)$$

with

$$I_\epsilon = I_a + I_c \qquad (52)$$

I_a being positive and I_c negative.

In the particular case of an isolated electrode carrying no net current we have $I_c = -I_a$ and hence

$$P_{\pi\epsilon} = (E_c - E_a)I_a \qquad (53)$$

The difference $E_c - E_a$ is equal to the affinity of the resultant purely chemical reaction divided by F and we are thus led back to the non-electrochemical power of irreversibility

$$P = \frac{A}{F} \times I_a = Av \geq 0 \qquad (54)$$

Further considerations of this type can be shown to bring a great deal of order in the electrochemical theory of corrosion phenomena.

The Neighborhood of Equilibrium—Use of Onsager's Reciprocal Relations.—Although the introduction in this thermodynamic theory of kinetic information such as that provided by Tafel's equation connecting overvoltage and current density is of very great interest we shall limit ourselves here to the neighborhood of equilibrium, *i.e.*, to the range of validity of the linear relations connecting reaction velocities and affinities. Let us consider two half-reactions 1 and 2 occurring in the same direction or in opposite directions at the same electrode. Their velocities will be linear functions of both electrochemical affinities provided the reversible potential differences of these reactions are sufficiently close to each other to allow the system to function in the close neighborhood of equilibrium. We then have

$$v_1 = L_1\tilde{A}_1 + L_{12}\tilde{A}_2 \qquad (55)$$

$$v_2 = L_{12}\tilde{A}_1 + L_2\tilde{A}_2 \qquad (56)$$

or, in terms of currents and overvoltages

$$I_1 = F^2(L_1\eta_1 + L_{12}\eta_2) \qquad (57)$$

$$I_2 = F^2(L_{12}\eta_1 + L_2\eta_2) \qquad (58)$$

formulas in which the Onsager reciprocal relation $L_{12} = L_{21}$ has been taken into account. The power of polarization is then

$$P_{\pi\epsilon} = F^2[L_1(E' - E_1)^2 + L_2(E' - E_2)^2 + 2L_{12}(E' - E_1)(E' - E_2)] \qquad (59)$$

or, in terms of the total current I

$$P_{\pi\epsilon} = \frac{I^2}{F^2(L_1 + L_2 + 2L_{12})} + F^2\frac{L_1L_2 - L_{12}^2}{L_1 + L_2 + 2L_{12}}(E_1 - E_2)^2 \qquad (60)$$

The existence of drag coefficients L_{12} different from zero would mean that polarization curves of single half-reactions are not additive when these reactions occur simultaneously at the same electrode. This additivity is often assumed in spite of considerable experimental evidence against its validity. Not only is the mutual influence corresponding to the L_{12} coefficients a theoretical possibility but its magnitude and direction might be such as to make one of the reactions occur in its otherwise non-spontaneous direction. In other words the *coupling* of an electrochemical half-reaction by one or several others is possible and should be looked for experimentally. Its existence could have consequences of very great practical interest.

States of Minimum Entropy Production.—A single electrode carrying a current I at a certain relative potential difference E' constitutes an open system in which several electrochemical affinities could be kept constant by means of suitable additions or removals of the various reactant and product species. Let us still consider the case of two simultaneous reactions and let us maintain the electrochemical affinity of reaction 1 constant by maintaining E' constant and the chemical affinity A_1 constant. There will then be a possible state of the system for which the power of polarization or the entropy production will be a minimum. On the basis of Prigogine's theorem[12] on steady states of minimum entropy production, which we are here extending to electrochemical systems, the reasoning is as follows: we differentiate $P_{\pi\epsilon}$ given by formula (59) with respect to E_2 at E' and $E_1 = A_1/F$ constant and obtain

$$\left(\frac{\partial P_{\pi\epsilon}}{\partial E_2}\right)_{E',E_1} = -2F^2[L_2(E' - E_2) + L_{12}(E' - E_1)] \qquad (61)$$

Setting this derivative equal to zero we see that $P_{\pi\epsilon}$ will be an extremum when

$$E_2 = \frac{E'(L_2 + L_{12}) + E_1L_{12}}{L_2} \qquad (62)$$

This extremum is a minimum since

$$\left(\frac{\partial^2 P_{\pi\epsilon}}{\partial E_2^2}\right)_{E',E_1} = 2F^2L_2 > 0 \qquad (63)$$

The value of the minimum is

$$P_{\pi\epsilon\min} = F^2\left(L_1 - \frac{L_{12}^2}{L_2}\right)(E' - E_1)^2 \qquad (64)$$

For this particular state of the system the currents are

$$I_1 = F^2\left(L_1 - \frac{L_{12}^2}{L_2}\right)(E' - E_1) \qquad I_2 = 0 \qquad (65)$$

During the transition of the system from its original state to that of minimum entropy production the electrochemical affinity of reaction 1 remains constant. That of reaction 2, however, will vary until the value

$$\tilde{A}_2 = F(E' - E_2) = -F\frac{L_{12}}{L_2}(E' - E_1) \qquad (66)$$

is reached.

Prigogine's theorem is easily generalized to the case of several simultaneous reactions. If, out of a total of n reactions, the affinities (or here electrochemical affinities) of k reactions, are kept constant the system may reach in the course of time a state of minimum entropy production in which the velocities of the n-k reactions which are not controlled become equal to zero (see de Groot[13]). These stationary states of minimum entropy production can be shown to follow a principle analogous to that of Le Chatelier concerning the "moderation" of disturbances.

It would be highly interesting to explore experimentally the possible applications of these theoretical considerations in the field of electrochemistry. In corrosion, for instance, the establishment of stationary states of minimum entropy

(12) I. Prigogine, Ref. 3, pp. 55–59.

(13) S. R. de Groot, ref. 4, pp. 195–207.

production might lead to the blocking of destructive reactions through the device of maintaining other reactions at constant electrochemical affinities. It seems likely that new light could thus be thrown on the problem of corrosion inhibition. For example, the electrochemical mechanism which we have proposed with Pourbaix[14] for the inhibition of the corrosion of iron by nitrites, chromates or even oxygen when present in sufficient amount lends itself to interesting further study on the basis of irreversible thermodynamics. Let us note in this connection that, through the approximate procedure of linearization of polarization curves, the practical range of usefulness of the above considerations can be considerably enlarged. We hope to return to this and other topics of theoretical and applied electrochemical thermodynamics in later communications.

(14) M. Pourbaix and P. Van Rysselberghe, *Corrosion*, **6**, 313 (1950).

ANODIC POLARIZATION OF PASSIVE AND NON-PASSIVE CHROMIUM–IRON ALLOYS

BY HERBERT H. UHLIG AND GLENN E. WOODSIDE

Corrosion Laboratory, Department of Metallurgy, Massachusetts Institute of Technology, Cambridge, Massachusetts

Received November 26, 1952

Anodic polarization data for 0–16.7% Cr–Fe alloys in 3% Na_2SO_4 are reported. Critical current densities for passivity accompanied by sudden reduction of anodic dissolution and a pronounced noble potential range from 150 ma./cm.^{2} for iron to 0.05 ma./cm.^{2} for 11.6% Cr. At 12% Cr and above, a critical current no longer exists; instead any small polarizing current produces a marked shift of potential in a noble direction. Small corrosion currents, therefore, can equipotentialize the surface and stifle the corrosion process in accord with the electrochemical mechanism of corrosion. Since 12% Cr and above mark the stable passive compositions (stainless steels) in solutions like Na_2SO_4, it appears that the property of so-called passive alloys to equipotentialize themselves is an important characteristic of passivity, and perhaps an essential condition to their remarkable resistance to corrosion. Coulometric measurements show that about 0.014 coulomb/cm.^{2} or less is concerned with the passivation process for the 9.2–16.7% Cr alloys and probably for other compositions as well. This corresponds at most to a few monolayers of substance on the passive surface. Thick oxide films, therefore, cannot possibly be the primary cause of passivity.

When iron is polarized as anode at moderate current densities in dilute sodium sulfate or sulfuric acid, the major reaction is $Fe \rightarrow Fe^{++} + 2e$. As the current is increased, a critical value is reached at which the potential suddenly changes to a value more noble by about 2 v., and the anodic reaction changes to

$$2OH^- \longrightarrow {}^1/_2O_2 + H_2O + 2e$$

accompanied by the reaction

$$Fe \longrightarrow Fe^{+++} + 3e$$

Iron is said to become passive, both because it assumes a more noble potential and because oxygen evolving at its surface resembles the behavior of a noble metal electrode. Also, the dissolution rate is appreciably less than that of an active iron anode.

Soon after the polarizing current is stopped, the electrode again assumes the active state. If the current is gradually decreased, the active state is achieved at a current density somewhat lower than is necessary to achieve the passive state when applying progressively higher currents.

Conditions that apply for achieving anodic passivity of iron–chromium alloys substituted for iron have not yet been studied. Information of this kind should be of value to a better understanding of passivity, particularly since passivity is established in a more stable form when the chromium content reaches 12% or more. This composition establishes the basis for the modern stainless steels.

Experimental Arrangement

Polarization data for the Cr–Fe alloys were obtained using the cell shown in Fig. 1. This was placed in an air thermostat maintained at 25 ± 1°. Two circular platinum cathodes 3.1 cm. in diameter are located 1 cm. from either side of the alloy anode. The latter measures approximately 1 cm. square by 2 mm. thick. The electrolyte is 3% Na_2SO_4. A tubulus, sealed at each end with asbestos fibers and filled with the same solution is mounted on one side of the anode close to the metal surface. The opposite end is immersed in a 0.1 *N* KCl solution into which an Ag–AgCl electrode also in 0.1 *N* KCl is immersed.

Potentials were measured using a vacuum tube potentiometer. No correction was made for liquid junction potentials, since these were assumed to be approximately constant throughout the measurements and, in any case, were small. Current was supplied usually by a high-voltage B battery through a high resistance, thereby maintaining constant current, actual values of which were read using a precision (± ¼%) milliammeter and also, for very small currents, by the potential drop across a precision 100-ohm resistance.

For many measurements, the sodium sulfate solution was first freed of chlorides by adding silver sulfate and removing excess silver by electrolysis for several hours between platinum electrodes. Contaminating heavy metals were removed simultaneously. The *p*H was then adjusted to 7 by adding sodium hydroxide. This purification procedure did not appear to be critical, since values of potentials were the same within the experimental error whether or not preelectrolysis was carried out.

Electrode materials consisted of electrolytic iron, and of laboratory melts of chromium–iron alloys. Alloys collected from three sources gave consistent results indicating that small differences in impurities are not important. Thermal history, however, was felt to be a significant factor, and, hence, all the alloys were heated in helium at 1000° and water quenched. Analyses are given in Table I.

Before measurements were made, the solutions were deaerated about one hour by bubbling nitrogen through them. Nitrogen was previously purified by passing it over copper turnings maintained at 400°. The gas entered the cell through a sintered glass disc providing a fine dispersion of gas bubbles, but during measurements the gas was bypassed through a glass tube at the side of the cell, so that bubbles did not impinge on the anode. This was necessary because stirring had some effect on the critical current for passivity, greater current being necessary the higher the stirring rate.

Preparation of Electrodes and Procedure.—The anode was attached to a nickel wire by spot-welding and then sealed into a glass tube using de Khotinsky Cement to cover the exposed wire and the spot-welded area. The electrode

TABLE I

ANALYSES OF ALLOYS

Alloys A, D, E, J were supplied by courtesy of the Electro Metallurgical Corporation. Alloys B, F, G, H, I were prepared in this Laboratory from ferrochrome and low metalloid iron with additions of manganese and silicon. Alloy C was supplied by courtesy of Armco Steel Corporation. All alloys were forged, followed by rolling or swaging, then water quenched from 1000°.

	Cr, %	C, %	Mn, %	Si, %
A	2.84	0.007		
B	3.54	.03	0.22	0.003
C	5.43	.099		
D	6.93	.016		
E	8.32	.018		
F	9.22	.09	0.34	.18
G	11.59	.07	.34	.17
H	12.22	.07	.30	.19
I	13.84	.06	.34	.25
J	16.70	.007		

was next pickled for a minute or less in hot 15 vol. % HNO_3–5% vol. HF, washed successively in three vessels of nitrogen-saturated water and quickly placed in the cell. The nitrogen was bubbled through the Na_2SO_4 solution for an additional 30 minutes in order to supplement the deaeration procedure carried out previously. Within this time, the open-circuit potential of the anode achieved a reasonably steady value. A small current was then impressed below the critical value for passivity until a constant measured potential was achieved, the corresponding potential was recorded and the current stopped. After the original open-circuit potential was regained, the measurement was repeated using a higher current. Eventually a current was reached at which the potential became considerably more noble and remained noble. This was designated as the critical minimum current for passivity.

A preconditioning treatment of the anode using a small current below the critical appeared necessary for reproducibility of measurements, perhaps in order to clean off the metal surface of adsorbed gas, ions, oxide, etc.; otherwise observed critical currents were erratically lower. The preconditioning usually gave an open-circuit potential slightly more active than before, confirming that the anode was cleaned by this treatment. Cathodic treatment of the electrode was less satisfactory, probably because of hydrogen entering the metal lattice where it could later escape and affect anodic polarization.

Reproducibility was no better than the scatter obtained in usual measurements of passivity. The critical current was established to ± 3% for iron, but could be determined with progressively less precision as chromium content of the alloy increased. One factor entering the larger percentage scatter for higher chromium alloys was the very small current necessary for passivity.

Electrodes polarized at currents below the critical quickly achieved the original open circuit value when the polarizing current was cut off, or reached a few hundredths volt more active, as mentioned previously. When the electrodes were polarized above the critical value for passivity, particularly for higher chromium–iron alloys, the original potentials were not regained, but instead some value more noble than the original. The critical currents on immediate repetition of the polarizing experiments were then always less. It was necessary to re-pickle the alloys in order to reproduce the original potentials and currents, especially for alloys of greater than 5% chromium.

Results

A plot of potential *versus* logarithm of polarizing current for iron and all the alloys is given in Fig. 2. Open-circuit potentials of the alloys are placed for convenience on the ordinate corresponding to 0.0001 ma./cm.^{2}. These potentials are slightly more noble as the chromium content increases. No particular pattern seems to be followed by polarizing potentials below the critical current density, but above the critical value, data fall on a typical Tafel overvoltage plot corresponding to oxygen evolution. The

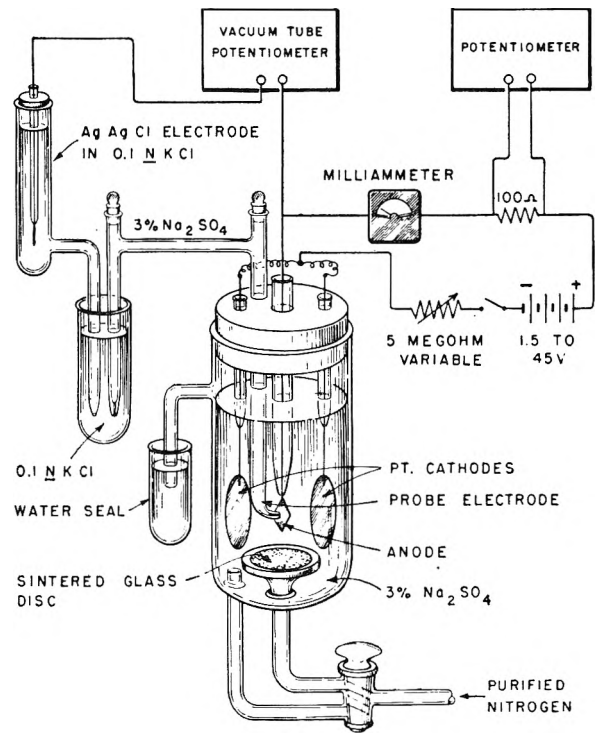

Fig. 1.—Sketch of polarization cell and auxiliary equipment.

equation for excess potential over the reversible oxygen potential, or in other words the Tafel equation for oxygen overvoltage η is given by

$$\eta = 0.83 + 0.10 \log i$$

where i is in milliamperes/cm.^{2}.

It is notable that a critical current density is no longer detected for alloys above 11.6% chromium. With the 12.2% chromium alloy or above, any applied current produces a potential more noble than before and as the current is increased the potentials become progressively more noble. At no time is there a sudden break in potential as is observed for the 11.6% or lower chromium alloys. This difference of behavior was carefully checked by repeated measurements on alloys containing 9 to 14% chromium.

These results imply that any small polarizing current will sensitively shift potentials of alloys containing more than 12% chromium in a noble direction, but for alloys of less than 12% chromium, appreciably more noble potentials are achieved only at current densities equal to or greater than the critical. However, critical current densities, when they exist, correspond to a substantial corrosion rate, so that such currents are not reached naturally in Na_2SO_4 solution. At 0.1 ma./cm.^{2}, for example, which is the critical current density for 9.2% Cr alloys, the corresponding corrosion rate is 250 m.d.d. (milligrams/sq. decimeter/day) or 0.045 i.p.y. (inches penetration/year), a value which exceeds the normal corrosion rate of iron (approximately 25–50 m.d.d.).

The relation of critical current density for passivity to chromium content is given in Fig. 3. Obviously, as the chromium content approaches 12%, the current necessary for passivity falls to very small values. Any corrosion process, therefore, accompanied by electric current in the neighborhood of 0.05 ma./cm.^{2} is expected to passivate the 11.6% chromium–iron alloy, and, hence, equivalent corrosion rates (in Na_2SO_4) are never greater than this value. But alloys above 12% chromium become progressively more noble for much smaller currents. It is obvious, therefore, that any corrosion process will quickly tend to equipotentialize the 12% Cr alloy surface, a tendency which in itself stifles the corrosion process in accord with the well known electrochemical theory of corrosion. Moreover, these alloys also tend to assume a noble potential in part because of the equipotentialization process.

The property of passive alloys to equipotentialize themselves through anodic polarization at low current densities appears to be an important characteristic of passivity and

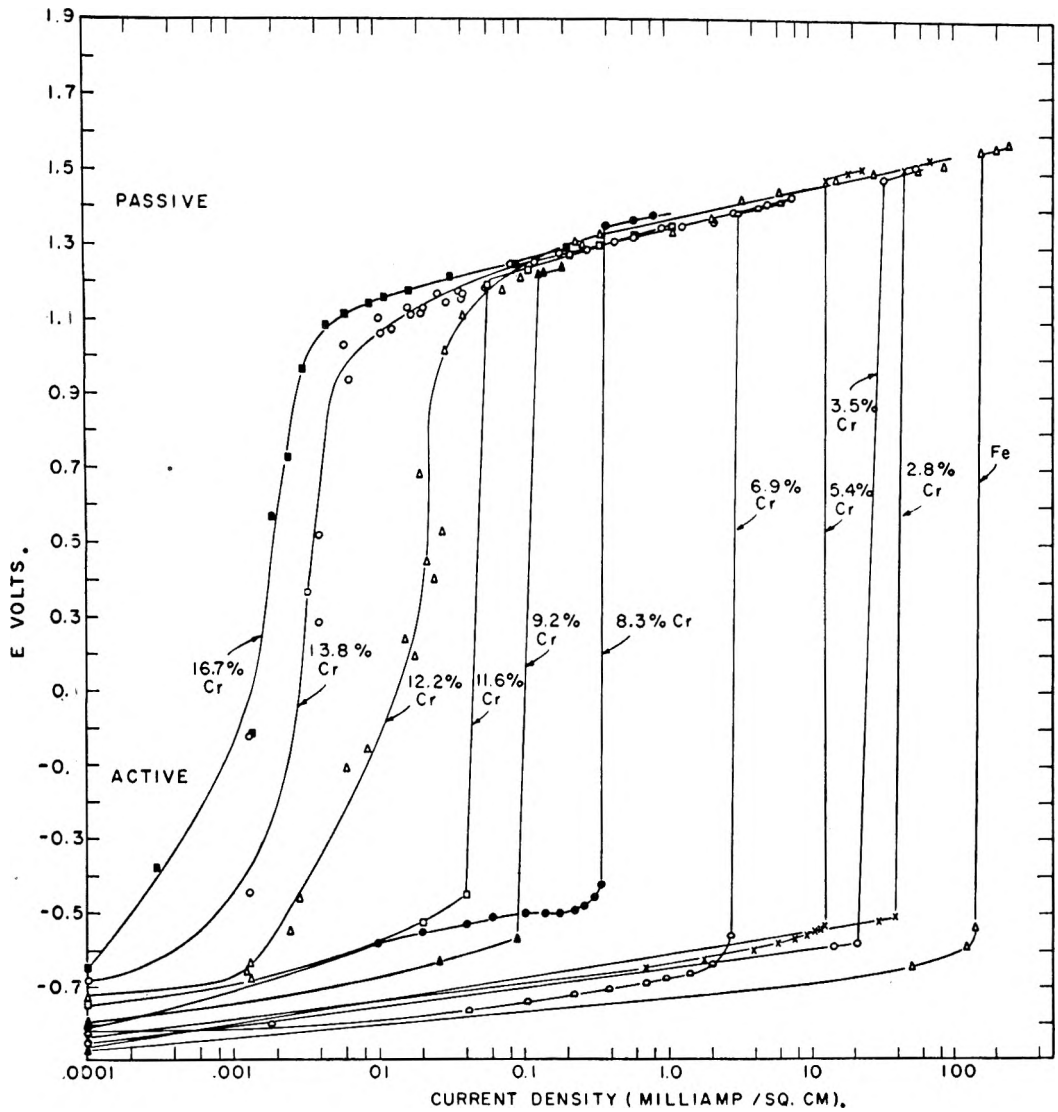

Fig. 2.—Anodic polarization characteristics of Cr–Fe alloys in 3% Na_2SO_4: potentials *vs.* Ag–AgCl in 0.1 *N* KCl, 25°.

perhaps an essential condition to their remarkable resistance to corrosion. The relation of passivity to polarization has been discussed previously by Mears and Brown.[1,2]

Amount of Substance on the Passive Alloy Surface.—Some measure of the number of equivalents concerned with change from active to passive state was obtained by coulometry. Preliminary data were obtained by recording the time, using a stopwatch, for the potential to progress from open-circuit values to an arbitrary value in the passive range. This could not be accomplished so simply for iron or the low chromium alloys because critical current densities for passivity are high and the corresponding times for passivation very brief. However, for alloys of greater than 9% chromium, the currents are small and, hence, several minutes are required to achieve passivity. From time–current measurements, the number of coulombs accompanying the passivation process can be calculated.

Information of this kind is assembled in Table II. In cases where the potentials did not reach 1.2 v., which was taken as the arbitrary passive potential, the time was extrapolated to this value of potential. The uncertainty of extrapolation was apparently less than the uncertainty of true surface area of the electrode, which may well have varied by a factor of two from a surface pickled once to another pickled several times. In addition, the values of coulombs/cm.^{2} are high to the extent that the anode reactions continue throughout the time

TABLE II

MEASURE OF EQUIVALENTS NECESSARY TO PASSIVATE CHROMIUM-IRON ALLOYS

Cr, %	Ma./cm.^{2}	Time to reach 1.2 v. *vs.* Ag–AgCl in 0.1 *N* KCl (sec)	Coulombs/cm.^{2}
9.2	0.18	70	0.013
	.18	57	.010
11.6	.18	125	.023
12.2	.18	100	.018
	.012	1350[a]	.016
13.8	.18	60	.011
	.006	1700[a]	.010
16.7	.007	1920[a]	.013

[a] Extrapolated.

(1) R. B. Mears *Trans. Electrochem. Soc.*, **95**, 1 (1949).

(2) R. B. Mears and R. H. Brown, *J. Electrochem. Soc.*, **97**, 75 (1950).

of measurement; hence, some current goes toward reactions other than those necessary to passivity. The data probably deserve repetition, therefore, at such time as the true current density can be determined parallel with true surface area measurements for each electrode and with corrections for extraneous reactions.

The average value of coulombs/cm.^{2} required for passivation of alloys listed in Table II is 0.014. This value can be compared with 0.08 coulomb/cm.^{2} necessary to passivate iron in 2 *N* NaOH at a current density of 0.01 ma./cm.^{2}, as reported by Kabanov, Burstein and Frumkin.[3] The passivation process in NaOH, of course, need not be the same.

Within the present experimental error of such determinations, there is no difference in the equivalents of substance necessary to passivate alloys below as compared with alloys above 12% chromium. The break in the potential *versus* current density curve for low Cr alloys and its absence for greater than 12% Cr alloys, therefore, is not related to any large difference in the equivalents of anodic reaction accompanying passivation.

The value 0.014 coulomb/cm.^{2} corresponds to 1.2×10^{-6} gram of oxygen/cm.^{2} of apparent alloy surface. A monolayer of close packed oxygen atoms corresponds to 0.15×10^{-6} g./cm.^{2} true surface, so that a roughness factor of 8 would be required if one assumes an adsorbed monolayer of oxygen atoms as primary cause of passivity. In this connection, it was recently determined that the amount of oxygen adsorbed on passive 18-8 stainless steel previously pickled corresponds to about 1.8 atomic oxygen layers (or 1 atom plus 1 molecule layer equivalent in either instance to 0.27×10^{-6} gram oxygen/cm.^{2} true surface),[4] so that the roughness factor assuming this situation need be only 4.5.

It can be concluded, therefore, that the amounts of oxygen required to anodically passivate chromium–iron alloys in sodium sulfate are not large, and,

(3) B. Kabanov, R. Burstein and A. Frumkin, *Discussions of the Faraday Soc.*, 259 (1947).

(4) S. S. Lord, Jr., and H. H. Uhlig, submitted to *J. Electrochem. Soc.*

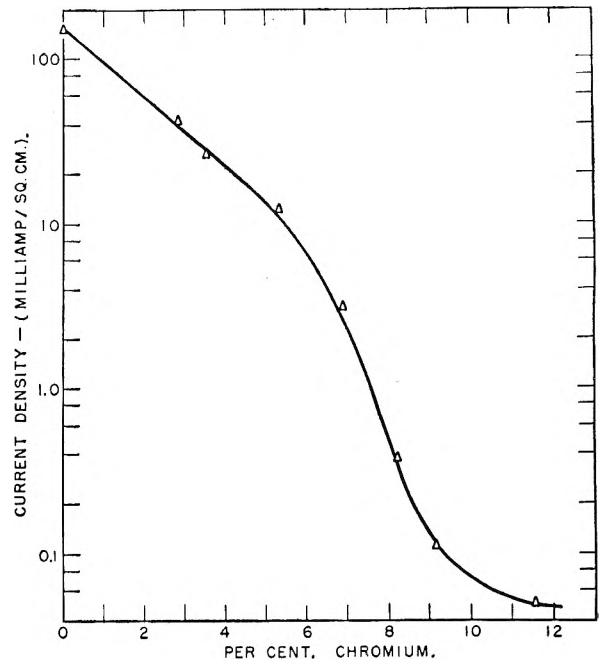

Fig. 3.—Critical current densities for passivity of the Cr–Fe alloys in 3% Na_2SO_4, 25°.

hence, thick oxide films cannot possibly be the primary cause of passivity. This is true of alloys just below as well as above 12% Cr. The view previously expressed at various times[5] that passivity is primarily accompanied by chemisorbed films in the order of monolayers of atoms or molecules is consistent with the presently reported facts.

Acknowledgment.—This research was supported by the Shell Fellowship Committee of the Shell Companies in the U. S. to whom the authors express their appreciation.

(5) I. Langmuir, *Trans. Electrochem. Soc.*, **29**, 260 (1916); *J. Chem. Soc., (London)* 518 (1940); H. H. Uhlig, *Trans. A.I.M.E.*, **175**, 710 (1948); *Chem. Eng. News*, **24**, 3154 (1946); H. H. Uhlig, editor, "Corrosion Handbook," John Wiley and Sons, Inc., New York, N. Y., 1948, pp. 24-33; H. H. Uhlig, *J. Electrochem. Soc.*, **97**, 215C (1950); "Metal Interfaces," *Am. Soc. Metals*, 312 (1952).

THE ADSORPTION OF IONS FROM BUFFER SOLUTIONS[1] BY SILICA, ALUMINA AND SILICA–ALUMINA GELS

BY C. J. PLANK

Socony-Vacuum Laboratories, A Division of Socony-Vacuum Oil Co., Inc., Research and Development Department, Paulsboro, New Jersey

Received October 20, 1951

The acidity of silica–alumina gel cracking catalysts apparently results from a residual ionic surface structure. Such a structure should possess considerably greater cation exchange capacity than silica or alumina gels, which are not good cracking catalysts. To compare the ionic adsorption properties of these three types of gels, measurements have been made with solutions of ammonium salts. The three gels were found to differ very widely in their adsorption characteristics. Primarily silica and silica–alumina gels are cation adsorbers. Alumina gel, on the other hand, is primarily an anion adsorber with some attendant ability to adsorb cations. Silica gel adsorbs ammonium ions from ammonium acetate and $(NH_4)_2HPO_4$ solutions, giving a slightly negative adsorption of the anions. It does not adsorb cations selectively from ammonium sulfate solutions. Alumina gel shows both anion and cation adsorption. The former is apparently due to a chemical exchange with –OH groups in the gel structure rather than a true anion exchange. The cation adsorption then is largely associated with the anion uptake, as required by electro-neutrality considerations. Silica–alumina gel exhibits the properties of a polybasic acid in which the acid sites vary over a wide pK_a range. It adsorbs only NH_4^+ ions from acetate and sulfate solutions. With ammonium sulfate solutions the equilibrium distribution of NH_4^+ and H^+ between gel and solution is similar to that shown by a true strong acid exchanger. However, with both acetate and sulfate solutions the total adsorption capacity of silica–alumina gel increases rapidly with increasing ionic strength of the solution, showing increased ionization of the weak acid sites on the catalyst. While the adsorption of NH_4^+ ions from ammonium acetate solutions by silica gel does not change much as the temperature is increased from 15 to 150°, the adsorption by silica–alumina gel quadruples within that temperature range. Silica–alumina gel adsorbs both NH_4^+ and $HPO_4^=$ ions from $(NH_4)_2HPO_4$ solutions. Apparently the acid centers are responsible for much of the NH_4^+ adsorption with the remainder, and all of the $HPO_4^=$ adsorption, being due to a chemical exchange of the $HPO_4^=$ for –OH groups attached structurally to the Al atoms.

The importance of synthetic silica–alumina gels as cracking catalysts has occasioned a considerable amount of research into the physical and chemical properties of these gels. One of the significant facts is that neither pure silica gel nor pure alumina gel is at all comparable to silica–alumina gel in cracking activity. In fact, the former is essentially inactive, while alumina is only slightly active. It is generally believed at present[2–4] that silica-alumina gel is acidic in nature, and that it is this acidic character which is responsible for the catalytic cracking activity of the gel.

Of course, it has long been known that synthetic alumino–silicate gels made at high *p*H have excellent zeolitic properties, if dried at temperatures no higher than about 200°. Thus, it is clear that as the sodium gel the gel structure has a very pronounced anionic character. It has been shown by the author in previous work[5,6] that this anionic character of silica–alumina hydrogel persists even when made at *p*H 7 or below and also after cation exchange with Al^{+++}, NH_4^+ or even H^+. Silica gel, of course, shows no such ionic character.

If silica–alumina gels do owe their cracking activity to surface acidity, they must preserve their ionic character, to some extent, even when calcined at high temperatures. Commercial catalysts are calcined at temperatures as high as 760° for several hours. Some early experiments made by the author, using *p*H color indicators along the lines indicated by Hartley and Roe,[7] showed that silica–alumina gels reacted to these indicators like very strong acids. Silica gel in similar experiments showed only a weakly acidic character. While silica–alumina adsorbed the acid form of indicators with pK as low as 1–2 (*e.g.*, metanil yellow), silica gel adsorbed the acid form only of those with pK above the range 3–4 (*e.g.*, methyl orange). It appeared, however, that quantitative data would be extremely difficult to obtain by this technique, so that another method was chosen to secure information as to quantitative differences among the three types of gels.

It was decided to use the adsorption of ions from ammonium salt solutions as a measure of the relative ionic character of the gels. The buffer solutions were chosen in order that the *p*H might be held within the limits where gel solubility is negligible. The greatest part of the work was done with ammonium acetate solutions since the ionization constants for ammonium hydroxide and acetic acid are so well known that *p*H measurements on the solutions serve as good checks on the ion analysis. The closeness of the checks was excellent as indicated in Table IV.

Experimental

A. Gels. Silica Gel.—Commercial silica gel of the desiccant type (*i.e.*, prepared at $pH < 0$) was used. Since this gel had been prepared under exceedingly acid conditions it was washed for weeks with redistilled water until the *p*H of the water showed no change after overnight contact with the gel. The samples were either dried before the tests to 125° for 16 hours or calcined overnight at 540°. Except where otherwise noted all gels were sized to 6–16 mesh.

Silica–Alumina Gel.—The Socony-Vacuum commercial silica–alumina bead cracking catalyst[8] was chosen as the gel to be tested. This particular sample was taken directly from the commercial drier (about 180°) instead of being tempered (at about 700°) so that the heat treating conditions could be controlled directly. The individual samples were dried at 125° or calcined at 540° before the tests. It was found unnecessary to wash this gel to eliminate excess hydrogen ion, since redistilled water placed on a sample of the gel for 24 hours showed no change in *p*H. However, as an added precaution the gel was washed about 5 times before use.

(1) Presented before the Colloid Division of the American Chemical Society at the Diamond Jubilee Meeting on September 7, 1951.

(2) R. C. Hansford, *Ind. Eng. Chem.*, **39**, 849 (1947).

(3) M. W. Tamele, *Discussions Farad. Soc.*, No. **8**, 270 (1950).

(4) C. L. Thomas, *Ind. Eng. Chem.*, **41**, 2564 (1949).

(5) C. J. Plank, *J. Colloid Sci.*, **2**, 413 (1947).

(6) C. J. Plank and L. C. Drake, *ibid.*, **2**, 399 (1947).

(7) G. S. Hartley and J. W. Roe, *Trans. Faraday Soc.*, **36**, 101 (1940).

(8) M. M. Marisic, U. S. Patent 2,384,217 (1945).

Alumina Gel.—The gel was prepared by making a sol by the Patrick[9] method from aluminum amalgam and acetic acid then gelling the sol with ammonia. The product was washed thoroughly and calcined at 540°.

The physical properties of the gels are shown in Table I.

TABLE I

PHYSICAL PROPERTIES OF THE GEL SAMPLES

Gel	Surface area, m.²/g.	Particle density, g./cc.	Real density, g./cc.	Pore volume, cc./g.	Pore diameter,[a] Å.
Silica-alumina[b]					
Oven dried	559	1.016	2.177	0.525	37
Calcined at 540°	510	1.057	2.318	0.510	40
Alumina					
Calcined at 540°	246	1.194	3.417	0.545	89
Silica					
Oven dried (180°)	698	1.211	2.143	0.359	22
Calcined at 540°	720	1.310	2.264	0.321	17

[a] Calcd. by method of Emmett and DeWitt (*J. Am. Chem. Soc.*, 65, 1253 (1945)). [b] 91% SiO_2–9% Al_2O_3 by wt.

B. Solutions.—All solutions were made directly from commercial reagent grade chemicals. However, in the case of the ammonium acetate solutions it was found that the *p*H obtained (25°) was 6.95, or slightly lower, instead of the desired 7.00 value. Therefore, the *p*H was adjusted to 7.00 by addition of aqueous NH_3 before the final dilution to the desired normality. The *p*H (25°) given by the $(NH_4)_2HPO_4$ solutions was 7.85–7.90 while that given by the ammonium sulfate solutions was 5.70–5.75. Although the normalities of the cation and anion were not exactly in stoichiometric proportions in the case of the phosphate and sulfate solutions, they were so near to equivalence that no adjustment was made and adsorption values were all based on analyzed values for the solution normalities. In the case of these two solutions the *p*H of the equilibrium solution did not serve as a very accurate check on the analyses.

C. Adsorption Experiments.—The technique used was extremely simple. Except where kinetic data were desired (which are not described here) the procedure was as follows.

A 100-ml. portion of the standard solution was pipetted into a 250-ml. erlenmeyer flask, the dried or calcined gel was added and the flask tightly stoppered. The flask was then placed in the water-bath held at 15 ± 0.2° and allowed to stand for 24 hours with occasional shaking. At the end of the 24-hour period, when equilibrium was shown to have been reached, the flask and mixture were shaken thoroughly for about 10 minutes and the gel was quickly filtered off. After warming to 25° the *p*H of the solution was taken (any calculations involving equilibrium *p*H were made using the value at 25°). Analyses of the equilibrium concentrations of the ions in solutions were made on the filtrate.

In the case of ammonium acetate some experiments were made at 85, 150 and 200°, as well as at 15°. For the two highest temperatures an entirely different technique had to be used, of course. For the sake of making direct comparison with the 15° runs, both methods were used at 85°. The method used at 15° was modified for the 85° runs only in that a round bottom flask equipped with a condenser stoppered at the top was used instead of a stoppered erlenmeyer flask.

The high temperature (150° and 200°) runs were made using the apparatus illustrated in Fig. 1. Here the gel sample was sealed in one end of the U-tube (A) and held there by a monel screen (S). The standardized solution was introduced into the tube through side arm (B) while the apparatus was in the position illustrated and the side arm was sealed off short. The U-tube was clamped (C—C) to a circular steel plate whose shaft (D) was activated by a cam in such a way that the tube turned first clockwise then counterclockwise through almost 180°. Thus the solution was stirred by flowing first toward one end then toward the other. Furthermore, since the gel sample did not fill its section of the bulb the gel was also stirred.

(9) W. A. Patrick, U. S. Patent 2,258,099 (1942).

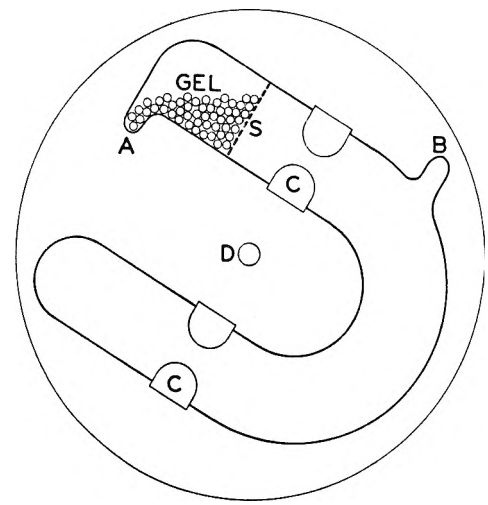

Fig. 1.—Apparatus for adsorption experiments at elevated temperatures: A, entrance for gel; B, entrance for soln.; C, clamps; D, shaft connected to circular plate; S, monel screen (20 mesh).

In these experiments only a 6-hour reaction period was taken to minimize the peptizing effect of the ammonium acetate solution on the gel. A gel of $^{12}/_{16}$ mesh was used so that equilibrium would be achieved more quickly than with the $^{6}/_{16}$ mesh samples usually used at 15°. Smaller mesh material could not be used since the monel screen which contained the gel was 20 mesh and it was found that any smaller size opening prevented free flow of the solution through the screen during the period of oscillation of the U-tube container. At the end of the 6-hour reaction period the U-tube was stopped in the position shown in Fig. 1 so that no excess solution would be in contact with the gel during the cooling period. After cooling the tube was opened at point (B), the solution drained off and filtered and *p*H measurement (25°) and analyses were made on the filtrate.

D. Analytical Methods. NH_4^+ Analysis.—A modified Kjeldahl technique was used for about half of the solutions. Excellent results (±0.5% of the actual value) were obtained by this method so long as the NaOH solution was standardized against the standard HCl solution under the same dilution condition as encountered in the analysis. The last half of the analyses for NH_4^+ were performed by the calcium hypochlorite method as described by Kolthoff and Stenger.[10] Results were comparable by both methods, with the latter being much more rapid. The results appeared to be accurate to at least ±0.5% of the actual concentration.

Anion Analyses.—The $HPO_4^=$ solutions were analyzed by the colorimetric method described by Woods and Mellon[11] which utilized the molybdenum blue reaction.

The $SO_4^=$ was generally determined by the gravimetric method of precipitation as $BaSO_4$.[12] However, during the latter stages of the investigation it was found that a fast accurate method was available utilizing ion exchange resins. This method was used especially in analyzing solutions equilibrated with the alumina gels where considerable adsorption occurred. The procedure is that of Samuelson[13] and is applicable to pure solutions such as were encountered in the present investigation. The solution was passed through a column containing a hydrogen-exchange resin (Dowex-50) wherein the ammonium ion was replaced by H^+ and the eluent was titrated for free H_2SO_4. The accuracy was apparently at least to ±0.5%.

The acetate ion was generally not adsorbed and only spot checks were made during the use of silica gel and silica-alumina gel to corroborate this fact. For these checks a distillation method analogous to the Kjeldahl method

(10) I. M. Kolthoff and V. A. Stenger, *Ind. Eng. Chem., Anal. Ed.*, **7**, 79 (1935).

(11) J. T. Woods and M. G. Mellon, *ibid.*, **13**, 760 (1941).

(12) J. H. Hildebrand and G. E. F. Lundell, "Applied Inorganic Analysis," John Wiley and Sons, Inc., New York, N. Y., 1929, p. 580.

(13) O. Samuelson, *Svensk Kem. Tid.*, **51**, 195 (1939); *C. A.*, **34**, 1271² (1940).

for the NH_4^+ was used. In these cases the solution was heated with H_3PO_4, the acetic acid vapors collected in standard NaOH solution and the mixture back titrated. It was found that 98.5% of the original acetate content was regularly recovered in the experiments utilizing the siliceous gels, as indicated by analysis using the above method.

In the experiments utilizing the alumina gels, acetate ion was positively adsorbed and it was found that the H^+-ion exchange method described for sulfate ion was equally applicable to the acetate analysis.

pH Measurement.—All *p*H measurements were made on a Beckman Model G *p*H meter using a glass electrode against a calomel (saturated KCl) electrode. With frequent standardization of the electrodes against standard buffer solutions, it was found that the accuracy of the *p*H determinations was about ±0.02 *p*H unit.

Results and Discussion

In connection with the presentation of the data the following should be pointed out. The amount of ion in milliequivalents, x, adsorbed by the gel is defined by the total amount of cation (or anion) held within the pores of the gel. On this basis

$$x = V_0(N_0 - N) + V_gN \qquad (1)$$

where x = milliequivalents of ion adsorbed, V_0 = total volume of solution (= 100 cc.), N_0 = original ionic normality, N = equilibrium ionic normality, and V_g = pore volume of the gel sample used. This definition follows from the fact that dried or calcined gel was placed in the solution so that a certain portion, V_g, of the volume, V_0, penetrated into the gel.

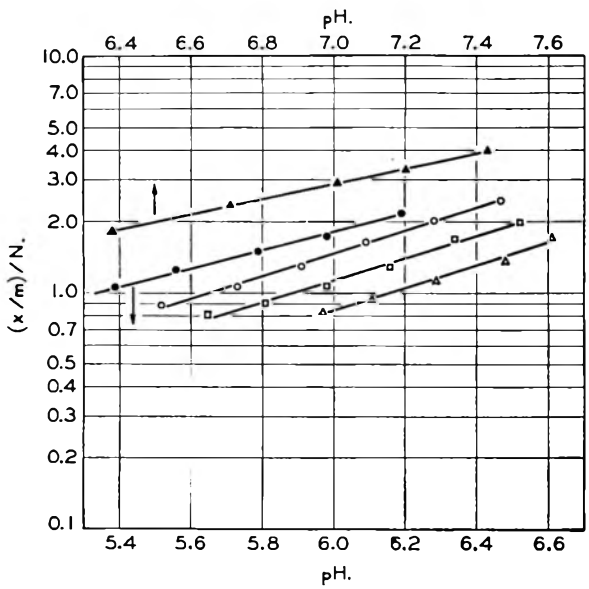

Fig. 2.—The variation of $(x/m)/N$ with *p*H for silica gel: ▲, 0.05 N $(NH_4)_2HPO_4$ with calcined silica gel; ●, 0.05 N NH_4OAc with calcined silica gel; ○, 0.05 N NH_4OAc with dried silica gel; □, 0.10 N NH_4OAc with dried silica gel; △, 0.20 N NH_4OAc with dried silica gel.

A. Silica Gel.—First of all, it is of primary interest that NH_4^+ adsorption by silica gel is small and highly dependent on the solution *p*H. As seen from the data of Table II, the NH_4^+ adsorption from 0.05 N $(NH_4)_2SO_4$ solution is such that the normality of the solution in equilibrium with the gel is greater than that of the initial solution. Apparently the silica gel is so weakly acidic that it adsorbs water preferentially to NH_4^+ from a solution of the *p*H range 3.8–4.0.

TABLE II

ADSORPTION OF NH^+ BY CALCINED SILICA GEL FROM $(NH_4)_2SO_4$ SOLUTION AT 15°

N_0, original solution normality; g, g. gel per 100 ml. soln. N, equilibrium normality; x, milliequivalents NH_4^+ adsorbed.

N_0	g	*p*H, 25°	$N_{NH_4^+}$	$x_{NH_4^+}$[b]
	8.00	4.00	0.0501	0.12
0.0502	16.00	3.88	.0504	.24
	32.00	3.83	.0514[a]	.39

[a] Final $SO_4^=$ normality for this run = 0.0521. [b] Meq. NH_4^+ adsorbed calcd. from equation $x = V_0(N_0 - N) + V_gN$.

With ammonium acetate solutions and $(NH_4)_2HPO_4$ solutions (Fig. 3) the NH_4^+ adsorption is small but measurable and in both cases it is quite dependent on *p*H.

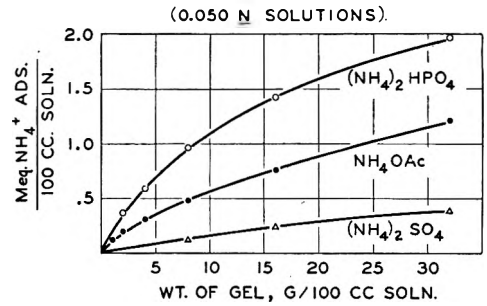

Fig. 3.—Adsorption by silica gel (0.050 N solutions).

The ratio of the milliequivalents of ion adsorbed per g. of gel to the normality of the same ion in solution was called R.

$$R = \frac{x/g}{N} \qquad (2)$$

where g = wt. of gel in g. This ratio is seen to be quite dependent on the *p*H of the solution at equilibrium. A plot of the *p*H *vs.* R on a semi-log scale, as in Fig. 2, shows a fair straight line relationship for ammonium acetate on oven dried silica gel and for both ammonium acetate and $(NH_4)_2HPO_4$ solutions on calcined silica gel. From the graph the following relationship holds for these systems

$$(x/g)/N = K[H^+]^{-p} \qquad (3)$$

The value of p for each of the systems can be calculated from the graph. For oven dried silica gel with 0.05 to 0.20 N NH_4OAc solutions $p = 0.50$, for calcined silica gel with 0.05 N NH_4OAc $p = 0.40$ while for calcined silica gel with 0.05 N $(NH_4)_2HPO_4$ $p = 0.33$.

It is also of interest to note that silica gel has a definite tendency toward negative adsorption for anions. At least this is true for $HPO_4^=$ and $SO_4^=$ ions due possibly to the very small pore size of the silica gel.

The data presented here for silica gel are not inconsistent with the theory expressed earlier by Kolthoff and Stenger[14] that cationic adsorption by silica gel is a secondary adsorption due to OH^- ion adsorption which is necessarily balanced by cation adsorption. Such a mechanism would explain the great dependence of the NH_4^+ ion adsorption

(14) I. M. Kolthoff and V. A. Stenger, THIS JOURNAL, **56**, 2113 (1932).

in the present experiments on the equilibrium *p*H of the solution.

B. Alumina Gel.—It would appear from the results of the alumina gel adsorption experiments (Fig. 4) that the adsorption is due primarily to an exchange of the anions in solution for structural OH groups which probably comprise much of the gel surface. That is, the gel does not behave at all as though it were an anion exchanger. The order of increasing adsorption for the ions ($CH_3CO_2^- < SO_4^= < HPO_4^=$) is the same as the order of increasing ability to complex with alumina.[15] If alumina were acting as a weakly basic anion exchanger, on the other hand, one would expect the order of increasing exchange to the $HPO_4^=$, $CH_3CO_2^-$, $SO_4^=$ to correspond with the decrease of *p*H.

The reactions involved are apparently of the type

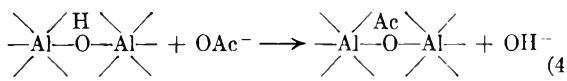

(4)

As would be expected from this equation and analogous ones for the other anions, the anion adsorption per gram decreases with increasing *p*H. All three of the anions tested show such a decreased adsorption with increasing *p*H.

It is assumed that in the experiments with sulfate and phosphate ions the reactions involved are strictly analogous to equation (4) in that one –OH group is replaced by one $SO_4^=$ or $HPO_4^=$ ion. That is, the resulting site on the gel surface would have an excess negative charge requiring cation adsorption for electroneutrality. The fact that NH_4^+ ion adsorption does occur with the sulfate and phosphate solutions to the extent, initially, of approximately one-half the anion adsorption (in meq./g.) is further evidence that a chemical exchange of the type indicated above is occurring. The fact that the NH_4^+ adsorption exceeds the value of 0.5 meq./meq. of anion adsorbed as the *p*H increases is due, probably, to OH^- adsorption which results in additional uptake of NH_4^+. With the acetate solution practically all the ammonium adsorption must be due to hydroxyl adsorption.

The data for the $(NH_4)_2HPO_4$ experiments are particularly interesting. The NH_4^+ adsorption in this case follows approximately the equation

$$\frac{(x/g)}{(N)_{NH_4^+}} = K(N_{HPO_4^=}) \qquad (5)$$

C. Silica-Alumina Gel.—The data obtained from the adsorption experiments with silica–alumina gel are interpreted to show one primary fact, namely, that the gel is a polybasic acid with a moderately high ionization constant. In this respect silica–alumina gel differs decidedly from silica gel, which is very weakly acidic, and alumina gel, which is basic (being primarily an anion adsorber). The acid centers on the gel are not constant in their acidity, but vary over a wide range of pK_a.

As with silica gel, ammonium acetate adsorption

(15) H. B. Weiser and E. B. Middleton, THIS JOURNAL, **24**, 53, 72 (1920); A. W. Thomas and R. D. Vartanian, *J. Am. Chem. Soc.*, **57**, 4 (1935).

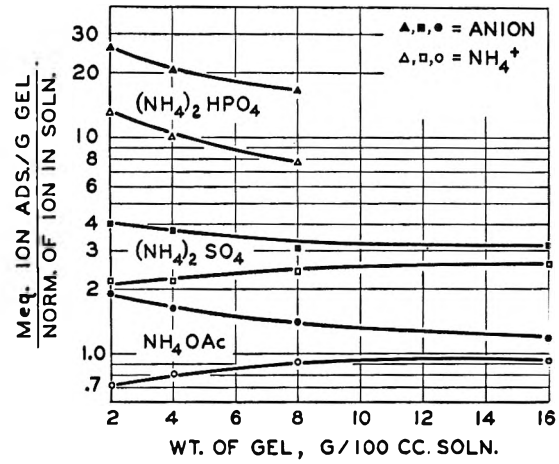

Fig. 4.—Adsorption by alumina gel (0.050 *N* solutions).

experiments were carried out with both calcined gel and gel which had been dried below 200°. From the results it was seen that the calcined gel possessed a more stable structure, as was expected, so that most of the experiments with ammonium sulfate and diammonium hydrogen phosphate were performed only with the calcined gel. As a result it seems most profitable to discuss primarily the properties of the calcined silica–alumina gel and include brief mention of the differences displayed by the oven-dried gel.

For a true strong acid exchanger it has frequently been found that an adsorption equation of the following type would express the conditions existing at equilibrium with a solution of ion A^+.

$$\frac{(A^+)_{ads}}{(H^+)_{ads}} = \frac{K(A^+)_{soln}}{(H^+)_{soln}} = \frac{\text{meq. } A_{ads}/\text{g.}}{\text{meq. } H_{ads}/\text{g.}} \qquad (6)$$

Furthermore, the total exchange capacity, *C*, is essentially constant for a strong acid exchanger so that the equation (6) becomes

$$\frac{x/g}{(Cg - x)/m} = \frac{x}{Cg - x} = \frac{K(A^+)_{soln}}{(H^+)_{soln}} \qquad (7)$$

Measurements were made to determine the total exchange capacity, *C*, of silica–alumina gel. The experiments were performed as follows. A weighed quantity of silica–alumina gel was placed in contact with exactly 100 ml. of ammonium acetate solution. After several hours the solution was drained off and replaced by a fresh 100-ml. batch. The *p*H of the solution was measured at 25° and the amount of NH_4^+ ion adsorbed was calculated. The process was repeated until no change in the *p*H of original ammonium acetate solution (7.00) was noted. Check runs were made in each case and the resulting checks were excellent. The results of these experiments are shown in Table III. For the calcined silica–alumina gel the total exchange capacity is a straight line function of the concentration of the solution used to measure it. That is

$$C = C_c + aN \qquad (8)$$

so that the gel is a weak acid exchanger.

A distinction is noted between the oven dried and calcined silica–alumina gel in the total adsorption capacity. The total adsorption capacity, *C*, for NH_4^+ in the presence of 0.05 *N* ammonium

TABLE III

TOTAL ADSORPTION CAPACITY OF SILICA–ALUMINA GEL TOWARD NH_4OAc AT pH 7.00

Wt. gel, g.	NH_4OAc, N	Meq. NH_4^+ ads./g.	Av.
	Calcined at 540°		
0.5	0.050	0.84	0.88
0.5	.050	0.90	
0.5	.100	1.20	1.19
0.5	.100	1.17	
0.5	.200	1.85	1.85
0.5	.200	1.85	
	Dried at 180°		
1.0	.050	1.32	1.31
8.0	.050	1.30	
1.0	.200	2.06	1.97
8.0	.200	1.89	

acetate is very considerably greater (approx. 50%) for the oven dried gel than for the calcined gel. On the other hand the adsorption capacity is not very greatly different for the same two materials with 0.20 N ammonium acetate (Table III). From these results it seems necessary to conclude that while the total concentration of acid centers present in the calcined gel may be almost as great as for the oven-dried gel, the strength of the acid centers are quite different.

TABLE IV

ADSORPTION OF NH_4^+ BY CALCINED SILICA–ALUMINA GEL FROM NH_4OAc SOLUTIONS AT 15°

g	pH (25°)	$N_{calcd.}$	x	R
		N_0, 0.0502		
0.40	6.28	0.0487	0.16	8.2
1.00	5.88	.0465	0.39	8.4
2.00	5.57	.0435	0.71	8.2
4.00	5.26	.0383	1.27	8.3
8.00	4.96	.0307	2.04	8.3
16.00	4.70	.0234	2.95	7.8
32.00	4.44	.0164	3.76[a]	7.9
		N_0, 0.100		
0.25	6.63	.0987	0.14	5.7
0.50	6.36	.0976	.26	5.3
1.00	6.05	.0953	.52	5.35
2.00	5.75	.0907	.98	5.4
4.00	5.47	.0837	1.79	5.35
8.00	5.17	.0720	3.07	5.3
		N_0, 0.200		
0.50	6.51	.1965	0.40	4.1
1.00	6.24	.1936	0.74	3.8
2.00	5.97	.1884	1.35	3.6
4.00	5.67	.1782	2.53	3.55
8.00	5.39	.1622	4.42	3.4

[a] Calculated from $N_{obs.} = 0.0150$. All the other observed values checked the calculated values of N within ± 0.0003 N.

Of course, this exchange capacity was measured at a pH = 7 and it would certainly change with the pH. For example, in the case of ammonium ion absorption from ammonium sulfate solutions the adsorption equilibrium is represented by equation (7), if C is defined as in equation (8). From the calculated values of C it is seen that at pH of about 4 the exchange capacity of calcined silica–alumina gel is about one-fourth that which it possesses at pH 7. Thus, there appears to be a substantial proportion (*i.e.*, 0.10 to 0.25 meq./g.) of the acid centers on the catalyst having a pK_a sufficiently low that they are highly ionized at pH 4. This is in decided contrast, of course, with silica gel which shows zero adsorption toward ammonium sulfate. Again, as with the ammonium acetate solutions, no anion adsorption occurs.

Merely for the sake of giving a rough indication of the acid strength of these centers the equation of Bradfield[16] was applied

$$p\mathrm{H} = pK + \log (\mathrm{salt})/(\mathrm{acid}) \qquad (9)$$

to compute the values indicated in Table V.

The adsorption of NH_4^+ ions from ammonium acetate solutions by calcined silica–alumina gel (Table IV) does not follow equation (7). Rather the adsorption equation is much simpler, namely

$$x/g = RN \qquad (10)$$

where R is essentially a constant for a given N_0. Or, more generally the equation becomes

$$x/g = (k_1/N_0 + k_2)N \qquad (11)$$

Equation (10) would follow from equation (6) if

$$(\mathrm{H}^+)_{ads} = \frac{R(\mathrm{H}^+)}{K}\ \mathrm{soln} \qquad (12)$$

a result not at all surprising on the basis that the gel acid is a weak acid. It is interesting to note that the adsorption of ammonium ion by silica–alumina gel from ammonium sulfate solution follows not only equation (7) but also equations (10) and (11).

Adsorption experiments carried out with diammonium hydrogen phosphate solutions and calcined silica–alumina gel (Table VI) showed a new phenomenon for this gel. This was anion adsorption in addition to cation adsorption. If the data for silica–alumina gel with $(NH_4)_2HPO_4$ solutions are considered along with those for alumina gel with $(NH_4)_2HPO_4$, it is concluded that the silica–alumina gel is showing a definitely dual function in this case. Apparently the acid spots are responsible for a portion of the NH_4^+ exchange while the 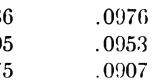 groups are responsible for the phosphate adsorption according to a chemical exchange reaction analogous to equation (4). In addition, further NH_4^+ exchange is caused by the phosphate adsorption, in a manner similar to that already discussed for alumina gel.

D. Experiments at Elevated Temperatures.— A few experiments were carried out to determine the change with temperature of NH_4^+ adsorption from ammonium acetate solutions by silica and silica–alumina gels. In order to make the proper comparisons in the change of adsorption with temperatures for the two different gels it was necessary to start with a batch of each gel which had been treated with ammonium acetate solution at the highest temperature to be encountered in the tests. This was 200° for the silica–alumina gel and 150° for the silica gel. It was found that after such a treatment followed by calcination to 540° subse-

(16) R. Bradfield, THIS JOURNAL, **35**, 360 (1931).

TABLE V

ADSORPTION OF NH_4^+ BY CALCINED SILICA–ALUMINA GEL FROM $(NH_4)_2SO_4$ SOLUTIONS AT 15°

N_0	g	pH (25°)	$N_{NH_4^+}$	$N_{SO_4^=}$	$x_{NH_4^+}$	$R_{NH_4^+}$	C^a	pK_a
0.0501 N NH_3^+	4.00	4.11	0.0466	0.0500	0.445	2.4	0.148	3.63
.0500 N $SO_4^=$	8.00	4.02	.0437		0.82	2.35	.147	3.66
	16.00	3.90	.0386		1.46	2.35	.150	3.71
	32.00	3.80	.0316		2.37	2.35	.141	3.80
.1003 N NH_3^+	2.00	4.23	.0982		0.31	1.6	.174	3.31
.1001 N $SO_4^=$	4.00	4.10	.0964		0.59	1.55	.171	3.32
	8.00	4.00	.0918		1.22	1.65	.186	3.39
	12.00	3.95	.0888		1.69	1.6	.176	3.35
	16.00	3.89	.0846		2.23	1.65	.184	3.41
.2006 N NH_3^+	2.00	4.14	.1978	.2015	0.48	1.2	.257	3.00
.2004 N $SO_4^=$	4.00	4.03	.1956	.2028	0.89	1.15	.245	3.01
	8.00	3.95	.1911	.2043	1.73	1.15	.242	3.02

[a] Calcd. from equation $\frac{x}{Cg-x} = K\frac{N}{[H^+]}$, if K is a true constant and = 5.0 $(10)^{-3}$. C = total exchange capacity at this pH range (meq./g.).

TABLE VI

ADSORPTION OF NH_4^+ AND $HPO_4^=$ IONS BY CALCINED SILICA–ALUMINA GEL FROM $(NH_4)_2HPO_4$ SOLUTIONS AT 15°

N_0	g	pH (25°)	$N_{NH_4^+}$	$N_{HPO_4^=}$	$x_{NH_4^+}$	$x_{HPO_4^=}$	$R_{NH_4^+}$	$R_{HPO_4^=}$
0.0502 N NH_4^+	2.00	7.21	0.0409	0.0468	0.97	0.36	11.8	3.8
	4.00	6.91	.0338	.0440	1.69	0.65	12.5	3.7
	8.00	6.38	.0219	.0362	2.92	1.47	16.7	5.1
.0500 N $HPO_4^=$	16.00	5.55	.0112	.0216	3.99	2.93	22.3	8.5
	32.00	5.40	.0040	.0084	4.66	4.20	36.5	15.6
.0989 N NH_4^+	1.00	7.57	.0932	.0968	0.62	0.17	6.65	1.75
	2.00	7.39	.0884	.0943	1.14	0.465	6.1	2.45
.0980 N $HPO_4^=$	4.00	7.15	.0792	.0894	2.13	1.04	6.7	2.9
	8.00	6.84	.0637	.0801	3.78	2.12	7.4	3.35
.1987 N NH_4^+	1.00	7.60	.1919	.1931	0.78	0.40	4.05	2.05
	2.00	7.48	.1853	.1899	1.53	0.815	4.15	2.15
.1961 N $HPO_4^=$	4.00	7.27	.1723	.1850	2.99	1.49	4.35	2.0
	8.00	7.05	.1481	.1739	5.67	2.93	4.75	2.1

quent exposure of the gel to ammonium acetate solution at lower temperatures had no further effect on the surface area, as shown in Table VII. Furthermore, check experiments carried out on the same batch of catalyst (with intermediate calcination) proved quite reproducible.

TABLE VII

TREATMENT OF GELS AT ELEVATED TEMPERATURES WITH 0.05 N AMMONIUM ACETATE—EFFECT ON SURFACE AREA

	Surface area (m.²/g.)
Silica–Alumina gel	
A, Original gel	510
B, A + 6 hr. in 0.05 N NH_4OAc at 200°	174
C, B + 6 hr. in 0.05 N NH_4OAc at 150°	184
Silica gel	
D, Original gel	720
E, D + 6 hr. in 0.05 N NH_4OAc at 150°	110
F, E + 6 hr. in 0.05 N NH_4OAc at 85°	106

The results of the tests are shown in Figs. 5 and 6. From these data it is seen that the acidity of silica–alumina gel continues to increase rapidly with increasing temperature, at least up to 200°. Silica gel also shows a slight increase in adsorption with temperature. However, the adsorption is still very small so that the discrepancy between the acidities of the two gels becomes much greater as the temperature increases.

Since the adsorption of NH_4^+ by silica–alumina gel from ammonium acetate solutions increases quite rapidly with temperature, it is not surprising that the acidity of some of the active sites is great enough at cracking temperatures (>430°) that they

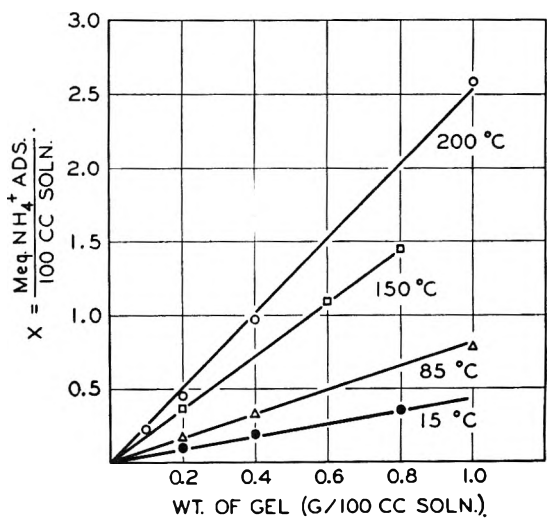

Fig. 5.—Effect of temperature on the NH_4^+ adsorption from 0.05 N NH_4OAc by calcined silica–alumina gel.

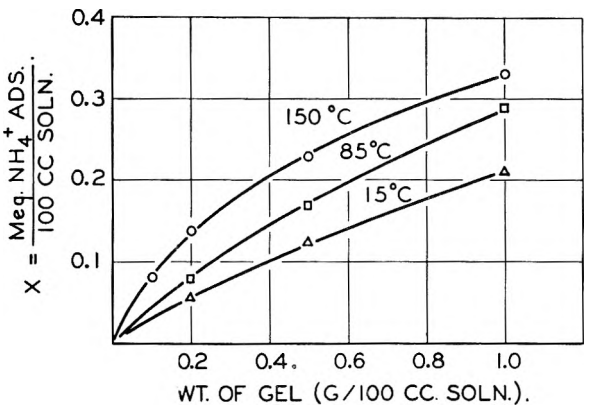

Fig. 6.—Effect of temperature on the adsorption of NH_4^+ by calcined silica gel from 0.05 N NH_4OAc solution.

can chemisorb bases as weak as quinoline quite strongly, as shown by Mills, Boedeker and Oblad.[17]

(17) G. A. Mills, E. R. Boedeker and A. G. Oblad, *J. Am. Chem. Soc.*, **72**, 1554 (1950).

It is apparent from the wide variation in acid strength of the different acid centers that the Al atoms are not all disposed in the structure in the same way. The most acidic spots are undoubtedly those intimately associated with silica in such a way that the Al atoms acquire a coördination number of 4 (*cf.* ref.[4]). However, it is not possible to say on the basis of the present data whether the acid centers showing low acid strength in the low temperature adsorption experiments do or do not acquire sufficient acidity at cracking temperatures to be important to the cracking reaction.

Acknowledgment.—The author acknowledges gratefully the assistance of members of the Inspection Section of the Socony-Vacuum Laboratories, Research and Development Division, and of Mr. J. L. Hammond in obtaining much of the analytical data. He also wishes to express his appreciation to the management of the Socony-Vacuum Laboratories for permission to publish this paper.

KINETICS AND THERMODYNAMICS OF THE STEADY STATE SYSTEM OF CATALASE WITH HYDROGEN PEROXIDE

BY ROLAND F. BEERS, JR.,[1-3] AND IRWIN W. SIZER

Department of Biology, Massachusetts Institute of Technology, Cambridge, Massachusetts

Received April 4, 1952

Equations for calculating the velocity constants of the two consecutive reactions between catalase and hydrogen peroxide from values of the over-all velocity constant and the concentration of the intermediate complex have been derived from steady state theory. The thermodynamic constants ΔH, ΔF and ΔS, of the consecutive reactions have been found to be the same and indicate that the rate determining steps are the same.

Introduction

Models of the kinetics of catalytic systems based on mathematical and chemical equations are essential for interpreting any theory for the mechanism of the action of a catalyst and for explaining the effects of inhibitors and accelerators on the catalyst-substrate system. On the basis of the mechanism of the catalase–hydrogen peroxide reaction proposed by several investigators,[4-6] catalase presents the unique feature of having a single substrate species which acts as both the acceptor (reductant) and donor (oxidant) molecule. In view of the fact that the hemes of catalase show no evidence of heme–heme interaction,[7] the reactions between catalase and peroxide are written thus by Chance[8]

$$FeOH + H_2O_2 \underset{k_2}{\overset{k_1}{\longleftrightarrow}} FeOOH + H_2O \qquad (a)$$

$$FeOOH + H_2O_2 \underset{k_{-4}}{\overset{k_4}{\longleftrightarrow}} FeOH + H_2O + O_2 \qquad (b)$$

where FeOH represents one heme of catalase. In the lowest range of hydrogen peroxide employed, the specific reaction rate (velocity constant, k_s) of the over-all reaction does not change in magnitude or order with variations in concentration of hydrogen peroxide.[10,11]

Theory.—The rate expressions for the substrate concentration, s, and the primary complex concentration, p, based upon the consecutive reactions (a) and (b) are

$$ds/dt = -k_1(e - p)s + k_2p - k_4ps \qquad (1)$$

and

$$dp/dt = k_1(e - p)s - k_2(p) - k_4ps \qquad (2)$$

(1) This work was done under an American Cancer Society, Inc., Fellowship recommended by the Committee on Growth of the National Research Council.

(2) The steady state analysis of this paper is from a thesis submitted by R. F. Beers, Jr., to the Massachusetts Institute of Technology in June 1951 in partial fulfillment of the requirements for the degree of Doctor of Philosophy.

(3) Naval Medical Research Institute, National Naval Medical Center, Bethesda 14, Maryland.

(4) B. Chance, *Biochem. J.*, **46**, 387 (1950).

(5) J. B. Sumner, A. L. Dounce and V. L. Frampton, *J. Biol. Chem.*, **136**, 343 (1940).

(6) B. Chance, *ibid.*, **180**, 947 (1949).

(7) B. Chance, *ibid.*, **179**, 1299 (1949).

(8) A recent paper by Chance[9] indicates that the active form of the substrate molecule is the undissociated acid, HOOH, and of the enzyme is the hydrated form, $FeOH_2$. Should this prove to be correct it does not alter the steady state theory discussed below. The reactions (a) and (b) become

$$FeOH_2 + H_2O_2 \underset{k_2}{\overset{k_1}{\longleftrightarrow}} FeH_2O_2 + H_2O$$

$$FeH_2O_2 + H_2O_2 \underset{k_{-4}}{\overset{k_4}{\longleftrightarrow}} FeOH_2 + O_2 + H_2O$$

(9) B. Chance, *J. Biol. Chem.*, **194**, 471 (1952).

(10) R. K. Bonnichsen, B. Chance and H. Theorell, *Acta Chem. Scand.*, **1**, 685 (1947).

(11) R. F. Beers, Jr., and I. W. Sizer, *J. Biol. Chem.*, **195**, 133 (1952).

where e is the total molar heme concentration. Adding (1) and (2) gives (*cf.* 12).

$$dp/dt + 2k_4ps = -ds/dt \quad (3)$$

The empirical rate formula for the substrate concentration after an induction period of a few micro-seconds as a function of the total heme concentration is

$$ds/dt = -k_s es \quad (4)$$

If we substitute (4) into (3) then

$$dp/dt + 2k_4ps = k_s es \quad (5)$$

But (4) is readily integrated to give

$$s = s^\circ \epsilon^{-k_s et} \quad (6)$$

where s° is the initial substrate concentration after the induction period. Substituting (6) into (5) and solving for p yields

$$\frac{p}{e} = \frac{k_s}{2k_4} - \left[\frac{k_s}{2k_4} - \frac{p^\circ}{e}\right]\epsilon^{[2k_4 s^\circ/k_s e][\epsilon^{-k_s et}-1]} \quad (7)$$

where p° is the initial primary complex concentration after the induction period. k_s has a value of approximately 10^7 l. mole^{-1} sec.$^{-1}$, while e is 10^{-9} M, and s° is 10^{-3} M for most experimental studies.[11] Substituting these values into (7) gives

$$\frac{p}{e} = \frac{k_s}{2k_4} - \left[\frac{k_s}{2k_4} - \frac{p^\circ}{e}\right]\epsilon^{(2k_4/k_s)10^6][\epsilon^{-10^{-2}t}-1]} \quad (7')$$

We observe that in less than a second the exponential term drops off to an insignificant value, since the magnitude of $2k_4/k_s$ is never less than unity. Equation (7), therefore, reduces to the approximation

$$p/e \cong k_s/2k_4 \quad (8)$$

Since e is constant p must be constant. Therefore

$$dp/dt \cong 0 \quad (9)$$

If, now, (1) is subtracted from (2) we have

$$ds/dt = -2k_1(e - p)s + 2k_2p \quad (10)$$

Substituting the value for p from (8) into (10) yields

$$ds/dt \cong -\left[2k_1\left(1 - \frac{k_s}{2k_4}\right) - \frac{k_2k_s}{k_4s}\right]es \quad (11)$$

But comparing (11) with (4) we observe that

$$2k_1\left(1 - \frac{k_s}{2k_4}\right) - \frac{k_2k_s}{k_4s} \cong k_s, \text{ or} \quad (12)$$

$$k_1 - \left[\frac{k_s}{2k_4}\right]\left[k_1 + \frac{k_2}{s}\right] \cong \frac{k_s}{2} \quad (13)$$

Therefore, if (6) and (13) are to be consistent, k_2/s must be small compared to k_1 (*cf.* 13). Equation (13) simplifies to the general equation for the over-all velocity constant[13]

$$k_s \cong \frac{2k_1k_4}{k_1 + k_4} \quad (14)$$

It should be pointed out that p/e and k_s are dependent variables (*cf.* 14). From (8) and (14) it can be shown that

$$1 - p/e \cong k_s/2k_1 \quad (15)$$

k_s, p and e are readily measured experimentally. Therefore, equations (8) and (15) can be used to calculate the values of k_1 and k_4.

The experimental activation energy (E_s) of the over-all reaction can now be resolved by equation (14) into the separate contributions of k_1 and k_4. Using the relation, $k = f \exp(-E/RT)$, where E is the "experimental energy of activation" and f is the temperature-independent "frequency factor"[15] equation (14) becomes when simplified

$$k_s \cong \frac{2}{\frac{\exp(E_1/RT)}{f_1} + \frac{\exp(E_4/RT)}{f_4}} \quad (16)$$

Experimentally, it has been shown[11,13] that $d^2(\ln k_s)/(1/T)^2 \cong 0$. This implies (as can be shown by requiring that in equation (16) the second derivative of $\ln k_s$ with respect to $1/T$ vanish) that

$$E_1 \cong E_4 \quad (17)$$

Moreover, if one substitutes $f_s \exp(-E_s/RT)$ for k_s in equation (16) and differentiates with respect to RT, it can be shown that

$$E_s \cong E_1 \cong E_4 \quad (18)$$

The conclusion, (17), can be reached in another way. From (8) and (15) can be derived

$$(e - p)/p \cong k_4/k_1 \equiv R_k, \text{ or} \quad (19)$$

$$R_k \cong f_4/f_1 \exp(E_1 - E_4)/RT \quad (20)$$

Therefore, unless $E_4 \cong E_1$, R_k (as measured by $(e - p)/p$) will vary as a function of temperature.[16]

Confirmation of the validity of this model can be established by determining whether p/e is a constant. Additional supporting data can be used to check equation (15) since all the variables of that equation have been published.[15,17] Chance[13] has shown with his rapid flow technique that p/e remains constant over a wide range of substrate concentration. The constancy of this ratio has also been confirmed when the notatin–glucose system is used as a continuous source of hydrogen peroxide.[4] We have repeated Chance's experiments with catalase coupled with a crude preparation of notatin plus glucose and have also found that p/e is constant. We have in addition established the fact that $(e - p)/p$ or R_k does not change within experimental error (5%) over the temperature range of 0–50°.[18]

Experimental

Apparatus.—For optical density measurements a Beckman spectrophotometer with 1 cm. path length quartz cuvettes and a hydrogen discharge lamp for a light source has been used. The cell compartment is temperature controlled with cooling coils.[11] Because the primary complex of catalase is unstable at high temperatures, it has been found necessary to construct a temperature controlled mixing apparatus which permits determinations of optical density immediately after mixing. Two 1-ml. tuberculin syringes (one for catalase, the other for the notatin system), encased in a water jacket connected in series with the cool-

(12) K. J. Laidler and J. M. Socquet, THIS JOURNAL, **54**, 519 (1950).

(13) Several authors have considered the second step, k_4, to be the rate determining process[6] in which case k_s and k_4 are assumed to be equal.[14] Part of this misinterpretation arose from a failure to realize that k_s is determined as a function of e while k_4 is determined as a function of p only. The same argument may be applied to k_1, which is a function of $(e - p)$.

(14) B. Chance and D. Herbert, *Biochem. J.*, **46**, 402 (1950); B. Chance, *J. Biol. Chem.*, **179**, 1341 (1949).

(15) J. A. Christiansen, *J. Colloid Sci.*, **6**, 213 (1951).

(16) A. C. Burton, *J. Cell. Comp. Physiol.*, **9**, 1 (1936).

(17) B. Chance, *J. Biol. Chem.*, **179**, 1311 (1949).

(18) R. F. Beers, Jr., and I. W. Sizer, *Federation Proc.*, **11**, 11 (1952).

ing coils of the spectrophotometer, are clamped in a horizontal position over the phototube housing unit.[18a]

Procedure.—Temperature equilibrium in the syringes is reached in less than a minute. During this time the operator adjusts the dark current and slit width of the spectrophotometer for use at 4050 Å. The plunger is pushed rapidly, emptying both syringes into the cuvette. A few bubbles of air are then forced from the air syringe through the solution in the cuvette and an optical density reading is taken. For active preparations of glucose oxidase the concentration of the primary complex of catalase remains constant for only a few seconds unless more air is bubbled through the solution. Each sample is checked three or four times by bubbling air into the system and taking density readings. The same solution is used for successive measurements of the absorption curve, until there is evidence that the optical density at 4050 Å. does not return to the initial value after aeration.

Results

The absorption curve of the primary complex is similar to that previously published by Chance.[19] The extinction coefficient reported for horse liver catalase ($E^{4050}_{mM-1} = 340$) has been used to calculate extinction coefficients of the primary complex. The deflection in the extinction coefficient at 4050 Å. produced by complex formation has been found to be between 45 and 50, the same as that reported by Chance. We have also observed that under anaerobic conditions the primary complex rapidly reverts to the uncombined form. The addition of a few bubbles of air makes possible the rapid restoration of the primary complex. At low concentrations of notatin, however, the primary complex is stable for periods up to 30 minutes, depending upon the temperature.

Since the rate of oxidation by glucose oxidase is zero order at high concentrations of glucose the steady state concentration of hydrogen peroxide under the experimental conditions specified may be assumed to be proportional to the concentration of the glucose oxidase. A hundred-fold dilution of the notatin (glucose constant) produced no change in the concentration of the primary complex (p/e is constant) in confirmation of Chance.[13]

Table I presents three typical sets of values of R_k at 2 and 45°. Since values at intermediate temperatures show no deviation, it is apparent that within experimental error there is no detectable change in concentration of the primary complex over this temperature range.

TABLE I

Exp.	Temp., ±0.5°	Control density	Sample density	No. samp.	±% dev.	p	$e - p$	R_k
A	3	681	582	4	0.5	99	201	2.03
	41	681	580	6	1.5	101	199	1.97
B	2	483	414	3	0.0	69	144	2.09
	43	483	418	4	0.0	65	148	2.27
C	2	620	534	6	1.5	86	191	2.22
	45	620	565	2	0.0	85	192	2.25

Average 2.14 ± 5% dev.

However, the concentration of the primary complex appears to fall with the age of the catalase preparation, although two separate shipments of catalase from the supplier had the same value. At higher temperatures in the presence of glucose and in the absence of any glucose oxidase, the optical density of the Soret band of catalase drops rapidly during the first 30 minutes. This does not appear to be related in any way to the formation of the secondary complex between catalase and hydrogen peroxide reported by Chance[4] and also observed by us.

(18a) R. F. Beers, Jr., and I. W. Sizer, *Anal. Chem.*, in press.

(19) B. Chance, *Acta Chem. Scand.*, **1**, 236 (1947).

Discussion

The validity of the proposed kinetic model of the catalase–hydrogen peroxide system has been verified by the agreement between the predicted and observed constancy of p/e over a wide concentration range of substrate. Additional confirmation should be obtained from the published values of k_s, k_1 and p/e. Table II quotes experimental values of k_s, k_1 and p/e for horse liver,[17] beef liver[11] and bacterial[13] catalase and calculated values of k_1, k_4 and R_k based on the given values for k_s and p/e.

TABLE II

SPECIFIC REACTION RATES × 10^{-6}

	Horse eryth. (4 hemes)	Bacterial (4 hemes)	Horse liver (3 hemes)	Beef liver (3 hemes)
k_s (exp.)	8.75	13.3	10.0	6.7
k_1 (exp.)	7.5	15.0		
k_1 (theory)	5.83	11.0	7.6	5.0
k_4 (theory)	17.5	16.5	15.0	10.0
$e - p/e$	0.25	0.40	0.33	0.33
R_k	3.0	1.5	2.0	2.0
Ref.	17	13	17	11

The large discrepancy between the theoretical and experimental values of k_1 in Table II is considerably in excess of any experimental error. Two compensatory errors have been made by previous workers in determining the value of k_1 from kinetic data.[13] The maximum reduction of the extinction coefficient at 4050 Å. has been taken as an indication of completion of the reaction between free catalase and hydrogen peroxide (treated essentially as an irreversible second-order process), while it actually represents a saturation of only 25% for horse erythrocyte and 40% for bacterial catalase. Correcting this error gives a value of k_1 too small because the rate of change of p is also a function of k_4. In calculating k_1 the assumption had been made that at sufficiently low concentrations the k_4 reaction could be neglected. However, as indicated from equation (10), k_1 exceeds k_1 for all catalase systems in which p/e is less than 0.5 ($R_k = 1$). Since the maximum value reported so far is only 0.4, k_4 cannot be neglected. Therefore, the published values of k_1 are in error and their similarity to the theoretical values cannot be used as an additional proof of the kinetic model.

In order to test quantitatively the validity of this kinetic model, either k_1 or k_4 should be known from experimental data. The simplest differential equation which may be integrated to solve for k_1 is obtained by eliminating k_4 by subtracting equation (4) from (2)

$$ds/dt - dp/dt = -2k_1(e - p)s \qquad (21)$$

A similar equation has been discussed by Chance.[13] However, a rigorous solution of (21) is not possible at the present time because adequate rate curves

for ds/dt and dp/dt for the initial pre-steady state period of the catalytic process have not been published. Solutions utilizing a differential analyzer have been discussed by Chance[20] in reference to unpublished data. It is not quite clear whether his theoretical values of k_1 calculated from equation (15)[20] are compared with published experimental values.[13] For the present the most accurate values of k_1 and k_4 can be determined only with steady state data.

The observation that R_k and the observed activation energy of k_s do not change with temperature[10,11,14] justifies the conclusion that k_s, k_1 and k_4 have the same activation energies.

From the statistical theory of reaction rates we may estimate the differences in the values of the two entropies and free energies of activation

$$k_{(1,4)} = (\kappa T/h)\epsilon^{-\Delta F_{(1,4)}/RT} = (\kappa T/h)e^{\Delta S_{(1,4)}/R}\, e^{-\Delta H_{(1,4)}/RT} \quad (22)$$

where κ is Boltzmann's constant, h Planck's constant, T the absolute temperature, R the gas constant, and ΔH is $E_{1,4} - RT$. The transmission coefficient is assumed to be unity.

Table III presents calculations of the various thermodynamic constants of three sources of catalase based on data reported in the literature and on the assumption that all three catalases are characterized by the fact that $E_1 = E_4$. Despite the wide variations in experimental activation energies, the entropies and free energies of activation are approximately the same.

TABLE III

EXPERIMENTAL ENERGY, FREE ENERGY AND ENTROPY OF ACTIVATION OF THE TWO REACTIONS, k_1 AND k_4, FOR A MOLAR CONCENTRATION OF HEME AT 25°

Source of catalase	Reaction	E_{exp}, kcal.	ΔF, kcal.	ΔS, e.u.
Horse erythrocyte (4 hemes)	k_1	1.7	7.54	−21.5
	k_4	1.7	6.94	−19.5
Bacterial (4 hemes)	k_1	1.4	7.2	−21.5
	k_4	1.4	6.96	−20.7
Beef liver (3 hemes)	k_1	0.6	7.60	−25.5
	k_4	0.6	7.23	−24.2

(20) B. Chance, "Modern Trends in Physiology and Biochemistry," E. S. G. Barron, Editor, Academic Press, Inc., New York, N. Y., 1951, p. 25.

Certain conclusions concerning the rate determining step may be made. The similarities of the heat, free energy and entropy of activation for k_1 and k_4 and the fact that the same substrate species is involved in both reactions indicate that the rate determining steps are the same in the two reactions. Diffusion of the substrate is the common denominator of both reactions, but the thermodynamic constants are not typical of a diffusion process. The decrease in randomness of the system encountered with each reaction process is no doubt related to the structural characteristics of the protein which set special steric requirements which must be fulfilled in the formation of the complex.

Non-linearity of the Arrhenius equation plot associated with many enzymatic processes has been attributed by various authors to a temperature sensitive equilibrium between active and inactive forms of the enzyme (see Kistiakowsky, *et al.*[21]). A possible explanation based on the requirement of two partial irreversible rate determining steps in an enzyme system has not been given serious consideration heretofore. The authors have extended Christiansen's treatment of non-catalytic systems to include the unique kinetics of catalase. From a theoretical standpoint it is important to note the possibility of a deviation from the Arrhenius equation on the basis of these two interpretations for the special case of catalase.

Acknowledgment.—The authors wish to thank Professors David F. Waugh and Charles D. Coryell for their helpful discussions on several aspects of this paper, and Mrs. June Rosenberg for her technical assistance.

Note Added September 17, 1952.—We are pleased to note that Chance, *et al.*,[22] have reached independently some of the general results (eq. (8) and (15) above) previously obtained by one of us.[2] Our present derivation, however, is somewhat more rigorous than our earlier, or than Chance's. On the subject of rigor, we should like to remark that in the current paper by Chance, *et al.*,[22] their attempt (pp. 308 ff.) to integrate dp/dt analytically is based on two contradictory requirements, *viz.*, that $s \cong s°$ (p. 308) and that $e \cong s°$ (p. 309). Also, in this integration, the appeal to "correction factors" from computer studies seems a further admission that the analysis has only descriptive value.

(21) G. B. Kistiakowsky and R. Lumry, *J. Am. Chem. Soc.*, **71**, 2006 (1949).

(22) B. Chance, D. S. Greenstein and F. J. W. Roughton, *Arch. Biochem. Biophys.*, **37**, 301 (1952).

STUDIES OF THE SOLVENT EXTRACTION BEHAVIOR OF THE TRANSITION ELEMENTS. I. ORDER AND DEGREE OF FRACTIONATION OF THE TRIVALENT RARE EARTHS

BY D. F. PEPPARD, J. P. FARIS, P. R. GRAY AND G. W. MASON

Contribution from the Chemistry Division, Argonne National Laboratory

Received April 9, 1952

The extractability of the lanthanides into tributyl phosphate from an aqueous hydrochloric acid phase and from an aqueous phase 8 to 15.6 *M* in nitric acid increases with increasing atomic number, paralleling the theoretical order of decreasing basicity. This order is inverted for the system TBP and a 0.3 *M* nitric acid aqueous phase. Yttrium falls in the position predicted from consideration of ionic radii. The logarithms of the distribution ratios of a given pair of lanthanides diverge with increasing acidity for relatively concentrated nitric acid solutions, so that the theoretical maximum mutual separation of the pair requires the use of concentrated nitric acid. Use of an inert diluent for the TBP decreases the extractability of the rare earths by a factor much larger than that predicted on the assumption of simple dilution. The lanthanides may be divided into two groups, the split occurring at any predetermined point, by control of certain variables in countercurrent fractionation. In this way a valuable thulium–lutecium fraction has been obtained from a mixed rare earth source. Consequently, by means of two successive divisions any individual lanthanide may, in principle, be isolated from its neighbors on both sides. The lanthanides, yttrium and scandium may be purified with respect to many common impurities by extraction from a salted phase. Scandium may be separated from the lanthanides and yttrium by extraction from hydrochloric acid.

Introduction

Studies of the fractionation of lanthanides by a liquid–liquid extractive technique have extended over the past fifteen-year period, the first work reported being that of Fischer, Dietz and Jübermann.[1] The reviews by Bock,[2] Quill[3] and Wylie[4] stress the importance of a continuous liquid–liquid extractive technique applicable to the fractionation of lanthanides. The present paper describes the study of tri-*n*-butyl orthophosphate, $(n\text{-}C_4H_9O)_3PO$, hereinafter referred to as TBP, as the organic phase using a solution of trivalent rare earth chlorides or nitrates as the aqueous phase, and reports the development of chemical techniques held applicable to the continuous fractionation of rare earths by means of countercurrent liquid–liquid extraction.

It is felt that the novelty of the TBP–nitric acid system, in comparison with previously reported systems, lies in the combination of the large distribution ratio for a given lanthanide under properly chosen conditions and the relatively sharp differentiation between adjacent lanthanides.

Experimental

General.—TBP was washed with two one-fifth volumes of aqueous 5% sodium carbonate before use in any of the experiments described. (The purpose of the sodium carbonate washes is to ensure the absence of trace quantities of phosphoric acid, monobutyl phosphoric acid and dibutyl phosphoric acid.) In all experiments, washed TBP was pre-equilibrated with respect to an aqueous phase identical to that under study except that it contained none of the element whose extraction was being investigated. In radioactive tracer studies, a quantity of tracer was added such that each milliliter of the feed solution corresponded to approximately 10^5 counts per minute under the counting conditions employed Equilibration periods of five minutes were found to be adequate. For radioactive assay, aliquots of the liquid were evaporated on a five-mil platinum disc. The number of counts per minute associated with such an aliquot was then determined by the usual means.[5] In the determination of K, the distribution ratio (concentration in the organic phase divided by the concentration in the aqueous phase at equilibrium), for tracer elements two sets of measurements were made for which the quantity of tracer used in one set differed from that used in the other by a factor of 25 or more.

In the study of lanthanide mixtures two methods of operation were employed. In the technique entitled "countercurrent distribution" by Craig[6] each separate portion of phase I remains in its given contactor in which it is contacted successively with separate portions of phase II. In the method of operation referred to as "pseudo countercurrent extraction" by Hunter and Nash[7] and discussed by them in some detail the phases are moved, batchwise, countercurrently, so that the batch analog of continuous column extraction results.

In the present work the pseudo-countercurrent extraction system was operated with both an extraction and a scrubbing section, the effluent aqueous scrub joining the influent aqueous feed and thus effecting reflux.

Spectrographic Assays.—The rare earth content of each organic phase was extracted into water. Each water re-extract, as well as each aqueous phase to be assayed, was washed with benzene or some similar solvent to remove traces of TBP. Aliquots were then converted to chlorides by repeated evaporation with hydrochloric acid. The resulting chloride solutions were assayed for rare earth content by the copper spark technique of Fred, Nachtrieb and Tomkins.[8]

Other Assays.—Total rare earth content was determined by the usual procedure of precipitation of an oxalate, from an aqueous solution, followed by ignition of the oxalate to an oxide. Prior to the oxalate precipitation the aqueous phases, or aqueous re-extracts of organic phases, were scrubbed as above to remove traces of TBP and evaporated to remove excess acid. From the total rare earth content and the relative values obtained by spectrographic assay the content of specific rare earths was calculated.

Acid content of aqueous phases (containing no salt) was determined by titration of a suitably diluted aliquot with aqueous sodium hydroxide, approximately 0.2 *M*, using phenolphthalein as indicator. Acid content of organic phases (containing no salt) was determined by the same technique except that the aliquot was diluted with absolute ethyl alcohol and the standard base was an ethyl alcohol solution. Acid content of feed (an aqueous phase containing salt) was determined in an approximate manner by electrometric titration of a diluted aliquot.

Sources of Materials.—TBP and Gulf Solvent BT were obtained from Commercial Solvents Corporation and Gulf Refining Company, respectively. The rare earths were ob-

(1) W. Fischer, W. Dietz and O. Jübermann, *Naturwissenschaften*, **25**, 348 (1937).

(2) R. Bock, *Angew. Chem.*, **62**, 375 (1950).

(3) L. L. Quill, *Record Chem. Progress*, **11**, 151 (1950).

(4) A. W. Wylie, *Roy. Australian Chem. Inst. J. Proc.*, **17**, 377 (1950).

(5) Beta counting was done on the first shelf of a Geiger–Müller counter filled with neon-amyl acetate gas with a window thickness of approximately 2 mg./cm.², using an aluminum absorber (12.5 mg./cm.²) to cut out stray alpha particles.

(6) L. C. Craig, *Anal. Chem.*, **21**, 85 (1949).

(7) T. G. Hunter and A. W. Nash, *Ind. Eng. Chem.*, **27**, 836 (1935).

(8) M. Fred, N. H. Nachtrieb and F. S. Tomkins, *J. Optical Soc. Am.*, **37**, 279 (1947).

tained as oxides and carbonates from Lindsay Light and Chemical Co.[9]

Results

It has been found that scandium may be separated from many of the elements frequently associated with it by extraction from a hydrochloric acid medium. Pertinent tracer data are given in Table I.

TABLE I

EXTRACTION OF TRACER[a] SCANDIUM, YTTRIUM AND PROMETHIUM INTO TBP FROM AQUEOUS HYDROCHLORIC ACID

Element	*K* for aq. HCl of indicated concn. 3.0 *M*	6.4 *M*	8.0 *M*
Sc	0.04	32	50
Y	< .001	0.001	0.05
Pm	< .001	<0.001	0.01

[a] Tracers used were 85-d Sc^{46}, 61-d Y^{91} and 3.7-y Pm^{147}.

The separation of a macro amount of Sc from macro amounts of Y and the rare earths is shown in Table II. A 250-ml. portion of feed, 6.0 *M* in HCl, containing 0.1 g. each of Sc and Y, approximately 0.3 g. each of La, Pr, Nd, Sm, Gd and Dy, and approximately 5 g. each of Al, Ca, Mg and Na was used as a feed to a system of two contactors each containing 100 ml. of pre-equilibrated TBP. The feed was followed by four 50-ml. portions of 6.0 *M* HCl and four 50-ml. portions of water.

TABLE II

SEPARATION OF MACRO SCANDIUM FROM MACRO YTTRIUM, RARE EARTHS AND CERTAIN OTHER CONTAMINANTS

Aq. phase no.	Recovery of added element, % Sc	Y	R.E.	Al, Ca, Mg, Na
1	<0.1	98.7	99.2	>99
2	0.5	1.0	0.6	<1
3	2.1	0.3	0.2	<0.05
4	8.2	<0.1	<0.1	<0.01
5	13.1	..	..	..
6	70.0	..	..	..
7	6.0	..	..	..
8	0.1	..	..	..
9	< .1	..	..	..

Although it is evident from Table II that the rare earths do not extract appreciably from 6.0 *M* HCl, further investigation showed that at high concentrations of HCl the extraction is much more efficient. The fractionation of the rare earths was demonstrated by the countercurrent distribution technique employing four contactors each containing 150 ml. of pre-equilibrated TBP and using a 50-ml. portion of feed 12 *M* in HCl. (In the terminology adopted *R* is the volume ratio of organic phase to aqueous phase in a given equilibration and *E* is the total number of contactors.) The feed containing approximately 0.4 g. of rare earths containing comparable quantities of Nd, Sm, Gd and Dy and quantities of Eu, Tb, Ho, Er and Yb about one order of magnitude smaller and a much smaller quantity of Lu, was followed by several 50-ml. portions of HCl scrubs of different concentrations. The results are shown in Fig. 1. For the sake of clarity only a few of the elements are included. For all experiments of this type reported the data have a probable error of less than one part in ten.

In order to demonstrate the fractionation among the lanthanides of higher atomic number more fully, scrubs 6–10 of Fig. 1 were combined, evaporated and converted to 13-ml. of feed 10 *M* in HCl. This feed was cycled through four 39-ml. portions of pre-equilibrated TBP and was followed by seven 13-ml. portions of 10 *M* HCl and six 13-ml. portions of water. The water scrubs were combined as scrub SX. The results are shown in Fig. 2. The Dy data nearly coincide with the Tb data and so are not reported, in the interest of clarity.

The following figures indicate the over-all fractionation achieved in the experiments represented by Figs. 1 and 2.

(9) The authors are indebted to Lindsay Light and Chemical Co. for supplying several rare samples gratis

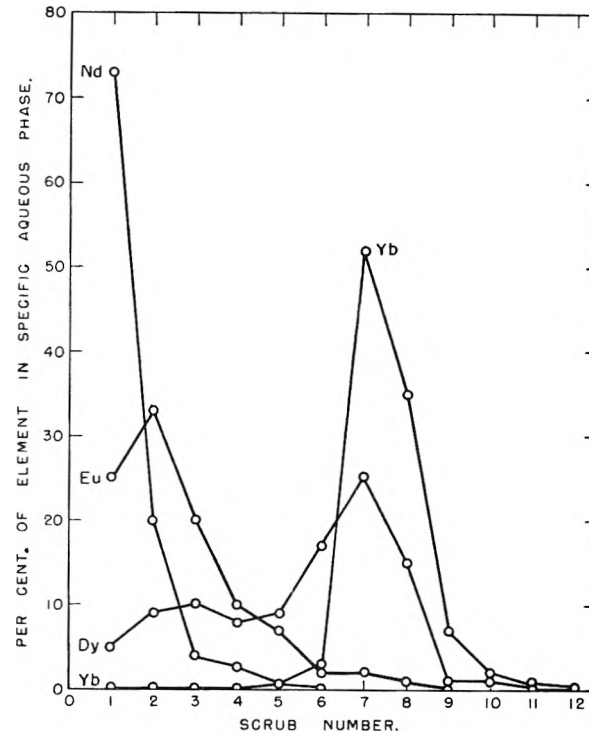

Fig. 1.—Distribution of rare earths in aqueous scrubs of tributyl phosphate; *E* = 4, *R* = 3; scrubs: 1–4, 12 *M* HCl; 5–8, 6 *M* HCl; 9–10, 1 *M* HCl; 11–12, water.

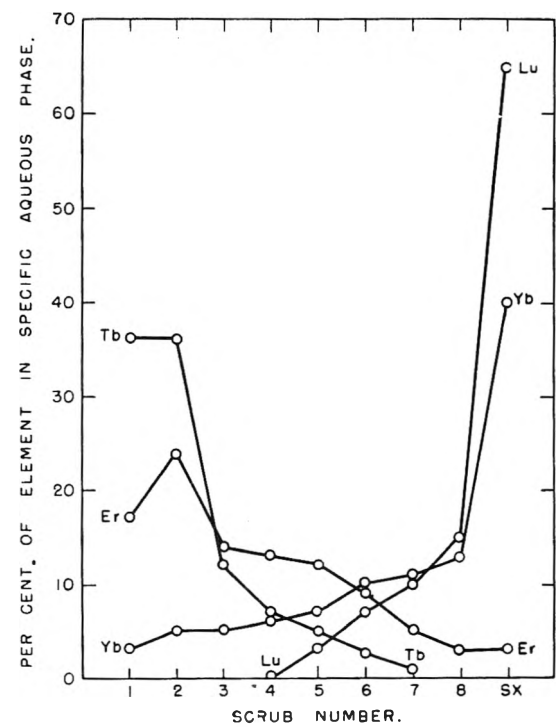

Fig. 2.—Distribution of rare earths in aqueous scrubs and aqueous re-extract of tributyl phosphate; *E* = 4, *R* = 3, scrubs 1–8, 10 *M* HCl; SX, combined aqueous re-extract.

From approximately 0.4 g. of feed rare earths containing approximately 1% Tm, 4% Yb and less than 0.5% Lu there was obtained approximately 8 mg. of product assaying 8% Tm, 66% Yb and 11% Lu. The respective percentage yields of Tm, Yb and Lu were 16, 33 and greater than 45. With respect to Yb, the approximate decontamination from various rare earths, expressed as the ratio of per cent. con-

tamination before fractionation to the per cent. contamination after fractionation, is: Eu, > 3000; Gd, 2000; Tb, 900; Dy, 600; Ho, 40; Er, 10; Tm, 2; and Lu, 0.7. Neodymium was obtained in 90% yield with the following approximate decontaminations from various rare earths; Sm, 2; Eu, 3; Gd, 4; Tb, 7; Dy, 15; and Yb, 200.

This series of experiments was extended, using feeds of various relative rare earth compositions, in order to establish that increasing extractability parallels increasing atomic number for all of the lanthanides. Consistently, Y fractionated between Dy and Ho, extracting only slightly less well than the latter. No inversions were found in a study involving HCl of concentrations ranging from 6 to 12 *M*.

Since one very important disadvantage associated with the system described is the necessity for using relatively dilute solutions of rare earths owing to the limited solubility of their chlorides in concentrated hydrochloric acid, an investigation of nitric acid–TBP systems was undertaken. The data of a preliminary survey are listed in Table III.

TABLE III

EXTRACTION OF LA, PM, Y AND SC INTO PRE-EQUILIBRATED TBP FROM VARIOUS AQUEOUS NITRATE PHASES[a]

Aqueous phase	*K* for: La	Pm	Y	Sc
7.2 *N* $Al(NO_3)_3$, 0.2 *N* HNO_3	>100	>500	>1,000	>1,000
10 *N* NH_4NO_3, 0.2 *N* HNO_3	..	~200	~200	>300
6 *N* NH_4NO_3, 0.2 *N* HNO_3	..	15	20	..
15.6 *N* HNO_3	0.33	3.6	125	>1,000

[a] The data pertain to 40-h La^{140}, 3.7-y Pm^{147}, 61-d Y^{91} and 85-d Sc^{46}.

From these data it may be concluded that the rare earths may be extracted very efficiently from a highly salted nitrate solution thereby purifying them from many commonly occurring contaminants. Only a trace of aluminum or ammonium ion extracts.

To demonstrate a purification of rare earths, an aqueous mixture of the respective nitrates containing approximately one gram each of La, Gd, Y, Sc, Al, Mg and Ca was converted to 100 ml. of solution saturated with respect to ammonium nitrate and approximately 0.2 *N* in HNO_3. This was cycled through four 100-ml. portions of pre-equilibrated TBP and was followed by six 25-ml. portions of aqueous scrub 10 *N* in NH_4NO_3 and 0.2 *N* in HNO_3. The scrubs were assayed for La, Y and Sc by cycling them through two more portions of TBP and analyzing these TBP phases. Analogously the solvent phases were analyzed for Al, Mg and Ca by cycling three more 50-ml. portions of ammonium nitrate scrub through them and assaying the composite of these aqueous phases. The results are shown in Table IV.

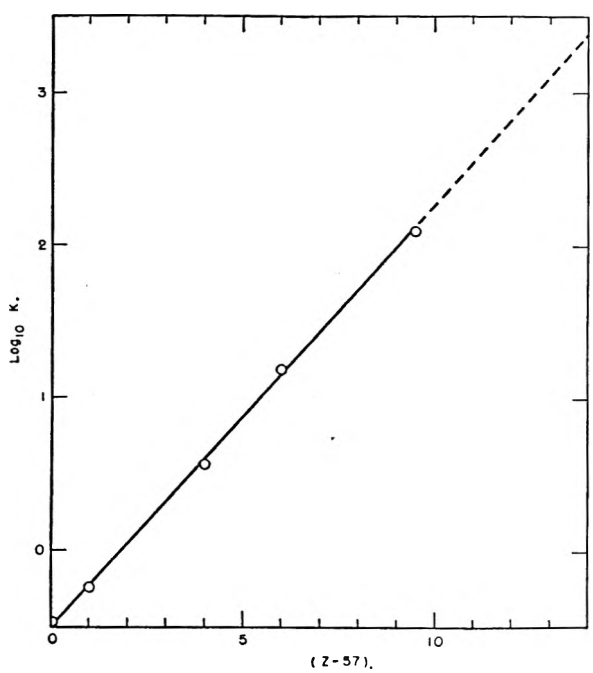

Fig. 3.—Variation of distribution ratio with atomic number for the system: 100% tributyl phosphate and 15.6 *M* HNO_3.

TABLE IV

EXTRACTION OF MACRO RARE EARTHS FROM COMMON CONTAMINANTS BY EXTRACTION INTO TBP FROM AMMONIUM NITRATE

Phase	Added element in phase, % La	Gd	Y	Sc	Al	Mg	Ca
Combined scrubs	1	<0.1	<0.1	<0.02	~100	~100	~100
Combined solvents	99	99.9	99.9	99.9	<0.1	<0.01	<0.1

Although the use of a metallic nitrate as a salting agent is advantageous in the separation of rare earths from accompanying impurities, it may be concluded, on the basis of the Pm and Y data of Table III, that for mutual fractionation of the rare earths a concentrated nitric acid phase is superior to a mixed nitrate–nitric acid phase. The data for the extraction of 40-h La^{140}, 275-d Ce^{144}(III), 3.7-y Pm^{147}, *ca.* 5.4-y $Eu^{152,154}$(III) and 61-d Y^{91} are shown in Fig. 3, the artificial atomic number 66.5 having been assigned to Y empirically, following the practice of Schubert,[10] since it has been found that in such a system Y fractionates in the Dy and Ho region.

Assuming the validity of the straight line of Fig. 3 the following expression results

$$\log K_Z = 0.28Z - 16.5$$

From the expression the ratio of the respective distribution ratios of successive rare earths is given as

$$(K_{Z+1})/(K_Z) = 1.9$$

It must be emphasized that this relationship is not necessarily valid for values of Z greater than 67. It is to be noted, further, that this expression applies to the extraction from 15.6 *M* HNO_3. When 12 *M* HNO_3 is used as the aqueous phase the ratio of the respective distribution ratios of successive rare earths is approximately 1.6.

The mutual separation of Y and Pm is shown in Fig. 4, the technique being countercurrent distribution. A sample of Y–Pm mixture totaling 3×10^6 counts per minute was processed as follows: the feed (2 ml., 12 *M* nitric acid) was contacted with six 3.6-ml. portions of a pre-equilibrated 50% washed TBP–50% dibutyl ether mixture. The resultant aqueous was labeled A. Five additional 2-ml. portions of 12 *M* nitric acid were cycled through the system of six contactors each containing 3.6 ml. of the solvent mixture. These scrubs were designated as B, C, D, E and F successively and the solvents in each contactor were labeled 1, 2, 3, 4, 5 and 6 successively, beginning with the first contactor. Aliquot portions of each phase were evaporated on two-mil platinum discs and beta counted.

The data of the foregoing experiment are indicated by the solid line of Fig. 4. The data of analogous experiments, identical to this except that Y and Pm tracers were used separately, are identified by the dotted lines of Fig. 4. The left tail of the dotted Y curve has been shown to be due to impurity in the tracer.

In order to approximate the conditions of maximum separability of a given pair of rare earths the variation of distribution ratio with nitric acid concentration was investigated. The results for Y and Pm, using TBP with and without diluent, are shown in Fig. 5. It is apparent that maximum separability between Pm and Y occurs at high nitric acid concentrations and that for concentrations to the left of the point of crossing of the curves the order of extraction is the reverse of that for concentrations to the right.

That the crossing of the corresponding curves for other rare earths also occurs is demonstrated in Figs. 6 and 7.

(10) J. C. Schubert in "Ion Exchange, Theory and Application," by F. C. Nachod, Academic Press, Inc., New York, N. Y., 1949, assigns the arbitrary "atomic numbers" of 56.5, 66.5 and 71.5 to Ac, Y and Sc, respectively, in order to fit these elements, as quasi rare earths, into the observed order of elution from a cation exchange resin.

TABLE V

PSEUDO-COUNTERCURRENT FRACTIONATION OF LANTHANIDES

12.00 ± 0.05 *M* HNO_3 scrub and feed, $q = 7$, $n = 4$, $R = 1.00$, $G/R = 1.33$

	Mg. of element per phase[a]							
	100% TBP		60% TBP		50% TBP		33% TBP	
Z	21P	21A	21P	21A	21P	21A	21P	21A
57	<0.04	0.6	<0.2	40	<0.2	40	<0.1	0.8
58	< .2	4	<1	80	<1	80	< .1	3
59	< .4	2	<2	8	<2	8	< .1	2
60	< .6	16	<1	40	<1	50	< .1	15
61	..	..	..	..	..	..	..	..
62	6	1	<2	12	<2	16	< .1	6
63	4	0.08	<0.2	<0.1	<0.2	<0.1	< .05	5
64	20	< .2	8	35	2	50	< .1	22
65	10	< .2	4	5	(2)?	10	< .05	11
66	60	< .2	150	40	70	100	2	60
39	40	.02	1800	60	1600	300	3	40
67	4	< .2	20	1	15	10	0.1	4
68	6	< .1	80	1	80	15	1	5
69	2	< .2	15	<0.2	15	1	0.5	2
70	6	< .04	40	0.1	40	1	2	4
71	..	..	5	<0.5	5	<0.5	3	..

[a] The symbols 21P and 21A refer, respectively, to the 40 ml. solvent and aqueous phases effluent from the twenty-first cycle. The TBP was diluted with Gulf Solvent BT. The feeds for the 100% and 33% TBP experiments were identical as were those for the 60% and 50% TBP experiments.

The feed, 200 ml. of a rare earth solution 12 *M* in HNO_3, was cycled through four 200-ml. portions of pre-equilibrated solvent (50% TBP–50% Gulf Solvent BT, by volume) and was followed by five 200-ml. portions of 12 *M* HNO_3. The effluent aqueous phases are labeled A-F, respectively, beginning with the effluent feed; and the water re-extracts of the individual solvent phases are identified as S1-S4, corresponding to the extractor numbers, in Fig. 6. Analogous results were obtained in an experiment identical to this except that the aqueous phase was 15.6 *M* in HNO_3 and the pre-equilibrated solvent was 25% TBP–75% Gulf Solvent BT. In this experiment Lu was detected in the S samples, since the absolute extractabilities were lower and therefore the quantities of Gd, Dy and Y in the S samples were not sufficiently high to mask the Lu in the assay procedure.

An extension of this series of experiments showed increasing extractability to parallel increasing atomic number for all of the lanthanides, using nitric acid of concentrations ranging from 8 to 15.6 *M* as the aqueous phase. The exact position of Y is somewhat doubtful, being nearly coincident with that of Ho.

In Fig. 7 the order of increasing extractability is seen to be inverted. These data were obtained by the preceding technique using four 300-ml. portions of pre-equilibrated 100% TBP and six 75-ml. portions of 0.3 *M* HNO_3, considering the feed as the first portion. The phases are identi-

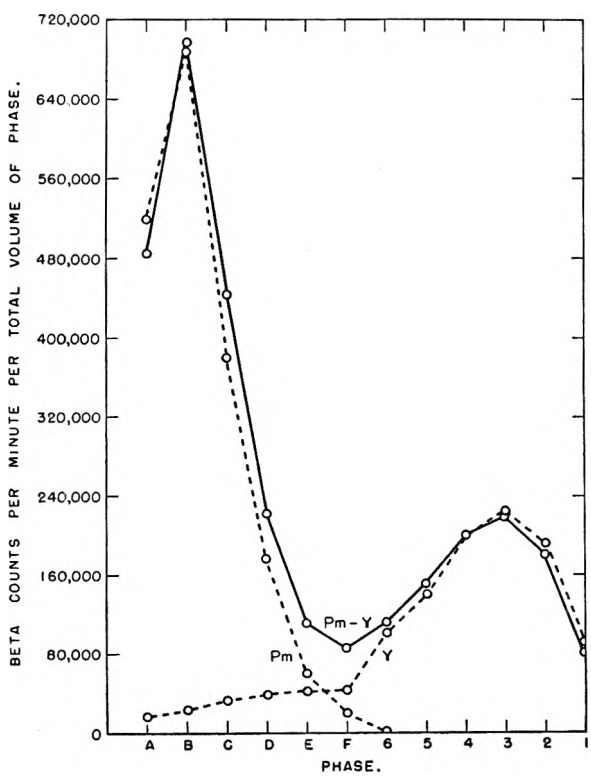

Fig. 4.—Separation of Y and Pm in the system: 50% tributyl phosphate–50% dibutyl ether and 12.0 *M* HNO_3.

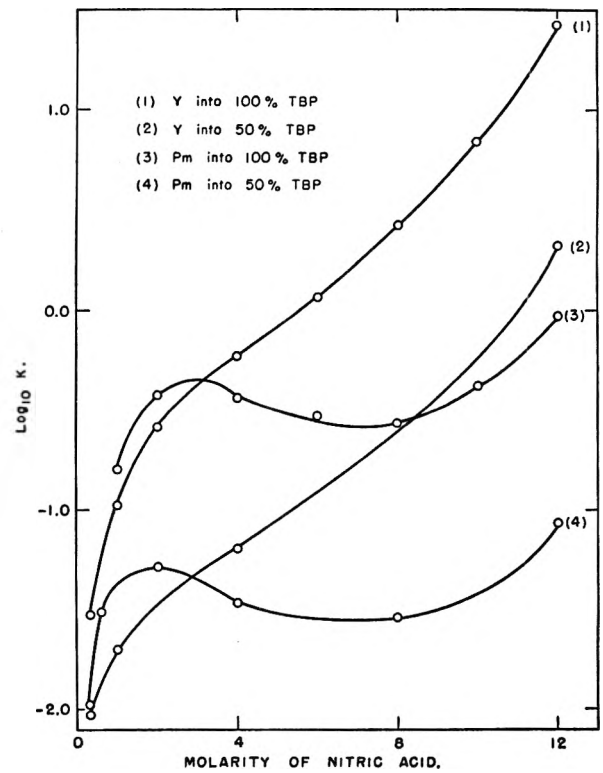

Fig. 5.—Variation of distribution ratio with aqueous HNO_3 concentration using 50% and 100% tributyl phosphate.

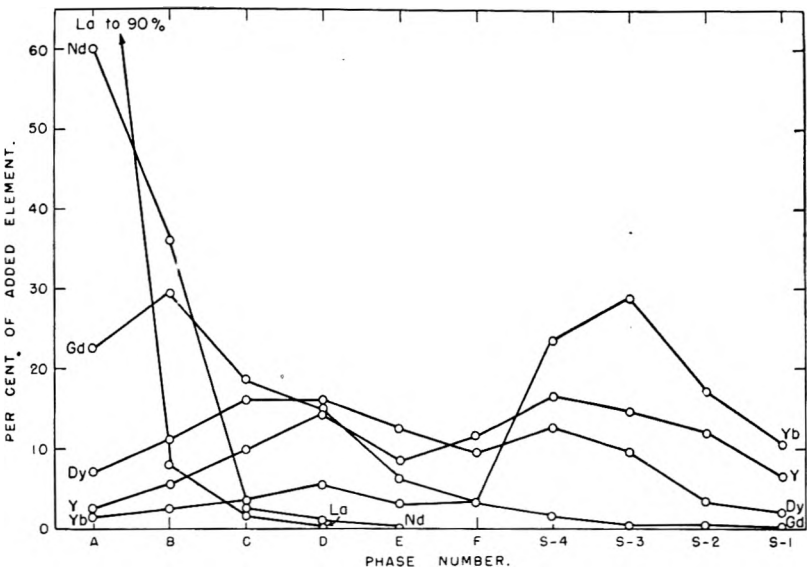

Fig. 6.—Fractionation of rare earths in the system: 50% tributyl phosphate–50% diluent and 12.0 M HNO_3.

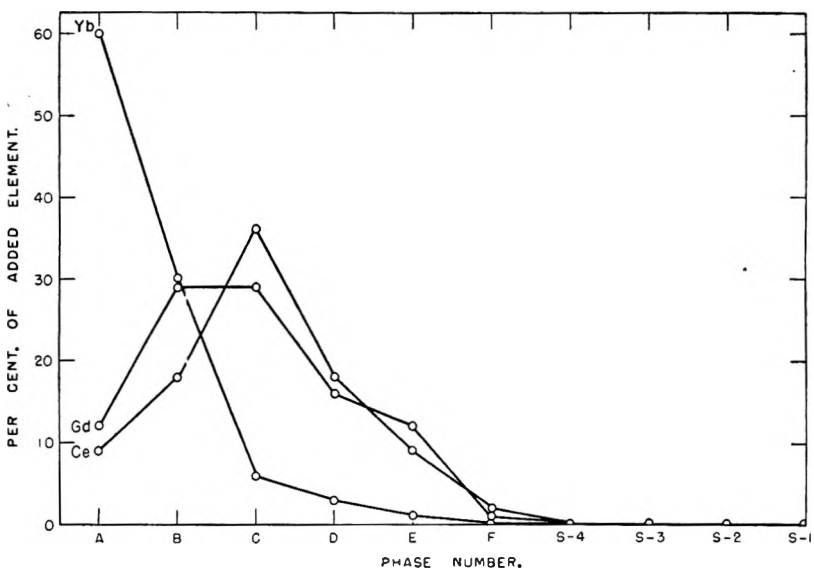

Fig. 7.—Fractionation of rare earths in the system: undiluted tributyl phosphate and 0.3 M HNO_3.

fied as in Fig. 6. The data of Fig. 8, in which the lines are drawn with an arbitrary slope of three, show the distribution ratio to approximate a third-power dependence on the concentration of TBP in dibutyl ether as diluent, using 11.5 M HNO_3 as the aqueous phase. The third-power dependence is approximately true also when 4 M HNO_3 is the aqueous phase, but in systems involving a 1 M HNO_3 aqueous phase the TBP dependence is approximately second power.

It is characteristic of the countercurrent distribution technique that certain of the product phases are quite dilute, with respect to lanthanide content, as compared with the feed. In order to establish whether there exists a large concentration effect on the separability of the lanthanides a series of pseudo-countercurrent experiments was performed. It was concluded that no large concentration effect exists.

Somewhat arbitrarily 12.00 M HNO_3 was chosen as the aqueous phase for the pseudo-countercurrent experiments, since it appeared to represent approximately the optimum HNO_3 concentration consistent with efficient rare earth fractionation and stability of solvent and diluent. Gulf Solvent BT, an inert liquid hydrocarbon, was adopted as a diluent on the basis of being more resistant than dibutyl ether to attack by nitric acid.

In the first pseudo-countercurrent experiments a center-feed, seven-stage, manually-operated system was used. (In the terminology adopted R is the volume ratio of the organic phase to the aqueous phase in a contactor in the extraction section, G is the corresponding ratio in a contactor in the scrubbing section, n is the number of the contactor into which the aqueous feed enters and q is the number of the contactor into which fresh organic extractant enters.) In this series of experiments the respective values of R and G were kept constant at 1.00 and 1.33, the concentration of HNO_3 in the aqueous phase was kept at 12.00 ± 0.05 M and the concentration of TBP in the solvent phase was varied, using Gulf Solvent BT as the diluent. Respective separate volumes of feed, scrub and solvent were 10, 30 and 40 ml.

In the later pseudo-countercurrent experiments a ten-stage, semiautomatic, mechanically-operated system with feed entry at the sixth stage was used. In this series of experiments the values of R and G were varied (keeping their ratio constant), the concentration of HNO_3 in the aqueous phase was kept at 12.00 ± 0.05 M and undiluted TBP was used as the solvent phase. Respective separate volumes of feed and scrub were 50 and 500 ml. The volume of solvent was either 125 or 500 ml.

The data for the seven-stage system are given in Table V and those for the ten-stage system in Table VI. It is apparent from these data that the position of the partitioning element is shifted toward the lower atomic numbers by increasing the concentration of TBP and by increasing the value of R, keeping other variables constant. The sharpness of fractionation increases with increasing q using approximate center feed, as predicted by theory[11] (see Fig. 9).

By use of an expression derived by Scheibel[12] it may be calculated that for a center-feed seven-stage system in which $R = G$, at the twenty-first cycle the effluent phases have attained 77% of the steady-state content of a substance corresponding to $RK = 1$ and greater than 77% of the steady-state content of all other substances extracting. For an analogous center-feed eleven-stage system the value is 47%. It is assumed that these approaches to steady-state operation were approximated in the experiments represented by the data of Tables V, VI and VII.

From the data of Tables V and VI, using the methods described in the Discussion Section, an experiment was designed for the purpose of fractionating a mixture of rare earth oxides (as obtained from Brazilian monazite) so that the effluent TBP phase would contain respectively 2, 8, 90,

(11) If F_A and F_P define the respective fractions of the element in question influent to the pseudo-countercurrent system which appear in the aqueous and organic phases effluent from the system at steady state then:

$$F_A = [\Sigma_0^{(n-1)} (GK)^i]/[\Sigma_0^{(n-1)} (GK)^i + (GK)^{(n-1)} \Sigma_1^{(q-n+1)} (RK)^i]$$

$$F_P = 1 - F_A$$

the assumptions being: the phases are completely immiscible, the volume of the composite aqueous phases is additive, and K is a true constant independent of concentration of the element considered and has the same value in both scrub and extraction sections. The scrub enters at number one contactor, the aqueous feed at the "nth" contactor, and the organic phase at the "qth" contactor.

(12) E. G. Scheibel, *Ind. Eng. Chem.*, **43**, 242 (1951).

TABLE VI

PSEUDO-COUNTERCURRENT FRACTIONATION OF LANTHANIDES

12.00 ± 0.05 *M* HNO_3 scrub, approx. 9 *M* HNO_3 feed, q = 10, n = 6, G/R = 1.11, undiluted TBP

		G of element per phase[a]			
		R = 1.00		R = 0.25	
Z	Element	40P	40A	40P	40A
57	La	<0.01	0.3	<0.01	0.3
58	Ce	..	..	..	..
59	Pr	< .04	.07	< .02	.06
60	Nd	< .01	.4	< .01	.4
61	Pm	..	..	..	..
62	Sm	1.7	.3	< .02	2.4
63	Eu	0.05	.005	.005	0.08
64	Gd	1.8	< .02	.4	1.0
65	Tb	0.2	< .01	.2	0.02
66	Dy	0.6	< .01	.7	.02
39	Y	1.5	< .01	1.4	< .01
67	Ho	0.03	< .01	0.04	< .02
68	Er	.1	< .01	.08	< .01
69	Tm	.01	< .005	.01	< .005
70	Yb	.02	< .005	.02	< .002

[a] The symbols 40P and 40A refer, respectively, to the effluent solvent and aqueous phases corresponding to the equilibration of the forty-fourth portion of feed.

TABLE VII

PSEUDO-COUNTERCURRENT FRACTIONATION OF LANTHANIDES[a]

		Composition (wt. %)	
		Feed	Product[b]
Z	Element	7.0 kg. oxide	72 g. oxide
57	La	16.1	<0.1
58	Ce	31.8	< .4
59	Pr	3.0	< .4
60	Nd	15.7	< .2
61	Pm	..	..
62	Sm	8.0	< .4
63	Eu	0.8	< .1
64	Gd	12.7	< .2
65	Tb	0.4	.4
66	Dy	3.2	5.1
39	Y	8.3	83.2
67	Ho	<0.2	1.2
68	Er	< .2	4.2
69	Tm	< .4	1.1
70	Yb	< .1	4.3
71	Lu	< .2	0.5

[a] Conditions: 12.00 ± 0.05 *M* HNO_3 scrub and feed, q = 10, n = 6, G/R = 2.00, R = 4.00, 60% TBP in Gulf Solvent BT. [b] The product is the lanthanide content of the composite TBP phase of 80 throughputs. The respective approximate fractional extractions of Gd, Dy and Y were 0.02, 2 and 10%. Probable approximate percentage yields of Ho, Er, Tm, Yb and Lu are 15, 60, 90, > 95 and > 99. > 98 and > 99% of the Dy, Y, Tm, Yb and Lu contained in the feed. Each portion of feed (750 ml.) contained 87.5 g. of lanthanides expressed as oxide, all cerium being reduced to cerium(III) by hydrogen peroxide. Following 40 throughputs to permit a close approach to steady-state operation 80 successive TBP extracts were composited and the product lanthanides removed by re-extraction into an aqueous phase.

The data for the 72 g. of product oxide obtained from 7.0 kg. of feed oxide are given in Table VII. The fractional extractions of Dy and Y agree very closely with the predicted values. It may be noted that on the basis of probable yields a Tm–Yb–Lu fraction in a yield in excess of 90% with an accompanying relative mass reduction of 90 was obtained.

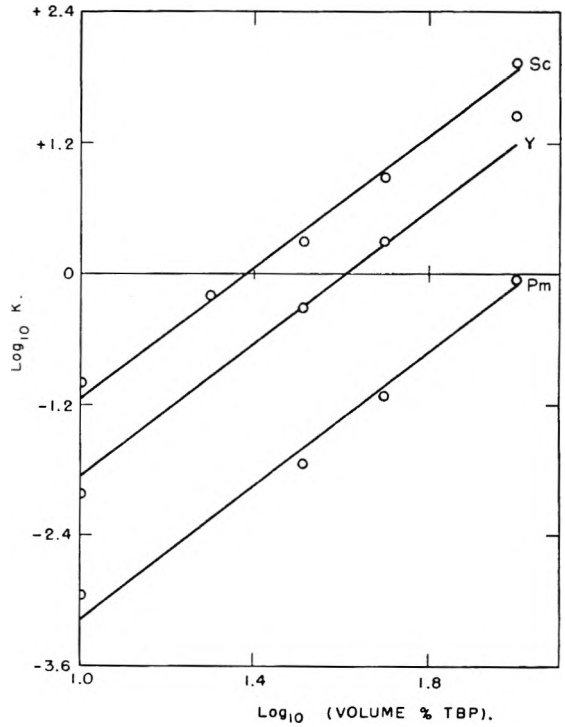

Fig. 8.—Variation of distribution ratio with concentration of tributyl phosphate in a tributyl phosphate–dibutyl ether solvent using 11.5 *M* HNO_3.

Discussion

In the extraction from hydrochloric acid and from nitric acid of moderate to high concentration, the extractability of the lanthanides into TBP increases with increasing atomic number, the order of increasing extractability paralleling the theoretical order of decreasing basicity as deduced by von Hevesy.[13] This order of increasing extractability is inverted for the case of dilute nitric acid.

In each of the systems investigated the extractability of Sc exceeds that of Y or any rare earths. Therefore, Sc may be purified quite efficiently with respect to Y and rare earth contamination by extraction into TBP from a hydrochloric acid solution.

In all of the present studies Y has been found to fractionate in the region of Ho, the position occupied in von Hevesy's basicity scale. According to the reasoning of Marsh,[14] fractionation of Y at this position implies ionic character of the Y and rare earth extracting species as opposed to covalent character which should result in fractionation of Y between Nd and Sm. The variation of fractionation position of Y has been reviewed by Moeller and Kremers.[15]

Assuming that equations of the following form adequately express the variation of K, at constant HNO_3 concentration, with respect to Z and with respect to the concentration of tributyl phosphate, respectively

$$\log K_1 = aZ - b$$
$$K = K_1(C_{TBP})^{\prime}$$

(13) G. von Hevesy, "Die seltenen Erden vom Standpunkte des Atombaues," Verlag von Julius Springer, Berlin, 1927.

(14) J. K. Marsh, *J. Chem. Soc.*, 118 (1947).

(15) T. Moeller and H. E. Kremers, *Chem. Revs.*, **37**, 97 (1945).

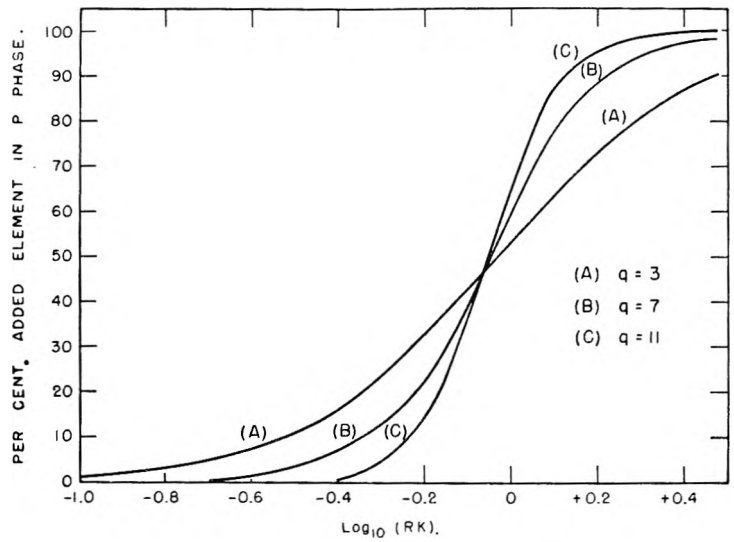

Fig. 9.—Theoretical steady state extraction in a system of an odd number of contractors with center feed, $G/R = 1.333$.

it follows that for constant K, Z_p is related to C_{TBP} as

$$dZ_p/d[\log C_{TBP}] = -f/a$$

where Z_p is the atomic number of the "partitioning element," *i.e.*, the element dividing approximately equally into the two effluent phases. Therefore, in the fractionation of the rare earths in a given system using nitric acid of a fixed concentration and TBP of various concentrations, a plot of the atomic number of the partitioning element against the logarithm of the per cent. concentration of TBP should be a straight line of slope $-f/a$.

For the system 12 M HNO_3–TBP (with Gulf solvent BT diluent) the respective approximate values of f and a are 3 and 0.2. Consequently for this system the slope should approximate -15. In the experiments reported in Table V the atomic numbers of the partitioning elements are 61, 65, 66 and 70. The plot of these numbers against the logarithm of the per cent. concentration of TBP is a straight line of slope -18. From such an experimental plot the concentration of TBP required, using the same system, to divide the rare earths at any atomic number between 61 and 71 may be obtained.

It is apparent that in order to place the point of division to the left of 61 some other variable must be changed. One of the simplest ways to accomplish such an end is to increase the value of R.

On the assumption that the ratio of the distribution ratios of successive rare earths in the 12 M HNO_3–TBP system is 1.6 the expression

$$(1.6)^{\Delta Z} = R_1/R_2$$

may be set up. Consequently, for a given system in which R is the only variable, the ratio of G to R being constant, the plot of the atomic number of the partitioning element against the logarithm of R should be a straight line of slope -5.

In the experiments reported in Table VI the partitioning elements have atomic numbers of 61 and 64. When plotted against the logarithms of the corresponding R values the points lie on a straight line of slope -5. From such an experimental plot the value of R required, using the same system, to divide the rare earths at any predetermined point may be obtained.

It is apparent that for the system 12 M HNO_3–TBP the partitioning point is far to the left for large values of R and far to the right for small values of R. Unduly large values of R may be avoided by use of a more concentrated HNO_3 phase, and inconveniently small values of R may be avoided by dilution of the TBP.

The increasing sharpness of the cut with increasing q[11] is shown graphically in the theoretical curves of Fig. 9. If the ratio of the K's for successive rare earths is a constant, then a definite increment in the abscissa of Fig. 9 corresponds to the difference between adjacent rare earths. Consequently, in principle, a vertical grid, with such a spacing, placed on Fig. 9 so as to cross a theoretical curve at a point corresponding to the extraction of one specific rare earth will also cut the same curve at points corresponding to the extraction of all of the other rare earths. In practice, this is very nearly true in the region in which the experimental value of F_P can be determined with sufficient accuracy to make such a determination valid, as may be shown by use of the data of Tables V and VI. Consequently, such a plot may be used to calculate the experimental K values of certain specific rare earths using a given combination of q, n, R and G in order to predict the behavior of the same chemical system using a different combination of q, n, R and G.

By such a process of reasoning it is concluded that Gd, differing from La by an increment of seven in atomic number, should have been separated from La with a decontamination factor of approximately 10^8 in the experiment reported in Table VI, $R = 0.25$, if the assumptions that $K_{(Z+1)} = 1.59K_Z$ and that the K values are independent of concentration in the ranges considered are valid. Since these assumptions are known to be approximated in fact, it seems safe to assume that the decontamination factor achieved was at least 10^5–10^6 as compared with the demonstrated decontamination factor of greater than 8. It may be noted that Gd was demonstrated to be decontaminated from Sm by a factor of approximately 30 in the same experiment.

By use of the continuous countercurrent extraction technique it seems likely, on the basis of the foregoing data, that the rare earths may be separated from non-rare earth impurities and fractionated into subgroups on an industrial scale. Large scale isolation of specific single rare earths in high purify also appears economically feasible.

Preliminary fractionation of the less abundant rare earths preparatory to final purification by an ion-exchange technique is another attractive possibility. For example (Table VII) a mass reduction of 90 for a Tm–Yb–Lu fraction has been obtained. Such a technique would permit the loading of a

larger quantity of the desired lanthanide on a given bed of exchanger.

The results of several experiments demonstrate the feasibility of using a TBP solution of the rare earths as the feed. Such an approach is especially promising, since the TBP feed may be prepared by contacting a solution of rare earth nitrates with TBP under conditions such that common contaminates such as Al, Mg, Ca, Na, etc., are removed before fractionation of the rare earths is undertaken. An equally important effect is the removal, by use of this procedure, of interfering ions such as phosphate and sulfate which lower the K's of the rare earths thereby shifting the position of the partitioning element to an atomic number higher than that calculated on the basis of data obtained using rare earths free from such ions.

It is felt that the major points of interest of this study, from the point of view of complex-forming tendencies of the lanthanides, are the remarkable constancy of the ratio of $K_{(Z+1)}$ to K_Z for a given TBP–nitric acid system and the inversion of the order of increasing extractability noted at approximately 3 M (in the aqueous phase) nitric acid. The explanation of the inversion is not known.

THE MECHANISM OF COAGULATION OF LYOPHOBIC SOLS AS REVEALED THROUGH INVESTIGATIONS OF SILVER HALIDE SOLS IN *STATU NASCENDI*[1]

By Božo Težak

In collaboration with E. Matijevic, K. Shulz, M. Mirnik, J. Herak, V. B. Vouk, M. Slunjski, S. Babić, J. Kratohvil and T. Palmar

Laboratory of Physical Chemistry, Faculty of Science, University of Zagreb, Zagreb, Yugoslavia

Received April 16, 1952

The coagulation values of several neutral electrolytes were determined for systems of silver halide sols in *statu nascendi* with various concentrations of stabilizing ions. The coagulations were observed tyndallometrically. The following electrolytes were tested: lithium, sodium, potassium, rubidium, cesium, calcium, uranyl, aluminum, thorium, and strychnine nitrate (sometimes of sulfate) in the cases of negative sols, and sodium nitrate, sulfate, dichromate, phosphate, acetate, propionate, butyrate, valerate and citrate in the cases of positive sols. In some systems the effect of hydrogen ion concentration was also systematically followed. Further, the coagulation values of potassium, barium, lanthanum and thorium nitrate in water–ethanol solutions were determined for negative sols of silver bromide. The development of some typical systems was observed also in water solutions of gelatin. It was shown that the systems with gelatin may be used for differentiation of the coagulation processes from the processes of growth of primary particles. In respect to the interpretation of the results it was pointed out that there is nearly linear relationship between the logarithm of the coagulation value and Bjerrum's critical distance for formation of stabilizing-coagulating ion-pairs. The similar relationship may be applied to systems with a changed dielectric constant (water–ethanol media).

In the process of precipitation of salts of small solubility from a solution of reacting electrolytes three stages may be distinguished: (1) nucleation, (2) regular or irregular growth, and (3) coagulation. All three stages are very dependent on the concentrational and other conditions of the precipitating system. By a systematical variation of the conditions, it may be possible to guide the precipitation in such a way that the stages (1) and (2) are very little affected thus allowing the examination of the practically isolated stage (3).

Actually, in a number of investigations we have been able to use the formation of heteropolar precipitates, especially, the precipitation of silver halides, as a very sensitive indicator for the coagulating effects of the neutral electrolytes.[2] The coagulation of such sols in *statu nascendi* should not be necessarily more complex than that of usual sols, while the simplicity of preparation of such systems, the definite ionic character of the colloidal particles, and the regularities of the phenomena observed, may be a valuable tool for clearing up not only the questions of the coagulating mechanism itself, but also its dependence on both controlling factors: that of the crystalline solid, and that of electrolytic solution, by which the composition of the critical transition layer on the surface of the precipitating particles, the so called methoric space,[3] is conditioned.

In this respect we are presenting a glimpse of several series of experimental results which may be taken as representative for the work done in our laboratory. For the experimental details and the potentialities of the method and technique used, our recent communications[4] may give the necessary information.

The Typical Precipitation Curve.—The starting point should be to ascertain the stability and instability regions of the typical precipitation curve[5] which may be obtained by taking the concentrations of the precipitation components reasonably small and constant, and varying systematically the excess

(1) Presented at the International Congress of Pure and Applied Chemistry, New York, September, 1951.

(2) B. Težak, *Z. physik. Chem.*, **191A**, 270 (1942); **192**, 101 (1943); *Arhiv kem.*, **19**, 19 (1947); B. Težak and E. Matijević, *ibid.*, **19**, 29 (1947); B. Težak, E. Matijević and K. Schulz, *ibid.*, **20**, 1 (1948); B. Težak, *ibid.*, **22**, 26 (1950); J. Herak and B. Težak, *ibid.*, **22**, 49 (1950); B. Težak, E. Matijević and K. Schulz, *J. Am. Chem. Soc.*, **73**, 1602, 1605 (1951); This Journal, **55**, 1558, 1567 (1951).

(3) Wo. Ostwald, *Kolloid-Z.*, **100**, 2 (1942); B. Težak, *Arhiv kem.*, **21**, 93, 96 (1949).

(4) B. Težak, E. Matijević and K. Schulz, *J. Am. Chem. Soc.*, **73**, 1602, 1605 (1951); This Journal, **55**, 1558, 1567 (1951).

(5) B. Težak, *Z. physik. Chem.*, **175A**, 219 (1935).

of the one of the ions from which the heteropolar crystal is composed.

On Fig. 1 the general feature of a typical precipitation curve (concentration tyndallogram) for the system 0.0001 *M* silver iodide in *statu nascendi* in aqueous solutions of various iodide (NaI) and silver ($AgNO_3$) ion activity, respectively, is given. The stabilization regions of the negative and positive systems show in longer periods of time characteristic changes, which are illustrated by the curves of Fig. 1. In recording such precipitation phenomena it is possible to make a rough distinction between very rapid, rapid, moderately rapid, slow and very slow processes of "development" or "aging." It may be assumed that the rapid processes are accomplished in time intervals varying from some fractions of a second to about 1 minute, the moderate in the course of 1 to 100 minutes, and the slow ones from about 2 hours to one week (100 to 10,000 minutes). For our purposes of primary importance are the transitional systems of rapid, moderately rapid and slow rate of change. The analysis of the kinetics of such precipitation processes was done elsewhere; as the critical time limit we chose 10 minutes for the systems of silver halides. The typical precipitation curve giving the turbidities of silver iodide 10 minutes after the preparation of the systems shows many different regions: (1) the complex solubility regions (−A and +A); (2) the so-called concentration maxima regions (−B and +B); (3) the stability regions (−C and +C); and (4) the so-called isoelectric or equivalency region (±D).

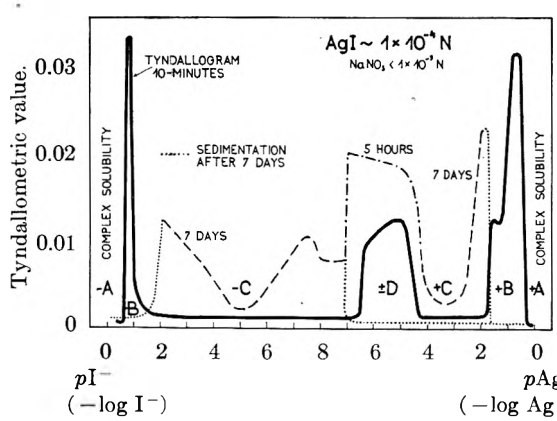

Fig. 1.—Typical precipitation curve of silver iodide for various excess of sodium iodide and silver nitrate, respectively.

The mode of action of neutral electrolytes on similar systems may be taken as decisive for distinction between the processes of crystalline growth and the agglomeration through coagulation. Figure 2 illustrates such effects. On the negative side there are the effects of sodium, barium and lanthanum nitrate, while on the positive side the corresponding influences are shown for sodium nitrate, sulfate and phosphate. The abscissas give, as in Fig. 1, the logarithm of activities of potential determining ions, and on the ordinates the logarithms of the critical concentrations for coagulation (coagulation values) are plotted. The situations given are those for 0.0001 *M* silver iodide 10 minutes after mixing of the components in water solution at 20° (the same conditions as for systems shown by the full line in Fig. 1). The upper portion shaded with slant lines illustrates the well advanced precipitation when sodium nitrate in critical concentrations was present in solution. The horizontal shading gives the growing portion of the precipitation region as a result of the effect of bivalent ions (barium nitrate and sodium sulfate, respectively), and the areas of vertical shading represent analogous effect of trivalent dominating ions (lanthanum nitrate and sodium phosphate). Similar relations were found with systems of silver chloride and silver bromide.

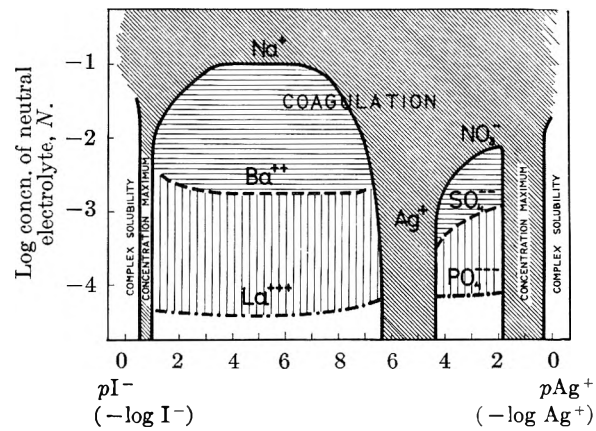

Fig 2.—Schematic presentation of critical coagulating concentrations of neutral electrolytes on systems of silver iodide given in Fig. 1.

The Gelatin Effect.—As an additional criterion for differentiation of the processes of coagulation from those of crystal growth, the gelatin effect on the precipitating system may be used. By observing the systems in the absence and in the presence of gelatin, it was possible to distinguish the crystallization from coagulation very sharply also in the cases where there are processes of mixed character. Thus, the region of isoelectric maxima, which by itself indicate the interaction of coagulating processes, may be examined with respect to its crystalline character. For example, with 0.5% gelatin it can be seen that the role of crystallization for the development of this isoelectric maximum is very different in cases of silver chloride, bromide and iodide (Fig. 3); the silver chloride and bromide

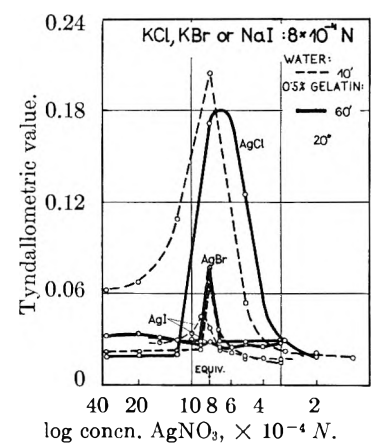

Fig. 3.—Effect of gelatin on precipitations of silver chloride, silver bromide and silver iodide in the equivalency region.

systems show, by application of gelatin, the retardation of the precipitation only, while in the case of silver iodide there is nearly complete inhibition. A similar effect is shown in Fig. 4 giving the concentration–tyndallograms for the systems: silver nitrate–potassium bromide–magnesium nitrate, without and with 0.001% gelatin, 10 and 60 minutes after mixing of the components.

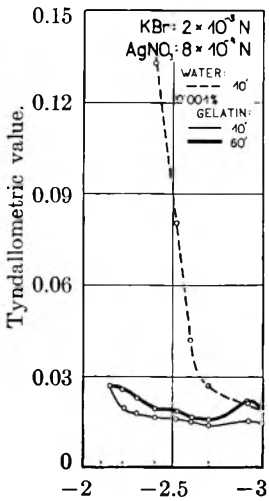

Fig. 4.—Effect of gelatin on coagulating action of magnesium nitrate.

In these, as in all other experimental systems referred to, the concentration data are given for whole volume of the solution, and the coagulation values are expressed as normalities of critical concentrations for coagulation 10 minutes after the preparation of the systems; the experimental temperature was 20°.

Coagulation of Negative Sols.—Generally, the effect of neutral electrolytes on silver chloride, bromide and iodide sols in *statu nascendi* are completely in accord with the old experiences of colloid science concerning the coagulation of lyophobic sols. For comparison, especially, may be taken the results from Kruyt's school.[6] As we are dealing with sols of very small concentrations (about 0.02 g./l.), in contrast to the usual coagulation experiments where much more concentrated sols were used, the results obtained are practically free from adsorption and other confusing effects. The relatively high precision and rapidity by which the coagulation values are determined, may give some preference to our method and technique in accumulation of data on which the theory of the coagulation could be built.

Figures 5 and 6 show the concentration tyndallograms illustrating the coagulation effects according to the rule of Schulze and Hardy, for sodium, calcium, aluminum and thorium nitrate and sulfate (Fig. 5), and according to the ionic sizes, for hydrogen, lithium, sodium, potassium, rubidium and cesium sulfate (Fig. 6), respectively; the concentration of silver bromide in *statu nascendi* amounted 1×10^{-4} *M*. On the abscissas there are the logarithms of concentration of the neutral electrolyte, and on the ordinates the tyndallometrical values, expressed in Sauer's units, 10 minutes after mixing of reacting components. The continuation of the linear trend of that part of the curve, which shows the greatest change in the rate of coagulation, indicates in its section with the axis of abscissas the critical concentration for coagulation (coagulation value). For the sake of brevity the majority of results presented here are such coagulation values.

Figure 7 gives a series of coagulation values for hydrogen, lithium, sodium, potassium, rubidium

(6) H. R. Kruyt and M. A. M. Klompé, *Kolloid-Beihefte*, **54**, 484 (1943).

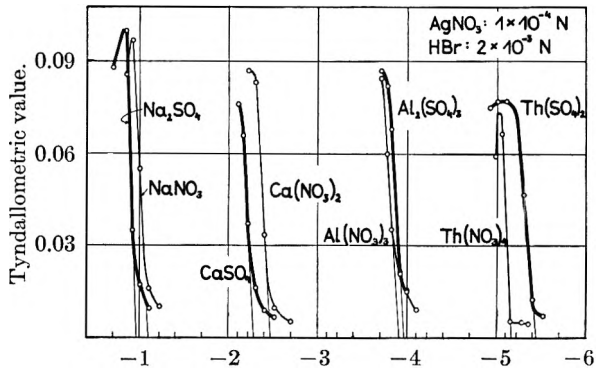

Fig. 5.—Critical coagulating concentrations of 1–1, 1–2, 2–1, 2–2, 3–1, 3–2, 4–1 and 4–2 neutral electrolytes for silver bromide sol in *statu nascendi*.

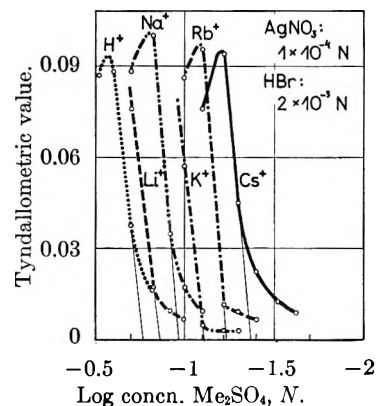

Fig. 6.—Critical coagulating concentrations of H, Li, Na, K, Rb and Cs sulfate for silver bromide sol in *statu nascendi*.

and cesium sulfate in a plot of the logarithm of coagulation value against logarithm of the concentration of the stabilizing bromide ion. Similar curves for nitrates are given in Fig. 8. The difference in the behavior between sulfates and nitrates should be noticed. The order of coagulation values is influenced also by the concentration region of the stabilizing ion.

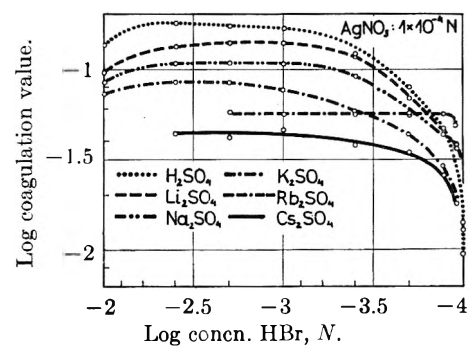

Fig. 7.—Coagulation values of H, Li, Na, K, Rb and Cs sulfate for silver bromide sols in presence of various concentrations of hydrobromic acid.

In Fig. 9 there are concentration tyndallograms once more, but showing the coagulation effects of various cations; aluminum and thorium nitrate change their coagulation values with "aging" of their water solutions; this effect can be explained by assuming the formation of various complex ions.

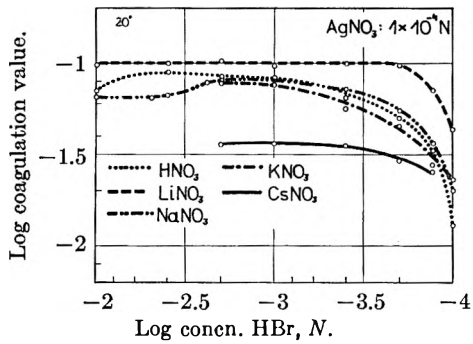

Fig. 8.—Coagulation values of H, Li, Na, K and Cs nitrate for silver bromide sols in presence of various concentrations of hydrobromic acid.

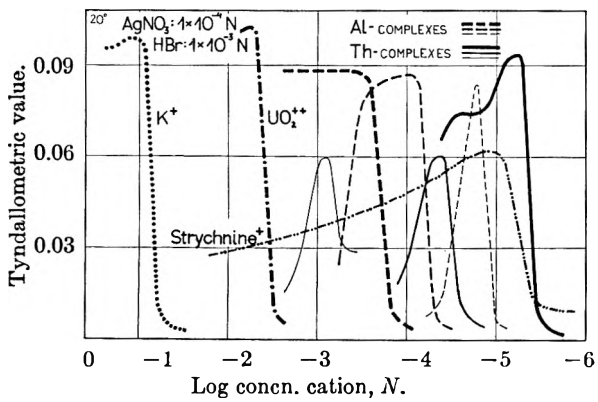

Fig. 9.—Critical coagulating concentrations of K, UO_2, Al, Th and strychnine nitrate for silver bromide sols in *statu nascendi*.

Coagulation of Positive Sols.—Similar coagulation effects are found with systems of silver halides with an excess of silver ions, but this time for the dominating anion of the electrolytic solution.

Since the hydrogen ion concentration may influence the coagulation values of the anions very greatly, systematic investigations were made of the systems where various amount of nitric acid was added. Figure 10 represents the variation of coagulation values of the salts of lower fatty acids with hydrogen ion concentration; ordinates give *p*H values as determined by glass electrode and the abscissas the logarithm of corresponding coagulation value.

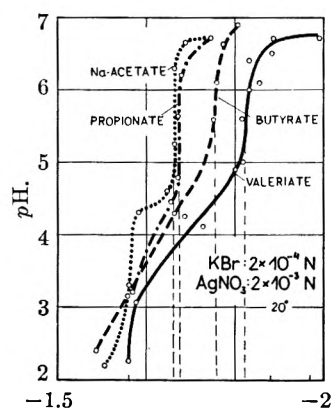

Fig. 10.—Plot of log of coagulation values of sodium acetate, propionate, butyrate and valerate *vs.* *p*H (nitric acid) for silver bromide sols in *statu nascendi*.

The coagulation values of sodium citrate in systems with various hydrogen ion concentration also were determined. Figure 11 gives change of the coagulation values of sodium citrate with *p*H value for systems where the concentration of silver nitrate was varied. If the logarithm of coagulation

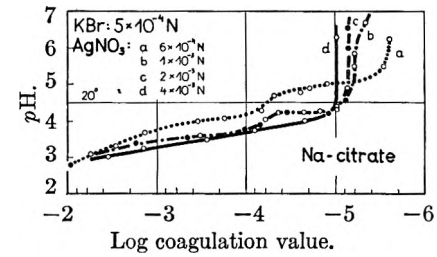

Fig. 11.—Plot of log of coagulation values of sodium citrate *vs.* *p*H (nitric acid) for the systems of silver bromide in presence of various concentrations of silver nitrate.

values corresponding to the same *p*H value and various concentrations of potential determining silver ion are taken, and plotted against the logarithm of the concentration of the stabilizing ion (abscissas), curves shown on Fig. 12 are obtained.

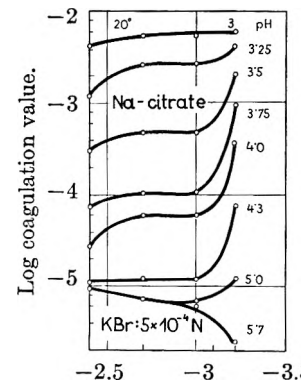

Fig. 12.—Coagulation values of sodium citrate for silver bromide sols in medium of various *p*H (nitric acid).

In Fig. 13 the tyndallograms are given for sodium nitrate, sulfate, dichromate, phosphate and citrate as an illustration of the rule of Schulze and Hardy.

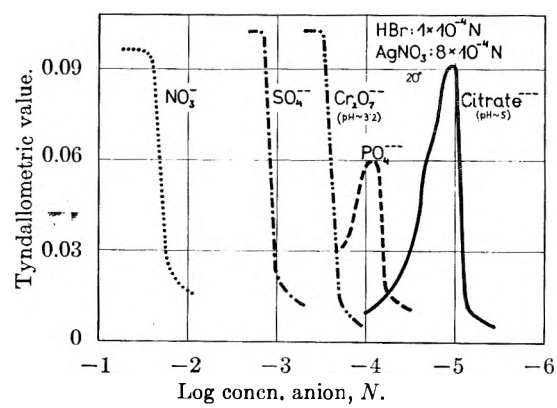

Fig. 13.—Critical coagulating concentrations of sodium nitrate, sulfate, dichromate, phosphate and citrate for silver bromide sols in *statu nascendi*.

Effect of Water–Ethanol Media.—For investigation of the influence of dielectric constant on coagulation value, water–ethanol mixtures were used, and

the coagulation values determined for various concentrations of the stabilizing ion.

On Fig. 14 the logarithms of coagulation values for potassium nitrate are plotted against the logarithm of the concentration of hydrobromic acid for various wt. % ethanol. Similar relations for

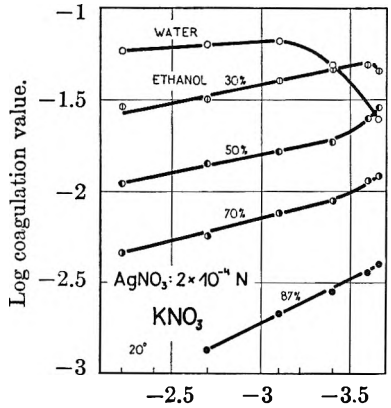

Fig. 14.—Effect of ethanol on the coagulation values of potassium nitrate for silver bromide sols in presence of various concentrations of hydrobromic acid.

barium and lanthanum nitrate are represented in Figs. 15 and 16, respectively. In all these cases the coagulation value systematically decreases as the content of ethanol is increased. This effect could be predicted from data on solubility and conductivity measurements. The electrical effects of interionic interactions are more pronounced in a medium with lower dielectric constant. But there are cases also where the opposite effect can be found.

Discussion

There are many theories of coagulation of hydrophobic sols. Some of them concentrate on the situation on the wall or in the double layer, the other stress the decisive influence of the electrolytic solution. All simple conceptions of the role of neutralization of particle charges (Linder and Picton), of the exchange of ions (Duclaux), of the critical electrokinetic potential (Powis), of the adsorption effects (Freundlich), have proved inadequate. The same may be said for Ostwald's[7] theory of the role of activity coefficient of the dominating ion in solution. In this respect the efforts of Verwey and Overbeek[8] cannot be taken as successful; on the contrary, they try, on the same line as Hamaker and others did, to solve the problem of colloidal stability by introducing the new undetermined factor, that of the attraction resulting from van der Waals–London forces.

In our attempt to interpret the coagulating mechanism we tried to find the relation between the role of the crystal, the composition of the transition layer (methoric layer) and the solution. The coagulation phenomenon itself is an abrupt, very sensitive, and characteristic process, that may be taken as an "internal signal" of correspondence

(7) Wo. Ostwald, *Kolloid-Z.*, **73**, 301 (1935); THIS JOURNAL, **42**, 981 (1939); *Kolloid-Z.*, **94**, 168 (1941).

(8) E. J. W. Verwey and J. Th. Overbeek, "Theory of the Stability of Lyophobic Colloids," Elsevier, New York, N. Y., 1948.

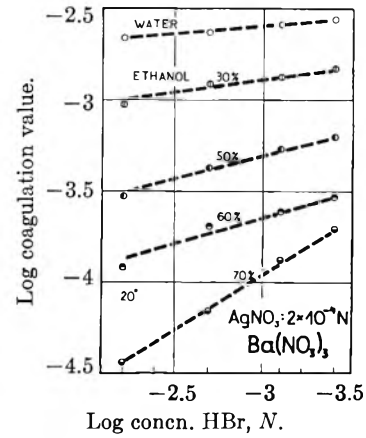

Fig. 15.—Effect of ethanol on the coagulation values of barium nitrate for silver bromide sols in presence of various concentrations of hydrobromic acid.

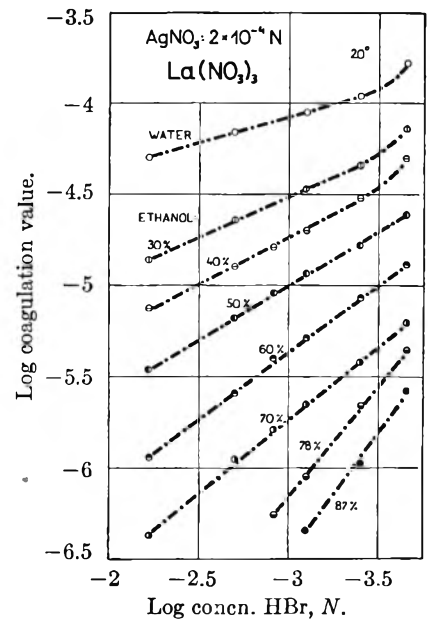

Fig. 16.—Effect of ethanol on the coagulation values of lanthanum nitrate for silver bromide sols in presence of various concentrations of hydrobromic acid.

between the states of systems under observation.

The significant effects of neutral electrolytes were studied on systems where it could be reasonably supposed that the process of the formation of primary particles was very little affected by such electrolytes. It may be that the sensibility of the systems is very much influenced by the dispersity of the particles, but as we always observed tyndallometrically the abrupt changes in the process of agglomeration of the primary particles of about 30 mμ to secondary structures of about 300 mμ, the results obtained may be taken as comparable. Therefore, as the factors in our experiments may be mentioned: (1) the character of the solid as reflected in the crystal lattice, the solubility of the crystalline phase and the specificity of the ions from which the colloidal particles are composed; (2) the characteristics and concentration of the lattice ion in excess; (3) the electrolytic composition of the media; (4) the dielectric properties of the media; and (5) the concentration of the precipi-

tated mass influencing the number and size of primary particles.

The experimental results already presented show some regularities which cannot be neglected. The behavior according to the Schulze–Hardy rule gives very expressively the valency effects, while the influence of ionic size is also very marked. Both groups of effects must be taken as dependent on the distribution of ions on the wall, in the methoric space, and in the solution. Within certain limits the joint regulating factor for the stability of the system is the distribution of the stabilizing ion, in the majority of cases of the lattice ion in excess. With respect to the amount of adsorbed stabilizing ions there are the results of Kruyt's[9] school. It may be taken for our systems that the adsorbed amount of the stabilizing ion corresponds to about 0.5% of the free surface of the colloid particles. Further, it is assumed that the stabilizing ions are distributed in a nearly uniform manner throughout the exposed surface. Thus the distances between neighboring stabilizing ions are about 30 Å. (one ion on 1000 Å.^{2}). For such a distribution it is possible to consider the interaction between the stabilizing ion and the ion in solution (counter ion) as a separate elementary process uninfluenced by the similar interactions in the neighborhood. Thus, many of the coulombic interactions of the association–dissociation equilibria related to the ion-pair formation in the solution must be fully reflected in the slightly modified circumstances where one of the partners of the ion-pair is fixed on the wall. This is our basic conception about the configuration of the boundary region.

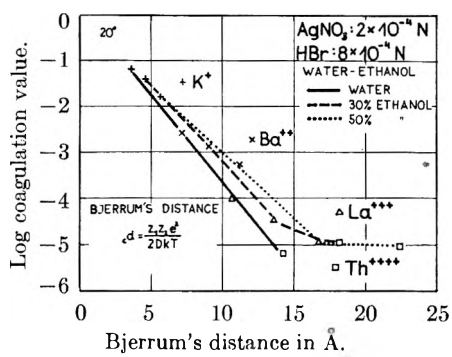

Fig. 17.—Plot of Bjerrum's distance in Å. *vs.* log of coagulation of K, Ba, La and Th nitrate for silver bromide sols for water, 30 and 50 wt. % ethanol media.

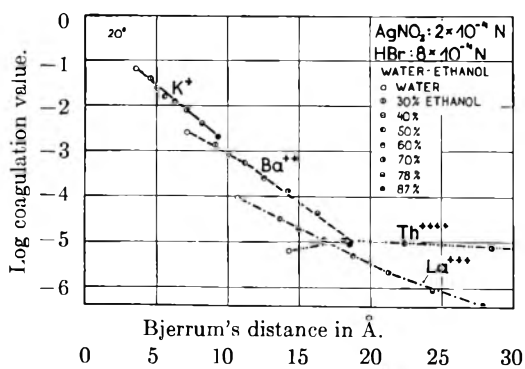

Fig. 18.—Plot of Bjerrum's distance in Å. *vs.* log of coagulation values of K, Ba, La and Th nitrate for silver bromide sols for water, 30, 40, 50, 60, 70, 78 and 87 wt.% ethanol media.

The first impulse for coagulation is certainly given by the disturbance of the dynamical equilibria maintained between the ionic charges distributed on the surfaces of the particles and the ions of the quasi-crystalline structure of the electrolytic solution. Thus the common elementary process which must be considered first is the formation of ionic pairs between the ions of opposite sign. We are dealing here primarily with systems of strong electrolytes where the ions are specially distributed. On the one side there are stabilizing ions fixed on the wall, and on the other side the statistical-kinetical distribution of the ions in solution. All these ions interact with each other but for us of special interest are possibilities of interaction of counter ions with ions of opposite sign. When interpreting such interactions we found especially valuable to use the concept of Bjerrum's critical distances[10] for the formation of ion-pairs

$$_cd = z^2e^2/2DkT$$

Figures 17 and 18 give such relationship between the logarithm of coagulation values and the Bjerrum distance corresponding to the stabilizing-coagulating ion interaction. Figure 17 gives these relationships for some of our systems of Figs. 14, 15 and 16. The linear course for water and 30 and 50 wt. % ethanol systems through the concentrational range from 0.1 to 0.00001 *N* is quite striking. Of course, there are special features for various systems; discrepancies are found quite often, but this relationship is worthwhile considering.

Generally, as to the character of the interaction between the stabilizing and the coagulating ion two cases may be distinguished: (1) when pure electrostatic associations prevail, (2) when associations are due to the combined electrostatic and chemical effects.

For a more general presentation of these relations based on the statistical distribution of the ions in solution, Fig. 19 may be used, where the legends are self explanatory.

Accordingly, it seems that the principal condition for coagulation of hydrophobic sols is the relation between the concentration of the associating and dissociating ions in the close neighborhood of the sol particles and in the solution in bulk. As the first named concentration is governed by the density of distribution of the stabilizing ions fixed on the wall, the critical stability–instability stage is reached when the distribution of the ions in solution is of greater density than that corresponding to the ions in the methoric space. The higher osmotic pressure of the ionic system in the interior of the solution may be taken in such circumstances as a cause for the diffusion of the solvent molecules from the methoric layer into solution, and thus—as a consequence—as working toward the diminution of the exposed surface. On the ground of such qualitative explanation also the quantitative expressions could be worked out which may follow

(9) E. J. W. Verwey and H. R. Kruyt, *Z. physik. Chem.*, **167A**, 137 (1933); A. Basiński, *Rec. trav. chim.*, **59**, 331 (1940).

(10) N. Bjerrum, *Kgl. Danske Videnskab. Selskab. Math.-fys. Medd.*, **7**, 9 (1926); "Selected Papers," Copenhagen, 1949, p. 108.

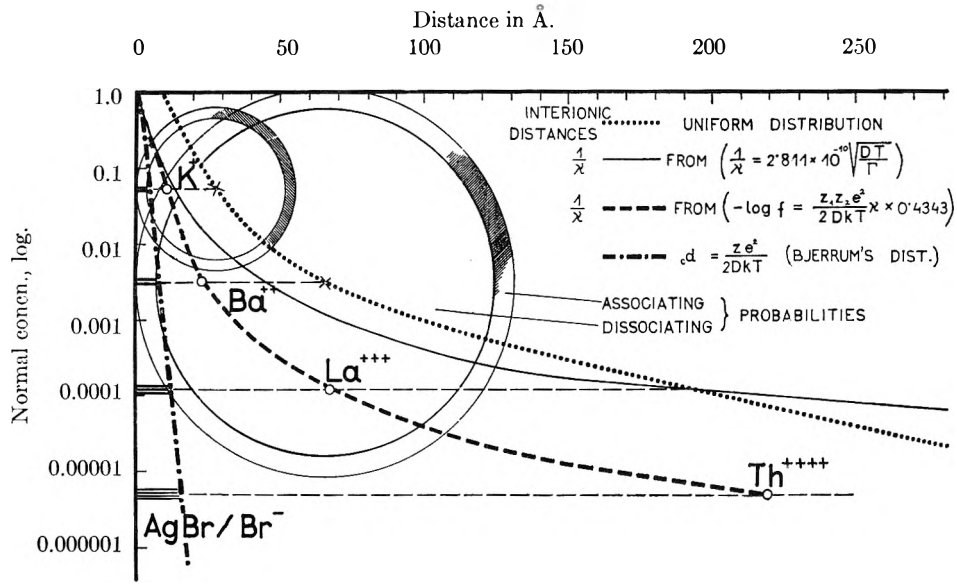

Fig. 19.—Schematic presentation of the relationship between critical distances (— · — · — line), thicknesses of ionic atmosphere (——— curve), and distances between ions when uniformly distributed in solution (. . . . . curve) *vs.* logarithm of coagulation value for ions of various valencies. The circles represent the ionic distribution spheres, while the partially shaded shells give probabilities of association of the stabilizing-coagulating ion-pairs.

the interpretation forwarded by Langmuir[11] concerning the role of attractive and repulsive forces in the formation of colloidal systems.

(11) I. Langmuir, *J. Chem. Phys.*, **6**, 873 (1938).

DIFFUSION IN A CENTRAL FIELD DUE TO VAN DER WAALS ATTRACTION

By R. S. Bradley

Department of Inorganic and Physical Chemistry, University of Leeds, Leeds, England

Received June 19, 1952

The influence of intermolecular attraction on the rate of diffusion has been studied for the evaporation of a drop at the center of a spherical enclosure and for diffusion of solute molecules up to another solute molecule. For the first example the effect is very small and no correction is necessary for diffusion coefficients deduced from observations on evaporating drops. For diffusion in solution the rate for a typical example may be increased by 28%.

Introduction

Several problems in physical chemistry depend on the theory of diffusion up to or away from a sphere, for instance the rate of coagulation of colloids, treated by Smoluchowski,[1] the evaporation kinetics for liquid drops and the collision frequency of molecules in solution.[2] It is usually assumed in these problems that the sole driving force for diffusion arises from the concentration gradient, whereas in fact there will be an additional force due to intermolecular attraction. This paper deals with the modification of the diffusion equations for spherical symmetry due to the presence of such intermolecular forces.

The problem of the kinetics of the coagulation of colloids has already been treated by Fuchs[3] and also by Tikhomirov, Tunitzky and Petrjanov.[4] The latter authors based their theory on the calculations of the writer on the interaction energy of spheres[5] and found at room temperature that the influence of interparticle forces might be expected to increase the coagulation constant by approximately 20% in comparison with their experimental increases of 25, 22 and 30% for mineral oil, tricresyl phosphate and sulfuric acid aerosols, respectively. It is the purpose of this paper to examine the problem for evaporation kinetics and for collision frequencies in solution (of importance in reaction kinetics in solution).

Diffusion Theory for Drops of Liquid Evaporating in a Gas.—A drop of liquid evaporates in a spherical enclosure which contains the gas and has absorbent walls. For spherical symmetry the diffusion equation may be written in the form

$$D\,\mathrm{d}^2(cr)/\mathrm{d}r^2 = r\mathrm{d}c/\mathrm{d}t \qquad (1)$$

(1) M. von Smoluchowski, *Z. physik. Chem.*, **92**, 129 (1918).

(2) R. S. Bradley, M. G. Evans and R. W. Whytlaw-Gray, *Proc. Roy. Soc. (London)*, **A186**, 368 (1946); J. Birks and R. S. Bradley, *ibid.*, **A198**, 226 (1949); R. S. Bradley and A. D. Shellard, *ibid.*, **A198**, 239 (1949); R. S. Bradley, *J. Chem. Soc.*, 1910 (1934); *Trans. Faraday Soc.*, **33**, 1185 (1937).

(3) N. Fuchs, *Z. Physik*, **89**, 736 (1934).

(4) M. V. Tikhomirov, N. N. Tunitzky and J. B. Petrjanov, *Acta Physicochim. U. R. S. S.*, **17**, 185 (1942).

(5) R. S. Bradley, *Phil. Mag.* **13**, 853 (1932); *Trans. Faraday Soc.*, **32**, 1088 (1936).

where D is the diffusion coefficient appropriate to the gas pressure, c the concentration of vapor molecules per cc., r the distance from the drop center, which is also the center of the sphere, and t the time. The evaporation will first be considered in the absence of a force field. Suppose that the enclosure is so large as to have virtually infinite radius and that the absorbent is such that the vapor pressure at the walls is virtually zero (if these conditions do not hold, corrections are easily made). A drop placed in such an enclosure will build up a vapor atmosphere which is graded in concentration from the drop surface to the wall, c being a function of the radius and of the time. The general solution is complicated, involving terms proportional to the time and others to the square root of the time, but if the time is sufficient the latter become negligible and an almost stationary state is reached. In experimental practice such a state is very quickly set up, with dc/dt virtually zero. The calculations of Luchak and Langstroth,[6] in which the approach to the stationary state is studied by successive approximations, support the view that little error is introduced by assuming such a state to be rapidly achieved.

In the stationary state the flux per spherical shell (X_0 molecules per second outwards) is independent of the radius of the shell, *i.e.*

$$X_0 = -4\pi r^2 D\, dc/dt = \text{constant} \qquad (2)$$

in agreement with (1) with $dc/dt = 0$. In the proximity of the drop we take the vapor molecular concentration to be c_0, *i.e.*, the value appropriate to the saturation pressure, it being assumed that $c = c_0$ at $r = R + d$, where R is the radius of the drop and d the molecular diameter (*cf.* Fig. 1). Refinements in the theory according to which a vapor envelope of concentration $<c_0$ is built up at some distance from the drop are neglected (*cf.* Bradley[2]). We also assume $c \to 0$ at $r \to \infty$. Hence

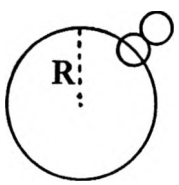

Fig. 1.

$$X_0 = 4\pi(R + d)Dc_0 \qquad (3)$$

If may be noted that $c = X_0/(4\pi Dr)$, and hence the vapor concentration does not drop linearly with radius.

In the presence of a force field the equation of diffusion becomes

$$-X = 4\pi r^2[D\, dc/dr + cD/(kT) \times dE(r)/dr] \qquad (4)$$

in place of equation (2), where X is the flux per spherical shell and where the second term on the right arises from the van der Waals force, which imparts a drift velocity according to Einstein's theory; $E(r)$ is the potential energy of a vapor molecule due to the presence of the liquid drop when the center of the latter is a distance r from the center of the molecule; k is the Boltzmann constant and T the absolute temperature.

Equation (4) may be integrated by multiplying throughout by

$$e^{\int \frac{dE(r)}{dr}\frac{dr}{kT}} = e^{E(r)/kT}$$

Taking $c \to 0$, $E(r) \to 0$ when $r \to \infty$, and $c = c_0'$ at $r = R + d$, we have

$$\frac{X}{4\pi D} = \frac{c_0' e^{E(R+d)/kT}}{\int_{R+D}^{\infty} \frac{e^{E(r)/kT}}{r^2}\, dr} \qquad (5)$$

Hence

$$\frac{X}{X_0} = \frac{c_0'}{c_0} \frac{e^{E(R+d)/(kT)}}{(R+d)\int_{R+d}^{\infty} \frac{e^{E(r)/kT}}{r^2}\, dr} \qquad (6)$$

Putting

$$c_0' = c_0 e^{-E(R+d)/kT}$$

according to Boltzmann's theory, we have

$$\frac{X_0}{X} = (R+d)\int_{R+d}^{\infty} \frac{e^{E(r)/(kT)}}{r^2}\, dr \qquad (7)$$

The value of $E(r)$ may be calculated using the method of the writer,[5] taking the energy between two molecules the centers of which are a distance r apart to be λ/r^6, *i.e.*, London[7] quantum mechanical forces of attraction are assumed and repulsion is neglected for simplicity. If the liquid drop contains q molecules per cc. the potential at P (Fig. 2)

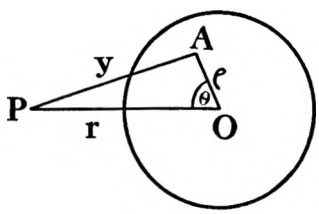

Fig. 2.

due to a polar element of volume $\rho^2 \sin\vartheta d\theta d\phi d\rho$ at A, this element being inside the sphere and distant ρ from the center, will be

$$-q\lambda\rho^2 \sin\theta\, d\theta d\phi d\rho/y^6$$

where $AO = \rho$, $PA = y$. Hence the potential at P due to a spherical shell of radius ρ and thickness $d\rho$ is

$$-\lambda q\rho^2\, d\rho \int\int \sin\theta\, d\theta d\phi/y^6$$

Since $PA^2 = y^2 = r^2 + \rho^2 - 2r\rho\cos\theta$, the potential at P due to the spherical shell is

$$\frac{-2\pi\rho q\lambda d\rho}{r}\int_{r-\rho}^{r+\rho} dy/y^5 = \frac{\pi\lambda q d\rho}{2r}\left[\frac{\rho}{(r+\rho)^4} - \frac{\rho}{(r-\rho)^4}\right] = Y d\rho$$

The potential of the whole sphere at P is

$$\int_0^R Y d\rho = \frac{\pi\lambda q d\rho}{2r}\left[\frac{-1}{2(r+R)^2} + \frac{r}{3(r+R)^3} + \frac{1}{2(r-R)^2} - \frac{r}{3(r-R)^3}\right]$$

or

$$E(r) = -\frac{4}{3}\pi\lambda q\, R^3/(r^2 - R^2)^3 \qquad (8)$$

Hence

$$X_0/X = (R+d)\int_{R+d}^{\infty} \frac{e^{-(4/3)\pi\lambda q R^3/[(r^2-R^2)^3 kT]}}{r^2}\, dr \qquad (9)$$

When the index of the exponential is sufficiently small the integral may be evaluated by expanding the exponential, giving as a first approximation

(6) G. Luchak and G. O. Langstroth, *Can. J. Research*, **A28**, 574 (1950).

(7) F. London, *Trans. Faraday Soc.*, **33**, 8 (1937).

$$\frac{X_0}{X} = 1 + \frac{4}{3}\frac{\pi\lambda q}{kT}(R+d)\left[\frac{1}{R^3(R+d)} + \frac{15}{16R^4}\log\frac{d}{R+d} + \frac{14}{16}\frac{(R+d)}{R^3 d} - \frac{(R+d)}{4Rd^2\ (2R+d)^2}\right] \quad (10)$$

If this method of expansion is not allowed (9) may be evaluated by graphical integration. As a typical example evaporative diffusion from n-$C_{16}H_{34}$ may be considered, using the data of the writer and Shellard[2]; λ may be calculated from the approximate formula due to London,[7] namely

$$\lambda = \frac{LV^2 \times 1.602 \times 10^{-12}}{3.04 \times 10^{62}} \quad (11)$$

where L is the latent heat of vaporization in cal. per mole, V is the molar volume, and λ is expressed in erg. cm.[6]. For n-$C_{16}H_{34}$, L = 19,170 cal. per mole, V = 292 cc., $q = 2.06 \times 10^{21}$ molecules per cc., $d = 9 \times 10^{-8}$ cm. We may assume R = 0.1 cm., T = 293°K., which gives by graphical integration that X_0/X differs from unity by only 2.5×10^{-6}. It follows that the correction is negligible and that diffusion coefficients calculated by this method may be accepted with confidence.

The Rate of Diffusion of Solute Molecules up to Another Solute Molecule.—(*Cf.* (2), last two references.) In this instance, assuming a steady state, with $c \to c_0$ at $r \to \infty$, we have

$$c = c_0 e^{-E(r)/kT} + X\frac{e^{-E(r)/kT}}{4\pi D}\int_\infty^r \frac{e^{E(r)/kT}}{r^2}\,dr \quad (12)$$

taking X as representing the flux inwards. D is an effective diffusion coefficient, *i.e.*, the sum of the diffusion coefficients of two molecules (*cf.* Smoluchowski[1]). Since $c = 0$ at $r = 2d$ (annihilation by reaction)

$$X = \frac{4\pi D c_0}{\int_{2d}^\infty \frac{e^{E(r)/kT}}{r^2}\,dr} \quad (13)$$

It follows that

$$X_0/X = 2d\int_{2d}^\infty \frac{e^{E(r)/kT}}{r^2}\,dr \quad (14)$$

where X_0 refers to the flux when $E(r) = 0$ for all values of r. If we write $E(r) = -\lambda_{12}/r^6$, we have

$$X_0/X = 2d\int_{2d}^\infty e^{-\lambda_{12}/(r^6 kT)}\,dr/r^2 = 1 - \lambda_{12}/(448 d^6 kT) \quad (15)$$

if the index of the exponential is sufficiently small. We may consider a hypothetical example for which $\lambda_{12} = 5 \times 10^{-57}$ erg cm.,[6] $d = 3 \times 10^{-8}$ cm. Then by graphical integration we find X/X_0 = 1.28 at 293°K., *i.e.*, the inclusion of the van der Waals force makes a considerable difference to the rate of diffusion.

THE EXCHANGE REACTION BETWEEN DEUTERIUM AND AMMONIA ON THE SURFACE OF METAL POWDERS

BY JOEL R. GUTMANN

Scientific Department, Israeli Ministry of Defence, Jerusalem

Received July 9, 1952

The isotopic exchange between ammonia and deuterium has been investigated on pure iron and nickel powders at temperatures between 210 and 319°. The exchange law has been calculated; it differs slightly from a first-order law. The experimental rate of exchange on iron is independent of the ammonia pressure and of the first order with regard to deuterium. The activation energy is 17.5 kcal/mole. A peculiar reversible poisoning effect has been found on the nickel catalyst.

It has been known for some time that on metal surfaces ammonia decomposes even at room temperature readily according to the following sequence of reactions[1,2]

$$NH_3 \longrightarrow NH_2 + H$$
$$NH_2 \longrightarrow NH + H$$
$$NH \longrightarrow N + H$$

The subsequent study of this process in the form of ammonia–deuterium exchange on an evaporated iron film,[3] led to the conclusion that this exchange is of zero order with regard to ammonia and of the order 0.5 regarding the deuterium; this was interpreted to mean that the rate determining step in the exchange is the combination of adsorbed NH_2 radicals with deuterium atoms. This simple picture of the situation has recently been obscured by the results of Weber and Laidler[4] and of Singleton, Roberts and Winter.[5] The former deduced from their experiments on a promoted iron powder (static system, higher pressures, temperatures below 200°) for the reaction rate a complicated dependence on the pressure of ammonia and on the 0.5th power of the deuterium pressure, whilst the latter on evaporated metal films and at somewhat higher temperatures (semi-flow system) observed the reaction to be of the first order with regard to deuterium, and with regard to ammonia either of zero order or even inhibited by this compound.[5]

The results of the present investigation which had been undertaken before the publications of Weber and Laidler[4] and of Singleton and co-workers,[5] are believed to contribute somewhat to the clarification of the situation. The experiments were carried out in a static system and at intermediate temperature, using both pure iron and nickel powders;

(1) H. S. Taylor and J. C. Jungers, *J. Am. Chem. Soc.*, **57**, 660 (1935).

(2) W. Frankenburger and A. Hodler, *Trans. Faraday Soc.*, **28**, 229 (1932).

(3) A. Farkas, *ibid.*, **32**, 416 (1936).

(4) G. Weber and K. J. Laidler, *J. Chem. Phys.*, **19**, 1090 (1951).

(5) J. Singleton, E. Roberts and E. Winter, *Trans. Faraday Soc.*, **47**, 1318 (1951).

(6) The important publication by Ch. Kemball, *ibid.*, **48**, 254 (1952), came into our hands only after the present paper had been submitted for publication. Kemball's results do not affect the aspects of the problems to which this investigation is devoted.

they appear to be in satisfactory accord with the results of Singleton, Roberts and Winter.[5]

Apparatus and Methods.—The apparatus used in the work, which could be evacuated to 10^{-6} mm. of mercury, is schematically reproduced in Fig. 1. The catalyst container R (60 cc.), made of Pyrex, is heated by an automatically regulated electric furnace of large heat capacity. With the thermocouple T, it was ascertained that during a run the temperature did not change by more than 1°. With the combined gas buret and Toepler pump P, first deuterium was transferred from the storage vessel into A and from there compressed into B, a vessel of known volume, in which the D_2 pressure was determined by means of the manometer C. In the same way, ammonia was then transferred into A and B. From the pressure of the mixture, read off the manometer C, its composition was determined with an accuracy of 1%. The mixture was then introduced into R and the pressure read off the manometer M. The whole system (outside the reaction vessel R) was evacuated, the trap T_1 cooled with liquid air and, from time to time, samples were withdrawn by a fine capillary (which extended into the center of R) into the sampling tube S (volume about 1 cc.). The dead volume of the capillary and the loss of material through sampling could be neglected.

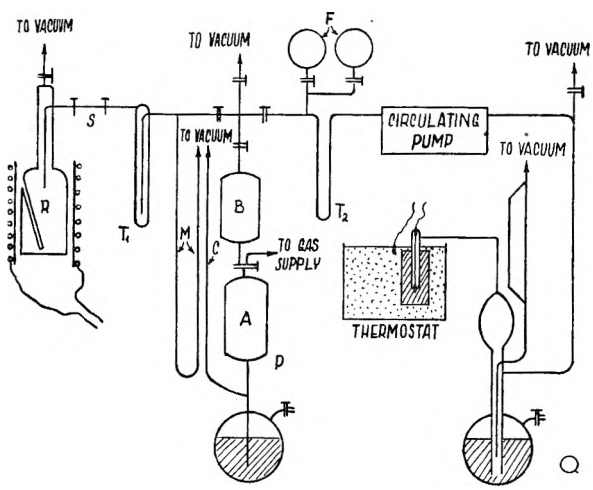

Fig. 1.—The apparatus.

The temperature range investigated was between 240 and 320°, the pressure range between 20 and 250 mm., for both deuterium and ammonia.

Materials.—Ammonia was dried by passage through calcium oxide, purified by fractional distillation *in vacuo* and stored over distilled sodium metal.

Deuterium was prepared by electrolysis of heavy water (d^{20}_4 1.10487), using anhydrous potassium sulfate as electrolyte and platinum electrodes, and was purified by passage through a palladium tube.

Hydrogen was obtained by electrolysis of a 30% sodium hydroxide solution and purified in the same manner.

As catalysts, one sample of nickel powder and two of iron powder were used; one was a commercial (May & Baker) reduced iron, the other had been prepared according to Vanino.[7]

They were reduced *in situ* by a stream of hydrogen for about 10 hours at 350° and outgassed at the same temperature until the pressure remained constant for some time. After this operation, the catalyst was only in communication with the remainder of the apparatus when hot; it was outgassed at 350° before and after each run. The catalysts did not change the deuterium content of 35 cc. D_2 by more than 0.5%, when kept in contact with the gas at 275° for one hour.

Analytical.—The exchange reaction was followed by measuring the decrease in the D content of the hydrogen by means of a thermal conductivity gage.[8] The samples in tube S were freed from ammonia by passage through the cold traps T_1 and T_2 and pumped into the gage Q by a one-stage mercury diffusion pump of small volume.[9] The pressure in the gage (tungsten spiral of 110 ohm resistance) was adjusted to about 50 mm. and measured by means of a cathetometer to 0.1 mm., sticking of the mercury being prevented by a drop of Apiezon oil. The gage head dipped into an oil thermostat, kept at about 32°, constant to ±0.02°. Measurements were made by the "constant resistance" method, the whole bridge circuit also being thermostated. When the gage head dipped directly into the oil thermostat, the bridge could not be accurately set to zero, but fluctuated erratically. This was found to be due to the fact that the glass wall was a little hotter than the thermostat and was unequally cooled through unequal streaming of the liquid. The gage head was therefore encased in a small copper block, thermal contact being provided by mercury. The block itself served as one of the electrical leads to the gage. This eliminated the fluctuations entirely.

The gage readings were checked by standard gas mixtures (storage flasks F). The D content of the samples could be determined to ±0.2%, but was usually measured to within 0.5%. The whole system outside the catalyst chamber did not cause any exchange between ammonia and deuterium to occur.

Results and Discussion

Whilst Singleton and co-workers[5] calculated the rate of the exchange reactions empirically as

$$K = K_e x_\infty$$

where K_e was obtained from the first-order plot of $-\log(1-\gamma)$ against the time t, a different, more theoretical, method was employed in the present investigation, following the lines suggested by Harris[10] for the kinetics of isotopic exchanges.

The equilibrium which in fact includes in addition to the starting materials all the species NH_2D, NHD_2, ND_3, HD and H_2, is treated by substituting the idealized equation: "light ammonia" + "heavy hydrogen" $\rightleftarrows$ "heavy ammonia" + "light hydrogen." The term "light (heavy) ammonia" includes all ammonia molecules that can exchange an H atom (D atom) for a D atom (H atom), the molecule NH_2D, for example, being counted twice as light and once as heavy ammonia.

Let us assume the forward and back reaction to have the same dependence on ammonia and hydrogen pressures, but the rate to differ by a factor $\epsilon = \overrightarrow{R}/\overleftarrow{R}$ due to the isotope effect. In practice, ϵ is 1.675 at 245° as calculated from the equilibrium composition. This treatment disregards the different reactivities of the isotopic species NH_3, NH_2D and NHD_2 in the forward reaction and of NH_2D, NHD_2 and ND_3 in the back reaction.

Starting from pure NH_3 and D_2, the *observable* rate of exchange can then be expressed as

$$\frac{dx}{dt} = \frac{a-x}{a}\frac{b-x}{b}\overrightarrow{R} - \frac{x^2}{ab}\overleftarrow{R} = \frac{\epsilon-1}{ab}\overleftarrow{R}\left(x^2 - \frac{\epsilon(a+b)}{\epsilon-1}x + \frac{\epsilon ab}{\epsilon-1}\right) \quad (1)$$

where $a = 3C_{\text{ammonia}}$; $b = 2C_{\text{hydrogen}}$; R is the *true* rate of exchange and the D content of the hydrogen is given by $(b-x)/b$.

Equation (1) presupposes tacitly that there is no marked difference in isotopic composition on the catalyst and in the gas phase. To check this point, pure NH_3 was made to react with mixtures of light and heavy hydrogen. The

(7) Vanino, "Handbuch der praeparativen Chemie," 3rd edition, Stuttgart, 1925, p. 626.

(8) H. W. Melville and J. L. Bolland, *Trans. Faraday Soc.*, **33**, 1316 (1937).

(9) H. P. Waran, *J. Sci. Instruments*, **1**, 53 (1923).

(10) G. M. Harris, *Trans. Faraday Soc.*, **47**, 716 (1951).

following table summarizes the results; it shows that the assumption made is reasonable.

Initial % D in hydrogen	Initial rate, v_0	$v_0/\%D$	
38.5	19	49	
54	24	45	mean 44
59	24	42	
100	46	46	

The solution of the differential equation (1) is

$$-\log(1-\gamma) + \log\left(1-\gamma\frac{a+b-\sqrt{(a-b)^2+\frac{4ab}{\epsilon}}}{a+b+\sqrt{(a-b)^2+\frac{4ab}{\epsilon}}}\right) = \frac{Rt}{2.3ab}\sqrt{(a-b)^2+\frac{4ab}{\epsilon}} \quad (2)$$

where $\gamma = x/x_\infty$; x_∞ = the value of x at equilibrium $= \frac{\epsilon}{\epsilon-1}\left(a+b-\sqrt{(a-b)^2+\frac{4ab}{\epsilon}}\right)$

The experimental results give good straight lines on plotting

$$-\log(1-\gamma) + \log\left(1-\gamma\frac{a+b-\sqrt{(a-b)^2+\frac{4ab}{\epsilon}}}{a+b+\sqrt{(a-b)^2+\frac{4ab}{\epsilon}}}\right)$$

against time. From the slope, R—the true reaction rate—could be evaluated and plotted against the ammonia and the hydrogen pressure.

As the isotopic correction term log

$$\left(1-\gamma\frac{a+b-\sqrt{(a-b)^2+\frac{4ab}{\epsilon}}}{a+b+\sqrt{(a-b)^2+\frac{4ab}{\epsilon}}}\right)$$

is only about 10% of the first-order term log $(1-\gamma)$, the experimental results are not accurate enough to show a marked difference between Singleton's and the present method of calculating the results. For the concentration range involved, furthermore, the numerical value of k (disregarding the isotope effect) differs from the value of R only by 3 to 7%. Both methods, however, are very sensitive to the equilibrium D content; reliance was, therefore, placed in the present study on the initial stages of the exchange, in which the reaction $NH_3 + D_2 \rightarrow NH_2D + HD$ predominates. The initial rate of the decrease of the D content at one single temperature was the same within about 10% for the whole range of pressure and composition.

Figure 2 summarizes the experimental results obtained with the first iron catalyst.

The partial pressures in the reaction vessel covered a range from 20 to 180 mm. for ammonia and from 25 to 220 mm. for deuterium, the composition varying from 25 to 87 volume per cent. of deuterium. Most runs were made at 245°, at which temperature the D content of the hydrogen dropped from 100 to about 90 in 10 minutes. Other runs were made at 210, 221, 271, 295 and 319°.

The solid lines represent the mean initial slope for every temperature, while the shaded area covers the deviations recorded from this value.

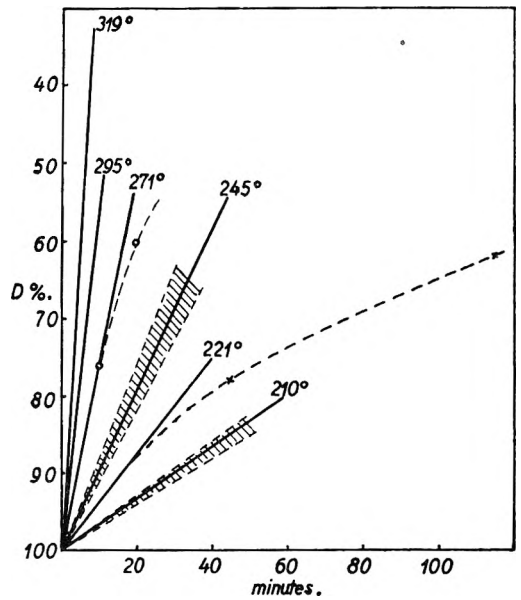

Fig. 2.—Change of D content of hydrogen interacting with NH_3 on reduced iron powder at different temperatures: dotted lines, actual reaction curve; solid lines, mean initial slope; shaded area, zone of deviations from mean.

These results show the exchange reaction to be independent (within 10%) of ammonia pressure and to be of first order in respect to deuterium. The catalyst appears to be almost completely covered by ammonia. From the plot of the logarithm of the initial velocity against the reciprocal of the temperature, an apparent energy of activation of 17.5 kcal./mole is calculated, which, of course, is independent of the reaction mechanism.

The results summarized in Fig. 2 for an iron catalyst give about the same picture as obtained by Singleton, *et al.*, for their tungsten catalyst at 697°K. The inhibitory effect of ammonia observed on their iron preparation, which could not

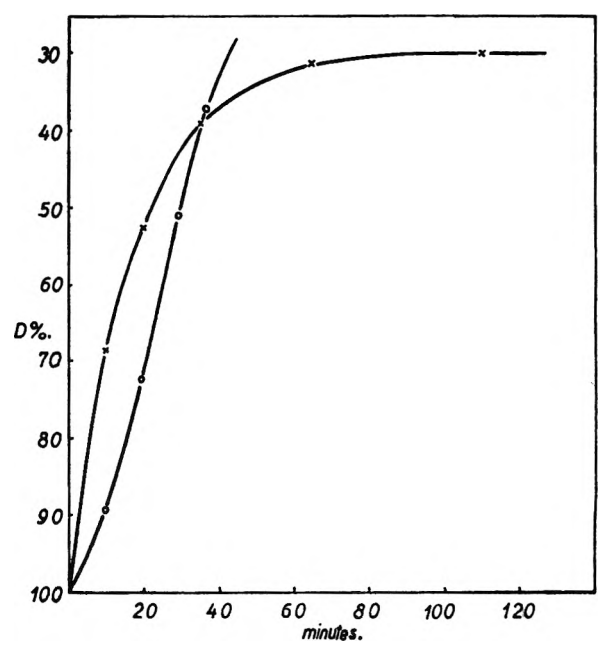

Fig. 3.—Change of D content of hydrogen interacting with NH_3 on nickel powder at 125°: x, normal near-first-order curve; o, poisoned S-shaped curve.

be detected in the present investigation, may be due to incomplete coverage of the surface by ammonia at their higher temperature.

The second iron catalyst studied decreased in activity from run to run, but the activity was restored by heating the powder with pure deuterium at 350°. The activation energy is slightly higher (19.8 kcal./mole). The restoration of the activity by reduction alone may point to a tenaciously held surface amide or nitride, as has been suggested. With nickel powder some similar phenomenon seems to occur: the runs were not well reproducible, and in some cases the rate of the exchange was slow in the beginning, but increased as the reaction proceeded. This increase in the activity during the run resulted in an S-shaped reaction curve, instead of the usual near-first-order curve (Fig. 3). Comparison of adjacent runs in which no such poisoning was observed, indicated an increase in the reaction rate with ammonia pressure.

Acknowledgment.—This investigation was carried out under the auspices of the Scientific Department, Israeli Ministry of Defence, and is published with its permission.

TRANSIENT SOLUTE DISTRIBUTIONS FROM THE BASIC EQUATION OF THE ULTRACENTRIFUGE

BY DAVID F. WAUGH[1] AND DAVID A. YPHANTIS

Department of Biology, Massachusetts Institute of Technology, Cambridge, Massachusetts

Received July 11, 1952

The behavior of small molecules in the ultracentrifuge has been examined by integrating, according to the method of Archibald, the basic centrifuge equation. Results for M = 1,000, 2,000 and 3,000 are given as concentration *versus* radial distance for centrifugation times of 2, 4, 5, 8 and 12 hours. The data were obtained by using a differential analyzer; individual values being accurate in general to 0.2%. In these calculations the molecules are assumed to be spheres of density 1.414 carrying a volume fractional kinetic water of $v = 0.5$. Calculations may be compared and molecular weights derived from the determination of R_s, the ratio of average solute concentration on the centrifugal side of a chosen boundary to the average solute concentration on the centripetal side. Values of R_s obtained from differential analyzer data have been used to determine the molecular weight range corresponding to a variation in v from 0 to 1.0. Over the range $0.32 < v < 0.71$ deviations of $\pm 5\%$ in M are expected. Approximations to the calculation of solute distribution have been examined. Results obtained by approximation are compared to those obtained by the differential analyzer by means of the ratio R_s. The approximate method has been used to calculate the effects of small physical errors on solute distribution and, through the ratio R_s, on the molecular weights calculated from solute distribution. The physical errors examined have been the positions of the meniscus and cell base and the position of an arbitrary fractionating plane near the center of the cell. The exact calculations have been extended to include other molecular weight ranges by choice of rotor angular velocity and centrifugation time. Under appropriate conditions the same calculations may be applied to new combinations of the parameters: partial specific volume, fractional kinetic water, particle density, solvent density and viscosity, and temperature as well as molecular weight and shape. Where a diffusion constant is known a molecular weight independent of shape or hydration may be determined.

The present discussion considers the behavior of small molecules ($M \leq 3{,}000$) in a centrifugal field. It is based primarily on the general ultracentrifuge equation deduced by Lamm[2] and the method for obtaining exact solutions as found by Archibald.[3a] To these exact solutions are compared the methods for obtaining approximate solutions, (Archibald[3b]), and the effects produced by changing parameters. The calculations are extended to include any near-spherical molecule having a density greater than the solvent density.

It has been clear for some time that many substances, and particularly those of biological importance, (a) have molecular weights in the range classified here as low, and (b) have not been prepared in chemically pure form. The over-all technique for treating small molecules has involved, in addition to a consideration of the Lamm equation, development of a method by which rotor temperature can be accurately measured and controlled[4] and a separation cell which fractionates its contents only after the normal sedimentation pattern has been established during a run.[5] Since the separation cell will handle low solute concentrations it is useful for examining the sedimentation patterns of pure materials as well as those of doubtful purity.

Certain techniques for handling ultracentrifuge data have been devised for cases where there is no formal boundary. Svedberg and Pedersen,[6] have suggested and Gutfreund and Ogston[7] have extended a procedure whereby sedimentation constants may be obtained for rapidly diffusing, slowly sedimenting molecules in the case where, in some region of the cell, the solute concentration is independent of position. Archibald[8] presents several noteworthy methods applicable to low molecular weight systems.

Other than the two specific considerations of Archibald,[3] we have been unable to find exact solutions of the Lamm equation applicable to the transient events taking place during sedimentation. Of particular interest are cases where a moving

(1) The authors wish to thank the Armour Laboratories for supporting this research.

(2) O. Lamm, *Ark. Mat. Astron. Fysik*, **21B**, No. 2 (1929).

(3) (a) W. J. Archibald, *Ann. N. Y. Acad. Sci.*, **43**, 211 (1942); (b) *J. Applied Phys.*, **18**, 362 (1947).

(4) D. F. Waugh and D. A. Yphantis, *Rev. Sci. Instruments*, **23**, 609 (1952).

(5) D. F. Waugh and D. A. Yphantis, to be published.

(6) T. Svedberg and K. O. Pedersen, "The Ultracentrifuge," Clarendon Press, Oxford, 1940, p. 23.

(7) H. Gutfreund and A. G. Ogston, *Biochem. J.*, **44**, 163-166 (1949).

(8) W. J. Archibald, THIS JOURNAL, **51**, 1204 (1947).

boundary cannot accurately be observed. In view of the above, and since these solutions have been extended to include other molecular weight ranges, the exact solutions obtained by the differential analyzer are given in detail.

The Centrifuge Equation.—Where the sedimenting properties of a solute are determined only by its sedimentation and diffusion constants (s and D), the transient distributions of solute within the cell can be predicted by the general centrifuge equation given by eq. (1)

$$\frac{\partial c}{\partial t} = D\left(\frac{\partial^2 c}{\partial r^2} + \frac{1}{r}\frac{\partial c}{\partial r}\right) - \omega^2 s\left(r\frac{\partial c}{\partial r} + 2c\right) \quad (1)$$

Here c is the solute concentration at a distance r cm. from the center of rotation and ω is the angular velocity (radians per sec.). It has been shown in several ways (see Archibald,[9] Svedberg and Pedersen[6]) that in dilute solutions the physical properties of the sedimenting molecule are related by eq. (2)

$$M(1 - V\rho_s) = RTs/D \quad (2)$$

where M is the molecular weight, D is the diffusion constant (cm.^{2}/sec.), V is the partial specific volume (cc./g.), ρ_s is the solvent density, and s the sedimentation constant (sec.). Equation (2) is generally used when the observation of a concentration gradient leads to measurements of s and D. The centrifuge has been used most often to examine molecular weights in excess of 5,000. For smaller molecules the unfavorable ratio of s to D precludes the formation of a sharp refractive index gradient with present equipment. For low values of s/D and dilute solutions refined optical methods may be unable to detect concentration distributions with sufficient accuracy.

Exact Solutions.—A closed solution for eq. (1) has not been obtained, for which reason it is not generally used. The mathematical procedure for obtaining exact solutions (Archibald[3a]) requires selection of physical parameters: the radii to the meniscus and cell base and appropriate values of s, D and ω. The meniscus and cell base used here are those which occur in the separation cell to be described elsewhere. It should be noted that the cell base is not that which exists normally in the Spinco Ultracentrifuge (Specialized Instruments Corporation, Belmont, California). Conformity with the conditions described here may be obtained by inserting a plastic base piece.

Table I lists a set of values of s and D corresponding to chosen values of M. The values of D were obtained using, in eq. (13), a solute partial specific volume of 0.707 and a fractional kinetic water of 0.50 cc. of water per cc. of solute (for other constants see eq. (13)). From these values of D corresponding values of s were calculated using eq. (2). Exact integrations of eq. (1) were obtained with the aid of a differential analyzer.[10]

TABLE I

SELECTED VALUES OF s AND D

(calculated from eq. 13)

Meniscus at r_a = 6.067 cm., base at r_b = 7.003 cm., ω^2 = $3.919 \times 10^{+7}$ (rad./sec.)^2.

Mol. wt.	D (cm.^{2}/sec.)	s (sec.$^{+1}$)
1,000	2.987×10^{-6}	0.356×10^{-13}
2,000	2.372	.565
3,000	2.073	.740

(9) W. J. Archibald, *Phys. Rev.*, **53**, 746 (1938).

The variable r, the radius to a point within the cell, varies from r_a (meniscus) to r_b (cell base). At the same time

$$z = \frac{\omega^2 s}{2D} r^2 \quad (3)$$

varies from z_a to z_b. Archibald finds that

$$\frac{c(z,t)}{c_0} = \frac{z_b - z_a}{e^{z_b} - e^{z_a}} e^z + \sum_{n=1}^{\infty} \frac{\int_{z_a}^{z_b} e^{-z} M(\alpha_n,1,z)dz}{\int_{z_a}^{z_b} e^{-z}\left\{M(\alpha_n,1,z)\right\}^2 dz} M(\alpha_n,1,z)e^{(\alpha_n-1)\tau} \quad (4)$$

where $\tau = 2\omega^2 st$ and t is time in seconds. In eq. (4) $M(\alpha_n,1,z)$, the eigenfunctions, are solutions to the equation

$$\frac{d^2M}{dz^2} + \left(\frac{1}{z} - 1\right)\frac{dM}{dz} - \frac{\alpha_n}{z} M_n = 0 \quad (5)$$

the α_n values (eigenvalues) are determined by the condition that, for $z = z_a$ and $z = z_b$

$$\frac{d}{dz} M(\alpha_n, 1, z) = M(\alpha_n, 1, z) \quad (6)$$

The differential analyzer was used to determine values of α_n and $M(\alpha_n, 1, z)$ by integration of eq. (5) subject to eq. (6). Three eigenfunctions (n = 1, 2, 3) were used in evaluating eq. (4).

The results are given in Tables II, III and IV. In each the first column gives the radial distance r, and the second the corresponding value of z. The latter is of use in calculating average concentrations since the volume increment, dV, is proportional to dz ($dV \propto rdr$). The fraction of the total solute to be found in a chosen sub-volume bounded by r_1 and r_2 will be given by

$$q_{1,2} = \frac{\int_{z_1}^{z_2} \frac{c}{c_0} dt}{z_a - z_b} \quad (7)$$

Consequently, if a boundary r_p be chosen within the cell, the ratio of the average concentration on the centrifugal side to that on the centripetal side is given by

$$\frac{\bar{c}_2}{\bar{c}_1} = R_s = \frac{\int_{z_p}^{z_b} \frac{c}{c_0} dz}{z_b - z_p} \Bigg/ \frac{\int_{z_a}^{z_p} \frac{c}{c_0} dz}{z_p - z_a} \quad (8)$$

or, noting that

$$\int_{z_a}^{z_b} \frac{c}{c_0} dt = z_b - z_a$$

$$R_s = \frac{\left(z_b - z_a - \int_{z_a}^{z_p} \frac{c}{c_0} dz\right)(z_p - z_a)}{\left(\int_{z_a}^{z_p} \frac{c}{c_0} dz\right)(z_b - z_p)} \quad (8a)$$

Equation (8a) is useful when errors on the centrifugal side of the boundary are objectionable.

As indicated in the introduction, an experimental technique has been devised by which the ratio R_s

(10) The differential analyzer No. 2 at the Massachusetts Institute of Technology was made available for this purpose.

TABLE II

DIFFERENTIAL ANALYZER SOLUTIONS GIVING SOLUTE CONCENTRATION RATIOS c/c_0 *vs.* RADIAL DISTANCE FOR M = 1,000 (see Table I)

		Values of c/c_0 for centrifugation times in hours						
r, cm.	z	0	2	4	5	8	12	∞
6.067	8.590	0.854	0.601	0.475	0.431	0.337	0.264	0.174
6.102	8.69	.932	0.659	.522	.474	.370	.291	.193
6.137	8.79	.992	.713	.568	.516	.405	.319	.213
6.172	8.89	1.033	.761	.611	.557	.439	.348	.235
6.207	8.99	1.055	.804	.653	.596	.474	.379	.260
6.241	9.09	1.061	.841	.692	.634	.509	.410	.288
6.275	9.19	1.054	.872	.728	.671	.544	.443	.318
6.309	9.29	1.036	.898	.761	.705	.579	.478	.351
6.343	9.39	1.014	.919	.792	.738	.614	.514	.388
6.377	9.49	0.991	.935	.820	.769	.649	.552	.429
6.410	9.59	.971	.948	.846	.798	.685	.592	.474
6.444	9.69	.958	.957	.869	.826	.722	.635	.524
6.477	9.79	952	.965	.891	.853	.760	.681	.579
6.510	9.89	.957	.970	.911	.880	.800	.730	.640
6.543	9.99	.968	.975	.932	.907	.842	.783	.707
6.575	10.09	.986	.980	.952	.935	.887	.841	.782
6.608	10.19	1.006	.985	.974	.965	.935	.905	.864
6.640	10.29	1.025	.992	.998	.997	.988	.974	.955
6.673	10.39	1.040	1.000	1.025	1.034	1.046	1.051	1.055
6.705	10.49	1.047	1.012	1.057	1.076	1.112	1.137	1.166
6.736	10.59	1.045	1.028	1.095	1.124	1.185	1.232	1.288
6.768	10.69	1.034	1.049	1.141	1.181	1.269	1.338	1.424
6.800	10.79	1.014	1.078	1.196	1.247	1.363	1.457	1.574
6.931	10.89	0.990	1.117	1.263	1.326	1.471	1.590	1.739
6.862	10.99	.967	1.168	1.344	1.419	1.595	1.739	1.922
6.894	11.09	.952	1.233	1.442	1.529	1.736	1.907	2.124
6.825	11.19	.953	1.318	1.559	1.659	1.897	2.095	2.348
6.956	11.29	.981	1.424	1.698	1.812	2.082	2.307	2.595
6.986	11.39	1.044	1.556	1.863	1.991	2.293	2.545	2.867
7.003	11.445	1.097	1.641	1.967	2.101	2.421	2.688	3.029

may be determined. Under given experimental conditions and the assumptions outlined at the start of this section, a ratio R_s corresponds to a particular molecular weight. The ratios R_s are used extensively below to compare solutions for the ultracentrifuge equation and to examine differences arising from changes in the various parameters.

Returning to Tables II, III and IV. The third and subsequent columns give the values of c/c_0 for centrifugation times of 0, 2, 4, 5, 8 and 12 hr. Figure 1 plots part of the data of Table III (M assumed to be 2,000).

Neglecting the higher eigenfunctions ($n \geqslant 4$) leads to large zero time errors. These decrease

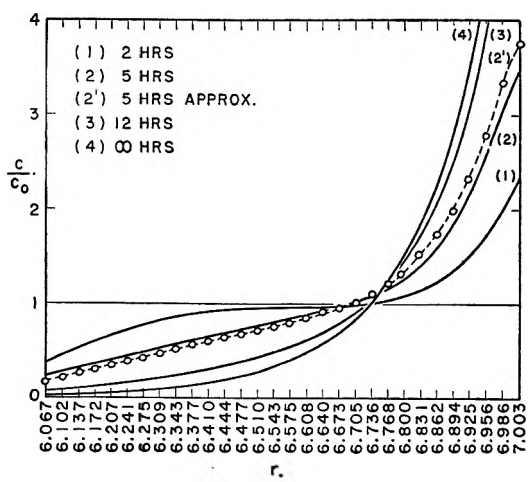

Fig. 1.—Concentration distribution curves for M = 2,000. The ordinate gives the ratio of concentration at time t to the initial concentration. The abscissa gives the radial position in cm.

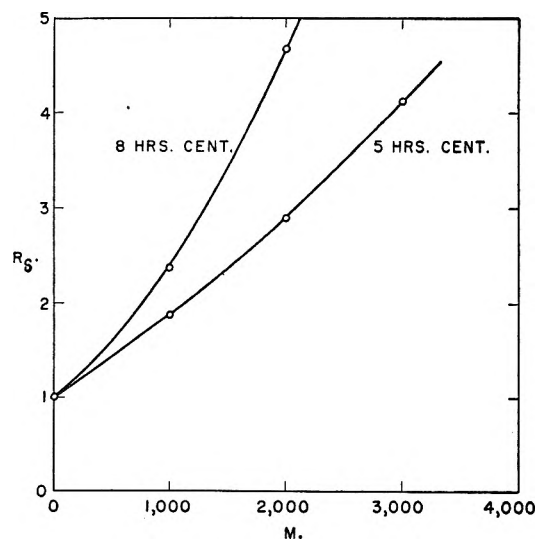

Fig. 2.—The concentration ratio R_s = average concentration on centrifugal side of r_p = 6.6 cm. to that on centripetal side. The ratio R_s is plotted against M for 5 and 8 hour centrifugation times. For further information see Table V.

TABLE III

DIFFERENTIAL ANALYZER SOLUTIONS GIVING SOLUTE CONCENTRATION RATIOS c/c_0 *vs.* RADIAL DISTANCE FOR $M = 2{,}000$ (see Table I)

		Values of c/c_0 for centrifugation times in hours						
r, cm.	z	0	2	4	5	8	12	∞
6.067	17.179	0.708	0.388	0.247	0.204	0.122	0.068	0.019
6.102	17.379	.830	.456	.291	.240	.144	.081	.023
6.137	17.579	.949	.533	.344	.284	.171	.097	.028
6.172	17.779	1.043	.607	.398	.330	.200	.115	.035
6.207	17.979	1.106	.686	.451	.376	.231	.134	.042
6.241	18.179	1.138	.735	.503	.423	.263	.154	.052
6.275	18.379	1.137	.788	.554	.469	.297	.177	.063
6.309	18.579	1.108	.831	.602	.515	.332	.202	.077
6.343	18.779	1.056	.866	.648	.559	.368	.229	.094
6.377	18.979	0.991	.892	.690	.601	.405	.259	.115
6.410	19.179	.924	.911	.728	.642	.444	.292	.140
6.444	19.379	.864	.924	.764	.681	.484	.329	.171
6.477	19.579	.823	.933	.796	.719	.526	.370	.209
6.510	19.779	.807	.939	.825	.755	.571	.416	.256
6.543	19.979	.822	.945	.853	.790	.619	.470	.312
6.575	20.179	.868	.951	.879	.826	.671	.532	.381
6.608	20.379	.940	.958	.906	.863	.730	.604	.466
6.640	20.579	1.030	.968	.935	.904	.798	.690	.569
6.673	20.779	1.126	.981	.968	.951	.876	.793	.695
6.705	20.979	1.212	.998	1.009	1.006	.970	.916	.849
6.736	21.179	1.274	1.020	1.059	1.075	1.083	1.066	1.037
6.768	21.379	1.298	1.050	1.126	1.161	1.221	1.249	1.266
6.800	21.579	1.275	1.090	1.213	1.272	1.393	1.473	1.546
6.831	21.779	1.206	1.149	1.331	1.417	1.609	1.750	1.889
6.862	21.979	1.097	1.235	1.490	1.607	1.880	2.092	2.307
6.894	22.179	0.954	1.350	1.696	1.850	2.218	2.514	2.818
6.925	22.379	.810	1.514	1.968	2.166	2.644	3.035	3.441
6.956	22.579	.706	1.747	2.327	2.575	3.182	3.681	4.203
6.986	22.779	.692	2.074	2.798	3.106	3.859	4.482	5.134
7.003	22.889	.742	2.303	3.115	3.459	4.302	4.999	5.729

exponentially with centrifugation time. For example, at two hr. the maximum estimated errors in c/c_0 are, for $M = 1{,}000$, 2,000, and 3,000, 0.003, 0.012, 0.1 (about 0.5, 5 and 8%). At four hours centrifugation the deviations are in the third decimal place except for $M = 3{,}000$ where they are less than 0.005. At five hours centrifugation all deviations are negligible. The accuracy of the differential analyzer itself is such that the errors in all final values are less than 0.2%.

By means of eq. (8a) the average solute concentrations on either side of a boundary may be computed. The values of R_s obtained from Tables II, III and IV for a boundary at $r_p = 6.60$ cm., are plotted against M in Fig. 2. The centrifugation times are five and eight hours (see also Table V).

Approximations.—Archibald[3b] has developed approximations to the eigenfunctions and eigenvalues for the case where $z_b - z_a \approx 1$. It is important to see whether these approximations can be extended to present cases where $z_b - z_a$ ranges from 3 to 9, and where α_n's are not necessarily large compared to z. Approximations to α_n values are obtained from

$$\sigma_n^2 = \left\{ -\frac{1}{4}\frac{z_a + z_b}{2} - \left(\alpha_n - \frac{1}{2}\right) \right\} \qquad (9)$$

where

$$\sigma_n = \frac{x_n}{2(z_b^{1/2} - z_a^{1/2})} \qquad (10)$$

and x_n is given by

$$x_n = n\pi + \tan^{-1}\left\{ \left(\frac{z_b^{1/2} - z_a^{1/2}}{x_n}\right)\left(\frac{1 + z_a}{z_a^{1/2}}\right) \right\} - \tan^{-1}\left\{ \left(\frac{z_b^{1/2} - z_a^{1/2}}{x_n}\right)\left(\frac{1 + z_b}{z_b^{1/2}}\right) \right\} \qquad (10a)$$

Equation (10a) was further approximated by Archibald as

$$x_n = n\pi + \frac{z_b^{1/2} - z_a^{1/2}}{n\pi}\left\{ \frac{1 + z_a}{z_a^{1/2}} - \frac{1 + z_b}{z_b^{1/2}} \right\} \qquad (10b)$$

The approximation (10b), valid for $z_b - z_a \approx 1$, is not strictly applicable when $z_b - z_a$ is in our range of ~3 to 9. For our computation, therefore, eq. (10a) was used and was solved by successive approximations for x_n. It should be pointed out that eq. (10a) was not always superior to eq. (10b), the latter frequently giving eigenvalues closer to those obtained by the differential analyzer. In any case, the α_n obtained through eq. (9), (10), and (10a), or (10b) are in good agreement with differential analyzer values.

The approximations to $M(\alpha_n, 1, z)$ are given by Archibald[3b] as

$$M(\alpha_n, z) = e^{z/2} z^{-\frac{1}{4}}\left\{ \cos\left(2\sigma_n z^{1/2} - \frac{3\pi}{4}\right) + K_n \sin\left(2\sigma_n z^{1/2} - \frac{3\pi}{4}\right) \right\} \qquad (11)$$

where

$$K_n = -\cot\left\{ \tan^{-1}\left[\frac{1}{2\sigma_n}\left(\frac{1}{z_a^{1/2}} + z_a^{1/2}\right)\right] + 2\sigma_n z_a^{1/2} - \frac{\pi}{4} \right\} \qquad (11a)$$

TABLE IV

DIFFERENTIAL ANALYZER SOLUTIONS GIVING SOLUTE CONCENTRATION RATIOS c/c_0 *vs.* RADIAL DISTANCE FOR M = 3,000 (see Table I)

		Values of c/c_0 for centrifugation times in hours						
r, cm.	z	0	2	4	5	8	12	∞
6.067	25.758	0.575	0.250	0.128	0.095	0.042	0.016	0.002
6.102	26.058	.749	.328	.169	.125	.056	.022	.002
6.137	26.358	.916	.411	.214	.159	.072	.028	.003
6.172	26.658	1.066	.495	.262	.197	.089	.036	.004
6.207	26.958	1.182	.578	.314	.238	.109	.043	.005
6.241	27.258	1.258	.657	.369	.280	.132	.053	.007
6.275	27.558	1.281	.727	.423	.326	.156	.064	.010
6.309	27.858	1.254	.787	.477	.373	.182	.076	.013
6.343	28.158	1.173	.836	.531	.420	.211	.091	.018
6.377	28.458	1.051	.873	.582	.467	.241	.108	.024
6.410	28.758	0.908	.898	.630	.514	.274	.126	.033
6.444	29.058	.759	.913	.675	.560	.309	.148	.044
6.477	29.358	.633	.920	.717	.604	.346	.174	.060
6.510	29.658	.557	.926	.756	.647	.386	.203	.081
6.543	29.958	.545	.929	.791	.689	.429	.240	.109
6.575	30.258	.620	.935	.824	.730	.477	.283	.149
6.608	30.558	.788	.949	.856	.773	.532	.338	.199
6.640	30.858	1.030	.968	.889	.818	.595	.406	.269
6.673	31.158	1.347	.999	.927	.868	.671	.496	.363
6.705	31.458	1.683	1.037	.970	.928	.767	.610	.490
6.736	31.758	1.989	1.083	1.028	1.003	.888	.763	.662
6.768	32.058	2.209	1.136	1.103	1.105	1.046	.965	.893
6.800	32.358	2.283	1.198	1.211	1.238	1.259	1.236	1.205
6.831	32.658	2.160	1.273	1.364	1.427	1.547	1.600	1.627
6.862	32.958	1.813	1.373	1.579	1.692	1.940	2.097	2.196
6.894	33.258	1.235	1.518	1.891	2.068	2.480	2.769	2.965
6.925	33.558	0.489	1.743	2.344	2.605	3.228	3.684	4.002
6.956	33.858	− .327	2.103	2.996	3.369	4.262	4.930	5.402
6.986	34.158	−1.042	2.673	3.937	4.450	5.694	6.630	7.293
7.003	34.318	−1.306	3.099	4.596	5.204	6.675	7.780	8.562

TABLE V

A TABULATION OF τ VALUES, CENTRIFUGAL TO CENTRIPETAL SOLUTE CONCENTRATION RATIOS OBTAINED FROM DIFFERENTIAL ANALYZER DATA ($R_{D.A.}$), AND A COMPARISON TO THOSE OF SOLUTE CONCENTRATION RATIOS OBTAINED BY APPROXIMATION

Time, hr.	M = 1,000			M = 2,000			M = 3,000		
	τ	$R_{D.A.}$	$R_{approx.}$	τ	$R_{D.A.}$	$R_{approx.}$	τ	$R_{D.A.}$	$R_{approx.}$
2	0.0201	1.322	1.321	0.0319	1.598	1.681	0.0418	1.807	2.082
4	.0402	1.687	1.696	.0638	2.401	2.531	.0835	3.155	3.617
5	.0502	1.871	1.884	.0797	2.890	3.048	.1044	4.118	4.71
8	.0804	2.396	2.424	.1275	4.661	4.91	.1670	8.47	9.69
12	.1205	2.974	2.992	.1913	7.470	7.81	.2506	18.45	20.81

Closest agreement between approximate and differential analyzer calculations is expected when z_a and z_b are small compared to α_1 (10 to 14 in this case); therefore when M is small. We have found best agreement for low M to occur if, instead of evaluating by numerical integration the integral

$$\int_{z_a}^{z_b} e^{-z}\,[M(\alpha_n, 1, z)]^2 dz$$

which occurs in eq. (4), it was taken as

$$\frac{z_b\, e^{-z_b} M_n(z_b) - z_a\, e^{-z_a} M_n(z_a)}{\alpha_n} \qquad (12)$$

Equation (12) was derived by Archibald[3a] in his treatment of exact solutions. We have used eq. (12) throughout in approximations.

In Fig. 1 the dotted line compares the approximation data with differential analyzer data for M = 2,000 and t = 5 hours. The agreement is better for M = 1,000 and worse for M = 3,000 as indicated in Table V which compares calculations by means of R_s values for r_p = 6.60 cm. In view of the extension which follows, we have included in Table V the values of τ corresponding to each molecular weight and time. Deviations in c/c_0 are smallest in the centripetal part of the centrifuge cell. Equation (8a), which has been generally used, integrates only through the centripetal region and is therefore preferable to eq. (8).

Analysis of Assumptions.—It is well known that spheres of radius r(cm.) in a medium of viscosity η (poise) have a diffusion constant D (cm.²/sec.) given by

$$D = \frac{kT'}{6\pi\eta r}$$

which, on appropriate substitution, becomes

$$D = 9.97 \times 10^{-10}\,\frac{T}{\eta}\left(\frac{\rho_p}{M(1+v)}\right)^{1/3} \qquad (13)$$

where ρ_p is the density of the anhydrous solute

(g./cc.) and v is the fractional volume of kinetic water (cc. water which effectively moves with the particle per cc. particles). The data of Table I were calculated using $T = 295.6°$, $\eta = 0.0967$, $\rho_p = 1.414$, $\rho_s = 1.0058$ and $v = 0.50$; the latter is approximately 0.35 g. of water per g. of molecules. It should be noted that a shape factor can be treated in a manner analogous to the treatment of the hydration effects discussed here.

The effect of varying v from 0 to 1.0 has been examined by calculating values of R_s for a boundary at $r_p = 6.60$ cm. and a centrifugation time of five hours. The ratio s/D was held constant; equivalent to assuming constant values for M, η, T, ρ_p and $V\rho_s$. Specific values of D were calculated from eq. (13). These were used in eq. (2) to obtain corresponding values of s, from which were obtained new values of τ. The latter were introduced into eq. (4) and values of R_s calculated from the resulting solute distribution. The results are shown in Fig. 3 for an assumed $M = 2{,}000$ and five hours centrifugation. The ratio R_s varies from 3.28 ($v = 0$) to 2.66 ($v = 1.0$). For a molecule having a fixed $v = 0.5$ this same range of R_s corresponds to a range of M from 1800 to 2300 as indicated by the right-hand ordinate. It should be noted that the range of v from 0 to 1.0 is considerably greater than that which would normally be encountered experimentally for small molecules. Over the range $v = 0.4$ to 0.7, M varies from 2050 to 1910. The percentage changes have been found to be approximately the same for $M = 1{,}000$ and $M = 3{,}000$ and for other centrifugation times.

Partial specific volume plays an important role in interpreting data obtained by centrifugation. For a constant ratio of s/D, the relationship between M and $(1 - V\rho_s)$ is predicted by eq. (2)

$$M_i(1 - V_i\rho_s) = M_j(1 - V_j\rho_s)$$

Assuming V to be of the order of 0.71, a 1% error in estimating V will lead to a 2.4% error in M. For a further discussion of parameters see Extension of Method.

Physical Errors.—Exact positions for the meniscus, fractionating plate (r_p) and cell base have been assumed. Experimentally deviations are expected, particularly in the position of the cell base. Such physical errors lead to deviations in R_s and to errors in M.

Plate Position.—Ratios R_s were computed for $r_p = 6.58$ cm. and compared with those for $r_p = 6.60$ cm., a relatively large Δr_p. Expressing errors up to 12 hr. centrifugation in terms of M; the maximum error is 1.8% and occurs at $M = 3{,}000$ and $t = 12$ hours ($R_s = 18.45$). For the experimentally useful range of $1.5 < R_s < 5.0$, the error in M is always less than 0.8%.

Meniscus Position.—Utilizing the approximate method, ratios R_s were calculated for $r_a = 6.017$ cm. (normally 6.067). The deviation, $\Delta r_a = 0.05$ cm., is well beyond any experimental error. For 2, 4, 5, 8 and 12 hours centrifugation the errors in M for $M = 1{,}000$ and $M = 3{,}000$ are, in per cent., −2.2, 0; −3.7, −4.3; −3.7, −4.7; −3.3, −4.4; −0.6, −3.1.

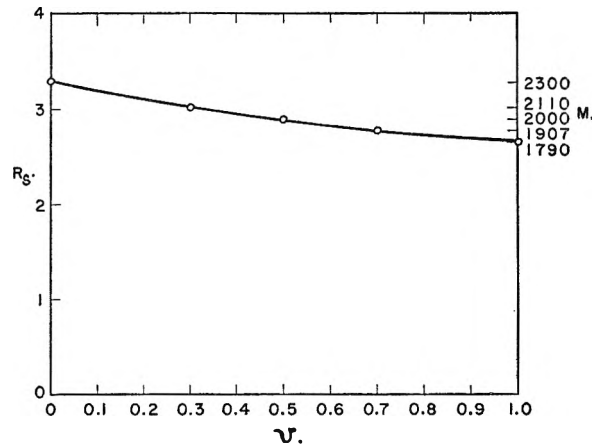

Fig. 3.—The effects of kinetic water, v (cc. water per cc. molecules), on the concentration ratio R_s for $M = 2{,}000$ and a centrifugation time of 5 hours. The right ordinate gives the corresponding molecular weight range for a molecule having $v = 0.5$.

Base Position.—Similarly ratios R_s were calculated for $r = 7.061$ cm. to be compared with those for the normal value 7.003 cm. Again the deviation, $\Delta r_b = 0.058$ cm., is large. For 2, 4, 5, 8, 12 hours centrifugation, the errors in M for $M = 1{,}000$ and $M = 3{,}000$ are in per cent., −1.6, −6.7; −2.8, −4.3; −2.4, −3.3; −1.1, −1.2; +2.8, +3.3.

Extension of Calculations.—The values $1M = 1{,}000$, $2M = 2{,}000$ and $3M = 3{,}000$ have been treated thus far. We have found it convenient and instructive to examine the procedures by which these calculations can be applied to other values of molecular weight either by a technique involving a measurement of R_s or by any more general technique involving a determination of $c(r, t)/c_0$.

In eq. (4) the eigenvalues α_n and the eigenfunctions $M(\alpha_n,z)$ are dependent eventually only upon z_a and z_b. When any set of experimental conditions leads to values of z_a, z_b and τ identical with those used in present calculations (condition I), the distribution of solute throughout the cell will be as calculated for these values. Let us examine the conditions under which the sedimentation pattern of a chosen molecular weight $f1M$ may, at ω_x^2 and t_x, be made equivalent to that for $1M$ at ω_i^2 and t_i. A value of $\tau_{1M,i}$ corresponds to t_i. Correspondingly we have $z_{a,1M}$ and $z_{b,1M}$. Values of ω_x^2 and t_x may be chosen for $f1M$ through condition I as follows. A value of ω_x^2 is given by values of z_a or z_b (for $1M$) using

$$\left.\begin{matrix} z_{a,1M} \\ z_{b,1M} \end{matrix}\right| = \frac{f1M(1 - V\rho_s)}{2RT}\omega_x^2 \left|\begin{matrix} r_a^2 \\ r_b^2 \end{matrix}\right. \qquad (14)$$

A value of the sedimentation constant s_x for $f1M$ is now calculated according to an assumed model; for example as is done for our model *via* eq. 2 and 13.

Upon substituting in eq. (15) values for $\tau_{1M,i}$, ω_x^2 and s_x a new value, t_x, is obtained which is the centrifugation time for $f1M$. Condition I is satisfied and the new values ω_x^2 and t_x will yield for $f1M$ the same solute distribution as the values ω_i^2 and t_i gave for $1M$.

$$\tau = 2\omega^2 st \qquad (15)$$

Since, very closely, $z_{2M}(r) = 2z_{1M}(r)$ and $z_{3M}(r) = 3z_{1M}(r)$, and $s_{2M} = (2)^{2/3}s_{1M}$ and $s_{3M} = (3)^{2/3}s_{1M}$, the values ω_x^2 and t_x for $f1M$ will satisfy condition I for $f2M$ and $f3M$; providing that the model does not change in shape or hydration. In this event the abscissa (M) of Fig. 2 relating R_s to M for five and eight hours centrifugation can be multiplied by a constant factor f by choosing appropriate values of ω_x and t_x. For example, the range shown in Fig. 2 may be extended by $f = 3$ (3,000 to 9,000) by using $\omega = 3.61 \times 10^3$ radians per second and $t = 7.21$ hours (curve 1) and $t = 11.54$ hours (curve 2) and by $f = 4$ (4,000 to 12,000) by using $\omega = 3.13 \times 10^3$ and $t = 7.94$ hours (curve 1) and $t = 12.70$ hours (curve 2).

In a similar manner the calculations may be made to apply to any new combination of the parameters V, v, ρ, η, etc., as well as M. It should be noted that a change in shape can be treated in a like manner to a change in v. In this respect it should also be noted that a change in v alone may be compensated for largely by a change in viscosity (therefore temperature) and that new values of ω and t need not be sought (see eq. 13).

When an accurate independent measurement of D (D_m) is available, the calculations and a measurement of R_s may be used to obtain an anhydrous molecular weight not subject to assumptions of shape or hydration. From this value a shape-hydration factor D_0/D_m may be obtained in the usual way.

D_m is used in eq. (2) along with $M = 1{,}000$, $M = 2{,}000$ and $M = 3{,}000$ to obtain values of s (s_1, s_2, s_3). The ratios s/D_m so obtained will give, for each M, the correct values of z_a and z_b. Equation (15) is now employed using these values of s, the value of ω used in calculations and experiments, and the experimental value of t, to obtain values of $\tau(\tau_1, \tau_2, \tau_3)$. Through the assumed values of M, each τ value corresponds to a value of R_s which can be obtained by interpolation in Table V. The paired values of R_s and M have been calculated for the experimental condition used and the assumption that $D = D_m$. The value of M corresponding to the measured value of R_s may now be determined. The extension of calculations given at the start of this section likewise applies to the situation where a value D_m is available.

KINETICS OF SURFACE REACTIONS IN THE CASE OF INTERACTIONS BETWEEN ADSORBED MOLECULES

BY KEITH J. LAIDLER

Department of Chemistry, The Catholic University of America, Washington, D. C.

Received July 14, 1952

The influence of interactions between adsorbed molecules on the absolute rates of surface reactions, with special reference to the parahydrogen conversion, is considered. It is shown that these interactions enter in two ways: they affect the number of dual surface sites and also the partition function for the surface sites. The rate equations are developed for the Bonhoeffer–Farkas mechanism for the parahydrogen conversion on tungsten and the two effects are shown to cancel exactly for a fully covered surface. In calculating absolute rates it is therefore correct to omit interaction terms.

Introduction

Recent work on adsorption[1-3] has indicated that there may frequently be strong repulsive interactions between atoms or molecules adsorbed on neighboring surface sites. It is therefore important to consider the effect of these interactions on the kinetics of surface reactions. Most treatments of surface reactions[4-8] neglect these effects: for example, in the calculations of the absolute rates of surface reactions interactions have usually not been considered, without any particular justification. In spite of this omission calculations of absolute rates have for the most part been remarkably successful and an explanation for this success is given in the present paper.

In two recent papers[9-10] absolute rate calculations have been made in which explicit account has been taken of the repulsive interactions. These calculations have been made for the Bonhoeffer–Farkas mechanism[11] for the parahydrogen conversion on tungsten. The equation employed for calculating the rates involves the application of collision theory and employs the expression derived by Peierls[12] for the number of bare neighboring sites on a surface. Employing an interaction energy of 4.4 kcal. derived from Trapnell's isotherm Eley[10] calculates that the number of bare dual sites is about 10^{-6} of the number that would be present if there were no repulsive forces. His absolute rates moreover are about 10^{-6} of the observed ones and on this basis Eley rejects the Bonhoeffer–Farkas mechanism. Laidler[7] on the other hand has neglected the repulsive forces, obtains good agreement and concludes that the Bonhoeffer–Farkas mechanism is acceptable.

At first sight, neglect of the repulsive forces of this magnitude would not appear to be correct.

(1) J. K. Roberts, *Proc. Roy. Soc.* (*London*), **A152**, 445 (1935).

(2) E. K. Rideal and B. M. W. Trapnell, *J. chim. phys.*, **47**, 126 (1950); *Faraday Soc. Discussion*, **8**, 114 (1950); B. M. W. Trapnell, *Proc. Roy. Soc.* (*London*), **A206**, 39 (1951).

(3) J. Weber and K. J. Laidler, *J. Chem. Phys.*, **18**, 1418 (1950); **19**, 1089 (1951).

(4) K. J. Laidler, S. Glasstone and H. Eyring, *ibid.*, **8**, 659, 667 (1940).

(5) S. Glasstone, K. J. Laidler and H. Eyring, "The Theory of Rate Processes," McGraw-Hill Book Co., Inc., New York, N. Y., 1941.

(6) K. E. Shuler and K. J. Laidler, *J. Chem. Phys.*, **17**, 1212 (1949).

(7) K. J. Laidler, THIS JOURNAL, **57**, 320 (1953).

(8) M C. Markham, M. C. Wall and K. J. Laidler, *ibid.*, **57**, 321 (1953).

(9) B. M. W. Trapnell, *Proc. Roy. Soc.* (*London*). **A206**, 39 (1951).

(10) A. Couper and D. D. Eley, *ibid.*, **A211**, 536 (1952).

(11) K. F. Bonhoeffer and A. Farkas, *Z. physik. Chem.*, **B12**, 231 (1931).

(12) R. Peierls, *Proc. Camb. Phil. Soc.*, **32**, 471 (1936).

Further consideration, however, reveals a serious objection to the rate equation employed by Trapnell and by Eley. The only way in which the repulsive forces appear in this equation is to diminish, by 10^{-6} or so, the concentration of bare dual sites. It is clear, however, that they should also enter in another way: by making the dual sites intrinsically improbable they should increase the rate of reaction per dual site. Expressed differently, the rate equation contained in its denominator the partition function for the dual site and this will be diminished by the repulsive interactions. There will clearly be some compensation between these two effects. On intuitive grounds the writer has previously assumed the compensation to be complete and has therefore neglected the interactions. The formal justification of this is now given. The proof will be given for the special case of the parahydrogen conversion on a well-covered surface, the rate of which is assumed to be controlled by the rate of adsorption of hydrogen. This case of the well-covered surface is the one of chief interest; when the surface is sparsely covered the interactions are of course unimportant owing to the small number of neighboring adsorbed species.

The statistical treatment of the adsorption is equivalent to that of Peierls[12] and Roberts.[13] Consider a central site S_0 surrounded by four neighboring sites S_1, S_2, S_3 and S_4. The isotherm for dissociative adsorption without interaction is

$$\theta/(1 - \theta) = Kp^{1/2} \qquad (1)$$

Suppose that S_0 is bare: then the probability P that S_1 is covered is given by

$$P/(1 - P) = K\zeta p^{1/2} = \kappa p^{1/2} \qquad (2)$$

Here ζ is a term that takes into account the interactions due to molecules surrounding the colony of five under consideration. If S_0 is occupied the probability P' that S_1 is occupied is given by

$$P'/(1 - P') = K\zeta e^{-V/kT} p^{1/2} = \kappa\eta p^{1/2} \qquad (3)$$

where V is the interaction energy and η is equal to $e^{-V/kT}$. Equations (2) and (3) give, for the probability that S_1 is bare when the surface is well covered ($P \to 1$ and $P' \to 1$)

$$1 - P = 1/\kappa p^{1/2} \quad \text{if } S_0 \text{ is bare} \qquad (4)$$

$$1 - P' = 1/\kappa\eta p^{1/2} \quad \text{if } S_0 \text{ is occupied} \qquad (5)$$

If the total number of sites per sq. cm. when the surface is bare is L, the concentration of bare single sites is

$$c_S = L(1 - P') \qquad (6)$$

The concentration of bare dual sites is given by

$$c_{S_2} = \frac{1}{2} s c_S (1 - P) \qquad (7)$$

where s is the coördination number, assumed to be 4 in this case. Equations (4)–(7) give rise to

$$\frac{c_{S_2}}{c_s^2} = \frac{s}{2L} \frac{1 - P}{1 - P'} = \frac{s\eta}{2L} \qquad (8)$$

The ratio of the partition function for a dual site, f_{S_2}, to that for two individual single sites, f_S^2, is $e^{-V/kT}/2 = \eta/2$; the numerator arises from the fact that the dual site has an energy V higher than that of two separate sites, while the denominator is the symmetry number of the dual sites.

The rate of adsorption, *i.e.*, the rate of reaction between gas molecules and bare dual sites, is equal to

$$v = c_g c_{S_2} \frac{kT}{h} \frac{f^{\ddagger}}{F_g f_{S_2}} e^{-E_0/RT} \qquad (9)$$

In terms of single sites instead of dual sites

$$v = \frac{s c_g c_s^2}{L} \frac{kT}{h} \frac{f^{\ddagger}}{F_g f_s^2} e^{-E_0/RT} \qquad (10)$$

Since the η cancel, it is clear that the interaction terms have no effect on the rate.[14] Equation (10) is the equation used in the following paper to calculate the rate of reaction by the Bonhoeffer–Farkas mechanism.

It appears, therefore, that in this case of a well-covered surface the interaction terms exactly cancel out of the rate expression, and that serious error arises from introducing the interaction term into the expression for c_{S_2} but neglecting its effect on f_{S_2}.

(13) J. K. Roberts, "Some Problems in Adsorption," Cambridge Univ. Press, London, 1939, p. 25; *cf.* A. R. Miller, "The Adsorption of Gases on Solids," Cambridge Univ. Press, 1949, p. 24.

(14) It should be noted that this conclusion involves the assumption, probably valid in most cases, that the partition function $f_{\ddagger}$ for the activated complex (which does not include the Boltzmann factor) is not affected by the repulsive interactions.

MECHANISMS OF SURFACE-CATALYZED REACTIONS. I. THE PARAHYDROGEN CONVERSION ON TUNGSTEN

BY KEITH J. LAIDLER

Department of Chemistry, The Catholic University of America, Washington 17, D. C.

Received May 23, 1952

The kinetic results of Farkas and of Eley and Rideal on the conversion of parahydrogen into orthohydrogen are discussed with reference to the adsorption data of Frankenburg and of Rideal and Trapnell. Various mechanisms for the reaction are considered and it is concluded that the only one that satisfactorily fits all of the data is the Bonhoeffer–Farkas mechanism in which the rate is controlled by adsorption of a hydrogen molecule on a bare dual surface site. According to this mechanism the rate is proportional to $(1-\theta)^2kp$ and if the variation of k with p is taken into account the mechanism explains the low reaction orders of close to zero; it also is consistent with the observed absolute rates. The Rideal mechanism, involving reaction between an adsorbed atom and a gaseous molecule or a van der Waals adsorbed molecule, is shown to be incapable of explaining either the order or the absolute rate.

Introduction

The conversion of parahydrogen into orthohydrogen at a tungsten surface has been the subject of careful experimental study[1–3] and of much theoretical discussion.[2,4–12] It was originally supposed that since adsorption involves dissociation into atoms the conversion proceeds *via* adsorption and evaporation

$$p\text{-}H_2 + W \rightleftarrows 2WH \rightleftarrows 2W + o\text{-}H_2 \qquad (1)$$

However the work of Roberts[13] appeared to indicate that desorption occurs too slowly for such a mechanism to be possible and as a result Rideal[5] proposed that reaction proceeds through interaction of a chemisorbed atom and a gaseous molecule or one held in a van der Waals layer

$$p\text{-}H_2 + WH \rightleftarrows HW + o\text{-}H_2 \qquad (2)$$

Later adsorption studies by Frankenburg[14] and by Rideal and Trapnell[8,10] indicated, however, that Roberts' surfaces were not as fully covered as he believed them to be and that at higher pressures than those used by Roberts the heats of adsorption fall to such low values that desorption can occur rapidly. In view of this there is no valid objection to the Bonhoeffer–Farkas mechanism on the basis of rates of desorption.

There still remain some problems in connection with the reaction and in particular the interpretation of the low order of reaction has given some difficulty.[11] In the present paper the reaction is discussed theoretically in a simple manner and it is shown that the low order and the absolute rate of the reaction can be satisfactorily interpreted on the basis of the Bonhoeffer–Farkas mechanism, but not on the basis of the Rideal mechanism. This conclusion is in agreement with that reached by Trapnell[10] on somewhat different grounds. It is to be emphasized that the present paper is concerned with the correlation of the experimental adsorption and kinetic data. Its conclusions are entirely independent of whether the data are to be interpreted in terms of surface heterogeneity or of repulsive interactions between adsorbed molecules.

Kinetics of the Conversion.—The salient facts regarding the conversion are as follows. The kinetics are strictly first order if the total pressure, *i.e.*, θ, is maintained constant. If, however, experiments are done using various initial pressures p_0 of pure parahydrogen, the rate is found to vary as p_0^n, where n is now much less than unity. Thus at temperatures between -78 and $-100°$ and with pressures between 1 and 20 mm. Eley and Rideal[2] obtained values of n varying between very close to zero and 0.5. There is a tendency for the order to be greater the lower the temperature; thus in one run at $-78°$ the order was 0.04 and in a comparable one at $-159°$ it was 0.16. Farkas[1] also found low orders, his values lying between 0.25 and 0.33. Farkas obtained an activation energy of 3.8 kcal.; while the values of Eley and Rideal varied from 1.0 to 3.8 kcal.; however, as emphasized by Rideal and Trapnell,[8] these values have no simple significance owing to the variation of θ with the temperature. The absolute rate of the conversion was found by Eley and Rideal to be 2.1×10^{18} molecules per sq. cm. per sec. at $-100°$, at a pressure of 1 mm.

The Bonhoeffer-Farkas Mechanism.—According to the mechanism of Bonhoeffer and Farkas[4,5] the rate of conversion is simply the rate of adsorption of parahydrogen and is therefore given by

$$v = k(1-\theta)^2 p \qquad (1)$$

It will first be shown that this expression for the rate is consistent with the low kinetic orders that are obtained experimentally.

At the temperatures and pressures used in the conversion experiments $1-\theta$ is found[8,14] to vary approximately as $p^{-0.2}$ so that $(1-\theta)^2$ varies as $p^{-0.4}$. The rate constant k depends on pressure through ΔH^*. In the pressure region of the experiments it may be seen from the data of Rideal and Trapnell[8] that a tenfold increase in pressure changes θ by about 0.02 unit, and this changes ΔH for

(1) A. Farkas, *Z. physik. Chem.*, **B14**, 371 (1931).
(2) D. D. Eley and E. K. Rideal, *Proc. Roy. Soc.* (*London*), **A178**, 429 (1941).
(3) D. D. Eley, *ibid.*, **A178**, 429 (1941).
(4) K. F. Bonhoeffer and A. Farkas, *Z. physik. Chem.*, **B12**, 231 (1931).
(5) K. F. Bonhoeffer, A. Farkas and K. W. Rummel, *ibid.*, **B21**, 225 (1933).
(6) E. K. Rideal, *Proc. Camb. Phil. Soc.*, **35**, 130 (1939).
(7) D. D. Eley, *Trans. Faraday Soc.*, **44**, 216 (1948).
(8) E. K. Rideal and B. M. W. Trapnell, *J. chim. phys.*, **47**, 126 (1950).
(9) E. K. Rideal and B. M. W. Trapnell, *Faraday Soc. Disc.*, **8**, 114 (1950).
(10) B. M. W. Trapnell, *Proc. Roy. Soc.* (*London*), **A206**, 39 (1951).
(11) G. D. Halsey, *Trans. Faraday Soc.*, **47**, 649 (1951).
(12) A. Couper and D. D. Eley, *Proc. Roy. Soc.* (*London*), **A211**, 536 (1952).
(13) J. K. Roberts, *ibid.*, **A152**, 445 (1935).
(14) W. G. Frankenburg, *J. Am. Chem. Soc.*, **66**, 1827 (1944).

adsorption by not more than about 1.0 kcal. Assuming a symmetrical potential energy barrier, this means that ΔH^* for adsorption will increase by about 0.5 kcal. when the pressure increases tenfold, and at $-100°$ the value of k is reduced by $10^{0.6}$. Under these conditions $(1 - \theta)^2 k$ therefore varies as $p^{-0.4} \times p^{-0.6}$, *i.e.*, as p^{-1}. The rate is therefore independent of p, *i.e.*, the kinetics are zero order.

A consideration of the reaction along these lines, taking into account the pressure variations of $1 - \theta$ and k, therefore leaves no difficulty in connection with the orders of reaction of close to zero that were observed experimentally. The variation in $(1 - \theta)^2 k$ that was deduced above represents the highest that is to be expected, so that under certain conditions the order will be higher. Smaller variations in $(1 - \theta)^2 k$ are to be expected the higher is θ, *i.e.*, at lower temperatures or higher pressures. It would therefore be predicted that the order will tend to increase at lower temperatures or higher pressures and this appears to be the case.

The plausibility of this interpretation of the reaction may be checked by an order of magnitude calculation of the rate at $-100°$ and a pressure of 1 mm. The rate is given by eq. (10) of the previous paper[15] and it will be assumed that $f_{\ddagger} = f_a$. The partition function for parahydrogen is 3.4×10^{22} at this temperature. The surface is about 90% covered, so that the concentration of bare single sites, c_s, is equal to $L(1 - \theta) = 10^{14}$ sites per sq. cm.; the coördination number s is assumed to be 4. Using these values the rate of the conversion is calculated to be

$$v = 6.0 \times 10^{18}\, e^{-E_1/RT} \text{ molecules cm.}^{-2} \text{ sec.}^{-1}$$

This is consistent with the experimental value of 2.1×10^{18} if there is a small activation energy.

(15) K. J. Laidler, THIS JOURNAL, **57**, 318 (1953).

This conclusion is to be contrasted with that of Couper and Eley[11] who, as discussed in the preceding paper,[15] employ an incorrect equation for calculating the absolute rate.

It may be concluded from the above that there is no major difficulty in interpreting the conversion on the basis of the Bonhoeffer–Farkas mechanism.

The Rideal Mechanism.—It does not seem possible to account for the results on the basis of the Rideal mechanism, as has also been concluded by Trapnell. If the reaction occurred between an adsorbed atom and a molecule in the gas phase the rate would be proportional to θkp. Now since the surface is fairly fully covered θ varies only very slightly with p, so that θkp varies approximately as $p^{-0.6} \times p = p^{0.4}$. It therefore is not possible to interpret on this basis the experimental orders which are close to zero. A lower pressure dependence may be obtained by assuming the hydrogen molecule to be adsorbed in a van der Waals layer, but the coverage in the second layer has to be quite considerable. Such a high coverage is not reasonable in view of the low adsorption heats for a van der Waals layer.

Absolute rate calculations also render this type of mechanism unlikely. The rate is now found to be $10^{20}\, e^{-E/RT}$ and this requires an activation energy of about 1.5 kcal. for agreement with the data. This is too low for this type of mechanism, involving the dissociation of a hydrogen molecule by interaction with an adsorbed hydrogen atom; a value of 7 kcal. applies to the reaction $H + p\text{-}H_2 \rightarrow o\text{-}H_2 + H$ even when the reacting atom is free and the Rideal mechanism should require a value at least as great as this.

The author is much indebted to Dr. B. M. W. Trapnell for valuable discussions and suggestions in connection with this paper.

MOLECULAR KINETICS AND MECHANISM OF METHANE-DEUTERIUM EXCHANGE REACTIONS ON NICKEL

BY MARIA CLARE MARKHAM, MARY COLMAN WALL AND KEITH J. LAIDLER

Department of Chemistry, The Catholic University of America, Washington, D. C.

Received May 23, 1952

The data of Kemball on the methane–deuterium exchange on evaporated nickel are discussed, mechanisms are formulated, and absolute rate equations derived. CH_3D is considered to be formed from adsorbed CH_3 and D, and the rate of production of CH_3D is shown to be approximately equal to the rate of adsorption of methane as methyl radicals. CH_2D_2, CHD_3 and CD_4 are considered to be formed by reaction between adsorbed methylene radicals and adsorbed deuterium atoms, and a treatment is given for the relevant statistical factors. Calculated rates for all four processes are in excellent agreement with the experimental ones.

Introduction

The object of the present paper is to consider recent data on the surface-catalyzed exchange reactions between methane and deuterium, to propose definite mechanisms, to formulate expressions for absolute rates, and to check the mechanisms by means of rate calculations.

The exchange reactions between methane and deuterium have recently been the object of careful experimental study by Kemball,[1] who used evaporated nickel surfaces. He measured the rates of formation of CH_3D, CH_2D_2, CHD_3 and CD_4, and determined an activation energy for each process. All of the rates were found to be proportional to the first power of the methane pressure. The rate of formation of CH_3D is inversely proportional to the square root of the deuterium pressure, while the rates of formation of CH_2D_2, CHD_3 and CD_4 are inversely proportional to the first power of the deuterium pressure. As suggested by Kemball, this result implies that the methyl radicals do not

(1) C. Kemball, *Proc. Roy. Soc.* (*London*), **B207**, 539 (1951).

TABLE I

RATES OF FORMATION OF CH_2D_2, CHD_3 AND CD_4 AT 500°K.

		Rate (molecules mg.$^{-1}$ sec.$^{-1}$ × 10^{-12})								
		CH_2C_2			CHD_3			CD_4		
P_{D_2} (mm. 0°)	P_{CH_4}	Calcd. (E = 32.0)	Calcd. (E = 33.0)	Obsd.	Calcd. (E = 32.0)	Calcd. (E = 33.0)	Obsd.	Calcd. (E = 32.0)	Calcd. (E = 33.0)	Obsd.
2.49	12.4	220	88	96	1260	380	340	2380	700	780
4.85	3.26	6	2.4	1.7	82	25	30	440	130	130
4.85	9.69	58	23	22	340	100	130	1100	440	460
14.4	3.20	0.8	0.3	0.4	18	5	5	140	40	36

rapidly undergo exchange with adsorbed deuterium atoms, but merely add on atoms to form CH_3D. The other deuterated methanes must then be formed in another manner, and the simplest hypothesis is that they are produced from adsorbed CH_2 radicals. Kemball has in fact produced evidence for two kinds of equilibria, one probably involving adsorbed CH_3 and the other adsorbed CH_2.

The exchange mechanisms formulated in the present paper are considerably more explicit than those of Kemball, but our discussion is, except in a few details, consistent with his. The general approach to the problem is similar to that given for the parahydrogen conversion.[2] The exchange processes occurring on the surface, *i.e.*, the production of absorbed CH_3D from adsorbed CH_3 and D and of adsorbed CH_2D_2, CHD_3 and CD_4 from adsorbed CH_2 and D, are considered to occur rapidly, the slow process in each case being the desorption of the products from the surface. Adsorption equilibrium, apart from exchange, is assumed to be established rapidly, and the concentrations of adsorbed CH_3 and CH_2 will therefore be calculated from the equilibrium expressions. The rate of removal of CH_3 from the surface, equal to the rate of adsorption of methane as CH_3, controls the rate of production of CH_3D, the proportionality factor being the statistical weight expressing the probability that an adsorbed CH_3 will pick up a D rather than an H. Similarly the rates of production of CH_2D_2, CHD_3 and CD_4 are controlled by the over-all rate of desorption of CH_2, which is initially equal to the rate of adsorption of methane as CH_2; the proportionality factors are now the statistical factors for the uptake of two, three and four deuterium atoms, respectively.

In the present formulation of the kinetic expressions the notation is the same as in previous publications.[2-6]

Formation of CH_3D.—Methyl radicals, hydrogen atoms and deuterium atoms are assumed to be adsorbed on single surface sites, and the rate of formation of CH_3D is the rate with which adsorbed CH_3 and D are desorbed together from the surface. The equilibria for deuterium adsorption may be written as

$$\tfrac{1}{2}D_2 + S \rightleftarrows S\text{-}D \qquad (I)$$

The equilibria involving H_2 and HD may be neglected since initially D_2 predominates. The surface is sparsely covered by methane and well covered by deuterium, so that the concentration of bare sites is given by the equations

$$L = c_S + c_{a'} \qquad (1)$$

and

$$c_{a'}/c_S = K' c_{g'}^{1/2} \qquad (2)$$

where the prime indicates deuterium. These equations give rise to

$$c_S = \frac{L}{1 + K' c_{g'}^{1/2}} \qquad (3)$$

$$\simeq L/K' c_{g'}^{1/2} \qquad (4)$$

for full coverage.

The rate of adsorption of methane as methyl radicals is

$$v = c_g c_S \frac{kT}{h} \frac{f_\pm}{F_g f_S} e^{-\epsilon_0/kT} \qquad (5)$$

$$= \frac{c_g}{c_{g'}^{1/2}} \frac{L}{K'} \frac{kT}{h} \frac{f_\pm}{F_g f_S} e^{-\epsilon_0/kT} \qquad (6)$$

$$= \frac{c_g}{c_{g'}^{1/2}} L \frac{kT f_\pm}{h} \frac{F_{g'}^{1/2}}{F_g f_{a'}} e^{-(\epsilon_0+\epsilon)/kT} \qquad (7)$$

since $K' = (f_{a'}/F_{g'}^{1/2} f_S) e^{\epsilon/kT}$ where ϵ is the energy of adsorption at 0°K. per deuterium atom. The treatment is seen to account correctly for the pressure dependence of the rate. This equation essentially gives the rate of desorption of CH_3D, since the probability that an adsorbed CH_3 will pick up a deuterium atom is close to unity on account of the high surface coverage by deuterium atoms.

Equation (7) has been applied to Kemball's data, taking $f_\pm$ and $f_{a'}$ as unity, and L as 13.6 × 10^{16} sites per milligram of catalyst, this value having been determined directly by Kemball. The partition functions were calculated from the free energy values given in the National Bureau of Standards tables. The value of 24.75 kcal. was used for E_0 [$=N(\epsilon_0 + \epsilon)$], being obtained from the experimental value of 24.0 kcal. by the addition of 3/4 RT. At 500°K. and deuterium and methane pressures of 2.49 mm. and 12.4 mm. the calculated rate is found to be 1.3 × 10^{14} molecules mg.$^{-1}$ sec.$^{-1}$, as compared with an experimental rate of 1.9 × 10^{14}. At pressures of 14.4 and 3.20, respectively, the calculated rate is 1.3 × 10^{13}, the observed 1.5 × 10^{13} molecules mg.$^{-1}$ sec.$^{-1}$. The agreement is seen to be very satisfactory.

Formation of CH_2D_2, CHD_3, CD_4.—In addition to being adsorbed as methyl radicals it must be assumed that methane is also adsorbed as methylene radicals, which are presumably attached to two surface sites

(2) K. J. Laidler, THIS JOURNAL, **57**, 320 (1953).
(3) K. J. Laidler, *Disc. Faraday Soc.*, **8**, 47 (1950).
(4) K. J. Laidler, THIS JOURNAL, **55**, 1067 (1951).
(5) K. J. Laidler, S. Glasstone and H. Eyring, *J. Chem. Phys.*, **8**, 667 (1940).
(6) S. Glasstone, K. J. Laidler and H. Eyring, "The Theory of Rate Processes," McGraw-Hill Book Co., Inc., New York, N. Y., 1941.

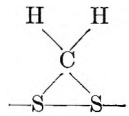

Whereas adsorbed methyl radicals can only add deuterium atoms, methylene radicals can undergo rapid surface exchange and be desorbed as CHD_3 and CD_4 as well as CH_2D_2.

The initial equilibria are

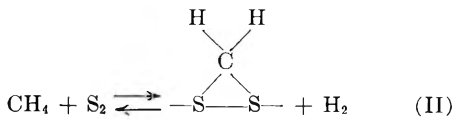

$$CH_4 + S_2 \rightleftharpoons \text{—S—S—} + H_2 \qquad \text{(II)}$$

and

$$\tfrac{1}{2}D_2 + S \rightleftharpoons S\text{-}D \qquad \text{(III)}$$

The methylenes only sparsely cover the surface, so that eq. (4) again gives the concentration of single sites. The concentration of dual sites is equal to $\frac{1}{2}\, sc_s^2/L$, where s is the coördination number, so that

$$c_{S_2} = \tfrac{1}{2}sL/K'^2c_{g'} \qquad (8)$$

The rate of adsorption of methane in the form of methylene is given by

$$v = c_g c_{S_2} \frac{kT}{h} \frac{f_\pm}{F_g f_{S_2}} e^{-\epsilon_0/kT} \qquad (9)$$

$$= \frac{1}{2^8} \frac{c_g}{c_{g'}} \frac{L}{K'^2} \frac{kT}{h} \frac{f_\pm}{F_g f_{S_2}} e^{-\epsilon_0/kT} \qquad (10)$$

$$= \tfrac{1}{2}s \frac{c_g}{c_{g'}} L \frac{kT}{h} \frac{f_\pm f_S^2 F_{g'}}{f_a^2 F_g f_{S_2}} e^{-(\epsilon_0+2\epsilon)/kT} \qquad (11)$$

Equation (11) also gives the total rate of desorption of CH_2 in the form of the various methanes, and is seen to give the correct pressure dependence for the formation of CH_2D_2, CHD_3 and CD_4. To obtain the rates of formation of these, eq. (11) must be multiplied by suitable statistical factors, as follows. It is assumed that surface equilibration is established rapidly compared with the rates of desorption. Let q be the probability of a deuterium atom being picked up, and $1 - q$ the probability of a hydrogen atom being picked up. Then the relative probabilities that an adsorbed CH_2 will form CH_2D_2, CHD_3 and CD_4 are $6(1 - q)^2q^2$, $4q^3(1 - q)$ and q^4. Kemball has listed experimental values of $q/(1 - q)$ and these are used in the following calculations; the theoretical interpretation of q is given in the Appendix.

Calculations were made by eq. (11) and using Arrhenius activation energies of 32 and 33 kcal.; Kemball actually obtained values of 34, 31 and 31 kcal. for the three reactions but it seems highly probable that the same value should apply to each. The E_0 values used were obtained by subtracting $1/2\ RT$ from the Arrhenius values. The partition functions $f_\pm$, f_S, f_a and f_{S_2} were taken as unity, L as 13.6×10^{16} per mg. (as determined by Kemball) and s as 4. The agreement between calculated and observed values is seen from Table I to be extremely good when the value of 33 kcal. is used.

APPENDIX

Theory of the Statistical Factors.—The problem is primarily to calculate the concentration of adsorbed hydrogen atoms ($c_{a''}$) in terms of the concentrations of gaseous methane and deuterium. These hydrogen atoms arise from the adsorption of methane as methylene radicals, so that in addition to reactions (II) and (III) above the adsorption process

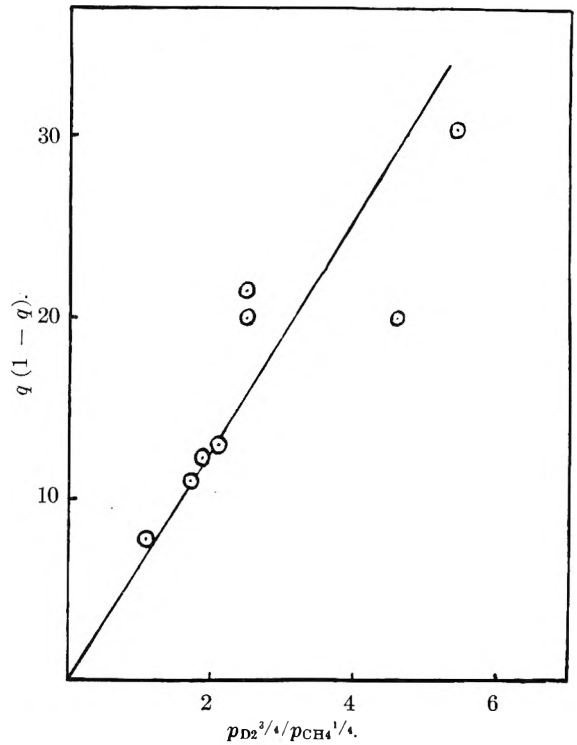

Fig. 1.—Plot of $q(1 - q)^{-1}$ *vs.* $p_{D_2}^{3/4}/p_{CH_4}^{1/4}$; *cf.* eq. (18).

$$\tfrac{1}{2}H_2 + S \rightleftharpoons S - H \qquad \text{(IV)}$$

must be considered. The equilibrium expressions corresponding to reactions (II) and (IV) are

$$c_a c_{g''}/c_g c_{S_2} = K \qquad (12)$$

and

$$c_{a''}/c_{g''}^{1/2} c_S = K'' \qquad (13)$$

c_{S_2} is given by eq. (8) above. Since an adsorbed methylene corresponds either to two adsorbed hydrogen atoms or to one gaseous hydrogen molecule it follows that

$$c_a = \tfrac{1}{2}c_{a''} + \frac{V}{S} c_{g''} \qquad (14)$$

where V is the gas volume and S the surface area. Equations (12), (13) and (14) give rise to

$$c_{a''}^4 + \frac{SK''^2L}{sV} c_{S_2} c_{a''}^3 - \frac{4SK''^4L^2K}{s^2V} c_g c_{S_2}^3 = 0 \qquad (15)$$

Consideration of the magnitudes of the quantities in this equation reveals that the second term can be neglected; hence

$$c_{a''} = \left[\frac{4SKK''^4L^2}{s^2V} c_g c_{S_2}^3\right]^{1/4} \qquad (16)$$

$$= \left[\frac{sSKK''^4L^5}{VK'^6}\right]^{1/4} \frac{c_g^{1/4}}{c_{g'}^{3/4}} \qquad (17)$$

Since $c_{a'}$ is essentially L, it follows that

$$\frac{q}{1 - q} = \frac{c_{a'}}{c_{a''}} = \left[\frac{VK'^6}{sSKK''^4L}\right]^{1/4} \frac{c_{g'}^{3/4}}{c_g^{1/4}} \qquad (18)$$

According to this a plot of $q(1 - q)^{-1}$ *vs.* $c_{g'}^{3/4}/c_g^{1/4}$ should be linear; such a plot is shown in Fig. 1, and it is seen that eq. (18) is consistent with the data.

ADSORPTION ON PROTEINS, THE GRAND PARTITION FUNCTION AND FIRST-ORDER PHASE CHANGES, ACCORDING TO APPROXIMATE STATISTICAL MECHANICAL THEORIES

BY TERRELL L. HILL

Naval Medical Research Institute, Bethesda, Md.

Received July 22, 1952

Adsorption on protein molecules in solution is an *actual* illustration of Gibbs' grand canonical ensemble. The transition in properties that occurs as the number of adsorption sites per protein molecule, B, gets very large is examined using the Bragg–Williams approximation. With sufficiently large attractive interactions between adsorbed molecules, the usual partition function, Q, based on an approximate theory (*e.g.*, Bragg–Williams), predicts a loop and first-order phase change for $B \to \infty$. A rigorous theory would give the thermodynamically stable equilibrium path instead of a loop in the two-phase region. Employment of the complete grand partition function, Ξ, instead of Q eliminates the loop and gives the stable equilibrium path even with an approximate theory. However, in this case a related deficiency in the theory replaces the loop difficulty, as must be expected. Fluctuations and the critical point are discussed. The above considerations apply to the Bragg–Williams approximation, the van der Waals equation, the Lennard–Jones and Devonshire theory of liquids, the quasi-chemical approximation for regular solutions, etc.

I. Introduction

Adsorption (or "binding") on protein molecules in solution is not only an important problem in its own right but is also an interesting *actual* illustration of Gibbs' grand canonical ensemble.[1] We examine in this paper the relations between protein adsorption with attractive interactions,[2] the grand partition function and first-order phase changes, using approximate statistical mechanical theories. Approximate theories of condensation of the van der Waals and Lennard–Jones and Devonshire type, phase splitting in "regular" solutions, etc., are related systems to which essentially the same considerations apply. However, it should be understood throughout the paper that while individual systems of the grand ensemble happen to have a physical significance in the protein adsorption problem, in referring to liquids, solutions, etc., the systems of the grand ensemble have only the usual abstract meaning of mental replicas of the single physical system.

While the language of this paper is that appropriate to adsorption on proteins, most of the discussion is in fact concerned with certain properties of approximate partition functions in relation to phase changes. In this connection, the partition functions written below do not include explicit contributions associated with the protein molecules themselves (*e.g.*, translation and rotation)—that is, the protein molecules are viewed as independent of each other and simply as furnishing sites for adsorption of solute molecules. We shall reserve for the future a more detailed discussion of protein binding, including interactions between protein molecules which depend on the amount of solute bound.

For recent papers using the grand canonical ensemble, see for example the work of Mayer, Kirkwood and others.[3-6]

(1) T. L. Hill, *J. Chem. Phys.*, **18**, 988 (1950).

(2) Adsorption of a gas onto very small particles (*e.g.*, dust in the atmosphere) is an equivalent system.

(3) W. G. McMillan and J. E. Mayer, *J. Chem. Phys.*, **13**, 276 (1945); J. E. Mayer, *ibid.*, **10**, 629 (1942); **19**, 1024 (1951); B. H. Zimm, *ibid.*, **19**, 1019 (1951).

(4) J. G. Kirkwood and R. J. Goldberg, *ibid.*, **18**, 54 (1950); J. G. Kirkwood and F. P. Buff, *ibid.*, **19**, 774 (1951).

(5) W. H. Stockmayer, *ibid.*, **18**, 58 (1950).

(6) H. C. Brinkman and J. J. Hermans, *ibid.*, **17**, 574 (1949).

II. Adsorption on Proteins and the Grand Partition Function

Consider a solution containing a very large number of protein molecules. Each protein molecule contains $B \geq 1$ equivalent sites for the localized adsorption of a solute from the solution. The chemical potential of the solute in solution is μ, its activity is a and its absolute activity is λ

$$\begin{aligned} \mu &= \mu^0(T) + kT \ln a \\ &= kT \ln \lambda \end{aligned} \qquad (1)$$

$\mu^0(T)$, a standard free energy, is a function of temperature only (the hydrostatic pressure on the solution is kept constant). We may consider each protein molecule as presenting an area $\mathfrak{a}$ (proportional to B). Then in this case the grand canonical ensemble consists of a large number of open "systems" ("system" = a protein molecule of area $\mathfrak{a}$, at temperature T, and with N adsorbed molecules) in equilibrium with a reservoir of adsorbate molecules at T and μ (solute molecules in solution). Let $Q(B,N,T)$ be the partition function for N molecules adsorbed on B sites, at T. Then the grand partition function[7] is

$$\Xi = \sum_{N=0}^{B} Q(B,N,T)\lambda^N \qquad (2)$$

The average number of adsorbed molecules per protein molecule is then[7]

$$\overline{N} = \left(\sum_{N=0}^{B} NQ\lambda^N \right) \Big/ \Xi \qquad (3)$$

Equation (3) is the adsorption isotherm, as it gives $\overline{N}(B,\lambda,T)$.

Special cases of eq. (3), derived from step-by-step equilibrium constants, have in fact been used for a long time[8-10] in treating the acid and base dissociation of, for example, polybasic acids and proteins, binding of ions and molecules on proteins, etc. To verify this connection we can write eq.

(7) R. H. Fowler and E. A. Guggenheim, "Statistical Thermodynamics," Cambridge University Press, 1939; G. S. Rushbrooke, "Introduction to Statistical Mechanics," Oxford University Press, 1949.

(8) E. J. Cohn and J. T. Edsall, "Proteins, Amino Acids and Peptides," Reinhold Publ. Corp., New York, N. Y., 1943, Chapter 20.

(9) G. Scatchard, *Ann. N. Y. Acad. Sci.*, **51**, 660 (1949).

(10) I. M. Klotz in "Modern Trends in Physiology and Biochemistry," Academic Press, New York, N. Y., 1952, edited by E. S. G. Barron.

(3) in conventional equilibrium constant form. Let us define $P(N)$ as $Q\lambda^N$. Then P is proportional to the probability that a given protein molecule will have N adsorbed molecules, or to the fraction or number of protein molecules with N adsorbed molecules. Then one finds, for example

$$\frac{P(N)a^{N'-N}}{P(N')} = \frac{Q(N)[\exp(-\mu^\circ/kT)]^{N'-N}}{Q(N')} \qquad (4)$$

Equation (4) has the usual equilibrium constant form with the proper relation to partition functions.

In the absence of interactions

$$Q = \frac{B!j^N}{N!(B-N)!} \qquad (5)$$

where $j(T)$ is the "intrinsic" partition function for adsorption on a particular site. Equations (3) and (5) give, of course, the Langmuir equation[7] for any $B \geq 1$,

$$\bar{\theta} = \bar{N}/B = j\lambda/(1+j\lambda) \qquad (6)$$

III. Adsorption on Proteins Using the Bragg–Williams Approximation

Even when there are strong attractive interactions between adsorbed molecules, it is easy to see that critical phenomena cannot occur if each protein molecule has only a few sites B. However, they can occur for B of the order of, say, 10^{23}, as is well known.[7] In this section we examine this rather instructive transition, using the grand partition function and the Bragg–Williams (B–W) approximation. As will be clear below, other approximate but more refined and complicated theories (*e.g.*, the quasi-chemical or Bethe approximation[7]) will lead to the same general results.

Experimental examples of protein binding with *attractive* interactions have been relatively rare; however, Colvin[11] has recently encountered a number of excellent examples of this type of behavior, with adsorption isotherms of the same form as those shown below.

We must mention first the essential features in the B–W approximation. Suppose each site has z nearest neighbor sites and the interaction free energy[12] between two adsorbed molecules on nearest neighbor sites is w. Then in this approximation[7]

$$Q = \frac{B!j^N}{N!(B-N)!}\exp(-\alpha N^2/B) \qquad (7)$$

$$\alpha \equiv zw/2kT$$

There will be appreciable geometrical difficulties[13] in arranging each site with z nearest neighbors for B too small (say $B < 10$). A partition function of this same form may also represent, approximately, electrostatic interactions[8-10] (α positive), interacting hydration effects,[11] etc.

The conventional treatment[7] of eq. (7) for B *very large* is to write

$$\mu/kT = \ln\lambda = -(\partial \ln Q/\partial N)_{B,T} \qquad (8)$$

or

$$j\lambda = \frac{\theta}{1-\theta}\exp(2\alpha\theta) \qquad (9)$$

where $\theta = N/B$. Equation (9) may also be found by "picking out the maximum term" in Ξ; that is, from

$$(\partial \ln Q\lambda^N/\partial N)_{B,T,\lambda} = 0 \qquad (10)$$

Equations (10) and (8) are identical. For sufficiently negative α, eq. (9) predicts a first-order phase change.[7] For example, eq. (9) gives the characteristic loop ACDEFG in Fig. 1 for $\alpha = -3$ and the critical curve in Fig. 2 for $\alpha = -2$.

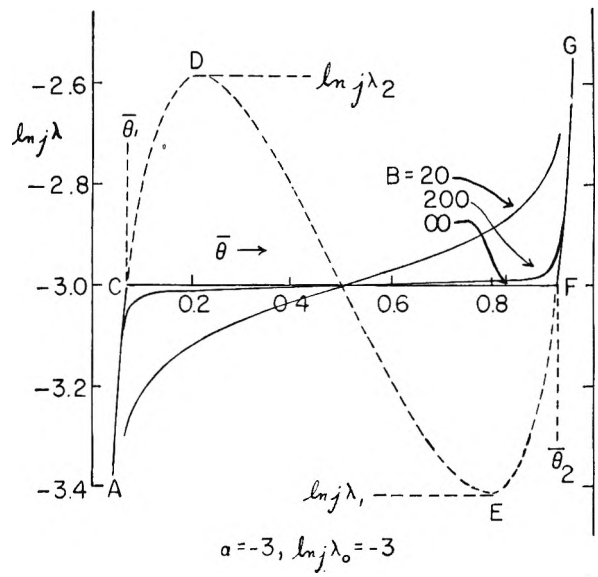

Fig. 1.—Adsorption isotherms in the form ln $j\lambda$ *versus* $\bar{\theta}$.

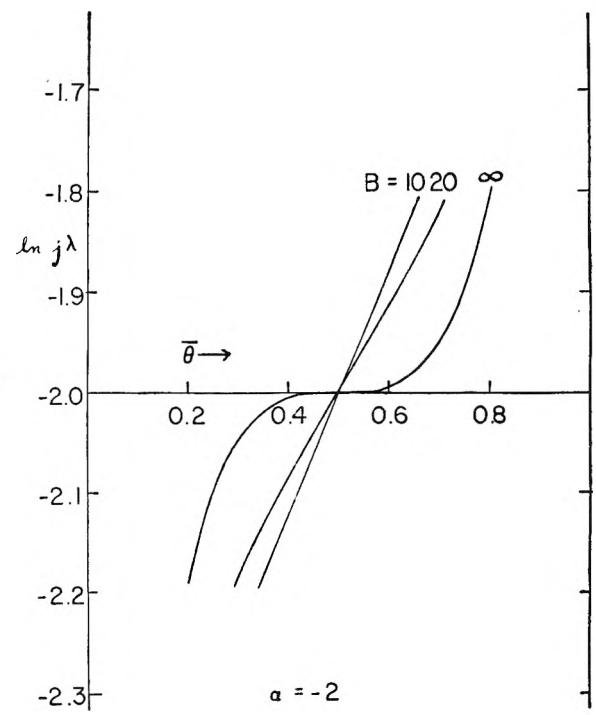

Fig. 2.—Adsorption isotherms in the form ln $j\lambda$ *versus* $\bar{\theta}$.

Phase Changes According to the Partition Function and the Grand Partition Function.—If we

(11) J. R. Colvin, *Canadian J. Chem.*, **30**, 320 (1952).

(12) E. A. Guggenheim, *Trans. Faraday Soc.*, **44**, 1007 (1948).

(13) The exact partition function for certain cases with $B \leq 12$ has been discussed by Scatchard,[9] M. F. Morales and J. Botts, *J. Chem. Phys.*, **16**, 587 (1948) and R. Peierls, *Proc. Roy. Soc.* (*London*), **A154**, 207 (1936).

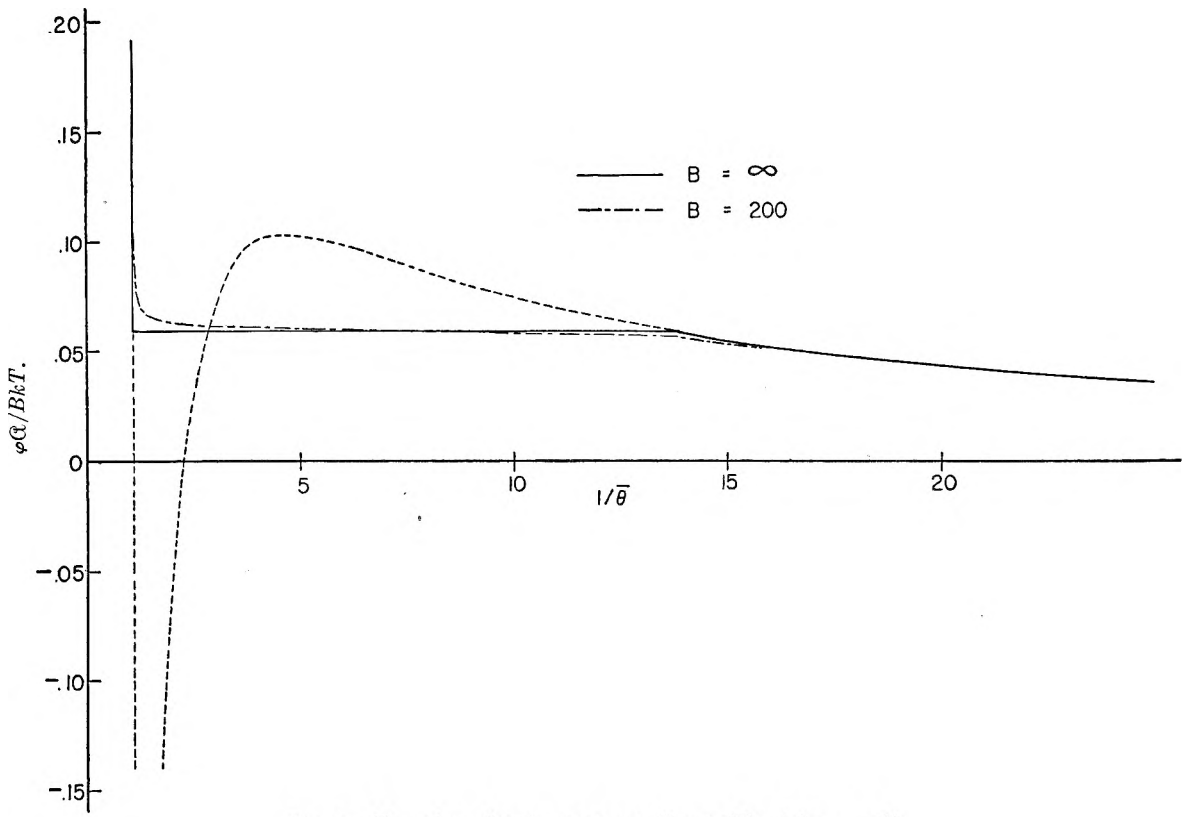

Fig. 3.—Equation of state, corresponding to Fig. 1 ($\alpha = -3$).

differentiate eq. (3) with respect to $\ln\lambda$, we get the well-known result of Gibbs

$$\left(\frac{\partial \ln \lambda}{\partial \bar{\theta}}\right)_T = \frac{B}{(N - \bar{N})^2} \qquad (11)$$

$$= -\frac{1}{\bar{\theta}^3}\left[\frac{\partial(\varphi\mathfrak{A}/BkT)}{\partial(1/\bar{\theta})}\right]_T \qquad (12)$$

where eq. (12) follows from thermodynamics.[13a] φ is the so-called surface or spreading pressure.[7] As the right hand side of eq. (11) cannot be negative, $\partial \ln \lambda/\partial\bar{\theta}$ is never negative and $\partial(\varphi\mathfrak{A}/BkT)/\partial(1/\bar{\theta})$ is never positive. That is, the complete grand partition function, in agreement with experiment and thermodynamics, cannot lead to a loop (even in an approximate theory) as encountered, for example, in Fig. 1 or with the van der Waals equation of state.

We now restrict ourselves temporarily to the case to N and B *very large* (of the order of 10^{23}). At an ordinary point (*i.e.*, not in a two-phase or critical region), experimentally and theoretically (*e.g.*, Figs. 1–3) the derivatives in eq. (11) and (12) are of the order of B^0. Then $(\theta - \bar{\theta})^2$ is of the order of B^{-1}, a very small quantity. Because of these extremely small fluctuations it is certainly legitimate, for an ordinary point, to pick out only the maximum term in Ξ (even in an approximate theory). Thus, for example, the branches AC and FG in Fig. 1 will be the same whether obtained from eq. (9) and (10) or from the complete Ξ. Let λ_0 be the value of λ at which two phases are in equilibrium, and let $\bar{\theta}_1$ and $\bar{\theta}_2$ be the values of $\bar{\theta}$ in the two phases (*e.g.*, Fig. 1). Then if we approach $\lambda = \lambda_0$ from two sides (A $\rightarrow$ C, G $\rightarrow$ F), at C the maximum term in Ξ is at $\theta = \bar{\theta}_1$ while at F the maximum term in Ξ is at $\theta = \bar{\theta}_2$. There are now two possibilities. (1) Consider a rigorous theory (*e. g.*, Mayer's theory of condensation or the Kramers–Wannier–Onsager–Kaufmann extension of the Ising model). It is generally accepted that, since a rigorous Q includes all possible configurations (even those configurations with two phases present simultaneously), Q and eq. (8) will in this case give the true equilibrium path CF rather than the loop CDEF. That is, eq. (8) has only one root for λ near and at λ_0. Then eq. (10), also, has only one root and Ξ only a single maximum term. As $\bar{\theta}$ passes from $\bar{\theta}_1$ to $\bar{\theta}_2$, the location of the maximum term in Ξ moves from $\theta = \bar{\theta}_1$ to $\theta = \bar{\theta}_2$ (see below also). Here, employment of this maximum term in Ξ (eq. (10)) is equivalent to the use of Q (eq. (8)). A loop is not encountered in either case. Also, of course, no loop is obtained from the complete Ξ (eq. (11)). (2) On the other hand, an approximate Q (*e.g.*, B–W, quasi-chemical, Lennard–Jones and Devonshire, van der Waals, etc.) which leads to a loop (eq. (8)) gives three roots in eq. (8) for $\lambda_1 < \lambda < \lambda_2$— and also in eq. (10). At $\lambda = \lambda_0$, P therefore has maxima at both C and F and a minimum in between. The loop in Fig. 1 is in fact the locus of

(13a) φ is the spreading pressure associated with an increase in B, but has this *thermodynamic* significance only when B is very large. When B is small, φ is *defined* by Eq. (13), and Eqs. (11) and (12) still hold provided B is held constant in the differentiations as well as T. For small (or large) B one can show that φ has the *thermodynamic* significance of a "spreading pressure" associated with an increase in the *total* surface area of all the protein molecules (considered distinguishable) by increasing their number at constant B. The number of protein molecules is assumed very large.

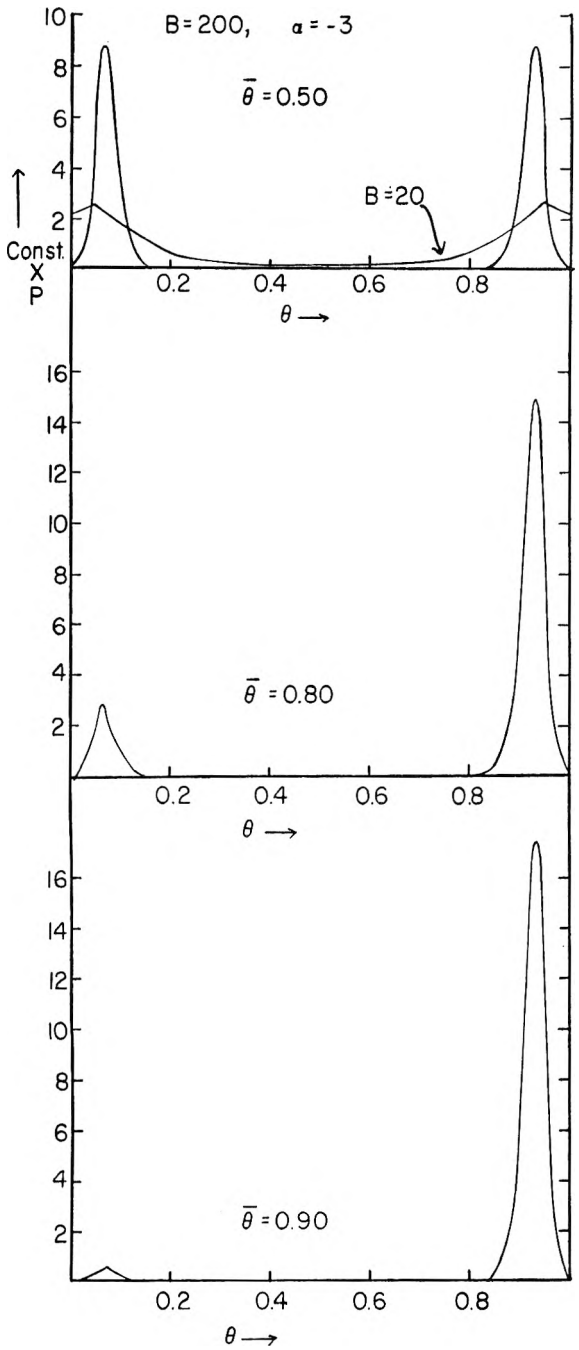

Fig. 4.—Transition from one phase to another in two-phase region, corresponding to Fig. 1.

the maxima and minimum in P (the thermodynamically impossible path DE locates the minimum; AD and EG the maxima). When $\bar{\theta} = \bar{\theta}_1$, there is a large maximum in P at $\theta = \bar{\theta}_1$ and an extremely small maximum at $\theta = \bar{\theta}_2$. This situation is reversed for $\bar{\theta} = \bar{\theta}_2$. In the transition, the $\theta = \bar{\theta}_2$ maximum is increased at the expense of the $\theta = \bar{\theta}_1$ maximum. In summary for an approximate Q: if Q (eq. (8)) gives ACDEFG, the complete Ξ gives ACFG; picking the *absolute* maximum term for each λ gives AC and FG; the indiscriminate use of eq. (10) gives ACDEFG.

Returning now to the situation with B not necessarily large, some of the points above, as well as the transition in behavior as $B \rightarrow \infty$, are illustrated in Figs. 1–6. Calculations for $B = 10$ and 20 were carried out by actual summation; for $B = 100$ and 200, intervals of $\Delta N = 5$ and numerical integration were used. Equations (2), (3), (7), and, in addition [7,13a]

$$\varphi\mathfrak{A} = kT \ln \Xi \qquad (13)$$

were employed in the calculations.[14]

Figure 1 shows ($B = 20$, 200, ∞; $\alpha = -3$) that the adsorption isotherm computed from the complete Ξ gradually approaches ACFG rather than ACDEFG as $B \rightarrow \infty$. Analogous curves are given in Fig. 2 at the critical ($B = \infty$) temperature, $\alpha = -2$. The $B = 200$ and ∞ curves of Fig. 1 are put in the alternative but thermodynamically equivalent form of an equation of state (eq. (13)) in Fig. 3.[13a] Figure 4 illustrates the transition, men-

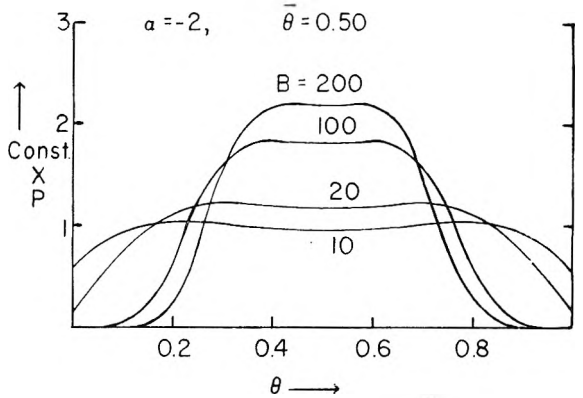

Fig. 5.—$P(\theta)$ for critical temperature and $\bar{\theta}$, corresponding to Fig. 2.

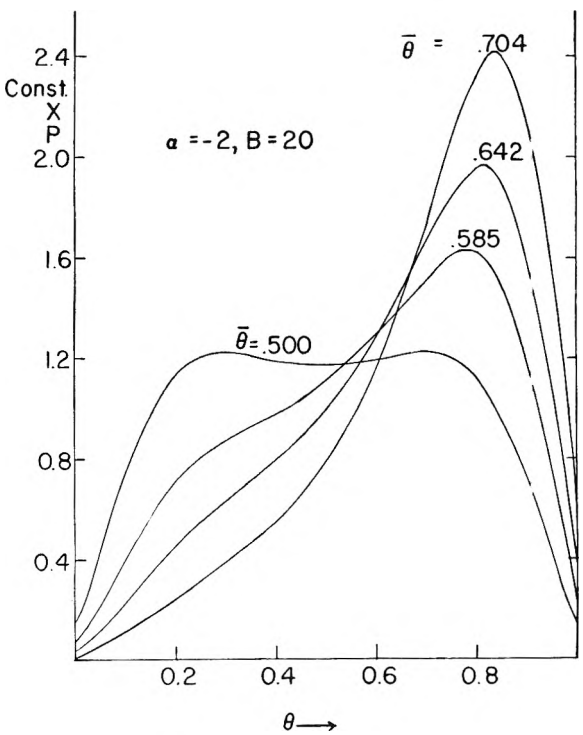

Fig. 6.—$P(\theta)$ for critical temperature and different values of $\bar{\theta}$, corresponding to Fig. 2.

(14) It is easy to prove that the symmetry apparent, for example, in Figs. 1 and 2 exists. This reduces the computations by a factor of about two.

tioned above, between the two maxima in $P(\theta)$ in the two-phase region (Fig. 1) for $\alpha = -3$, $B = 200$ and $\bar{\theta} = 0.50, 0.80$ and 0.90. The curves shown are normalized to unity. The $\bar{\theta} = 0.50$ case includes P for $B = 20$. Figure 5 gives $P(\theta)$, normalized to unity, at the critical temperature ($\alpha = -2$) and critical $\bar{\theta}$ ($\bar{\theta} = 0.50$), for $B = 10, 20, 100$ and 200. Figure 6 also refers to $\alpha = -2$, and shows $P(\theta)$ for $B = 20$ and several different values of $\bar{\theta}$.

For practical purposes, Fig. 4 shows "phase separation" even with B only 200. As $B \rightarrow \infty$, the behavior of $P(\theta)$ is the same except that the peaks get extremely sharp. Any approximate theory with a Q leading to loops will give $P(\theta)$ curves of this type—for reasons already discussed. As is well-known, the reason the loops (from Q) are obtained is that such theories restrict themselves implicitly to configurations with uniform macroscopic density throughout the system.[15] A rigorous Q will contain all possible configurations, including those representing two phases present simultaneously (non-uniform macroscopic density). Now, as is apparent in Fig. 1, the grand partition function eliminates the loops discussed above but the implicit restriction mentioned persists in $P(\theta)$ (Fig. 4), as must be expected. That is, according to Fig. 4, in the two-phase region with $B = \infty$ ($\bar{\theta}_1$ and $\bar{\theta}_2$—see above), a single protein molecule (a system in the grand ensemble) must have $\theta = \bar{\theta}_1$ or $\theta = \bar{\theta}_2$, but no intermediate value is possible except for extremely small fluctuations about $\bar{\theta}_1$ and $\bar{\theta}_2$. This is obviously unsatisfactory. This effect, which appears when the grand partition function is used with approximate theories of this type, replaces and is equivalent to the loop defect found when Q is employed in treating such theories. A rigorous theory will give a single maximum in $P(\theta)$ in the two-phase region, as discussed above, corresponding to the (experimental) fact that within a single system of the grand ensemble both phases can be present simultaneously.

Fluctuations in the Bragg-Williams Approximation. (a). Ordinary Point. B and $\bar{N}$ Large.—There is a single maximum in $P(N)$ (except for a second very small "embryonic" maximum[15] for $\lambda_0 < \lambda \leqslant \lambda_2$ and $\lambda_1 \leqslant \lambda < \lambda_0$, associated with the loop in Fig. 1—see above and also below). From eq. (7), an expansion of $\ln (P/P_{\max})$ about $N = N_{\max} = \bar{N}$ gives

$$\ln(P/P_m) = -\beta(N - \bar{N})^2 \qquad (14)$$

$$\beta = \frac{\alpha}{B} + \frac{1}{2\bar{N}} + \frac{1}{2(B - \bar{N})} \qquad (15)$$

Hence

$$\overline{(N - \bar{N})^2} = 1/2\beta \qquad (16)$$

in agreement with eq. (9) and (11). β is of the order of B^{-1} and hence $\partial \ln \lambda/\partial\bar{\theta}$ (eq. (11)) is of the order of B^0, as observed experimentally (for an ordinary point).

With regard to the relative height of the "embryonic" maximum[15] mentioned above: suppose we consider $\ln \lambda = \ln \lambda_0 + \Delta \ln \lambda$ in Fig. 1, where $\Delta \ln \lambda$ is small. Let P_2 be the value of P at the maximum in P just above (*i.e.*, by $\Delta \ln \lambda$) F and let P_1 be the value of P at the "embryonic" maximum in P just above C. Then on expanding $\ln P_2/P_1$ in powers of $\Delta \ln \lambda$, one finds

$$P_2/P_1 = \exp[(\Delta \ln \lambda)(\bar{N}_2 - \bar{N}_1)] \qquad (17)$$

where $\bar{N}_1$ and $\bar{N}_2$ are the values of $\bar{N}$ at C and F, respectively. For example, if $\Delta \ln \lambda = \Delta \ln j\lambda = 10^{-2}$ (compare Fig. 1) and $\bar{N}_2 - \bar{N}_1 \cong B = 10^5$, then $P_2/P_1 = \exp(10^3)$.

(b). Two Phase Point. B and $\bar{N}$ Large.—In the two-phase region, there are two comparable maxima as in Fig. 4. Then obviously $\overline{(N - \bar{N})^2}$ is of the order of B^2, and $\partial \ln \lambda/\partial\bar{\theta}$ (eq. (11)) is of the order of B^{-1} (compare, for example, $B = 20$ and 200 in Fig. 1 at $\bar{\theta} = 1/2$).

As a rough illustration of the corresponding situation for a rigorous theory, suppose $\ln \lambda$ varies linearly with N (*i.e.*, no loop) from N_1 (and λ_1) to N_2, with slope $\Delta \ln \lambda/\Delta N$. Then we can obtain an expression for $Q(N)$ and hence $P(N) = Q\lambda^N$ by integration of $d \ln Q = -\ln \lambda \, dN$. We find that $P(N)$ has a single maximum at

$$N_m = (\ln \lambda - \ln \lambda_1) \frac{\Delta N}{\Delta \ln \lambda} + N_1$$

which travels from N_1 to N_2, and that (in agreement with eq. (11), (14) and (16))

$$P/P_m = \exp\left[-\frac{1}{2}\frac{\Delta \ln \lambda}{\Delta N}(N - N_m)^2\right] \qquad (18)$$

If $\Delta \ln \lambda/\Delta\theta$ is of the order of B^{-1}, then [ ] in eq. (18) is of the order of $-(\theta - \theta_m)^2$. Thus a single extremely broad maximum replaces the two sharp maxima above—but in both cases $\overline{(N - \bar{N})^2}$ is of the order of B^2.

(c). Critical Point. B and $\bar{N}$ Large.—If we expand $\ln P/P_m$ about $N = \bar{N} = B/2$ at the critical temperature and critical λ, the result is

$$\ln(P/P_m) = -\frac{4(N - \bar{N})^4}{3B^3} - \frac{32}{15}\frac{(N - \bar{N})^6}{B^5} - \ldots \qquad (19)$$

The "flat top" in Fig. 5 is of course due to the missing term in $(N - \bar{N})^2$. The leading term of the series gives $\overline{(N - \bar{N})^2}$ of the order of $B^{3/2}$ [intermediate between B (ordinary point) and B^2 (two-phase point)] and $\partial \ln \lambda/\partial\bar{\theta}$ of the order of $B^{-1/2}$. B^2 is of course the upper limit for the order of $\overline{(N - \bar{N})^2}$ and Zimm[3] believes that a rigorous theory of gas condensation may give this order of magnitude for $\overline{(N - \bar{N})^2}$ at the critical point. Incidentally, if the leading term in eq. (19) involves $(N - \bar{N})^{2n}$, then $\overline{(N - \bar{N})^2}$ is of the order of $B^{2-(1/n)}$.

By repeated differentiation of eq. (3), one finds in addition to eq. (11)

$$\frac{\partial^2 \ln \lambda}{\partial\bar{\theta}^2} = -\frac{B^2\overline{x^3}}{(\bar{x^2})^3} \qquad (20)$$

$$\frac{\partial^3 \ln \lambda}{\partial\bar{\theta}^3} = -\frac{B^3[\overline{x^4} - 3(\bar{x^2})^2]}{(\bar{x^2})^4} + \frac{3B^3(\bar{x^3})^2}{(\bar{x^2})^5} \qquad (21)$$

(15) Although this restriction is unsatisfactory for a complete equilibrium theory, it happens to be of some physical interest because just this feature is involved in metastable states, nucleation, hysteresis, etc.

where $x = N - \bar{N}$. One can then deduce the orders of magnitude given in Table I. In particular, $\partial^3 \ln \lambda/\partial\bar{\theta}^3$ is of order unity at the critical point—the same conclusion obtained simply from eq. (9).

TABLE I

BRAGG–WILLIAMS THEORY

Point	$\partial \ln \lambda/\partial\bar{\jmath}$	$\partial^2 \ln \lambda/\partial\bar{\jmath}^2$	$\partial^3 \ln\lambda/\partial\bar{\theta}^3$
Ordinary	B^0	B^0	B^0
Critical	$B^{-1/2}$	0 (by symmetry)	B^0
Two-phase	B^{-1}	B^{-1}	B^{-1}

The discussion of the first (eq. (12)) and higher derivatives associated with the equation of state is essentially equivalent and will be omitted.

(d). Energy Fluctuations.—The connection between energy fluctuations and heat capacity is well known. We consider this point briefly here in relation to the above discussion. Consider a Q of the form[7]

$$Q = j(T)^N \sum_{\mathfrak{N}} g(\mathfrak{N},N,B) \exp(-\mathfrak{N}w/kT) \quad (22)$$

where g is the number of configurations with exactly $\mathfrak{N}$ nearest neighbor pairs. The rigorous partition function in the gas condensation problem can be put in essentially equivalent form—so eq. (22) is actually rather general. Differentiating[16] eq. (22) twice with respect to $-w/kT$ (compare eq. (11)) we find

$$(kT^2/w^2)(C_a - C_i) = \overline{(\mathfrak{N} - \bar{\mathfrak{N}})^2} \quad (23)$$

where C_a is the heat capacity at constant area (volume, in a three dimensional problem), C_i is the "internal" heat capacity associated with $j(T)$, and $\bar{\mathfrak{N}}w$ is the average potential energy of the system. Now experimentally and theoretically, $C_a - C_i$ is of the order of Bk, even in a critical or two-phase region,[17] and hence $\overline{(\mathfrak{N} - \bar{\mathfrak{N}})^2}$ is of the order of B. For large B, there is thus a sharp maximum in the terms of the sum in eq. (22) and it is legitimate to use the maximum term only, even in a two-phase region and with an approximate theory (unlike the situation with the grand partition function—see above).

As an example, consider the quasi-chemical approximation[18] with $z = 4$. Let $R = g \exp(-\mathfrak{N}w/kT)$. Then on expanding about $\mathfrak{N} = \bar{\mathfrak{N}} = \mathfrak{N}_{max}$ (B and N large)

$$\ln(R/R_m) = -\beta'(\mathfrak{N} - \bar{\mathfrak{N}})^2 \quad (24)$$

$$\overline{(\mathfrak{N} - \bar{\mathfrak{N}})^2} = 1/2\beta' \quad (25)$$

(16) Here we take w independent[12] of T.

(17) Using three dimensional language, in a two-phase region C_p is (virtually) infinite because $dT = 0$ when heat is absorbed by the two-phase system at *constant pressure*. But if the same system absorbs heat at *constant volume*, in general $dp \neq 0$ and $dT \neq 0$, so C_v is finite.

(18) We use the g, due to Chang, given on p. 310 of Rushbrooke.[7]

$$\beta' = \frac{1}{4B}\left[\frac{1}{(\bar{\mathfrak{N}}/2B)} + \frac{1}{1 - 2\theta + (\bar{\mathfrak{N}}/2B)} + \frac{2}{\theta - (\bar{\mathfrak{N}}/2B)}\right] \quad (26)$$

where $(\bar{\mathfrak{N}}/2B)$ is determined by the familiar relation

$$\frac{(\bar{\mathfrak{N}}/2B)\,[1 - 2\theta + (\bar{\mathfrak{N}}/2B)]}{[\theta - (\bar{\mathfrak{N}}/2B)]^2} = \exp(-w/kT) \quad (27)$$

IV. van der Waals' Equation

Van der Waals' equation is based on a partition function very similar to the B–W partition function. A completely analogous discussion can be given replacing φ by p and $\mathfrak{a}$ by V. However, we merely indicate that

$$Q = \frac{1}{N!}(B - N)^N \left[\left(\frac{2\pi mkT}{h^2}\right)^{3/2} b\right]^N \exp(\alpha' N^2/B) \quad (28)$$

$$\alpha' = a/bkT,\ B = V/b$$

Also, in place of eq. (19), we find

$$\ln(P/P_m) = -\frac{243}{64}\left[\frac{(N - \bar{N})^4}{B^3} - \frac{3(N - \bar{N})^5}{5B^4} + \ldots\right] \quad (29)$$

Hence the general remarks about the B–W critical point apply here also.

V. Two Component Solution—Bragg–Williams Approximation

In this section we put the usual B–W treatment[7] of a *condensed* binary solution in the same language as the earlier adsorption discussion, so that the same results will apply. Suppose we have N_I molecules of I and N_{II} of II. Then

$$Q = f_I^{N_I} f_{II}^{N_{II}} \frac{(N_I + N_{II})!}{N_I!\,N_{II}!} \exp\left[-\frac{zw}{2kT} \times \frac{N_I N_{II}}{(N_I + N_{II})}\right] \quad (30)$$

$$w = 2w_{I,II} - w_{I,I} - w_{II,II}$$

where $w_{I,II}$ is the nearest neighbor interaction free energy[12] between a molecule of type I and one of type II, etc. The partition function of pure liquid I is $f_I^{N_I}$, where f_I is a function of T only (for present purposes). Now put $N_I + N_{II} = B$ = constant, and $N_I = N$. Then $P = Q\lambda_I^{N_I}\lambda_{II}^{N_{II}}$ becomes

$$P = \text{const.}\ \frac{B!}{N!(B - N)!} \exp\left(\frac{zw}{2kT} \times \frac{N^2}{B}\right)\left[\frac{f_I\lambda_I}{f_{II}\lambda_{II}} \exp\left(-\frac{zw}{2kT}\right)\right]^N \quad (31)$$

This is formally identical with eq. (2) and (7). Equation (31) gives $\bar{N}(\lambda_I/\lambda_{II})$. This result and the Gibbs–Duhem equation determine the vapor pressure curves $\lambda_I(\bar{N})$ and $\lambda_{II}(\bar{N})$.

SURFACE AREA ANALYSIS BY MEANS OF GAS FLOW METHODS. I. STEADY STATE FLOW IN POROUS MEDIA[1]

BY GERARD KRAUS, JOHN W. ROSS AND L. A. GIRIFALCO

Applied Science Research Laboratory, University of Cincinnati, Cincinnati 21, Ohio

Received July 29, 1952

Steady state flow rates have been measured on packed columns of powders ranging in BET surface area from 0.30 to 8.0 square meters per gram. By treating the Poiseuille and Knudsen flow contributions to the total permeability independently it is possible to calculate two surface areas from the flow data. The experimental evidence suggests that the surface area deduced from the Poiseuille flow contribution represents the geometric area of the particles, while the Knudsen flow area is to be identified with the total surface of the continuous pore space. In no case do steady state flow areas include the surface of blind pores.

Introduction

Several years ago Rigden,[2] and independently Arnell[3] showed how the well known Kozeny–Carman law[4,5] for the flow of fluids through porous media must be modified for gases in order to include the contribution due to Knudsen flow. The resulting permeability equation has, in various forms, been used by a number of authors[2,3,6,7] to measure the internal surface area of porous media and of packed beds of particles. It is readily shown that all forms of the equation reported may be reduced to the expression

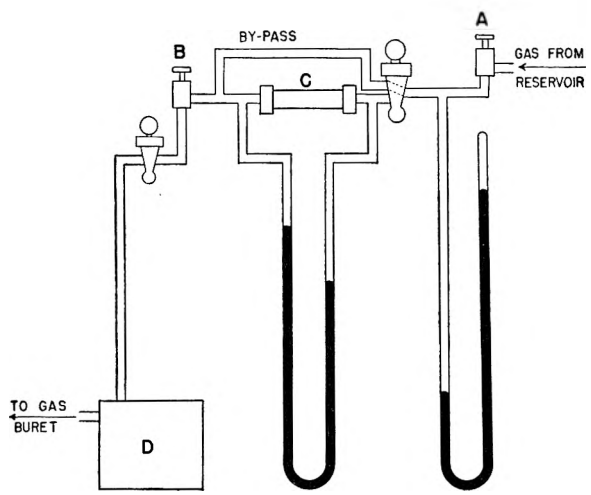

Fig. 1.—Schematic diagram of steady state flow apparatus.

$$Q \equiv \frac{1}{\Delta P} \times \frac{dn}{dt} \times \frac{l}{A} = \frac{\epsilon^3}{k(1-\epsilon)^2 S_v^2 \eta RT} \times \bar{P} + \frac{Z\epsilon^2\pi}{(1-\epsilon)S_v\sqrt{2\pi MRT}} \quad (1)$$

where

dn/dt is the flow rate in moles/sec.
ΔP is the pressure drop across the porous medium, dynes/cm.^{2}
l is the length of porous medium in cm.
A is the cross-sectional area of porous medium in cm.^{2}
ϵ is the porosity = void volume/total volume
k is a constant dependent on the geometry of the porous medium
S_v is the specific surface area of the porous medium in cm.^{2}/cm.^{3} of solid
η is the viscosity of the gas in poises
R is the gas constant
T is the absolute temperature, °K.
$\bar{P}$ is the mean pressure in the porous medium, dynes/cm.^{2}
M is the molecular weight of the gas
Z is a constant

The constant k in the first (Poiseuille flow) term is known to be very close to 5.0 for random pored media[6] and attempts have been made to establish

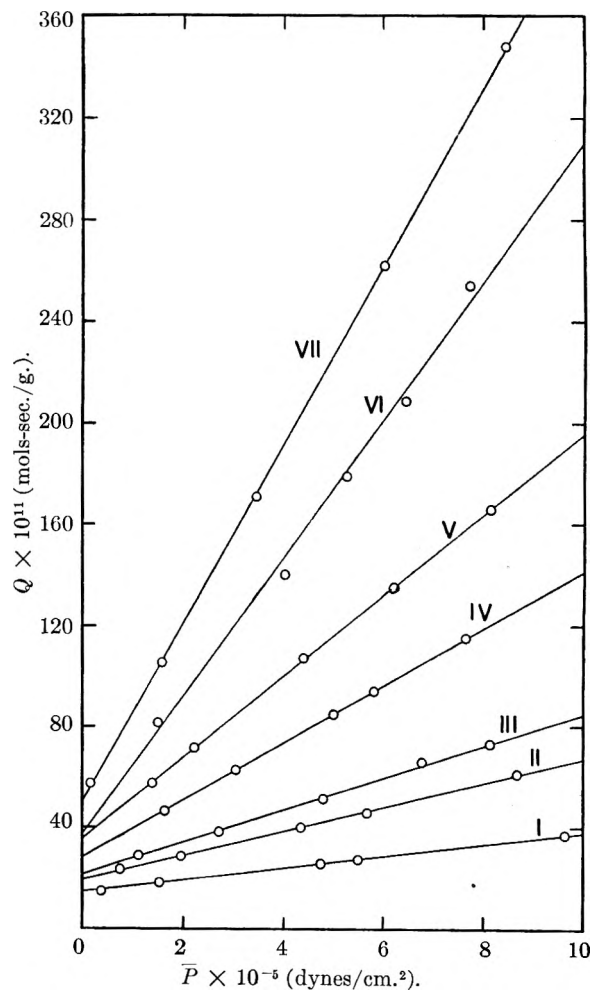

Fig. 2.—Specific flow rates for seven fractions of glass microspheres, hydrogen.

(1) Presented before the Division of Colloid Chemistry of the American Chemical Society, Atlantic City, New Jersey, September, 1952.

(2) P. J. Rigden, *J. Soc. Chem. Ind.*, **66**, 130 (1947).

(3) J. C. Arnell, *Can. J. Research*, **24A**, 103 (1946); **25A**, 191 (1947).

(4) J. Kozeny, *Ber. Wien. Akad.*, **136** (IIa), 271 (1927).

(5) P. C, Carman, *Disc. Faraday Soc.*, **3**, 72 (1948).

(6) R. M. Barrer and D. M. Grove, *Trans. Faraday Soc.*, **47**, 826 (1951).

(7) F. A. Schwertz, *J. Applied Phys.*, **20**, 1070 (1949).

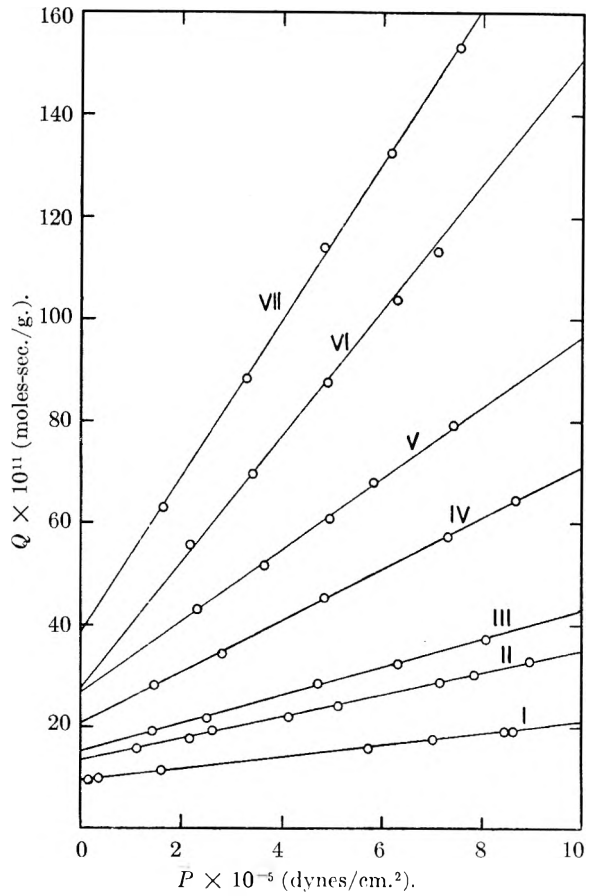

Fig. 3.—Specific flow rates for seven fractions of glass microspheres, helium.

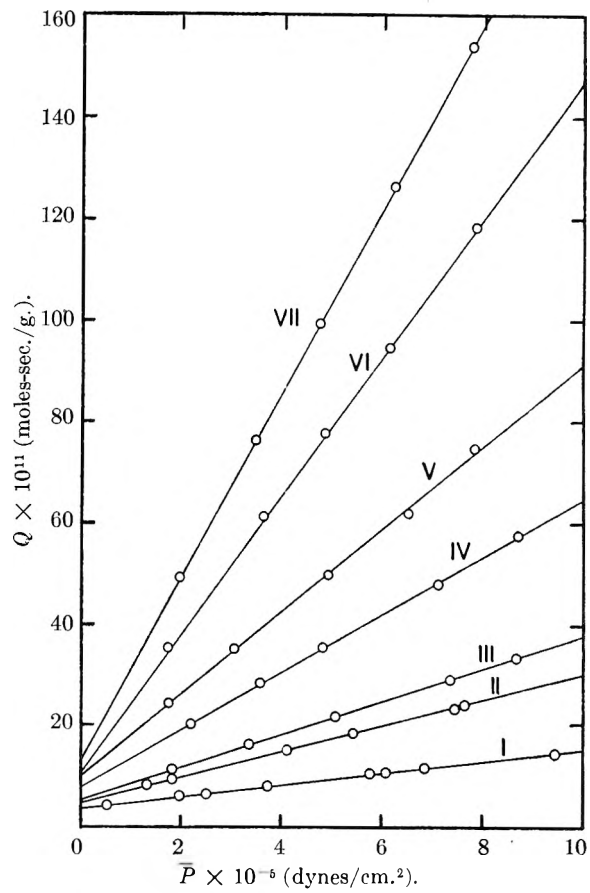

Fig. 4.—Specific flow rates for seven fractions of glass microspheres, nitrogen.

certain generalizations[8,9] regarding the constant Z in the second (Knudsen flow) term of equation (1). Unfortunately, virtually all such deductions have been based on values of Z computed from equation (1) on the assumption that the surface areas governing the Poiseuille and Knudsen contributions to the total flow rate are identical, so that effectively the Knudsen term is discarded as a possible source of new information.

In a recent theory of Knudsen flow in porous media Derjaguin[10] derived an expression for the flow rate which is easily shown to be identical with the second term of equation (1) provided $Z = 48/13\pi$. Measurements performed in this Laboratory have yielded consistently larger surface areas deduced from the Knudsen flow term—with $Z = 48/13\pi$—than from the Poiseuille term. Since permeability surface areas have long been suspected of representing a "rounded off" surface[6,7] it was decided to undertake a detailed investigation as to the physical significance of both the Poiseuille and Knudsen flow areas. The results of this study are reported in two papers, of which the present article is confined to steady state measurements, while the companion paper[11] deals with transient state experiments.

(8) P. C. Carman, *Nature*, **160**, 301 (1947).

(9) P. C. Carman and J. C. Arnell, *Can. J. Research*, **26A**, 128 (1948).

(10) B. Derjaguin, *Compt. rend. acad. sci. U.R.S.S.*, **53**, 623 (1946).

(11) G. Kraus and J. W. Ross, THIS JOURNAL, **57**, 334 (1953)

Experimental

Permeability measurements were made on seven fractions of glass microspheres, $BaSO_4$, $PbCrO_4$, TiO_2 and CuO. The glass microspheres were furnished by the Minnesota Mining and Manufacturing Co. as "Pavement Marking Beads" and were fractionated by sedimentation. The remaining four powders were either C.P. or reagent grade.

The gas flow apparatus is shown in Fig. 1. The in-going gas was passed over P_2O_5 into a reservoir maintained at approximately atmospheric pressure by means of a mercury check valve. Two Hoke High Vacuum valves (Schaar & Co.), A and B, were used to adjust the pressure on the in-going side of the porous medium cell C and the pressure difference across the cell to the desired levels. After running through the pump D the gas was collected in a gas buret. By keeping the volume between A and B small, steady state is reached quite rapidly. Flow rates were measured by timing the outflow of 60 cc. of gas at atmospheric pressure. Several readings were taken until the observed rate was found to be constant. All experiments were conducted at 27 ± 2°.

The densities of the powders were determined pycnometrically using dicyclohexyl as the displacement fluid.[12] Where available, literature values were used (I.C.T.). Gas viscosities were taken from a recent tabulation of Hirschfelder, Bird and Spotz.[13]

The nitrogen adsorption data were obtained on a standard volumetric adsorption apparatus.[14] The nitrogen adsorption areas were calculated by means of the simple Brunauer, Emmett and Teller equation[15] and also by the relative method of Harkins and Jura.[16]

The geometric surface areas of the glass microspheres were

(12) W. R. Ruby and R. P. Loveland, *ibid.*, **50**, 345 (1946).

(13) J. O. Hirschfelder, R. B. Bird and E. L. Spotz, *Chem. Revs.*, **44**, 205 (1949).

(14) P. H. Emmett, *Advances in Colloid Sci.*, **1**, 1 (1942).

(15) S. Brunauer, P. H. Emmett and E. Teller, *J. Am. Chem. Soc.*, **60**, 309 (1938).

(16) W. D. Harkins and G. Jura, *ibid.*, **66**, 1366 (1944).

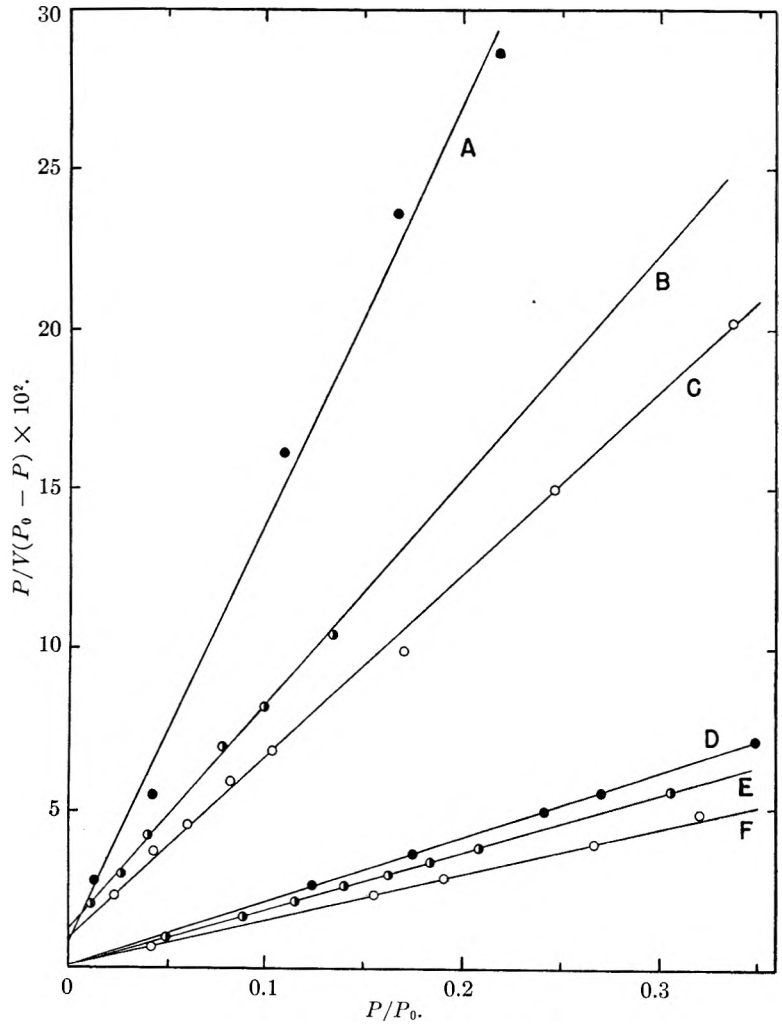

Fig. 5.—BET plots of adsorption data used in calculating surface areas: A, CuO; B, glass spheres IV; C, glass spheres II; D, $BaSO_4$; E, $PbCrO_4$; F, TiO_2.

obtained by preparing photomicrographs of each fraction and measuring the particle diameters. Three to six hundred particles were measured on each fraction and the mean diameter $\bar{D}$, standard deviation σ and skewness α_3 of the distribution computed. The specific surface area per gram is then

$$S = \frac{1}{\rho} \times \frac{6(\bar{D}^3 + \sigma^2)}{\bar{D}^2 + 3\bar{D}\sigma^2 + \sigma^3\alpha_3}$$

where ρ is the density of the particles.

Results and Discussion

Figures 2 to 4 show the specific flow rates Q plotted against the mean pressure $\bar{P}$ for the seven fractions of glass microspheres. The slopes and intercepts were determined by the method of least squares and the surface areas calculated from the slopes using $k = 5.0$. These areas are compared with the photomicrographic areas in Table I. It is readily seen that the agreement between data obtained with different gases is excellent and that there is generally good correlation with the photomicrographic areas.

Figure 5 shows BET plots for fractions II and IV and the four powders of non-spherical particle shape. Flow rates for these powders are given in Figs. 6 and 7. The BET surface areas are compared with flow areas deduced from both the slopes and intercepts (with $Z = 48/13\ \pi$) in Table II.

TABLE I

COMPARISON OF PHOTOMICROGRAPHIC AREAS WITH POISEUILLE FLOW AREAS FOR GLASS MICROSPHERES

Fraction no.	Gas	Flow area, m.²/g.	Photomicrographic area, m.²/g.
	H_2	0.409	
I	He	.401	0.410
	N_2	.415	
	H_2	.290	
II	He	.286	.258
	N_2	.285	
	H_2	.201	
III	He	.179	.182
	N_2	.191	
	H_2	.174	
IV	He	.174	.151
	N_2	.174	
	H_2	.104	
V	He	.105	.112
	N_2	.104	
	H_2	.0810	
VI	He	.0804	.0904
	N_2	.0804	
	H_2	.0622	
VII	He	.0627	.0607
	N_2	.0613	

TABLE II

COMPARISON OF FLOW AREAS WITH NITROGEN ADSORPTION AREAS

Powder	Gas	Flow areas, m.²/g. Poiseuille term	Flow areas, m.²/g. Knudsen term	Nitrogen adsorption areas, m.²/g. BET	Nitrogen adsorption areas, m.²/g. HJ
CuO	H_2	0.073	0.17	0.30	0.31
	He	.067	.19		
Glass spheres IV	H_2	.17	.29	.37	.38
	He	.17	.28		
Glass spheres II	H_2	.29	.47	.55	.59
	He	.29	.47		
$PbCrO_4$	H_2	2.1	3.73	3.75	4.01
	He	1.9	3.63		
$BaSO_4$	H_2	1.9	4.46	4.68	4.97
	He	1.9	4.04		
TiO_2	H_2	6.0	8.37	7.97	8.26
	He	4.8	8.02		

It is apparent that the surface areas deduced from the Knudsen flow term are in all cases larger than the Poiseuille flow areas. For TiO_2 and $PbCrO_4$ the Knudsen flow and nitrogen adsorption areas are equal within experimental error, while for the remaining powders the Knudsen areas are smaller.

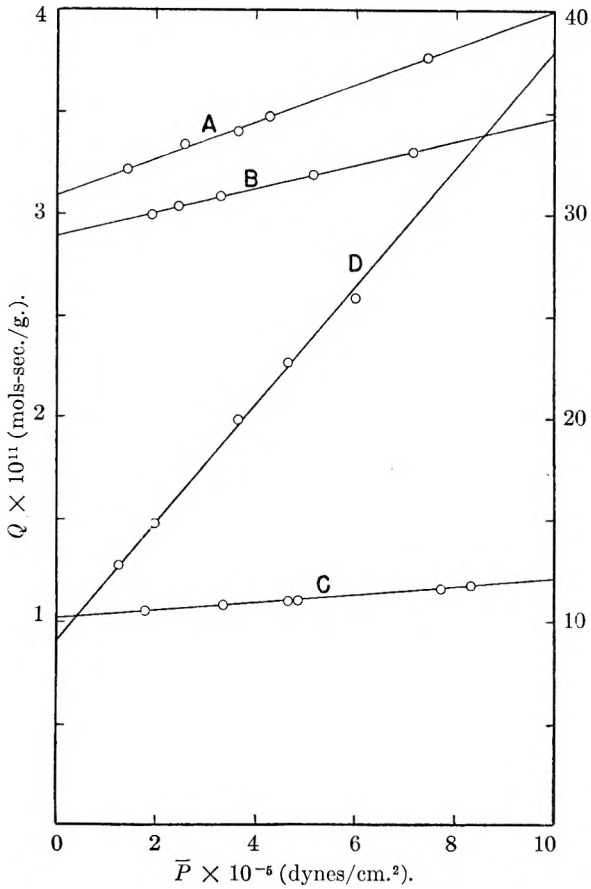

Fig. 6.—Specific flow rates (hydrogen) for powders of non-spherical particle shape: A, $PbCrO_4$; B, TiO_2; C, $BaSO_4$; D, CuO. Right hand scale for CuO only.

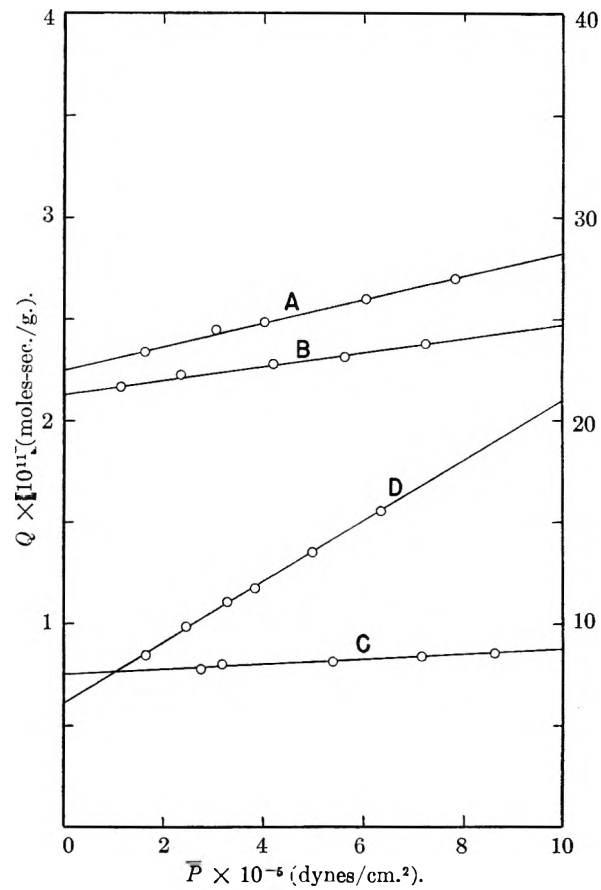

Fig. 7.—Specific flow rates (helium) for powders of non-spherical particle shape: A, $PbCrO_4$; B, TiO_2; C, $BaSO_4$; D, CuO. Right hand scale for CuO only.

An interpretation of these results may be obtained upon consideration of some of the characteristic features of the flow mechanisms involved. In Poiseuille flow the velocity is zero at the pore wall and hence most of the flow takes place through regions closer to the center of the pores. One might expect therefore that roughness on a molecular scale would have very little effect on the Poiseuille permeability and that the surface areas deduced from the slopes of the flow rate curves are essentially geometric areas, as is indeed the case with the glass microspheres of Table I. The situation is quite different with regard to Knudsen flow. In this case the flow rate is governed by collisions of the gas molecules with the pore walls and it appears plausible that the controlling surface area should be nearer to the total internal surface of the porous medium. This would lead us to expect agreement of the Knudsen flow areas with the adsorption areas, were it not for the possibility of the occurrence of blind pores in the particles proper.

It is clear that no steady state flow method can be capable of picking up the surface area of "blind" pores, for gas in such pores would simply be immobilized, contributing nothing to the steady state flow rate. Consequently the Knudsen flow areas would be expected to be smaller than the BET surface areas in such cases. It may be concluded therefore that the steady state Knudsen flow area represents the total surface area of the continuous pore space and that glass, copper oxide and, to a much lesser extent, barium sulfate contain blind pores. Further evidence for this interpretation is given in Paper II of this series,[11] in which the question of blind pore space is considered in some detail.

Acknowledgment.—This investigation was supported by the Office of Ordnance Research, U. S. Army, under Contract No. DA33-008 ord 123.

SURFACE AREA ANALYSIS BY MEANS OF GAS FLOW METHODS. II. TRANSIENT STATE FLOW IN POROUS MEDIA[1]

BY GERARD KRAUS AND JOHN W. ROSS

Applied Science Research Laboratory, University of Cincinnati, Cincinnati 21, Ohio

Received July 29, 1952

Transient state flow rates in the Knudsen flow region have been measured on a series of powders previously investigated by steady state flow methods. Surface areas calculated from the transient flow data using nitrogen were found to agree exceedingly well with nitrogen adsorption areas, even in cases where steady state measurements yield too small a surface area. Helium flow measurements result in somewhat larger areas suggesting that more surface is accessible to the smaller helium molecules than is to nitrogen.

Introduction

It has been shown in the preceding paper[2] that steady state flow rates of gases in porous media in the region of Knudsen flow may be used to evaluate a surface area which in some instances agrees very closely with the Brunauer–Emmett–Teller[3] nitrogen adsorption area. In other cases, however, the flow area is found to be definitely less, a behavior indicating the presence of blind pores. Barrer and Grove,[4] in a recent publication, suggest the possibility of obtaining a total surface, including blind pores, by conducting the flow measurements in the transient state. The present investigation represents a test of this hypothesis based on comparison with nitrogen adsorption surface areas.

Theoretical

In the theory of Barrer and Grove[4] the surface area of the porous medium is introduced as follows. The specific flow rate for Knudsen flow (written as a diffusion coefficient) for a straight cylindrical capillary is

$$D = \frac{4r}{3}\sqrt{\frac{2RT}{\pi M}} \qquad (1)$$

where r is the capillary radius, R is the gas constant, T is the absolute temperature and M is the molecular weight of the gas. The diffusion constant is measured by the time-lag method[4-5] giving

$$D = k^2 l^2/6L \qquad (2)$$

where L is the "time lag" necessary for establishment of steady state extrapolated to zero flow, l is the length of the porous medium, and k is a tortuosity factor (taken as equal to $\sqrt{2}$) allowing for the fact that the capillaries are not straight. Finally the expression

$$r = \frac{2\epsilon}{(1-\epsilon)S_v} \qquad (3)$$

is used to introduce the specific surface area S_v (per unit volume of solid), ϵ being the porosity. By combining equations (1) to (3) and setting $k = \sqrt{2}$, it is found that

$$S_v = \frac{8\epsilon}{1-\epsilon} \times \frac{L}{l^2}\sqrt{\frac{2RT}{\pi M}} \qquad (4)$$

It is readily shown that this equation is not consistent with the specific flow rate deduced from Derjaguin's theory[6] as used in the present study[2]

$$\frac{1}{\Delta P} \times \frac{dn}{dt} = \frac{48}{13}\frac{\epsilon^2 A}{(1-\epsilon)S_v l} \times \frac{1}{\sqrt{2\pi MRT}} \qquad (5)$$

where dn/dt is the flow rate in moles per second, ΔP is the pressure drop across the porous medium, and A is the cross-section of the porous medium. By definition

$$D \equiv \frac{L}{\epsilon A} \times \frac{RT}{\Delta P} \times \frac{dn}{dt} = \frac{24}{13}\frac{\epsilon}{(1-\epsilon)S_v}\sqrt{\frac{2RT}{\pi M}} \qquad (6)$$

It will be noted that the total cross-sectional area of the pores appears as ϵA, for clearly the diffusion coefficient must be based on the *open* cross-section of the porous medium. In the flow experiment D is simply

$$D = l^2/6L \qquad (7)$$

without the use of a tortuosity factor, as the internal pore structure is already accounted for in equation (5). It follows from equations (6) and (7) that

$$S_v = \frac{144}{13}\frac{\epsilon}{1-\epsilon} \times \frac{L}{l^2}\sqrt{\frac{2RT}{\pi M}} \qquad (8)$$

which is exactly 18/13 times the surface calculated by the method of Barrer and Grove.[4]

In view of the experimental results to follow, it is important to note here that both equations (1) and (5) are based on the assumption of inelastic collisions of the gas molecules with the pore walls.

Experimental

The apparatus used (Fig. 1) consisted essentially of two 4-liter reservoirs connected through the cell holding the powder. A mercury manometer D was used to measure the pressure on the high pressure side and a calibrated thermocouple vacuum gage was used to determine the pressure on the discharge side. The actual quantity of gas flowing through the porous medium during an experiment was found to be always quite small, making the use of a manostat on the high pressure side unnecessary. The inlet pressure must, of course, be at all times much larger than the pressure on the outgoing side so that the pressure gradient may be regarded as constant. In operation the entire system was evacuated and flushed twice with the appropriate gas. The system was then pumped down to approximately 1 to 2 microns of mercury and shut off from the pumps by

(1) Presented before the Division of Colloid Chemistry of the American Chemical Society, Atlantic City, New Jersey, September, 1952.

(2) G. Kraus, J. W. Ross and L. A. Girifalco, THIS JOURNAL, **57**, 330 (1953).

(3) S. Brunauer, P. H. Emmett and E. Teller, *J. Am. Chem. Soc.*, **60**, 309 (1938).

(4) R. M. Barrer and D. M. Grove, *Trans. Faraday Soc.*, **47**, 826, 837 (1951).

(5) R. M. Barrer, "Diffusion in and Through Solids," Cambridge Press, 1951, p. 19.

(6) B. Derjaguin, *Compt. rend. acad. sci. U.R.S.S.*, **53**, 623 (1946).

TABLE I

TRANSIENT FLOW AND NITROGEN ADSORPTION AREAS

Powder	l, cm.	ϵ	Transient Knudsen flow: Helium L, min.[a]	Helium S, m.²/g.	Nitrogen L, min.[a]	Nitrogen S, m.²/g.	Nitrogen adsorption: BET S, m.²/g.	HJ S, m.²/g.
CuO	60.32	0.420	2.12	0.37	4.8	0.31	0.30	0.31
Glass spheres, II	42.10	.388	0.895	0.64	2.04	0.55	.55	.59
$PbCrO_4$	15.31	.652	.86	4.60	1.92	3.89	3.75	4.01
$BaSO_4$	26.94	.377	7.0	5.45	16.0	4.75	4.68	4.97
TiO_2	15.31	.724	0.80	8.85	1.89	7.90	7.97	8.26

[a] Time lags L based on at least three experiments.

closing stopcock G. Stopcocks E and F were closed and the desired inlet pressure established by bleeding gas into reservoir A through H. At zero time stopcock F was opened and the gas allowed to diffuse through the cell C into reservoir B. Figure 2 shows a typical flow rate curve. The time lag L is obtained by extrapolation of the straight line, steady state portion of the curve to the initial pressure in the cell and discharge reservoir. It is not necessary that this pressure be zero.[5] Several runs were made in each determination, using various inlet pressures. In order to ensure essentially pure Knudsen flow, it is important that these pressures be sufficiently small to cause the mean free path of the molecules to exceed the pore dimensions. With powders of unknown particle size the pore dimensions are, of course, also unknown. In such cases it is best to take time lag measurements over a range of inlet pressures and to extrapolate to zero pressure. Both procedures were found to give the same limiting time lag within experimental error.

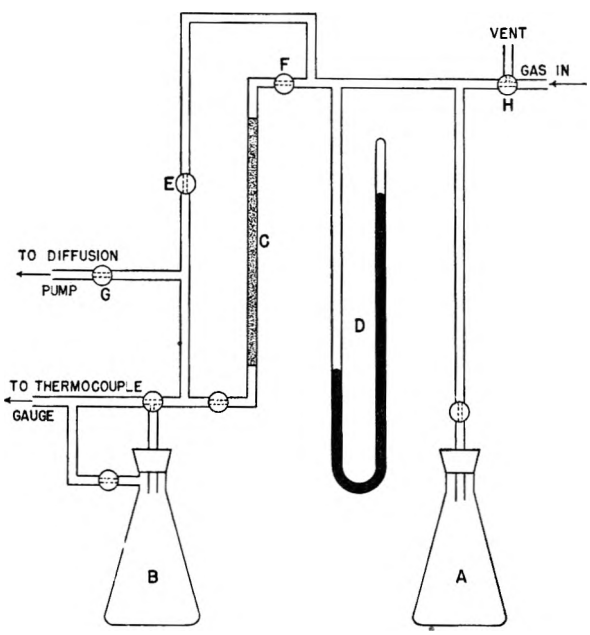

Fig. 1.—Schematic diagram of transient state flow apparatus.

The powders investigated were the same as in paper I, and all flow measurements were carried out at 30 ± 2°. Surface areas from nitrogen adsorption isotherms were calculated by the Harkins–Jura[7] relative method as well as by the BET method. The cross-sectional molecular area for nitrogen was taken as 16.2 square ångströms.[8]

Results and Discussion

In Table I are given the flow data for the six powders investigated along with the surface areas calculated by equation (8) and the BET and HJ areas. The agreement between nitrogen flow and nitrogen adsorption areas is easily within the experimental accuracy of either method, and it is apparent that the method of calculation of Barrer and Grove[4] (equation 4) leads to results which are some 28% too low.

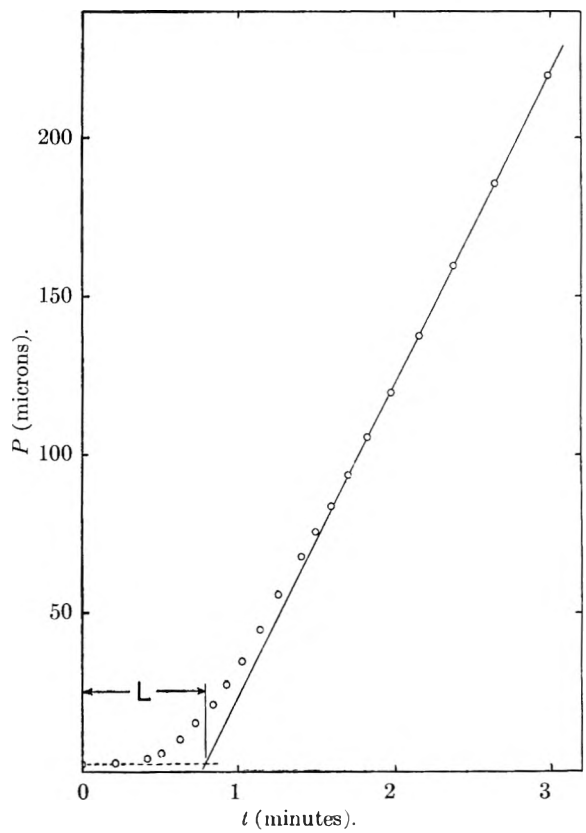

Fig. 2.—Typical flow rate curve, helium through TiO_2.

Transient flow areas obtained with helium are from 12 to 19% higher than the nitrogen flow or adsorption areas. A possible explanation of this behavior may lie in the smaller size of the helium molecule, for it is conceivable that helium could penetrate into extremely minute crevices and channels inaccessible to nitrogen. In this case neither the nitrogen flow nor the adsorption methods could be expected to include the surface area of these pores. This interpretation does not appear unreasonable in view of the known fact that densities of powders determined by helium displacement are invariably larger than liquid displacement densities.[9-10]

There are two other phenomena which could cause deviations from equation (6) and hence lead to erroneous surface areas. The first of these is ad-

(7) W. D. Harkins and G. Jura, *J. Am. Chem. Soc.*, **66**, 1366 (1944).

(8) R. T. Davis, T. W. DeWitt and P. H. Emmett, THIS JOURNAL, **51**, 1232 (1947).

(9) R. C. Smith and H. C. Howard, *Ind. Eng. Chem.*, **34**, 938 (1942).

(10) R. P. Rossman and W. R. Smith, *ibid.*, **35**, 973 (1943).

sorption of the gas on the surface, leading to a larger time lag and an apparently higher surface area. It is clear, however, that in the case of helium this is extremely improbable. The other alternative is the possibility of specular reflection of molecules at the walls of the capillaries. Derjaguin[6] has shown that for 100% specular reflection the coefficient 24/13 in equation (6) becomes equal to 8/3; in intermediate cases the value of this coefficient may be assumed to lie somewhere between the two extremes. It follows that if specular reflections were involved, D would be larger than indicated by equation (6) and hence the use of equation (8) would lead to surface areas which are too small. Exactly opposite results were observed with helium. Thus, the mechanism advanced in the preceding paragraph appears to be the most plausible explanation for the larger helium flow areas.

Despite the success of the transient state flow method in predicting surface areas, it should be mentioned that the use of the time lag method is not always free from objection. The time lag method for measuring diffusion coefficients can only be exact as long as Fick's second law is valid and the diffusion coefficient is a constant. While this is true for transient Knudsen flow through packed particles containing no blind pores, the presence of blind channels must introduce deviations from Fick's second law and produce a time dependent diffusion coefficient. Furthermore, the time lag must be a function of blind pore volume as well as area. This objection is probably not a serious one as long as the blind pore volume is small compared to its area, as must be the case with the rather fine powders used in the present study. We may, however, visualize a situation in which there are a few large blind pores such as might occur in some consolidated porous media. Because of the immobilization of gas in the blind pores, the time lag will now be larger than it would be if no blind pores were present. At the same time, however, the internal surface of the medium is hardly affected by the few large blind pores, so that the use of the time lag method will result in too large a value for the surface area.

The various physically distinct surface areas which may be derived from gas flow experiments offer an interesting method for the study of surfaces. By combining steady state and transient experiments it is possible to obtain a fairly complete picture of the structure of a porous medium, giving such information as total surface, surface area of blind pores (by subtraction of the steady state from the transient state Knudsen area), and at least in some cases geometric surface.[2] From these, such quantities as mean particle size, mean pore diameter and surface roughness factor are readily calculated.

Acknowledgment.—This investigation was supported by the Office of Ordnance Research, U. S. Army, under Contract No. DA33-008 ord 123.

LIQUID METALS. I. THE VISCOSITY OF MERCURY VAPOR AND THE POTENTIAL FUNCTION FOR MERCURY

BY LEO F. EPSTEIN AND MARION D. POWERS

General Electric Company, Knolls Atomic Power Laboratory,[1] Schenectady, New York

Received July 29, 1952

It is shown that, contrary to the results of earlier studies, an excellent fit to the data on the viscosity on mercury vapor can be obtained using a Lennard-Jones 6–12 potential, in spite of the fact that X-ray scattering measurements indicate that this substance is more nearly represented by a 6–9 potential. Viscosity measurements, like second virial coefficient studies, do not appear to be sufficient by themselves to determine the repulsive power uniquely. In this study, the 6–12 parameters $\epsilon/k = 851 \pm 32$°K. and $r_0 = 3.25_3 \pm 0.04_4$ A. are obtained. A detailed survey of the previous studies of the potential function for mercury indicates that the values obtained from the viscosity are quite consistent with the other data. Certain difficulties in the determination of r_0 and related quantities from X-ray scattering data are pointed out.

Introduction

The viscosity of a gas which satisfies a Lennard-Jones 6–12 potential

$$U_{12}(r) = \epsilon[(r_0/r)^{12} - 2(r_0/r)^6] \qquad (1)$$

(in which ϵ is the depth of the potential energy curve, occurring at r_0) has been shown by Hirschfelder, Bird and Spotz[2] in a brilliant study of the transport properties of gases, to be given by

$$\eta = (C/\sigma^2)(MT)^{1/2}\,[V/W^2(2)] \qquad (2)$$

where the constant

$$C = 266.93 \times 10^{-7} \qquad (3)$$

if η is in poises, σ in Å., and ϵ/k in °K. is defined by $U_{12}(\sigma) = 0$, and is given by

$$\sigma = r_0/2^{1/6} = 0.8909 r_0 \qquad (4)$$

M is the molecular weight of the gas. The quantities V and $W^2(2)$ are quite complicated functions of ϵ/kT which have fortunately been calculated and tabulated over a wide range of the independent variable.[2]

In attempting to apply eq. 2 to mercury vapor, Hirschfelder and his associates were at once confronted by the fact that the experimental evidence seemed to indicate that Hg did not in fact satisfy a 6–12 potential. The liquid mercury X-ray scattering data of Hildebrand, Wakeham and Boyd[3] lead to a 6–9 rather than a 6–12 potential function.

(1) The Knolls Atomic Power Laboratory is operated for the United States Atomic Energy Commission by the General Electric Company under Contract No. W-31-109 Eng-52.

(2) (a) J. O. Hirschfelder, R. B. Bird and E. L. Spotz, *J. Chem. Phys.*, **16**, 968 (1948); (b) J. O. Hirschfelder, R. B. Bird and E. L. Spotz, *Trans. Am. Soc. Mech. Engrs.*, **71**, 921 (1949).

(3) J. H. Hildebrand, H. R. R. Wakeham and R. N. Boyd, *J. Chem. Phys.*, **7**, 1094 (1939).

However, if the $U(r)$ function defined by eq. 1 is fitted to the X-ray data, the 6–12 parameters

$$\epsilon/k = 1522°\text{K.}; \quad \sigma = 2.5\ \text{Å}. \qquad (5)$$

are obtained. With these parameters, Hirschfelder, *et al.*, computed the viscosity of Hg vapor over the range 491 to 883°K., with somewhat disappointing results: the calculated and observed values found in this way differed by −5.0% at 491°K. and +2.9% at 883°K. This poor agreement was attributed to the crudeness of the approximation in fitting a 6–9 $U(r)$ curve to a 6–12 equation and to the fact that mercury vapor is not, in fact, adequately represented by a 6–12 potential.

The implications of this conclusion are most important, if true. It is well known that it is not possible to unequivocally establish the exponent of r occurring in the repulsive part of the potential function from the second virial coefficient and similar measurements; so that if it could be shown that the transport properties such as the viscosity are much more dependent upon the repulsive power, so that differentiation between a 6–12 and a 6–9 potential can be effected, it is clear that a powerful tool for determining the repulsive parameters would be available. It is, therefore, somewhat disappointing to find that this conclusion does not appear to be supported by the data on mercury vapor.

By altering the parameters used, rather considerably perhaps, but within entirely acceptable limits, eq. 2 may be made to fit the available data quite well even when a 6–12 potential is used. It, therefore, does not follow, in this case at least, that the viscosity data can be used to distinguish between a 6–12 and a 6–9 potential.

Experimental Data and Least Square Analysis of Viscosity.—The available experimental data on the viscosity of mercury vapor[4] are listed in Table I.

TABLE I

VISCOSITY OF MERCURY VAPOR (POISES)

t, °C.	Observer	$\eta \times 10^{+7}$, exptl.	$\eta \times 10^{+7}$, empirical (eq. 7)	Deviation, %	$\eta \times 10^{+7}$, theor. (eq. 2, 5, 8)	Deviation, %
218	3	4709	4637	+1.5	4739	−0.6
219.5	3	4672	4653	+0.4	4753	−1.7
223.5	3	4689	4694	−0.1	4793	−2.2
273	4	4940	5203	−5.3	5277	−6.8
281	3	5310	5226	+1.6	5355	−0.8
300.5	3	5501	5489	+0.2	5546	−0.8
301	4	5320	5494	−3.3	5551	−4.3
330	3	5831	5798	+0.6	5835	−0.1
352	4	6078	6030	+0.8	6051	+0.4
380	4	6540	6329	+1.7	6326	+3.3
421	3	6856	6770	+1.2	6730	+1.8
439.5	3	7029	6970	+0.8	6912	+1.7
496	3	7610	7589	+0.3	7471	+1.8
565	3	8343	8358	−0.2	8154	+2.3
588.5	3	8632	8623	+0.1	8387	+2.8
607	3	8766	8833	−0.8	8571	+2.2
610	3	8802	8867	−0.7	8601	+2.3
				±1.7		±2.6

(4) (a) S. Koch, *Wied. Ann.*, **25**, 618 (1885); **32**, 194 (1887); (b) H. Braune, R. Basch and W. Wentzel, *Z. physik. Chem.*, **A137**, 176, 447 (1928).

A plot of η against T is nearly linear, and passes through the origin, suggesting an equation of the form

$$\eta = AT + BT^2 \qquad (6)$$

Determining the constants A and B by the method of least squares, weighing all points equally, the equation obtained is

$$10^7\eta/T = 8.692 + 1.5265 \times 10^{-3}T \qquad (7)$$

Values of the viscosity computed using this equation are given in Table I and plotted in Fig. 1. The root mean square per cent. deviation

$$\pm\sqrt{\frac{\Sigma(\%\ \text{deviation})^2}{\text{No. of measurements}}} \qquad (8)$$

of the 17 experimental points may be taken as a measure of the fit of the equation to the experimental data. For eq. 7, this quantity is ±1.7%.

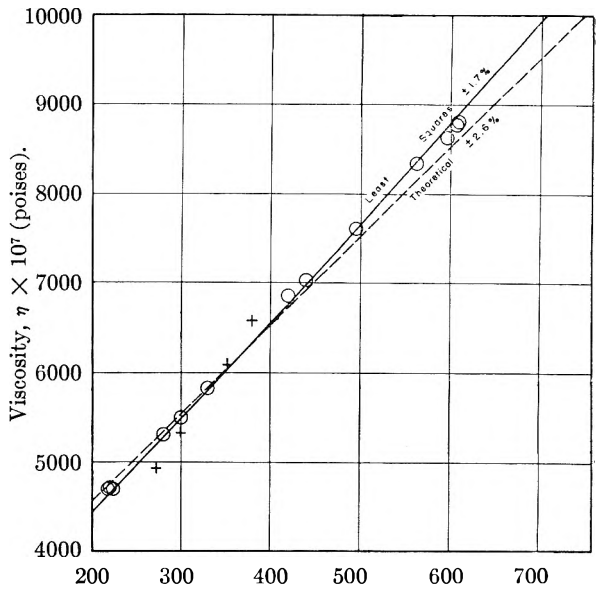

Fig. 1.—The viscosity of Hg vapor: ○, Braune, Basch and Wentzel (1928); +, Koch (1885, 1887); ——, least squares ±1.7%; theoretical - - -, ±2.6%.

Theoretical Computation of Viscosity of Mercury Vapor.—Equation 2 can be rewritten as

$$\eta = (CM^{1/2}/\sigma^2)(\epsilon/k)^{1/2} f(kT/\epsilon) \qquad (9)$$

where

$$f(kT/\epsilon) = (kT/\epsilon)^{1/2}\,[V/W^2(2)] \qquad (10)$$

$f(kT/\epsilon)$ is nearly linear in (kT/ϵ), and a plot of $(\epsilon/kT)\ f(kT/\epsilon)$ using the Hirschfelder, Bird and Spotz tables[2b] reveals a striking peculiarity: the slope of this function, plotted against (kT/ϵ), is positive only in the relatively short region from

$$0.6 \leqslant (kT/\epsilon) \leqslant 1.0 \qquad (11)$$

In this range, by the method of least squares, it is found that

$$f(kT/\epsilon) = +0.6177(kT/\epsilon) + 0.01270(kT/\epsilon)^2 \qquad (12)$$

with a maximum deviation from this equation of

less than 0.06%.[5] From eq. 9 and 12

$$\eta = (CM^{1/2}/\sigma^2)(\epsilon/k)^{1/2}\,[0.6177(k/\epsilon)T + 0.01270(k/\epsilon)^2T^2] \quad (13)$$

Now over the whole experimental range from 491 to 883°K., η/T is positive according to eq. 7. From the inequality (11), it follows that (kT/ϵ) can vary only from 0.6 to 1.0 for these limits in the temperature and so ϵ/k can be uniquely determined to fall within the limits

$$818.6 < \epsilon/k\ (°\text{K.}) < 883.2 \quad (14)$$

These values are fairly close together, so that the mean value may be taken, and it may be concluded that these data yield

$$\epsilon/k = 851 \pm 32°\text{K.} \quad (15)$$

ϵ/k is thus uncertain by about $\pm 3.8\%$. Substituting this value of ϵ/k in eq. 13, and equating the result to the experimental viscosity points, a series of σ values is obtained, one for each observation, ranging from 2.856 to 2.995 Å. Again, these limits are fairly close together and determining the mean and the standard deviation from the mean

$$\sigma = 2.89_8 \pm 0.03_9\ \text{Å}. \quad (16)$$

The corresponding value of r_0, from eq. 4, is then

$$r_0 = 3.25_3 \pm 0.04_4\ \text{Å}. \quad (17)$$

Using these parameters, the viscosity can be computed and the resulting values are given in the penultimate column of Table I. The root mean square per cent. deviation of the theoretical equation is $\pm 2.6\%$, *i.e.*, the fit to the theoretical equation is only slightly inferior to that using an empirical least square formulation. The data are also plotted in Fig. 1 for ready visualization.

The method of determining the Lennard-Jones parameters given here may appear to be somewhat involved. A more direct procedure for determining ϵ/k and r_0 is to be preferred, but no such technique was found; a straight-forward least-square analysis, for example, did not lead to credible results. It has been pointed out to the authors[6] that "The ϵ/k limits depend on the temperature range covered. It is conceivable that η/T would be positive over a wider range of temperatures, and thus a wider variation in ϵ/k would result." The validity of this argument is unquestionable, but in the absence of Hg vapor viscosity data outside the range considered here, the relatively narrow limits given in eq. 14 appear to be the best that can be obtained at the present time. When data on Hg vapor are obtained which are more accurate, or cover a wider range of temperatures, the methods as well as the results of this analysis may require amendment.

The difference between the values of the parameters obtained from the X-ray data (eq. 5) and those derived from the viscosity measurements (eq. 15 and 16) should not be alarming. There is, as will be shown below, considerable doubt about the position and depth of the potential minimum for Hg (r_0 and ϵ) as well as the value of the cross-over point σ which is related to the repulsive potential power. It appears from the available evidence that the latter may in fact be closer to 9 than it is to 12; but the value of ϵ/k seems to be much less than the older one obtained by Hildebrand, Wakeham and Boyd. At this stage of knowledge of the potential function for mercury, the skeptical chemist will find it difficult to reject the parameters (eq. 15 and 17) on the basis of disagreement with experiment.

It would be extremely interesting, of course, to compute the function equivalent to $[V/W^2\ (2)]$ for the 6–9 potential

$$U_9(r) = \epsilon[2(r_0/r)^9 - 3(r_0/r)^6] \quad (18)$$

This has not as yet been done, although it is hoped that with the availability of high speed mechanical computing equipment, such tables may be forthcoming in the future. With these tables, the depth and position of the minimum in the potential curve which gives the best fit to the viscosity data might be significantly different from those found above. It is to be expected that the transport properties of gases (viscosity, thermal conductivity, self-diffusion, etc.) will be much more strongly dependent upon the repulsive power than the properties derived from equilibrium measurements, the second virial coefficient for example.

The Potential Function for Mercury.—Over the last twenty odd years, there have been many attempts to determine the potential function for mercury. The earliest is that of Hassé and Cook[7] who tried to derive it from a study of the viscosity of mercury vapor. Since they used a Lennard-Jones 4–8 potential, instead of the theoretically demanded[8] inverse sixth power attraction, their results

$$\epsilon/k = 2564°\text{K.},\ r_0 = 2.05\ \text{Å}.,\ \sigma = 1.72\ \text{Å}. \quad (19)$$

are of little more than historical interest.

Hildebrand, Wakeham and Boyd,[3] working with the X-ray scattering data of Boyd and Wakeham,[9] concluded that the data were best satisfied by a 6–9 potential with

$$\epsilon/k = 1553°\text{K.},\ r_0 = 2.86\ \text{Å}.,\ \sigma = 2.50\ \text{Å}. \quad (20)$$

Recently, Kerr and Lund[10] carried out an analysis of the X-ray scattering measurements of Campbell and Hildebrand.[11] They obtained their best fit to the data with the repulsive power $s = 8.3$ and the parameters

$$\epsilon/k = 985°\text{K.},\ r_0 = 2.97\ \text{Å}.,\ \sigma = 2.58\ \text{Å}. \quad (21)$$

The most ambitious attempt to derive a theoretical expression for the potential function is prob-

(5) F. G. Keyes in *Trans. Am. Soc. Mech. Engrs.*, **73**, 589 (1951), presents an empirical equation for $f(kT/\epsilon)$ covering the wider range $0.35 < x < 300$ where $x = kT/\epsilon$. This equation

$$f(x) = 0.629x - 1.3445x^{1/2}/10^{3.1428/x} - 16.27x^{1/2}/10^{6.9055/x^{1/2}}$$

yields an average deviation in $x^{-1/2}f(x)$ of 0.0055. Equation 12 above, while limited in applicability to the narrower range $0.6 < x < 1.0$ is much more accurate within those limits: the maximum deviation in $x^{-1/2}\,f(x)$ is 0.0003.

(6) J. H. Hildebrand and B. Alder, private communication, Feb. 14, 1952.

(7) H. R. Hassé and W. R. Cook, *Proc. Roy. Soc. (London)*, **125A**, 196 (1929).

(8) (a) F. London, *Z. physik. Chem.*, **B11**, 222 (1930); (b) H. Ekstein and M. Magat, *Compt. rend.*, **199**, 264 (1934).

(9) R. N. Boyd and H. R. R. Wakeham, *J. Chem. Phys.*, **7**, 958 (1939).

(10) R. H. Kerr and L. H. Lund, *ibid.*, **19**, 50 (1951).

(11) J. A. Campbell and J. H. Hildebrand, *ibid.*, **11**, 330 (1943).

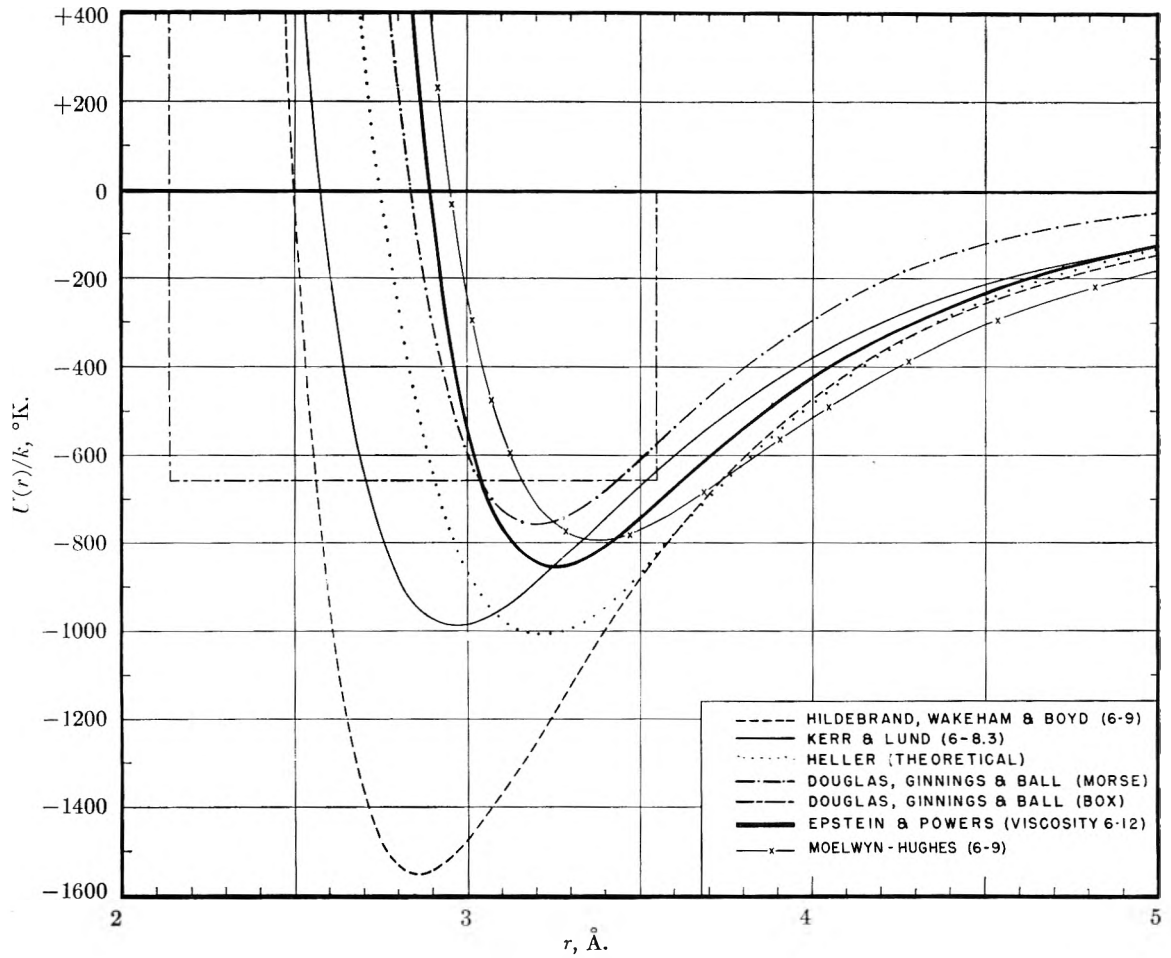

Fig. 2.—The potential function of mercury.

ably that of Heller.[12] For the repulsive term, he used the form $A \exp(-r/\rho)$ derived theoretically for He by Slater and Kirkwood[13] and successfully applied by Born and Mayer[14] in representing the repulsive term in alkali halide crystals. Heller's treatment is concerned, strictly speaking, with the theoretical computation of the attractive part of the potential function, and this was carried out to terms in r^{-12} to take higher multipoles into account. This analysis does not predict the value of r_0: for this Heller used 3.20 Å., which was previously chosen by Kuhn.[15] r_0 should be slightly larger than the measured value of the distance of closest approach in solid Hg,[16] 3.00 Å. at −46°,[17] and the value used is an average obtained from (a) the density of liquid Hg assuming it to be made up of close-packed spheres (3.25 Å.) and (b) from the data on Ag amalgams (3.09 Å.) and Pb–Hg mixtures (3.24–3.28 Å.). Heller's complete equation is

$$\begin{aligned} U(r)\,(\text{ergs}) = {} & +2.5846 \times 10^{-8} \exp(-2.8473 \times 10^{+8} r) \\ & -2.296 \times 10^{-58} r^{-6} \\ & -1.252 \times 10^{-73} r^{-8} \\ & -6.487 \times 10^{-89} r^{-10} \\ & -4.234 \times 10^{-101} r^{-12} \end{aligned} \qquad (22)$$

where r is in cm. From this

$$\epsilon/k = 998°\text{K.}, \; r_0 = 3.20 \text{ Å.}, \; \sigma = 2.77 \text{ Å.} \qquad (23)$$

Douglas, Ball and Ginnings[18] computed a table of second virial coefficients for Hg for temperatures up to 500°. To fit these data, they concluded that, from the spectroscopic data, the best fit could be obtained by using the Morse function

$$U(r) = \epsilon[\{1 - e^{-a(r - r_0)}\}^2 - 1] \qquad (24)$$

where

$$a = \pi\omega c\sqrt{m/\epsilon} \qquad (25)$$

and

$$r_0 = 3.2 \text{ Å.}, \; \omega = 36 \text{ cm.}^{-1}, \; \epsilon/k = 755°\text{K.} \qquad (26)$$

This equation gives $\sigma = 2.84$ Å. Because no analytical method is known for determining the second virial coefficient $B(T)$ from a Morse potential function, these authors resorted to numerical integration. The resulting data were found to fit the equation

$$B(T) = 56.4 - 43.82 \exp(+655/T) \qquad (27)$$

(12) R. Heller, *J. Chem. Phys.* **9**, 154 (1941).
(13) J. C. Slater and J. G. Kirkwood, *Phys. Rev.*, **37**, 682 (1931).
(14) M. Born and J. E. Mayer, *Z. Physik*, **75**, 1 (1932).
(15) H. Kuhn, *Proc. Roy. Soc.* (*London*), **A158**, 230 (1937).
(16) The structure of solid Hg can be considered to be derived from face-centered cubic packing by shortening of a body diagonal. This leads to a structure in which each mercury atom has six coplanar neighbors at a distance of 3.47 Å. and six other neighbors, three in each of the adjacent planes, at a much smaller distance of 3.00 Å. *Cf.* R. W. G. Wyckoff, "Crystal Structures," Vol. I, Interscience Publishers, Inc., New York, N. Y., 1948.
(17) M. C. Neuberger, *Z. anorg. u. allgem. Chem.*, **212**, 40 (1933).
(18) T. B. Douglas, A. F. Ball and D. C. Ginnings, *J. Research Natl. Bur. Standards*, **46**, 334 (1951).

But this expression corresponds not to the original Morse function used, but rather to the form[19]

$$B(T) = (2\pi N/3)\sigma^3 - (2\pi N/3)(\rho^3 - \sigma^3)[\exp(+\epsilon/kT) - 1] \quad (28)$$

which is derived from the "box" potential

$$U(r) = \begin{cases} + & \infty \text{ for } r < \sigma \\ - & \epsilon \text{ for } \rho > r > \sigma \\ & 0 \text{ for } r > \rho \end{cases} \quad (29)$$

with

$$\epsilon/k = 655°\text{K.}, \rho = 3.55 \text{ Å.}, \sigma = 2.14 \text{ Å.} \quad (30)$$

The fact that this potential reproduces the data on the second virial coefficient derived from a Morse function must be due to the basic insensitivity of $B(T)$ to the form of the potential function.

Recently, Moelwyn-Hughes[20] has evaluated the potential function of Hg entirely from the properties of the liquid—vapor pressure, density, compressibility, thermal expansion, etc. His results lead directly to the Lennard-Jones 6–9 type of potential (eq. 18) with a relatively small uncertainty in the value of the repulsive exponent. His parameters are

$$\epsilon/k = 795°\text{K.}, r_0 = 3.38 \text{ Å.}, \sigma = 2.95 \text{ Å.} \quad (31)$$

in quite good agreement with the results obtained from vapor viscosity data (eq. 15 and 17).

These functions are plotted in Fig. 2. It will be seen that the $U(r)$ curve derived above (eq. 1, 15 and 17) from viscosity data agrees quite well with the other curves for mercury.

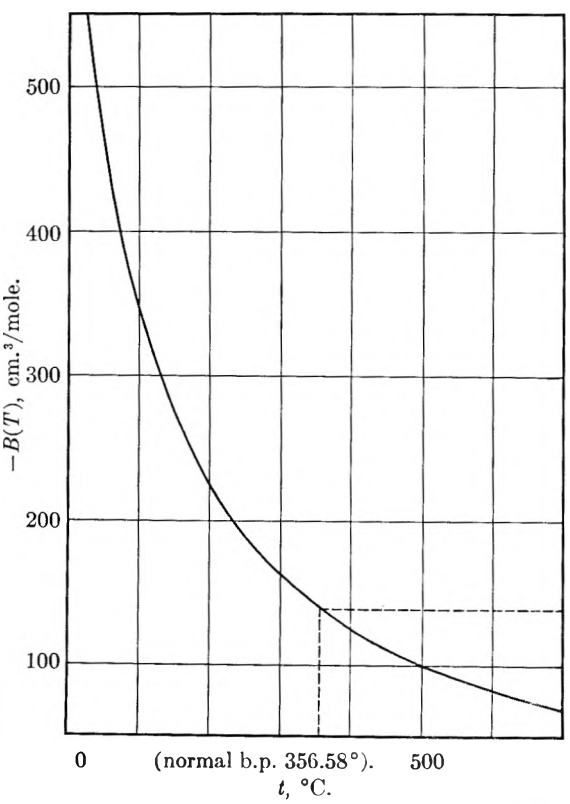

Fig. 3.—Second virial coefficient for mercury vapor, based on a Lennard-Jones 6–9 potential with $r_0 = 3.25$ Å. and $\epsilon/k = 775°$K.

There have been a large number of attempts to determine the energy of dissociation of Hg_2 from spectroscopic data.[15,21] Most of the more recent values of this constant come out around 1.4 to 1.6 kcal./mole ($\epsilon/k = 704$ to 805°K.) although a few determinations[21e,f] have led to considerably higher values. Gaydon[22] prefers the value 1.38 ± 0.07 kcal./mole ($\epsilon/k = 694 \pm 35$°K.) found by Winans and Heitz.[21g] Herzberg[23] in the first edition of his book gives a value corresponding to $\epsilon/k = 926$°K. while in the second edition, he lists the value $\epsilon/k = 696$°K. There is thus a wide margin of disagreement among authorities on the proper value for this constant, and the value of 851°K. obtained in eq. 15 falls well within the limits of uncertainty.

There appears to be some basis for concern with the r_0 values obtained from X-ray scattering: both the Hildebrand, Wakeham and Boyd value (2.86 Å.) and that of Kerr and Lund (2.97 Å.) are less than the shortest observed value in solid Hg (3.00 Å.). It would be most surprising if the value in the expanded liquid phase is smaller than that in the solid, and it seems most probable that r_0 falls in the range 3.2 to 3.3 Å. This anomaly has also been pointed out by Moelwyn-Hughes.[20] The reasons for this discrepancy are obscure, but thought-provoking. That the X-ray scattering technique is fundamentally capable of yielding results in good agreement with the gas viscosity data is apparent from the table below, for argon.

Workers	Reference	Method	ϵ/k, °K.	r_0, Å.
Eisenstein and Gingrich	28, 10	X-Ray (Hildebrand's)	117	3.76
Eisenstein and Gingrich	10	X-Ray (Kerr and Lund's)	104	3.80
Hirschfelder, Bird and Spotz	2b, 29, 30	Viscosity	124.0	3.827

Measurements of X-ray scattering in liquids are subject to a great deal of error, in the experimental details and in interpretation, as has been pointed out by Campbell and Hildebrand[11] and by Gregg and Gingrich[24]; and mercury is a particularly difficult liquid to handle because of the high absorption correction needed, the ready formation of oxide films, and fluorescent radiation emitted by the sample.[25]

While there have been a great many investiga-

(19) J. A. Beattie and W. H. Stockmayer, "Reports on Progress in Physics," Vol. VII, The Physical Society (London), 1940, p. 195.

(20) E. A. Moelwyn-Hughes, THIS JOURNAL, **55**, 1246 (1951).

(21) (a) W. Finkelnburg, *Physik. Z.*, **34**, 551 (1933). (b) E. Koernicke, *Z. Physik*, **33**, 219 (1925). (c) H. Kuhn and K. Freudenberg, *ibid.*, **76**, 38 (1932). (d) T. Mrozowski, *ibid.*, **104**, 230 (1936); *Acta Physica Polonica*, **2**, 81 (1933); **3**, 215 (1934). (e) J. G. Winans, *Phys. Rev.*, **37**, 101, 897 (1931). (f) T. Subbaraya, *Proc. Indian Acad. Sci.*, **1**, 166 (1934). (g) J. G. Winans and M. P. Heitz, *Phys. Rev.*, **65**, 65 (1944).

(22) A. G. Gaydon, "Dissociation Energies," Chapman and Hall, London, 1947, p. 209.

(23) G. Herzberg, "Molecular Spectra and Molecular Structure. I. Diatomic Molecules," 1st Ed., Prentice-Hall, Inc., New York, N. Y., 1939, p. 488; *ibid.*, 2nd Ed., D. Van Nostrand Co., Inc., New York, N. Y., 1950, p. 537.

(24) R. Q. Gregg and N. S. Gingrich, *Rev. Sci. Instruments*, **11**, 305 (1940).

(25) C. A. Barrett, "Structure of Metals," McGraw-Hill Book Co., Inc., New York, N. Y., 1943, p. 227.

tions of X-ray scattering by liquid Hg,[9,11,26] of these only two[3,9-11] have been thoroughy analyzed to date. There are wide discrepancies in the position reported for the peaks in $(\sin\theta)/\lambda$ (*cf.* ref. 11). Gingrich[27] in a critical review of X-ray scattering in liquid elements gives most weight to the Debye and Menke values which lead to an r_0 of 3.23 Å., in much better agreement with the result obtained from viscosity measurements (eq. 17) than it is with other X-ray data. It is to be hoped that a definitive study of this point will be forthcoming in the near future, and studies of this kind have been initiated here.[28-30]

(26) (a) R. W. G. Wyckoff, *Am. J. Sci.*, **5**, 455 (1923). (b) C. V. Raman and C. M. Sagani, *Nature*, **120**, 514 (1927); *Ind. J. Physics*, **2**, 97 (1927-1928). (c) J. A. Prins, *Physica*, **6**, 315 (1926). (d) M. Wolf, *Nature*, **122**, 314 (1928); *Z. Physik*, **53**, 72 (1929). (e) P. Debye and H. Menke, *Physik. Z.*, **31**, 348 (1930). (f) F. Sauerwald and W. Teske, *Z. anorg. allgem. Chem.*, **210**, 247 (1933). (g) V. I. Danilow and V. E. Neimark, *J. Exptl. Theoret. Phys.* (*U. S. S. R*), **5**, 724 (1935).

(27) N. S. Gingrich, *Rev. Modern Phys.*, **15**, 90 (1943).

(28) A. S. Eisenstein and N. S. Gingrich, *Phys. Rev.*, **62**, 261 (1942).

At the present time, it appears that the best $U(r)$ curve that can be drawn for Hg is probably a 6–9 function (*cf.* eq. 18) with $r_0 = 3.25 \pm 0.04$ Å. and $\epsilon/k = 775 \pm 20$°K., the mean of the spectroscopic value (eq. 26) and Moelwyn-Hughes' value (eq. 31). Using these parameters and the recently published tables for a 6–9 gas,[31] the second virial coefficient of Hg vapor has been computed. This is presented in graphical form in Fig. 3. The deviation from ideality at the normal boiling point,[32] 356.58°, amounts to 0.27% in exact agreement with the value recently deduced from experimental data by Busey and Giauque.[33]

(29) H. L. Johnston and E. R. Grilly, THIS JOURNAL, **46**, 948 (1942).

(30) V. Vasilesco, *Ann. Phys.* (*Paris*), Ser. II, **20**, 292 (1945).

(31) L. F. Epstein and C. J. Hibbert, *J. Chem. Phys.*, **20**, 752 (1952).

(32) J. A. Beattie, B. E. Blaisdell, and J. Kaminsky, *Proc. Am. Acad. Sci.*, **71**, 375 (1937).

(33) R. H. Busey and W. F. Giauque, *J. Am. Chem. Soc.*, **75**, 806 (1953); private communication from Professor Giauque, Sept. 9, 1952.

ELECTROKINETIC PROCESSES IN PARALLEL AND SERIES COMBINATIONS

BY PHILIP B. LORENZ

Petroleum Experiment Station, U. S. Bureau of Mines, Bartlesville, Oklahoma

Received August 4, 1952

When two porous media exhibiting electrokinetic effects are combined in parallel or in series, the ordinary laws of combination of electrical resistance are slightly altered. The exact laws are derived by a general treatment, which also gives combination laws for permeability, streaming effects, electro osmotic effects and cell constant. The law of combination for cell constant is different according to the type of process being considered.

The familiar laws of combination of electrical resistances R are derived from Ohm's law and from the conditions imposed by Kirchhoff's laws on the current I and potential drop E across conductors when they are connected in parallel or in series. These conditions for a series combination of two conductors are $E_1 + E_2 = E$, and $I_1 = I_2 = I$, where the subscripts refer to the individual conductors and no subscript is used for the combination. For this case, it is convenient to use Ohm's law in the usual form $E = RI$. For a parallel combination $E_1 = E_2 = E$, and $I_1 + I_2 = I$, and it is convenient to write Ohm's law as $I = GE$, where $G = 1/R$ is the conductance.

Similarly, laws of combination of hydrodynamic resistance, W, of a porous solid can be derived from Darcy's law[1] and the conditions imposed on volume flow rate V and pressure differential P. The usual form of Darcy's law is $V = KP$, where $K = 1/W$ is the permeability. However, when a porous solid is permeated by a conducting liquid, the laws of combination of both permeability and electrical resistance are somewhat altered if electrokinetic effects also take place. In this paper the correct combination laws are developed, not only for resistance and permeability, but also for streaming and electroösmotic quantities. Such laws are important in interpreting measurements on geological formations whose permeability, electrical resistance and electrokinetic properties are not uniform; and in the laboratory in measuring these properties on packed beds of particles or fibers that must be supported in a measuring cell by a rigid porous medium with different properties.

Overbeek and Wijga[2] have derived combination laws for some of these properties, but their results are only approximately correct because their assumed conditions were not completely valid, and their quantities R and W were not defined exactly.

Development of the Basic Equations.—We now have four variables, E, I, P, V, which are governed by *two* equations[3,4]

$$I = L_{11}E + L_{12}P$$
$$V = L_{21}E + L_{22}P$$

As in the case of Ohm's law, it is convenient to have various forms of these equations. Four different forms are possible in which the independent variables are, in turn, E and P, E and V, I and V, and I and P. The notation becomes less cumbersome if we use the symbols R, G, W and K, where they are appropriate, with $M = L_{12} = L_{21}$ for the "electropermeability."[4] Another convenient symbol, B, was introduced by Mazur and Overbeek[3]

(1) M. Muskat, "The Flow of Homogeneous Fluids through Porous Media," McGraw-Hill Book Co., Inc., New York, N. Y., 1937, p. 71.

(2) J. Th. G. Overbeek and P. W. O. Wijga, *Rec. trav. chim.*, **65**, 556 (1946).

(3) P. Mazur and J. Th. G. Overbeek, *ibid.*, **70**, 83 (1951).

(4) P. B. Lorenz, THIS JOURNAL, **56**, 775 (1952).

in equations analogous to 3 below. It is an electrokinetic resistance coefficient. The four pairs of equations are

$$I = GE + MP \quad (1a)$$
$$V = ME + (\alpha K)P \quad (1b)$$
$$E = RI + (BK)P \quad (2a)$$
$$V = (MR)I + KP \quad (2b)$$
$$E = (\alpha R)I + BV \quad (3a)$$
$$P = BI + WV \quad (3b)$$
$$I = (1/\alpha R)E + (M/\alpha K)V \quad (4a)$$
$$P = (B/\alpha R)E + (1/\alpha K)V \quad (4b)$$

where $\alpha = 1 + M^2/KG = 1 + B^2/RW$. (The factor $1 - Q$ of a previous paper[4] is equal to $1/\alpha$.) It should be emphasized that R is the resistance when $P = 0$ and K is the permeability when $I = 0$. The coefficients are distributed so that $RG = WK = 1$. It is also found that $BM = 1 - \alpha$. It is worth noting that

$$W/G = R/K = -B/M \quad (5)$$

The total electrical resistance, permeability, electropermeability, etc., of a parallel or series combination are defined as R, K, M, etc., in the above equations. The individual quantities for each member of a combination are defined by similar equations with appropriate subscripts. Taking equations 1 as an example, it is important to remember that, although E and P are independent, E_1 and P_1 are not independent in a combination, and the same is true of individual equations for other members of the combination. We use these individual equations and the conditions for parallel or series combinations to eliminate the dependent variables, which for two members are I, I_1, I_2, V, V_1, V_2, E_1, E_2, P_1 and P_2. In the resulting equations between the independent variables E and P, we set the coefficient of each variable equal to zero.

Combination Laws for R, K and M. Parallel Combinations.—The conditions are

$$\begin{aligned} I_1 + I_2 &= I \\ V_1 + V_2 &= V \\ E_1 = E_2 &= E \\ P_1 = P_2 &= P \end{aligned} \quad (6)$$

By combining these conditions with the six equations having the form of (1), we get

$$(G_1 + G_2 - G)E + (M_1 + M_2 - M)P = 0$$
$$(M_1 + M_2 - M)E + (\alpha_1 K_1 + \alpha_2 K_2 - \alpha K)P = 0$$

Hence

$$G = G_1 + G_2 \text{ or } \frac{1}{R} = \frac{1}{R_1} + \frac{1}{R_2} \quad (7)$$
$$M = M_1 + M_2 \quad (8)$$
$$\alpha K = \alpha_1 K + \alpha_2 K_2 \quad (9)$$

Equations 7, 8 and 9 can be derived, less conveniently, from equations 2 or 4. Equation 9 shows that the "permeability at $E = 0$," αK, follows the law of combination usually used for the permeability K. Another form of equation 9 can be derived from 6 and equations with the form of 2, as

$$M_1R_1I_1 + K_1P + M_2R_2I_2 + K_2P = MRI + KP \quad (10)$$
$$R_1I_1 + B_1K_1P = R_2I_2 + B_2K_2P = RI + BKP \quad (11)$$

From equation 11 and making use of 5

$$\begin{aligned} R_1I_1 &= RI + (M_1R_1 - MR)P \\ R_2I_2 &= RI + (M_2R_2 - MR)P \end{aligned} \quad (12)$$

From 7 and 8

$$\begin{aligned} (M_1R_1 - MR) &= (R/R_2)(M_1R_1 - M_2R_2) \\ (M_2R_2 - MR) &= -(R/R_1)(M_1R_1 - M_2R_2) \end{aligned} \quad (13)$$

Combining 12 and 13 and substituting into 10

$$M_1RI + (M_1R/R_2)(M_1R_1 - M_2R_2)P + M_2RI - (M_2R/R_1)(M_1R_1 - M_2R_2)P + (K_1 + K_2)P = MRI + KP$$

Equating coefficients of P

$$K = K_1 + K_2 + R(M_1/R_2 - M_2/R_1)(M_1R_1 - M_2R_2)$$
$$\text{or } K = K_1 + K_2 + (R/R_1R_2)(M_1R_1 - M_2R_2)^2 \quad (14)$$

The last term is a correction term to the usual law of combination for permeability (at $I = 0$). This correction term for a parallel combination of n components is

$$\sum_{i=1}^{n} M_i(M_iR_i - MR)$$

In a similar way, equations 4 lead to the relation

$$\frac{1}{\alpha R} = \frac{1}{\alpha_1 R_1} + \frac{1}{\alpha_2 R_2} + \frac{\alpha_1 K_1 \alpha_2 K_2}{\alpha K}\left(\frac{M_1}{\alpha_1 K_1} - \frac{M_2}{\alpha_2 K_2}\right)^2 \quad (15)$$

where the last term is a correction term to the ordinary law of combination in dealing with resistance at $V = 0$. The correction term for n components is

$$\sum_{i=1}^{n} M_i\left(\frac{M_i}{\alpha_i K_i} - \frac{M}{\alpha K}\right)$$

Series Combinations.—The conditions are

$$\begin{aligned} E_1 + E_2 &= E \\ P_1 + P_2 &= P \\ I_1 = I_2 &= I \\ V_1 = V_2 &= V \end{aligned} \quad (16)$$

In the same manner as before, we find

$$\alpha R = \alpha_1 R_1 + \alpha_2 R_2, \text{ or} \quad (17)$$
$$R = R_1 + R_2 + (K/K_1K_2)(M_1R_1 - M_2R_2)^2 \quad (18)$$
$$\frac{MR}{K} = \frac{M_1R_1}{K_1} + \frac{M_2R_2}{K_2} \quad (19)$$
$$1/K = 1/K_1 + 1/K_2 \quad (20)$$
$$\frac{1}{\alpha K} = \frac{1}{\alpha_1 K_1} + \frac{1}{\alpha_2 K_2} + \frac{\alpha_1 R_1 \alpha_2 R_2}{\alpha R}\left(\frac{M_1}{\alpha_1 K_1} - \frac{M_2}{\alpha_2 K_2}\right)^2 \quad (21)$$

For a series combination of n components, 18 and 21 become

$$R = \sum_{i=1}^{n} R_i\left[1 + \frac{M_i}{K_i}(M_iR_i - MR)\right] \quad (18a)$$

$$\frac{1}{\alpha K} = \sum_{i=1}^{n} \frac{1}{\alpha_i K_i}\left[1 + \alpha_i M_i R_i\left(\frac{M_i}{\alpha_i K_i} - \frac{M}{\alpha K}\right)\right] \quad (21a)$$

Combination Laws for Electrokinetic Properties. Streaming Potential.—We define

$$S \equiv (E/P)_{I=0} = BK = -MR \quad (22)$$

In parallel, using 8

$$S/R = S_1/R_1 + S_2/R_2$$

In series, using 19

$$S/K = S_1/K_1 + S_2/K_2$$

Streaming Current.—We define

$$i \equiv (I/P)_{E=0} = M$$

In parallel

$$i = i_1 + i$$

In series

$$\frac{iR}{K} = \frac{i_1R_1}{K_1} + \frac{i_2R_2}{K_2}$$

Electroösmotic Flow.—The quantity $(V/I)_{p=0} = MR$ follows the same laws as S. The quantity $(V/E)_{p=0} = M$ follows the same laws as i.

Electroösmotic Pressure.—We define

$$p \equiv (P/E)_{V=0} = B/\alpha R = -M/\alpha K \qquad (23)$$

In parallel

$$\alpha Kp = \alpha_1K_1p_1 + \alpha_2K_2p_2$$

In series

$$\alpha Rp = \alpha_1R_1p_1 + \alpha_2R_2p_2$$

Cell Constant.—A porous medium can be regarded as a sort of conductivity cell with an apparent cell constant

$$J = \kappa^0R$$

where κ^0 is the specific conductivity of the liquid in bulk.

Actually J will vary with electrolyte concentration because of surface conductance. Using the laws of combination of R, we find, for parallel combinations

$$1/J = 1/J_1 + 1/J_2 \qquad (24)$$

and, for series combinations

$$\alpha J = \alpha_1J_1 + \alpha_2J_2 \qquad (25)$$

or, from 18

$$J = J_1 + J_2 + (K/K_1K_2)(M_1R_1 - M_2R_2)^2 \qquad (26)$$

At high concentrations of electrolyte, surface conductance disappears along with other electrokinetic effects. The cell constant determined in this range is the true cell constant, J°. In parallel combinations, from 24

$$1/J^\circ = 1/J^\circ_1 + 1/J^\circ_2 \qquad (27)$$

In series combinations, from 25 or 26

$$J^\circ = J^\circ_1 + J^\circ_2 \qquad (28)$$

Instead of dealing with an apparent cell constant, we can deal with an apparent conductivity, κ, defined by

$$J^\circ \equiv \kappa R \qquad (29)$$

For parallel combinations, then

$$\frac{1}{\kappa R} = \frac{1}{\kappa_1R_1} + \frac{1}{\kappa_2R_2}$$

and for series combinations

$$\kappa R = \kappa_1R_1 + \kappa_2R_2$$

Cell Constant in Electrokinetic Formulas.—The standard expression for streaming potential and electroösmosis in circular capillaries is

$$i = -S = \frac{\zeta\epsilon}{4\pi\eta\kappa^0}$$

For an arbitrary porous medium, this equation amounts to a definition of the ratio $\zeta\epsilon/\eta$. Combining it with 22 and 29

$$M = \frac{\zeta\epsilon}{4\pi\eta\kappa}$$

When the ratio $\zeta\epsilon/\eta$ is the same for each member of a combination, we find from 8 that, in parallel

$$1/J^\circ = 1/J^\circ_1 + 1/J^\circ_2 \qquad (30)$$

which agrees with 27. However, for a series combination, 19 gives

$$\frac{R}{J^\circ K} = \frac{R_1}{J^\circ_1K_1} + \frac{R_2}{J^\circ_2K_2} \qquad (31)$$

Equation 31 can also be written

$$C = \frac{W_1R_1C_1 + W_2R_2C_2}{R(W_1 + W_2)} \qquad (31a)$$

where $C = 1/J^\circ$ is the "conductance capacity" of the porous medium. In this notation 28 becomes

$$1/C = 1/C_1 + 1/C_2 \qquad (28a)$$

Equations 31a and 28a were given by Overbeek and Wijga,[2] who showed that, with circular capillaries, the two formulas give different results when κ_1 is different from κ_2. This occurs when two capillaries in series have different surface conductances.

If R had been defined as the resistance at $V = 0$,[5] formulas 27–31 for J^0 and C would be the same, but 24–26 would become

parallel: $$\frac{1}{\alpha J} = \frac{1}{\alpha_1J_1} + \frac{1}{\alpha_2J_2} \qquad (24a)$$

series: $$J = J_1 + J_2 \qquad (25a, 26a)$$

Thus the combination law for apparent cell constant depends on the exact nature of the conductive process. The reason that the law of series combination for J^0 is different for electrokinetic processes from those for purely conductive processes is related to the fact that the law of combination for $1/R$ differs from the law of combination for M. Because of this, when electrokinetic and conductive processes occur simultaneously in combinations, charges tend to be accumulated or depleted at the junction points, which produces a non-uniform electric field in the combination. In this way, the contribution of each member is influenced by its relative properties (K_1/K and R_1/R).

An equation similar to 31a can be derived for the "permeability capacity," defined by Manegold[6] for circular capillaries as

$$C_D \equiv K/(r^2/8\eta)$$

Substitution into formulas 9 or 20 is of no value, since r^2 generally does not have an independent meaning for a combination. However, when we combine with 23 and with the standard expression for electroösmotic pressure in circular capillaries

$$p = \frac{2\zeta\epsilon}{\pi r^2}$$

these results

$$M = \frac{\zeta\epsilon}{4\pi\eta}\alpha C_D$$

As before, when $\delta\epsilon/\eta$ is the same for each member of a combination, we find from 19

$$C_D = \frac{R_1W_1\alpha_1(C_D)_1 + R_2W_2\alpha_2(C_D)_2}{RW\alpha}$$

Acknowledgment.—The author is grateful to Prof. J. Th. G. Overbeek for stimulating correspondence on the matters discussed herein.

(5) Formulas 9 and 12 of Overbeek and Wijga are precisely correct only for this definition of R, while their formulas 8 are correct only for our original definition. Similar statements apply in reverse order to their symbol W.

(6) E. Manegold and K. Solf, *Kolloid-Z.*, **55**, 273 (1931).

MOLAR POLARIZATIONS OF ISOMERIC PROPYL AND BUTYL MERCAPTANS

BY SIMÃO MATHIAS

Departamento de Quimica, Faculdade de Filosofia, Ciencias e Letras, Universidade de São Paulo, São Paulo, Brazil

Received August 14, 1952

The dielectric constant and density of benzene solutions of isomeric propyl and butyl mercaptans have been measured at 25°. The molar polarizations of these compounds have been calculated and the results compared with the ones corresponding to analogous isomeric halides. It is shown that the sum of the atomic plus orientation polarization is much more sensitive to structural influences than the electronic polarization.

In a previous study carried out by the present author[1] with the purpose to investigate the relation between the refractivity and the molecular structure of isomeric propyl and butyl mercaptans, it was found of interest to compare the refractivity results with the electric dipole moments and Raman frequencies of these compounds available in the literature. This comparison was extended to the corresponding propyl and butyl halides. As very few data were found for the dipole moments of these mercaptans, it seemed desirable to measure the dielectric constant of these compounds, both in the vapor phase and in solution, with the purpose of supplying further material for the comparative study of their physical properties. In the present paper the results of the measurements in benzene solution will be reported.

Experimental Part

Substances.—The preparation and purification of the mercaptans used in the present work have been described before.[1] The benzene used as a solvent (thiophene-free from Eastman Kodak Company) was purified by washing with concentrated sulfuric acid followed by dilute sodium hydroxide solution. It was dried over phosphorus pentoxide for a few days and distilled through a fractionating column. The fraction of constant boiling point 77.4° (699.2 mm.) had the values d^{25}_4 0.8736 and $n^{25}D$ 1.4978. Measurements of the boiling point, refractive index and density of the benzene were frequently made in order to test its purity.

Physical Measurements.—Density measurements were carried out by the pycnometric method previously described.[1]

For the determination of the dielectric constants of the solutions a resonance apparatus similar to the one described by Kalderbank and Le Fèvre[2] was used. A quartz crystal having a frequency of about 1000 kc./sec. and a 1LB4 radio tube were employed. The milliammeter had its shunt removed in order to increase the sensitivity of the point of initial resonance, which was taken as the null point. The precision condenser was of the type 722N from General Radio Company. The dielectric cell differed from the one described by Le Fèvre[3] by having three[4] concentrical cylinders instead of two, thus improving the shielding of the high potential. The cylinders, made of brass, were chrome-plated and fixed rigidly by means of mica spacers. The temperature of the cell was kept constant at 25° to within ±0.01°. The temperature of the room was maintained at 25.0 ± 0.1°. The cell had in air at 25° a replaceable capacity of 84.6 $\mu\mu$F. This value was calculated by the equation

$$C_0 = C_{air} - \frac{\epsilon C_{air} - C_{benz}}{\epsilon - 1}$$

where C_0 is the replaceable capacity of the cell, C_{air} its capacity when filled with air, and C_{benz} its capacity when filled with benzene. The dielectric constant of benzene $\epsilon = (C_{benz} - C')/(C_{air} - C')$ was taken as 2.2725 at 25°, C' is the fixed non-replaceable capacity associated with the leads.[4]

Results and Discussion

Table I summarizes the results of the measurements in benzene solution. The three columns show, respectively, the weight fraction of the mercaptan w_2, the dielectric constant of the solution ϵ_{12}, and the specific volume of the solution v_{12}. The numbers in parentheses are extrapolated values. The molar polarization of the mercaptan at infinite dilution P_2 was calculated by the method of Halverstadt and Kumler.[5] The ϵ_{12} *vs.* w_2 and v_{12} *vs.* w_2 curves were plotted and found to be straight lines, but the actual results were obtained by the usual statistical method of least squares. The molar refractivity for infinite wave length R_∞, which has been previously reported,[1] was taken as equal to the electronic polarization P_E, the difference $P_2 - P_E$ being the sum of the atomic plus orientation polarization P_{A+O}. Table II gives the different types of molar polarization which can be obtained under the present conditions. The estimated accuracy of the values for P_2 is about 0.2%.

The electric dipole moment was not calculated, as this would require the introduction of an arbitrary value for the atomic polarization. The approximation suggested by Groves and Sugden[6] that $P_E + P_A$ could be considered as $1.05P_E$ or, as done by many authors, the inclusion of the atomic polarization in the value of the electronic polarization calculated from the refractive index for the sodium D line may involve considerable error, particularly in the present case, when we are considering closely related isomeric compounds.

Relatively few measurements of dielectric constants of mercaptans have been performed. The first work reported on such compounds is that of Hunter and Partington[7] in 1931. These authors measured the dielectric constant and density of ethyl, *n*-propyl and *n*-butyl mercaptan in benzene solution at 20°. Walls and Smyth[8] published in 1933 the results of an investigation undertaken with the object of comparing mercaptans and sulfides with the corresponding oxygen compounds. Two mercaptans, *n*-butyl and *n*-amyl,

(1) S. Mathias, *J. Am. Chem. Soc.*, **72**, 1897 (1950).

(2) K. E. Kalderbank and R. J. W. Le Fèvre, *J. Chem. Soc.*, 1951 (1948).

(3) R. J. W. Le Fèvre, *Trans. Faraday Soc.*, **34**, 1127 (1938).

(4) See F. Fairbrother, *Proc. Roy. Soc. (London)*, **A142**, 173 (1933).

(5) I. F. Halverstadt and W. D. Kumler, *J. Am. Chem. Soc.*, **64**, 2988 (1942).

(6) L. G. Groves and S. Sugden, *ibid.*, 971 (1935); 1779 (1937).

(7) E. C. E. Hunter and J. R. Partington, *ibid.*, 2062 (1931); 2812 (1932).

(8) W. S. Walls and C. P. Smyth, *J. Chem. Phys.*, **1**, 337 (1933).

TABLE I

DIELECTRIC CONSTANT AND SPECIFIC VOLUME OF BENZENE SOLUTIONS OF PROPYL AND BUTYL MERCAPTANS AT 25°

w_2	ϵ_{12}	v_{12}
	Propyl mercaptan	
0.000000	(2.274)	(1.1447)
.009703	2.304	1.1451
.014396	2.318	1.1454
.022207	2.341	1.1458
.033506	2.377	1.1463
.043125	2.405	1.1467
	Isopropyl mercaptan	
0.000000	(2.275)	(1.1446)
.008444	2.301	1.1454
.015244	2.324	1.1459
.030337	2.370	1.1472
.046879	2.422	1.1486
	Butyl mercaptan	
0.000000	(2.276)	(1.1445)
.011606	2.306	1.1451
.020364	2.329	1.1455
.028944	2.352	1.1459
.044952	2.395	1.1468
.053629	2.415	1.1472
	Isobutyl mercaptan	
0.000000	(2.273)	(1.1448)
.023053	2.333	1.1460
.037097	2.367	1.1468
.041352	2.379	1.1470
.043063	2.383	1.1472
.049199	2.401	1.1474
	s-Butyl mercaptan	
0.000000	(2.274)	(1.1446)
.017815	2.322	1.1458
.021865	2.334	1.1460
.029577	2.356	1.1465
.040407	2.386	1.1472
.054172	2.421	1.1481
	t-Butyl mercaptan	
0.000000	(2.272)	(1.1446)
.010148	2.300	1.1456
.021474	2.331	1.1468
.031334	2.357	1.1478
.038810	2.379	1.1486
.050676	2.411	1.1498

TABLE II

MOLAR POLARIZATIONS (IN CC.) OF PROPYL AND BUTYL MERCAPTANS AT 25°

Mercaptan	P_2	ΔP_2	P_E	ΔP_E	P_{A+O}	ΔP_{A+O}
Propyl	70.58	0.00	23.10	0.00	47.48	0.00
Isopropyl	72.70	+2.12	23.20	+ .10	49.50	+2.02
Butyl	76.47	0.00	27.63	.00	48.84	0.00
Isobutyl	75.97	−0.50	27.66	+ .03	48.31	−0.53
s-Butyl	78.69	+2.22	27.69	+ .06	51.00	+2.16
t-Butyl	80.05	+3.58	27.90	+ .27	52.15	+3.31

were measured in benzene solution at 25 and 50°. Ethyl mercaptan in the same solvent was also measured at 15° by Wang[9] in 1940.

(9) Y. L. Wang, *Z. physik. Chem.*, **B45**, 323 (1940).

In order to compare the literature data with the results reported in the present work the total molar polarizations at infinite dilution of *n*-propyl and *n*-butyl mercaptan were calculated by exactly the same method referred to above, starting from the original values reported in the literature. From the data of Hunter and Partington one obtains for P_2 at 20°, 66.69 cc. for the *n*-propyl, and 68.43 cc. for the *n*-butyl mercaptan. Though these values are not strictly comparable with the ones listed in Table II, they are presumably too low, as the value of the molar polarization at infinite dilution, for polar molecules in a non-polar solvent, usually increases with a decrease in temperature. From the data of Walls and Smyth[10] the value 75.14 cc. is obtained, which is slightly lower than ours.

Table II shows that both P_2 and P_{A+O} vary in a much more pronounced way than the electronic polarization, in relation to the branching of the carbon chain. With the exception of isobutyl mercaptan, which shows a slight diminution in the value of these properties, P_2 and P_{A+O} increase with departure from the normal chain, in the same order as the molar refractivity and dispersivity,[1] *i.e.*, from propyl to isopropyl and from butyl to secondary and to tertiary butyl mercaptan.

Valuable information is obtained when these results are compared with the ones for the corresponding alkyl halides. The dielectric constants and densities of these compounds have been measured by many authors, in various solvents, and in the vapor phase. Most appropriate for the present

TABLE III

MOLAR POLARIZATIONS (IN CC.) OF PROPYL AND BUTYL HALIDES AT 20°

Chloride	P_2	ΔP_2	P_E	ΔP_E	P_{A+O}	ΔP_{A+O}
Propyl	101.6	0.0	20.3	0.0	81.3	0.0
Isopropyl	109.5	+ 7.9	20.5	+ .2	89.0	+ 7.7
Butyl	107.3	0.0	24.8	.0	82.5	0.0
Isobutyl	105.4	− 1.9	24.9	+ .1	80.5	− 2.0
s-Butyl	117.2	+ 9.9	24.9	+ .1	92.3	+ 9.8
t-Butyl	123.2	+15.9	25.1	+ .3	98.1	+15.6
Bromide						
Propyl	104.6	0.0	23.1	0.0	81.5	0.0
Isopropyl	117.5	+12.9	23.3	+ .2	94.2	+12.7
Butyl	111.9	0.0	27.5	.0	84.4	0.0
Isobutyl	110.7	− 1.2	27.6	+ .1	83.1	− 1.3
s-Butyl	127.0	+15.1	27.7	+ .2	99.3	+14.9
t-butyl	136.5	+24.6	28.0	+ .5	108.5	+24.1
Iodide						
Propyl	101.8	0.0	27.8	0.0	74.0	0.0
Isopropyl	114.4	+12.6	28.2	+ .4	86.2	+12.2
Butyl	107.8	0.0	32.3	.0	75.5	0.0
Isobutyl	108.0	+ 0.2	32.4	+ .1	75.6	+ .1
s-Butyl	121.3	+13.5	32.7	+ .4	88.6	+13.1
t-Butyl	129.8	+22.0	...	...	...	...

(10) The dielectric constant and density values reported by Walls and Smyth for *n*-butyl mercaptan show a considerable deviation from linearity when plotted against concentration; four of the seven solutions measured by them had a molar concentration higher than 10%. In the calculation from their data by the method of Halverstadt and Kumler only the three more dilute solutions were taken into consideration. In this case, the curves obtained could be considered as linear.

purpose are the measurements of Parts[11] made in benzene solution at 20°. The total molar polarization at infinite dilution of the isomeric propyl and butyl halides were calculated, from his original values, by the same method of Halverstadt and Kumler using the graphical modification. The electronic polarizations were obtained by calculating the molar refractivity for infinite wave length by the method of Wulff[12] from data selected by Timmermans.[13] The results are listed in Table III.

It is seen that in every series of halides, the same general gradation is observed as in the case of the corresponding mercaptans. The deviations are, however, much more pronounced. For instance, while *t*-butyl mercaptan shows for P_2, in relation to the normal compound, a positive deviation of about 4.5%, *t*-butyl chloride and bromide are, respectively, 18.9 and 28.5% higher than the corresponding normal halide.

(11) A. Parts, *Z. physik. Chem.*, **B7**, 327 (1930); **B12**, 312 (1931).
(12) P. Wulff, *ibid.*, **B21**, 368 (1933).
(13) J. Timmermans, "Physico-Chemical Constants of Pure Organic Compounds," Elsevier Publ. Co., Inc., New York, N. Y., 1950.

In the case of the isobutyl compounds, where the deviations are relatively small (Tables II and III), it is of interest to point out that, from the four butyl isomers, the isobutyl is the only one to which it has not been possible to ascribe a definite value for the C–X (X = SH, Cl, Br, or I) stretching frequency on the basis of Raman and infrared investigations.[14]

The above results show that in the case of the isomers under consideration the sum of the atomic plus orientation polarization is much more sensitive to structural influences than the electronic polarization. An exact information about the atomic polarization in the present case is of considerable importance in clarifying the results obtained by Raman and infrared studies referred to above. In order to obtain this information unambiguously measurements in the vapor phase are being carried out in this Laboratory.

Acknowledgment.—The author gratefully acknowledges the financial assistance given by the Rockefeller Foundation to this Laboratory.

(14) I. F. Trotter and H. W. Thompson, *J. Chem. Soc.*, 485 (1946). See also ref. 1.

THE COPOLYMERIZATION OF BUTADIENE AND ALPHA-METHYLSTYRENE IN EMULSION AT 12.8°[1]

BY J. W. L. FORDHAM AND H. LEVERNE WILLIAMS

Research and Development Division, Polymer Corporation Limited, Sarnia, Ontario, Canada

Received September 2, 1952

Several monomer ratios of α-methylstyrene and butadiene have been copolymerized in a low temperature emulsion copolymerization recipe at 12.8°. As the content of the former in the monomers increased, the initial rate of conversion went through a maximum (when about one-half of the monomers was α-methylstyrene), and the ultimate conversion decreased. Simultaneously the regulating index for the mixed tertiary mercaptans increased and the intrinsic flow time of the polymer in solution decreased. The value of r_1 where α-methylstyrene is monomer-1 was 0.010. The value of r_2 was 1.55. The values of Q and e (0.71 and −0.1, respectively) for the substituted styrene based on butadiene as the reference monomer were comparable with reported values based on other reference monomers. A twofold increase in the regulator with an α-methylstyrene content equal to 30% of the monomers resulted in an increase in the initial rate of conversion and a decrease in the regulating index.

Introduction

An increasingly extensive adoption of the process for the manufacture of phenol and acetone from cumene through the hydroperoxide intermediate may result in the production of large quantities of the monomer α-methylstyrene as a by-product. Presumably this monomer arises as a result of the dehydration of the intermediate carbinol formed in conjunction with the hydroperoxide. It was of interest to investigate the copolymerization of α-methylstyrene with butadiene and to compare the results with those obtained when styrene was used with butadiene. The experimental data obtained with various monomer ratios and amounts of regulators in a low temperature emulsion copolymerization recipe and a discussion of these data are presented in this report.

Results and Discussion

The experimental data with varying monomer ratios and varying amounts of regulator are in Table I.

The time conversion data show that the ultimate conversion decreased as the α-methylstyrene content of the monomers increased. This decrease in ultimate conversion, observed also in the preparation of the copolymers for calibration of the refractometric method of analysis for bound α-methylstyrene gives some indication of the difficulty with which α-methylstyrene homopolymerizes by a free radical mechanism. The initial rate of conversion went through a maximum when about one-half of the monomer was α-methylstyrene with a decrease in rate as the α-methylstyrene content increased still more. A twofold increase in the weight of the regulating mercaptans resulted in an increase in the initial conversion rate. The rate of copolymerization of α-methylstyrene and butadiene is somewhat slower than that of styrene and butadiene. In the synthetic rubber range (about 70% butadiene in the charge) the rate at 12.8° is quite comparable with the rate in the same type

(1) Presented before the Division of Polymer Chemistry, American Chemical Society, Atlantic City, N. J., September, 1952.

TABLE I

EFFECT OF MONOMER RATIO AND WEIGHT OF REGULATOR ON POLYMERIZATION DATA

Reaction time, hr.	Conv., %	Bound α-methyl-styrene, %	Residual mercaptan, %	[η]
α-Methylstyrene/butadiene 10.0/90.0, MTM 0.240				
2.0	14.3	6.5	69.5	1.27
3.0	23.0	6.5	48.5	1.65
4.0	26.7	6.5	47.0	1.70
6.0	42.4	6.6	33.0	1.96
7.5	51.6	6.6	21.5	2.49
9.0	55.3	6.5	19.0	2.58
11.5	67.4	7.0	20.0	3.65
16.0	84.9	7.8	2.0	3.29
24.0	91.5	8.3	1.0	2.79
α-Methylstyrene/butadiene 30.0/70.0, MTM 0.240				
1.5	6.7	19.0	82.5	0.70
3.5	14.3	19.1	86.0	0.56
6.0	29.8	19.4	41.5	1.08
7.5	41.4	20.0	29.0	1.55
9.5	49.4	20.3	16.0	1.67
16.0	63.1	21.4	8.5	2.01
24.0	82.0	22.7	1.5	2.65
48.0	75.8	22.4	6.0	2.39
α-Methylstyrene/butadiene 50.0/50.0, MTM 0.240				
2.0	11.6	33.2	67.5	0.98
3.0	18.7	33.5	50.5	1.30
4.0	25.2	34.0	42.5	1.34
5.5	42.3	35.5	21.5	1.59
7.0	54.1	36.7	18.5	1.55
8.0	60.1	37.4	16.5	1.71
12.0	67.6	38.5	12.0	1.92
48.0	76.5	39.8	9.0	2.23
α-Methylstyrene/butadiene 70.0/30.0, MTM 0.240				
3.0	6.3	47.7	79.0	0.99
4.0	24.0	49.4	40.0	0.77
6.0	33.1	50.7	29.0	1.03
8.0	39.0	51.7	23.5	1.09
16.0	50.3	53.1	15.5	1.12
144.0	57.1	54.9	13.0	1.13
α-Methylstyrene/butadiene 90.0/10.0, MTM 0.240				
4.7	7.5	64.7	76.0	0.50
8.0	10.9	65.6	65.5	.52
12.0	16.6	67.7	51.5	.53
16.0	22.0	70.1	42.5	.53
19.0	26.0	70.7	36.0	.55
97.0	28.4	72.0	35.0	.65
α-Methylstyrene/butadiene 30.0/70.0, MTM 0.480				
1.5	14.9	19.3	75.5	0.60
2.5	23.1	19.3	68.5	.77
4.0	33.8	19.7	58.5	.99
5.0	41.5	20.0	40.0	1.09
6.5	48.8	20.3	26.5	1.17
8.0	55.1	25.4	27.0	1.08
11.5	68.4	21.9	10.5	1.58
16.0	81.5	21.9	4.5	1.97
24.0	88.2	24.0	2.5	1.77

of recipe at 5.1° when butadiene and styrene are used.[2]

(2) J. M. Mitchell, R. Spolsky and H. L. Williams, *Ind. Eng. Chem.*, **41**, 1592 (1949).

Values of r_1 and r_2 were calculated by extrapolating bound α-methylstyrene-conversion curves to 0% conversion to obtain the compositions of the copolymers formed initially from monomers of definite compositions and then utilizing the linear method of calculation.[3] The values of r_1, r_2 and r_1r_2 obtained from the slopes of these plots are in Table II along with values obtained at 45°[4] and calculated for 60° from the results obtained at the other two temperatures.

TABLE II

COPOLYMERIZATION DATA

Polymn. temp., °C.	Constants r_1	r_2	r_1r_2
Butadiene–styrene			
−18[5]	0.38	1.37	0.52
5[6]	.64	1.38	0.89
45[7]	.65	1.83	1.19
Butadiene–α-methylstyrene			
12.8	0.010	1.55	0.016
45.0	.18	1.20	.22
60.0	.57	1.08	.62

From the values of r_1 it is evident that the tendency of α-methylstyrene to homopolymerize in this system decreases as the temperature decreases. For comparison the corresponding values of r_1 and r_2 for styrene and butadiene are included. For styrene the decrease in r_1 with a decrease in temperature is not nearly as pronounced as with α-methylstyrene and there is less change in r_2.

Based on the arbitrary choice of 1.00 and −0.8 as the values of Q and e, respectively, for styrene at 60° the corresponding values for butadiene at the same temperature are 1.33 and −0.8.[8] The values of Q and e for α-methylstyrene with butadiene as the reference monomer are 0.71 and −0.1, respectively. The value of Q is in good agreement with those reported in the literature with other reference monomers, particularly methyl methacrylate. The value of e is negative in agreement with reported values but its magnitude is smaller as would be expected from the lower polymerization temperature.[7]

When the residual mercaptan results are plotted values of the regulating index of the mixed tertiary

TABLE III

REGULATING INDEX OF MERCAPTAN

α-Methyl-styrene in charge, %	Mercaptan parts/100 parts monomer	Regulating index
10	0.24	3.0
30	.24	3.3
50	.24	3.4
70	.24	4.0
90	.24	4.2
30	.48	1.7

(3) M. Fineman and S. D. Ross, *J. Polymer. Sci.*, **5**, 259 (1950).

(4) G. U. Glasgow and J. A. Reynolds, Report to Office of Rubber Reserve, Oct. 9, 1946.

(5) R. J. Orr and H. L. Williams, *Can. J. Chem.*, **29**, 270 (1951).

(6) R. D. Gilbert and H. L. Williams, *J. Am. Chem. Soc.*, **74**, 4114 (1952).

(7) J. M. Mitchell and H. L. Williams, *Can. J. Research*, **27F**, 35 (1949).

(8) C. C. Price, *J. Polymer Sci.*, **3**, 772 (1948).

mercaptans, defined as $r = -\mathrm{d} \ln R/\mathrm{d}P$ where R = the residual regulator and P = fractional conversion, can be calculated from the slopes of the initial linear portions of the curves. The results are in Table III.

As the α-methylstyrene content of the monomers increased, the regulating index increased. This indicates that a copolymer radical with a terminal α-methylstyrene group tends to react with the regulator more easily than the butadiene-terminated radical and under similar conditions the number average molecular weight of the copolymer with a high α-methylstyrene content should be lower than that with a low α-methylstyrene content. This dependence of regulating index on monomer content is not observed with MTM and styrene at $-18°$[6] or with n-dodecyl mercaptan and styrene at 45°.[6] In general the value of the regulating index obtained with 0.240 pt. of MTM and 30 pt. of α-methylstyrene at 12.8° was slightly lower than the value obtained with styrene under similar conditions at 5°.[9] With 30 pt. of alpha-methylstyrene the regulating index decreased when the amount of mercaptans was doubled. The initial regulation would be relatively poor at higher concentrations of these mercaptans. At $-18°$ with the α-methylstyrene replaced by styrene a similar increase in amount of regulator present results in an increase in the value of the regulating index.[6]

The intrinsic flow time–conversion data show that the intrinsic flow time decreased appreciably as the α-methylstyrene content of the monomers increased. This decrease may be related to the decrease in number average molecular weight indicated by the regulator disappearance data but is largely due to the effect of the bound α-methylstyrene content of the copolymer on the relationship between intrinsic viscosity and number average molecular weight. As the styrene content of a styrene–butadiene copolymer is increased, the intrinsic viscosity of the copolymer of fixed molecular weight is decreased. Presumably the same phenomenon will be present for α-methylstyrene–butadiene copolymers. This decrease in intrinsic flow time with a decrease in the butadiene content of the monomer is also observed with butadiene and styrene copolymerized under varied conditions.[6,8]

Experimental

Standard polymerization technique was used throughout these experiments. The copolymerization (50 g. of monomer) were conducted in 8-oz. peroxide bottles each of which was provided with a polyvinyl chloride–butyl rubber self-sealing gasket system to permit syringe injection. Agitation was provided by end-over-end rotation of the bottles in a constant temperature bath thermostated at 12.8°. The solution of dextrose digested for 10 min. at reflux temperature was added to the emulsifier solution and this combined solution was added to the bottles followed by the regulator solution and the butadiene in that order. Evaporation of a slight excess of butadiene was used to expel air from the bottles and nitrogen pressure was used with the low butadiene ratios to ensure a positive pressure inside the bottles throughout polymerization. After a pre-emulsification time of 20 min. the activator solution, which had previously been aged under nitrogen for 30 min. at 60°, was injected, and after further rotation for 10 min. the initiator solution was injected to start the reaction. Injection of a dispersion containing 0.305 pt. per 100 pt. of monomers of the shortstop 2,5-di-*t*-butylhydroquinone (Tennessee Eastman Corporation) was used to stop polymerization at the desired time.

The composition of the various solutions mentioned in the previous paragraph based on 100 pt. of total monomers is as follows: *dextrose solution*, dextrose 1.00, KOH 0.040 and water 40.0; *emulsifier solution*, Dresinate 214 (solids) 4.70, Daxad 11 0.100, KOH 0.090, KCl 0.500 and water 130.0; *regulator solution*, MTM variable and α-methylstyrene 91.0–butadiene (100%); *activator solution*, $FeSO_4 \cdot 7H_2O$ 0.140, $K_4P_2O_7$ 0.177 and water 10.0; *initiator solution*, cumene hydroperoxide (100%) 0.100 and α-methylstyrene 9.0.

All materials used were of commercial grade with the exception of the electrolytes which were laboratory chemicals and the α-methylstyrene which was Eastman Research grade and was used as received. The butadiene was 97.5% material manufactured at Polymer Corporation, Limited. Dresinate 214, a potassium disproportionated rosinate supplied by the Hercules Powder Company, contained 80% solids. Daxad 11, a product of the Dewey and Almy Chemical Company, contained at least 77% polymerized sodium alkyl naphthalene sulfonates and no more than 15% inert ingredients. The regulator MTM consisting of 60% *t* C_{12} SH, 20% *t* C_{14} SH and 20% *t* C_{16} SH was manufactured by the Phillips Petroleum Company. Cumene hydroperoxide, a product of the Hercules Powder Company, was 68% pure.

For each bottle the following determinations were made: conversion, bound α-methylstyrene, residual regulator and intrinsic flow time. The bound α-methylstyrene and residual regulator were determined using unstopped latex removed by syringe immediately prior to stopping; the other two determinations were made on stopped latex. Conversion of monomer to polymer was determined by the unvented solids technique, and the bound α-methylstyrene content of the copolymer by measurement at 60.2° of the refractive index of a dry thin film of copolymer obtained on coagulation of the latex in ethanol with two subsequent ethanol washes. Residual regulator in the latex was determined by amperometric titration.[10] The intrinsic flow time, defined as $[t] = \lim_{c \to 0} (\ln t_r/e)$ where t_r = relative flow time and c = concentration of the copolymer in g./100 ml. of solution, was determined at 31.3° by the vistex method[11] with 80:20 benzene–isopropyl alcohol as the original solvent and benzene the diluting solvent in an Ubbelohde viscometer in which the flow time for the original solvent was 104.6 seconds.

In order to calibrate the refractometric method of determining bound α-methylstyrene samples were prepared by copolymerizing for 240 hours at 50.3° various ratios of α-methylstyrene to total monomers in the recipe: α-methylstyrene 100.0–butadiene, water 180.0, MTM 0.500, sodium soap flakes 5.00 and $K_2S_2O_8$ 0.300 parts by weight.

All ingredients were added to the bottles before these were capped in order to avoid syringe injections and hence to minimize losses during polymerization. For a reason that will be apparent from the report copolymers of 100% conversion could not be obtained. Consequently the bound α-methylstyrene content of each of the two copolymers con-

TABLE IV

POLYMERIZATION DATA FOR COPOLYMERS FOR CALIBRATION

α-Methylstyrene/total monomers $\times 10^2$	Conv., %	$n^{60}D$	Bound α-methylstyrene, %
10.0	98.9	1.5121	10.1
20.0	98.1	1.5207	19.3
30.0	97.0	1.5283	27.8
40.0	94.5	1.5355	36.5
60.0	85.7	1.5531	53.4
70.0	77.9	1.5620	61.5
80.0	65.9	1.5714	69.7
90.0	47.6	1.5810	79.0

(9) H. F. Windsor, cited in ref. 6.

(10) I. M. Kolthoff and W. E. Harris, *Ind. Eng. Chem., Anal. Ed.*, **18**, 161 (1946).

(11) D. A. Henderson and N. R. Legge, *Can. J. Research*, **B27**, 666 (1949).

taining the lowest percentages of substituted styrene was calculated on the assumption that the unreacted α-methylstyrene was recovered quantitatively by a careful steam distillation. For the copolymers with higher α-methylstyrene content the assumption was made that all the butadiene had reacted.

The experimental data for the calibration copolymers are in Table IV. The relationship between refractive index and bound α-methylstyrene content for these copolymers is not as linear as is that for styrene–butadiene copolymers and the refractive indices are higher for the same per cent. bound monomer. The results obtained at high bound α-methylstyrene contents are subject to error because of the difficulty of determining the refractive index of a copolymer with a high α-methylstyrene content.

Acknowledgments.—The authors thank Polymer Corporation Limited for permission to publish this paper. The assistance of S. Butler, A. Johnston, J. Borunsky and G. Vincent is acknowledged.

ANALYSIS OF MULTILAYER GAS ADSORPTION ISOTHERMS USING THE CONCEPT OF SURFACE HETEROGENEITY

BY J. M. HONIG[1]

Department of Chemistry, University of Minnesota, Minneapolis 14, Minn.

Received September 3, 1952

The heterogeneous surface model discussed in the literature has been extended to cover the case of multilayer gas adsorption. The applicability of the theory to the adsorption of nitrogen on rutile at 77°K. is discussed.

The interpretation of gas adsorption isotherms in terms of a heterogeneous surface model has been discussed extensively in the recent literature.[2-8] These discussions are all based on the assumption that surface sites associated with the same adsorption energy are covered in accordance with the Langmuir law.[5,9] The use of such a model ought therefore to be limited to cases where only a monolayer of adsorbate is formed on the surface.

In this paper a very simple extension of the theory is presented which permits application of the heterogeneous surface model to multilayer adsorption systems. The significance of the results obtained with this theory is also discussed.

Previous attempts to apply the concepts of surface heterogeneity to multilayer adsorption systems have been limited. McMillan[10] as well as Walker and Zettlemoyer[11] have assumed the existence of surface sites associated with two different adsorption energies. The resulting isotherm equations fit experimental data over a surprisingly wide range of surface coverage.

The present discussion is an extension of the work just cited. It rests on the assumption that all sites of equal adsorption energy are filled according to the BET isotherm equation[5,12]

$$\theta_\epsilon = \left(\frac{1}{1-x}\right)\left(\frac{1}{1+[(1-x)/x]\beta e^{-(\epsilon-\epsilon_L)/kT}}\right) \quad (1)$$

where the variable parameter $(1/\beta)e^{(\epsilon-\epsilon_L)/kT}$ is analogous to the fixed parameter c of the BET theory.[5,12] θ_ϵ represents the fraction of the surface sites associated with energy ϵ which are covered, $x = p/p_0$ is the relative pressure, ϵ and ϵ_L represent, respectively, the energy of adsorption and of liquefaction of the gas. From statistical considerations one finds[13] that β is related to the ratio of the internal partition functions for the adsorbed and liquid phases, respectively.

Now let $dF(\epsilon)$ represent the fraction of all sites whose associated energy is in the range ϵ to $\epsilon + d\epsilon$; the total surface coverage is then given by (compare refs. 3 and 4)

$$\theta(x) = \int_\epsilon \theta_\epsilon dF(\epsilon) = \frac{1}{1-x}\int_{\epsilon_m}^{\infty} \frac{dF(\epsilon)}{1+[(1-x)/x]\beta e^{-(\epsilon-\epsilon_L)/kT}} \quad (2)$$

$$= \frac{1}{1-x}\int_0^{\infty} \frac{dF(\Delta\epsilon)}{1+[(1-x)/x]\mu e^{-\Delta\epsilon/kT}}$$

In equation (2) ϵ_m represents the lowest adsorption energy encountered on the surface. The substitutions $\Delta\epsilon = \epsilon - \epsilon_m$ and $\mu = \beta e^{\epsilon_L/kT}$ were used to obtain the integral at the bottom. This equation is a generalization of those cited in references 10 and 11.

Using equation (2) the distribution of adsorption energies among surface sites may now be calculated in one of two ways. One may select *a priori* a number of different functions for substitution in place of $F(\epsilon)$ in (2), carry out the integration, compare the experimental data with the calculated isotherm equations, and then decide which of the selected functions gives the best fit. Alternatively, one may use the inversion procedure suggested by Sips[3a,b] with minor modifications. Let

$$dF(\Delta\epsilon) = f(\Delta\epsilon)d\Delta\epsilon \quad (3)$$

$$z = e^{\Delta\epsilon/kT} - 1 \qquad x = \mu/(y-1+\mu)$$

$$\theta\left(\frac{\mu}{y-1+\mu}\right) = L(y) \qquad h(z) = f(kT\ln(z+1))$$

$$g(z) = kT\,h(z)$$

(1) The James Forrestal Research Center, Princeton University, Princeton, N. J.

(2) T. L. Hill, *J. Chem. Phys.*, **17**, 762 (1949).

(3) (a) R. Sips, *ibid.*, **16**, 490 (1948); (b) *ibid.*, **18**, 1024 (1950).

(4) G. Halsey and H. Taylor, *ibid.*, **15**, 624 (1947).

(5) S. Brunauer, "The Adsorption of Gases and Vapors," Vol. I, Princeton University Press, Princeton, N. J., 1943.

(6) E. Cremer, *J. chim. phys.*, **46**, 411 (1949).

(7) V. A. Crawford and F. C. Tompkins, *Trans. Faraday Soc.*, **46**, 504 (1950).

(8) J. Zeldovitsh, *Acta Physiochim. U. R. S. S.*, **1**, 961 (1934).

(9) I. Langmuir, *J. Am. Chem. Soc.*, **40**, 1361 (1918).

(10) W. G. McMillan, *J. Chem. Phys.*, **15**, 390 (1947).

(11) W. C. Walker and A. C. Zettlemoyer, THIS JOURNAL, **52**, 47 (1948).

(12) S. Brunauer, P. Emmett and E. Teller, *J. Am. Chem. Soc.*, **60**, 390 (1938).

(13) T. L. Hill, *J. Chem. Phys.*, **14**, 263 (1946).

TABLE I

THEORETICAL ISOTHERM EQUATIONS REPRESENTING THE ADSORPTION OF N_2 ON RUTILE AT 77.78°K.

Designation	Distribution density function, $kt\,f(\epsilon)$	Adsorption isotherm, $n =$	N_m, m mole/g.	Constants	$\mu = \beta e^{\epsilon_L/kt}$
A	$\delta(\epsilon - \epsilon_1)$ [a]	$\frac{n_m}{1-x}\frac{cx}{1-x+cx}$ [b]	0.179	$c = 368$ [b]	....
B	$[\ln \gamma]^{-1}$	$\frac{n_m}{1-x}\frac{1}{\ln\delta}\ln\frac{(\gamma-\beta)x+\beta}{(1-\beta)x+\beta}$	.183	$\gamma = 7.52 \times 10^5$	0.120
C	$\frac{\sin \pi d}{\pi} z^{-d}$ [c]	$\frac{n_m}{1-x}\left(\frac{x}{(1-\beta)x+\beta}\right)^d$	.180	$d = 0.104$	.0561
D	$\frac{1}{2}\frac{\sin \pi d}{\pi d}\frac{z^{-d}}{1+(2\cos\pi d)z^{-d}+z^{-2d}}$ [c]	$\frac{n_m}{1-x}\frac{2}{1+[1+\beta(1-x)/x)]^d}$	.181	$d = 0.161$	.0848

[a] Dirac delta function. [b] $c = \frac{1}{\beta} e^{(\epsilon_1 - \epsilon_L)/kT}$. [c] $z = e^{\Delta\epsilon/kT} - 1$, $\Delta\epsilon = \epsilon - \epsilon_m$.

with which (2) becomes

$$M(y) \equiv L(y) \times \frac{y-1}{y-1+\mu} = \int_0^\infty \frac{g(z)\,dz}{y+z} \quad (4)$$

which is the Stieltjes transform of $g(z)$. The integral may be inverted according to the standard procedure[2,3,14] by use of the relation

$$g(z) = [M(ze^{-\pi i}) - M(ze^{\pi i})]/2\pi i \quad (5)$$

which yields $F(\epsilon)$ *via* (3).

In what follows the theory will be applied to adsorption data of nitrogen on rutile.[15] Since it was the easier to use, the first of the two methods was employed to correlate the adsorption data with an energy distribution. The four functions listed in Table I and illustrated in Fig. 1 were substituted in (2); the resulting isotherm equations are also listed in Table I. They were fitted to the data using the constants shown in the third column of the table. A comparison of the theoretical and experimental data is shown in Fig. 2. The solid curve represents the smoothed out isotherm drawn through the experimental points; the various types of circles represent points on the isotherm computed from the four isotherm equations listed in the table.

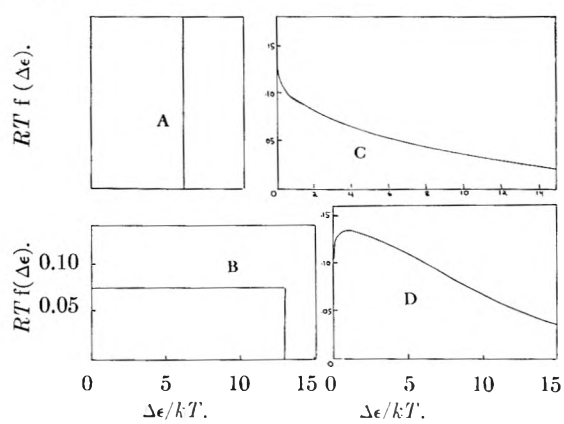

Fig. 1.—Possible distributions of adsorption energies among surface sites.

Figure 2 shows that the BET isotherm equation (equation A of Table I corresponding to the energy density distribution A, in which all sites have the same adsorption energy ϵ_1) represents the data only in the very limited region $0.90 \leq \theta \leq 1.4$. The equation fails very badly in the region of low surface coverage, where the effects of surface heterogeneity become of great importance. By contrast, the isotherm equations corresponding to the energy density distributions B, C or D coincide with the experimental data from the lowest measured surface coverages up to $\theta = 1.4$.

In addition to the calculations made in connection with Fig. 2 it was attempted to fit the data to other types of equations. These were based on models involving localized[16–20] or mobile[21–23] adsorption in the presence or absence of lateral interactions on smooth surfaces. All such attempts met with failure. From this evidence and from Fig. 2 it is to be concluded that the concept of surface heterogeneity is essential to account for the nitrogen adsorption on rutile at 77.7°K.

Unfortunately, it is also evident from Fig. 2 that the theoretical isotherm equations $\theta(x)$ are not very sensitive to the particular distribution functions selected for substitution in eq. (2). The three distribution functions fit the data equally well. Similarly, good agreement with experimental results can be obtained by use of a two-step distribution function for $F(\epsilon)$ (corresponding to the use of a linear combination of two Dirac delta functions for $f(\epsilon)$), as has been shown previously.[10,11] It follows that a mere comparison of theoretical and experimental data is not sufficient for the determination of the "correct" distribution of adsorption energies among surface sites.

On the other hand, the theory is able to exclude certain distribution functions from consideration. Thus, distribution A of Table I is clearly unsatisfactory; also, any function $f(\epsilon)$ which stays bounded away from zero as ϵ approaches infinity will render the integral (2) divergent and is thus unsuitable. The best that can be done in this adsorption system is to distinguish between distribution functions compatible and incompatible with the data.

(14) D. V. Widder, "The Laplace Transform," Princeton University Press, Princeton, N. J., 1941, Chap. VIII.

(15) J. M. Honig and L. H. Reyerson, THIS JOURNAL, **56**, 140 (1952).

(16) R. Fowler and E. Guggenheim, "Statistical Thermodynamics," Cambridge University Press, 1939, Chap. X.

(17) A. M. Miller, "Adsorption of Gases on Solids," Cambridge University Press, 1949, Chap. II.

(18) J. K. Roberts, "Some Problems in Adsorption," Cambridge University Press, 1939, Chap. II.

(19) F. Volkenshtein, *Zhur. Fizicheskoi Khimii*, **21**, 163 (1947)

(20) M. Dole, *J. Chem. Phys.*, **16**, 25 (1948).

(21) T. L. Hill, *ibid.*, **14**, 441 (1946).

(22) T. L. Hill, *ibid.*, **15**, 767 (1947).

(23) A. B. D. Cassie, *Trans. Faraday Soc.*, **41**, 450 (1945).

The failure of equation (2) above $\theta = 1.4$ is not surprising, since in its derivation it was assumed that adsorption in the second and higher layers occurs with the heat of liquefaction. In more refined derivations such an assumption must be eliminated along the lines indicated in recent publications.[24-28] Even without this refinement, however, the present theory gives a fit over wider ranges of surface coverage than the corresponding theory, mentioned in the introduction, which is based on the Langmuir equation.[15] For $x \ll 1$ adsorption isotherms A, B and C of Table I reduce, respectively, to the Langmuir isotherm and to two other isotherms discussed recently by Sips.[3]

Column 3 of Table I is of interest, for it shows that n_m, the quantity of adsorbate required for monolayer coverage of the surface, is practically independent of the four distribution functions used in eq. (2). This is obviously related to the well known fact that the BET isotherm equation, despite its failings, generally yields correct n_m values. Secondly, it is seen from the table that the parameter β varies with the type of function substituted for $f(\epsilon)$, although in the derivation of eq. (2) it is assumed to be independent of ϵ. This tends to confirm the hypothesis made by Hill[2] that the partition function of the adsorbed phase is itself a function of the adsorption energy.

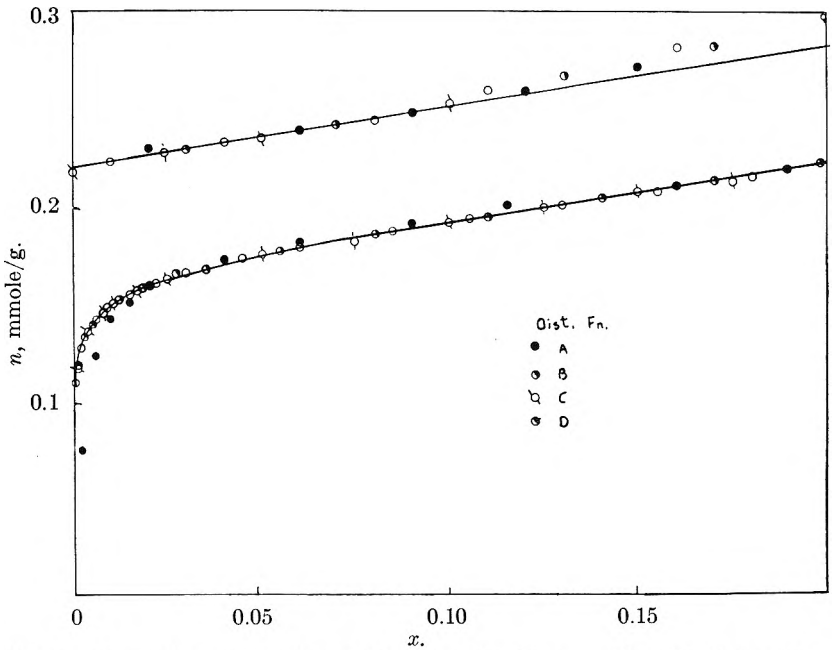

Fig. 2.—Comparison of experimental isotherm for N_2 on rutile with those calculated using the distribution functions of Fig. 1 in the heterogeneous surface model.

It is of interest that the uniform energy density distribution B covers a range of energy $\Delta\epsilon/kT = 13.5$, which at liquid nitrogen temperatures corresponds to $\Delta\epsilon = 2100$ cal./mole. Since the heat of liquefaction of N_2 at its boiling point is roughly $\Lambda = 1330$ cal./mole[29,30] we obtain approximately[31] $\epsilon_L = (1/2)kT + \Lambda = 1410$ cal./mole. Assuming for averaging purposes that the lowest ϵ value is effectively ϵ_L it is seen that the range of adsorption energies covered by the distribution B lies between 1410 and 3510 cal./mole with an average value of $\bar{\epsilon} = 2460$ cal./mole.

(24) G. Halsey, *J. Chem. Phys.*, **16**, 931 (1948).
(25) T. L. Hill, *ibid.*, **17**, 590 (1949).
(26) T. L. Hill, *ibid.*, **17**, 668 (1949).
(27) W. G. McMillan and E. Teller, THIS JOURNAL, **55**, 17 (1951).
(28) W. G. McMillan and E. Teller, *J. Chem. Phys.*, **19**, 25 (1951).
(29) L. I. Dana, *Proc. Am. Acad. Arts Sci.*, **60**, 241 (1925).
(30) W. F. Giauque and J. O. Clayton, *J. Am. Chem. Soc.*, **55**, 4879 (1933).
(31) T. L. Hill, *J. Chem. Phys.*, **17**, 106 (1949).

A COMPARISON OF THE EFFECTS OF SEVERAL SOLUBILIZED C_6-HYDROCARBONS ON THE VISCOSITY OF A POLYSOAP SOLUTION[1]

BY ULRICH P. STRAUSS AND LIONEL H. LAYTON[2]

School of Chemistry, Rutgers University, New Brunswick, New Jersey

Received September 5, 1952

The effects of solubilized hexane, hexene, cyclohexane, cyclohexene and benzene on the viscosity of a 2% solution of a polysoap, prepared by the partial quaternization of polyvinylpyridine with *n*-dodecyl bromide, were compared in order to find out what structural features of benzene are responsible for its anomalous viscosity behavior. It was found that none of the aliphatic hydrocarbons showed the viscosity maximum which was observed when increasing amounts of benzene were solubilized in the polysoap solution. A new method for measuring the solubilities of the hydrocarbons in the solution gave results in close agreement with values determined by a previously described technique. The solubilities of the hydrocarbon increased in the order in which they are listed above. These results indicate that both cyclization and the introduction of a double bond increase the solubility of a hydrocarbon, but that neither of these factors is responsible for the viscosity anomaly shown by benzene. The anomaly is most likely due to some property connected with the aromatic nature of benzene. Perhaps the ease with which electronic displacements may be induced in benzene molecules makes possible their solubilization not only in the lipophilic but also in the polar regions of the polysoap molecules.

Introduction

It has recently been shown that polysoaps, which are polymers to whose chain structure soap molecules are chemically attached, solubilize hydrocarbons in water just as simple soaps do.[3] Each polysoap molecule acts as a prefabricated soap micelle. By means of viscosity measurements we have found polysoap molecules to undergo considerable changes in their structure upon solubilization. Depending on the solubilizate, two distinct types of behavior have been observed. On the addition of isoöctane or *n*-dodecane and other straight chain aliphatic hydrocarbons to a polysoap solution, the viscosity decreases uniformly until hydrocarbon saturation is reached.[4] With benzene and other aromatic hydrocarbons or heptyl alcohol, on the other hand, the viscosity goes first through a maximum.[5,6] While in the case of ordinary soaps a difference in solubilization behavior toward non-polar and polar compounds has long been recognized,[7] benzene has customarily been considered as belonging to the "non-polar" variety. It is therefore of special interest to find out what in our case causes it to behave like heptyl alcohol rather than like isoöctane. In order to get an idea as to what feature in the benzene structure is responsible for this "anomalous" behavior, we have made a solubilization study comparing benzene with other C_6-hydrocarbons which have some structural features in common with benzene while differing in others. The results of this study which includes *n*-hexane, hexene-1, cyclohexane, cyclohexene and benzene are presented in this paper.

Experimental

Materials.—**Polysoap No. L 1153** was prepared by the partial quaternization of poly-2-vinylpyridine (our sample No. J 3258[5]) with *n*-dodecyl bromide employing essentially the method of preparation described previously.[3] The polysoap contained 7.16% nitrogen, 15.72% bromine and 0.45 meq. of hydrogen ion per gram.[8] From these analytical data it follows that 29.7% of the nitrogens were quaternized with *n*-dodecyl bromide while 8.7% carried hydrogen bromide.

The aliphatic hydrocarbons, *n*-hexane, hexene-1, cyclohexane and cyclohexene were "pure grade, minimum purity 99 mole per cent." Phillips Petroleum Company products. They were redistilled before use.

Eastman Kodak (777) benzene, thiophene-free, was redistilled.

Procedure.—Sealed glass ampules containing the polysoap solution and the desired quantity of hydrocarbon were tumbled end over end in a water-bath thermostated at 25° for at least four days to attain equilibrium. The solutions were then transferred into a Bingham viscometer[9] whose constant $(pt)_0$ for water was 13,210 gram seconds per square centimeter. The viscosity was then measured at 25°.

The method of preparing the ampules has already been described.[4] Because of the high volatility of the C_6-hydrocarbons, all the special precautions which had been found necessary for benzene[5] had to be observed in this study, too. Moreover, for samples containing less than 20 mg. of hydrocarbon, the special stock dilution method used previously for isoöctane[4] was employed.

The method by which the hydrocarbon solubility is determined from the viscosity results has been described previously.[4] This method has also been used in this study, but, in addition, a new technique for the determination of the solubility in polysoap solutions has been applied and tested. This technique is more cumbersome than the old method, but it is useful in cases where the old method lacks in precision. The new method is applied as follows: Hydrocarbon in excess of saturation is added to the polysoap solution contained in an ampule. Equilibrium is reached by tumbling which must be slow enough to avoid emulsification. After the ampule is allowed to stand in the bath for 24 hours to let the excess hydrocarbon rise to the top, the saturated solution is drawn into a hypodermic syringe, care being taken to avoid picking up excess hydrocarbon. Portions of the saturated solutions are then introduced into smaller ampules where they are subdiluted in known proportions. These solutions are then tumbled to equilibrium, and from their measured viscosities their hydrocarbon concentrations are calculated by means of the previously determined viscosity–concentration relationship. Since the ratio by which the saturated solution was subdiluted is known, the value of the hydrocarbon concentration in the saturated solution can be calculated. In this manner a value for the solubility is obtained from each subdilution. The values obtained from the subdilutions of at least two independently prepared saturated solutions are then averaged to give the best representative value for the hydrocarbon solubility. All the care necessary to avoid losing the volatile hydrocar-

(1) Paper presented at the American Chemical Society Meeting, Division of Colloid Chemistry, Atlantic City, N. J., September 16, 1952.

(2) These results will be contained in a thesis to be submitted by L. H. Layton to the Graduate School of Rutgers University in partial fulfillment of the requirements for the degree of Doctor of Philosophy.

(3) U. P. Strauss and E. G. Jackson, *J. Polymer Sci.*, **6**, 649 (1951).

(4) E. G. Jackson and U. P. Strauss, *ibid.*, **7**, 473 (1951).

(5) L. H. Layton, E. G. Jackson and U. P. Strauss, *ibid.*, **9**, 295 (1952).

(6) U. P. Strauss and L. H. Layton, unpublished results.

(7) See, for instance, H. B. Klevens, *Chem. Revs.*, **47**, 1 (1950).

(8) The nitrogen and bromine analyses were performed by W. Manser, Mikrolabor der E. T. H., Zurich, Switzerland.

(9) E. C. Bingham, "Fluidity and Plasticity," McGraw-Hill Book Co., Inc., New York, N. Y., 1922.

bons during transfer, and all corrections for the presence of hydrocarbon in the vapor spaces above the solutions, must, of course, be applied in this technique, too.

Results and Discussion

The experimental results are given in Fig. 1 where the reduced viscosity, η_{sp}/C (C = polysoap concentration in grams per 100 ml., and η_{sp} = specific viscosity with respect to water as the solvent), is plotted against the hydrocarbon concentration, K. The contrast between the two types of behavior which we have discussed in the Introduction is evident. The results show that regardless of structure, none of the aliphatic hydrocarbons investigated follows the complex behavior of benzene. On addition of an aliphatic hydrocarbon, the reduced viscosity decreases almost linearly, with a slight upward curvature,[10] until saturation is reached; addition of more hydrocarbon does not affect the viscosity any further so that at the saturation point the curve experiences a sharp break and continues as a horizontal straight line.[11] The break indicates the solubility limit of the solubilizate. The solubilities of the aliphatic hydrocarbons, K_s, obtained in this way, are given in the first column of Table I. The more complicated benzene curve also experiences a break at saturation, but the break is not sharp enough to allow the determination of the solubility with much precision.[5] We have therefore used the new method involving the subdilution of saturated solutions which has been described under Procedure. The method has not only been applied to benzene, but to all the hydrocarbons studied, and the results are given in the second column of Table I. The agreement with the values in the first column is satisfactory, and indicates that we may have confidence in the new method. As a test of the precision of the new method in the case of benzene, the K-values of the sub-diluted solutions have been calculated from the K_s-value determined by the new method, and the corresponding points (represented by squares in Fig. 1) are shown to fall on the established benzene curve within the experimental error.

TABLE I

SOLUBILITIES OF C_6-HYDROCARBONS

Hydrocarbon	K (g./100 ml.) By old method[a]	By new method[a]	Solubility in water, g./100 ml.	S, g./100 ml.	S/C g./g.
n-Hexane	0.157	0.157	0.012[b]	0.145	0.0725
Hexene-1	.203	.213	(.02)[c]	.19	.095
Cyclohexane	.284	.293	.008[b]	.280	.140
Cyclohexene	.382	.393	.013[b]	.375	.1875
Benzene	...	.970	.179[d]	.791	.395

[a] For explanation see text. [b] J. W. McBain and K. J. Lissant, THIS JOURNAL, 55, 655 (1951). [c] Estimated value. [d] R. L. Bohon and W. F. Claussen, *J. Am. Chem. Soc.*, 73, 1571 (1951).

(10) In the first investigation of this kind,[4] this curvature was too small to be noticeable, but it has since been observed in several other studies. The curvature indicates that the more compact the polysoap molecules become the less efficient a given amount of hydrocarbon is at contracting them further.

(11) For better legibility, the experimental points corresponding to excess hydrocarbon are omitted in Fig. 1. However, in each case the horizontal line which is determined by these points is indicated by a dashed line labeled with the name of the appropriate hydrocarbon

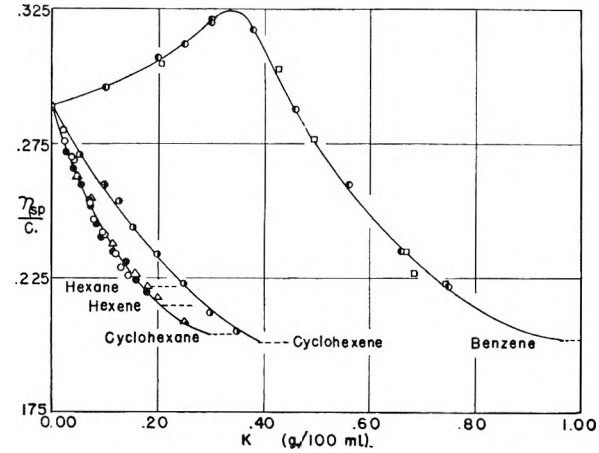

Fig. 1.—The effect of C_6-hydrocarbons on the reduced viscosity of a 2.00% polysoap solution: ○, hexane; ●, hexene; △, cyclohexane; ◑, cyclohexene; ◐, benzene. Test of new subdilution method for benzene: □, subdilutions from solutions saturated with benzene, using 0.970 g./100 ml. as the benzene concentration of the saturated solution (see text).

To obtain the true solubilization limits, *i.e.*, the solubilities of the hydrocarbons due to the presence of the polysoap alone, we must subtract the solubilities of the hydrocarbons in water from the average K_s-values. The results, denoted by S, are given in the fourth column of Table I. Finally in column 5, we have given S/C which represents the solubility of hydrocarbon per gram of polysoap. A comparison of these solubilities indicates that ring formation, *i.e.*, going from hexane to cyclohexane or from hexene to cyclohexene, approximately doubles the solubility, whereas the introduction of a double bond, both with hexane and cyclohexane, increases the solubility by about one-third of its value. While this is hardly enough evidence to prove the general validity of these "rules," it is nevertheless tempting to apply them to the calculation of the expected solubility of benzene. Starting with the S/C value of cyclohexene, the expected S/C value of benzene would be 0.33, which is at least of the right order of magnitude. It is quite conceivable that the aromatic nature of benzene is responsible for the difference between the "calculated" and the experimental values.

If we compare the effect of the hydrocarbons on the reduced viscosity of the polysoap solution, we find that, gram for gram, hexane, hexene and cyclohexane depress the reduced viscosity by about the same amount while cyclohexene depresses it by less. The reason for this is not clear. Changing the concentrations to volume or mole units does not appreciably affect the situation. However, all four aliphatic hydrocarbons follow the same simple type of behavior. In the case of isooctane and *n*-dodecane this behavior was previously found to be independent of polysoap concentration and dependent only on the hydrocarbon to polysoap ratio, and was therefore interpreted as a simple contraction of the polysoap molecules induced by the solubilized hydrocarbon.[4] With benzene, on the other hand, the viscosity goes through a maximum and, as has been shown in a previous paper,[5]

the height of the maximum increases sharply with the polysoap concentration of the solution to which the benzene is added. This indicates that the solubilized benzene affects not only the size, but even more the interaction potential of the polysoap molecules, so that, depending on the amount of benzene solubilized, the polysoap molecules become more or less prone to form aggregates.

To come back to our question as to what structural feature of benzene causes this behavior, the results obtained with cyclohexane, which, incidentally, resembles benzene also in most physical properties,[12] hexene and cyclohexene show that neither cyclic structure nor a double bond nor the combination of the two is responsible. The most important remaining feature in which benzene differs from the other hydrocarbons investigated is its aromatic character. It is quite conceivable that the ease with which electronic displacements may be induced in the aromatic nucleus by electric fields may cause the benzene molecules, when they happen to be in the polar region of a polysoap molecule, to become highly polarized and as a consequence to be held there by strong attractive forces. It has been shown previously[5] that with such an assumption, namely, that the benzene is solubilized not only in the hydrocarbon portion but also in the polar region of the polysoap molecule, the observed viscosity maxima can be explained, and, furthermore, that the similarity in the effects produced by benzene and heptyl alcohol can be understood.

It is of interest that viscosity maxima as a result of benzene solubilization have also been observed in 10% sodium oleate solutions.[13,14] It is evident that our explanation for polysoaps also fits the sodium oleate case.

One feels tempted to compare the induced aggregation of polysoap molecules by benzene with the aggregation of the protein, fibrinogen, brought about by the enzyme, thrombin. This phenomenon is of biological importance because it is responsible for the clotting of blood. While the mechanism in this latter case is believed to be quite different from ours, involving a chemical change of the fibrinogen molecule,[15] we nevertheless feel that the analogy is worthy of attention.

Acknowledgment.—This investigation was supported by research grants from the Office of Naval Research, the Research Corporation, and the Rutgers Research Council.

(12) Compare, for instance, the following physical properties of benzene and cyclohexane (given in that order): vapor pressures at 25° = 95.1 and 97.8 mm.; critical temperatures = 562 and 554°K.; critical pressures = 47.1 and 40.4 atm.; normal boiling points = 80.1 and 80.7°; freezing points = 5.5 and 6.6°; densities at 25° = 0.874 and 0.774 g./ml.

(13) A. Hahne, *Z. dtsch. Öl.- u. Fettind.*, **45**, 245 f (1925).

(14) M. Kiessig and W. Philippoff, *Naturwissenschaften*, **35**, 593 (1939).

(15) K. Laki, *Science*, **114**, 435 (1951).

ELECTRON MICROSCOPIC STUDIES OF SOME PARAFFINIC SODIUM SOAPS[1]

BY MORTON L. E. CHWALOW[2]

Temple University, Philadelphia, Penna.

Received September 22, 1952

Electron microscopic investigations of the crystalline structures formed by the paraffinic sodium soaps, from sodium butyrate ($NaC_4H_7O_2$) through sodium stearate ($NaC_{18}H_{35}O_2$), show these to consist, primarily, of ribbon-like fibers, which in the higher molecular weight soaps occasionally form closed rings. The maximum widths of these fibers decrease as the molecular weights of the soaps increase. As is known from previous diffraction studies, sodium soap molecules align themselves with the long axes of their hydrocarbon chains parallel and with their ionic ends adjacent to each other, thus forming bimolecular laminae. On the basis of the above and a realization of the layer lattice nature of these soaps a model is proposed in which the long axes of the hydrocarbon chains are oriented essentially normal to the planes of the above noted ribbon-like fibers. Use of this model plus analysis of the van der Waals forces acting between the adjacent hydrocarbon chains and the forces prevailing in the ionic layer, lead to a direct explanation of the structures and structural changes observed electron microscopically.

I. Introduction

The general purpose of this investigation was to study the effect of regular variations in molecular weight and structure on the gross morphologies of a set of crystalline compounds characterized by such variations. This work includes both experimental electron microscopic studies of an appropriate set of compounds and an explanation of the morphologies and morphological changes observed therein based on analysis of the prevailing molecular structures and forces.

The straight chain paraffinic sodium soaps, ranging from sodium butyrate ($NaC_4H_7O_2$) to sodium stearate ($NaC_{18}H_{35}O_2$) offer an ideal array of such compounds. They differ regularly from each other, in molecular weight, by an integral multiple of the molecular weight of two CH_2 groups. Their molecular structures are that of essentially ionic crystals attached to one end of long hydrocarbon chains differing from each other only in integral multiples of the length associated with two CH_2 groups.

In the following the essentially fibrous morphologies of the various soaps, as revealed by the electron microscope, will be discussed first. These structures and the variations therein will then be explained in terms of the molecular orientations within the soap fibers as inferred from diffraction studies, and on the basis of a theory which accounts

(1) Materials and equipment (RCA) were provided by Socony-Vacuum Laboratories.

(2) Frankford Arsenal, Philadelphia, Penna.

for both the van der Waals forces operating between the hydrocarbon chain portions of adjacent soap molecules, and the ionic forces prevailing between the ionic portions of these molecules.

II. Electron Microscopy. Experimental

The morphologies of all the straight chain paraffinic sodium soaps, ranging from sodium butyrate through sodium stearate were investigated electron microscopically. The soaps were prepared in each case by the saponification of Eastman Kodak high purity grade fatty acids. These acids (butyric through stearic) were additionally purified by once recrystallizing from U.S.P. ethanol. The saponification of each acid was carried out by adding a carbonate-free solution of sodium hydroxide in U.S.P. ethanol and water, to an ethanol solution of the acid. The water and ethanol were then evaporated and the solid soaps were dried in vacuum at 80°.

The soaps were all prepared and analyzed at the Socony-Vacuum Laboratories under the supervision of Dr. J. R. White whose generous supply of these, for the purpose of this investigation, is acknowledged. Chemical analysis showed the impurity content due to elements not present in the sodium soaps to be negligible. Acidimetric determinations showed that each sodium soap was contaminated by similar soaps of different molecular weights by less than 5%.

The electron microscopic investigations were all carried out with the standard RCA-EMU electron microscope. The resolving power was determined to be between 50 and 100 Å. during these investigations. The micrographs were taken at a magnification of twelve thousand diameters at which best resolutions were attained with the instrument used.

For this investigation, specimens were prepared as the residues of 0.02% distilled water solutions of the soaps. For the most part formvar substrates were used. When not, the conventional supporting screens were merely dipped into the solutions and then allowed to dry in either air or vacuum. Drying of the specimen could proceed in either air or vacuum without perceptibly affecting the morphology of the material.

In order to increase contrast the specimens which were produced on formvar substrates were shadowcast[3] with gold. The thickness of the shadowcasting layer was approximately 1000 Å. The shadowcasting beam of gold was directed at an angle of approximately 60° to the normal to the surface of the specimen. The gold was evaporated from tantalum ribbon filaments shaped to provide a small source of the metal beam.

In order to minimize sampling and observation errors, two precautions were taken. A minimum of twenty-four specimens of each soap were investigated and these investigations extended over a two-month period. Of much greater importance was the choice of a wide molecular weight range of soaps for investigation. The differences observed between the characteristic structures of the soaps at the extremes of the molecular weight range and, generally, between soaps varying significantly in molecular weight were so great as to ensure confidence in the conclusions drawn. Before proceeding with this discussion a terminology which will remain consistent throughout will be adopted. The primary structure characteristic of all the soaps is a ribbon-like (length > width > thickness) fiber. The term thickness will be used to denote the minimum fiber dimension, the term length the maximum fiber dimension and the term width the remaining fiber dimension.

As just noted the paraffin sodium soaps are characterized primarily, by a ribbon-like fibrous structure. In the higher molecular weight soaps these fibers occasionally form closed rings. Further, the characteristic soap fibrous structures decrease in width with increasing molecular weight of the soap. All the above is illustrated in Figs. 1, 2, 3 and 4.

Fig. 1.—Na butyrate typical sheet-like fiber.

Fig. 2.—Na caprylate.

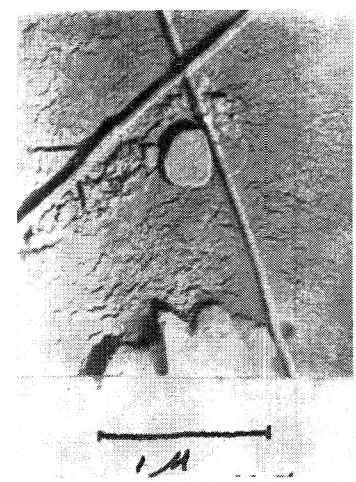

Fig. 3.—Na palmitate fibers and rare plates.

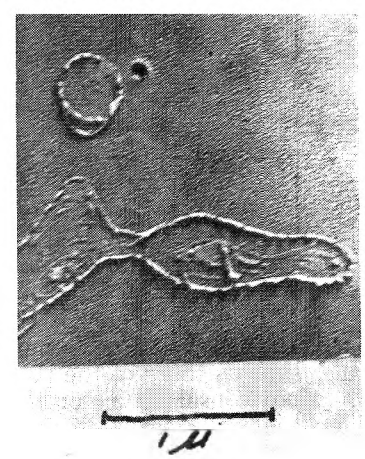

Fig. 4.—Na stearate fiber and closed structure.

(3) R. C. Williams and R. W. G. Wyckoff, *J. Applied Phys.*, **17**, 23 (1946).

III. Theory of the Structures and Structural Changes Observed Electron Microscopically

The paraffinic sodium soaps are the sodium salts of molecularly linear (completely saturated hydrocarbon chains) fatty acids. X-Ray diffraction investigations[4,5] of such materials reveal unit cells having two relatively short axes whose lengths are simply related to the packing diameters and interatomic spacings of saturated hydrocarbon chains. The remaining axis of the unit cell is much longer than the other two and is directly related to twice the length of the fatty acid chain. As would be expected, this type of structure is characterized by X-ray powder patterns consisting of many short spacings associated with the distances between adjacent hydrocarbon chains and one long spacing directly associated with the lengths of the molecular chains. It also has long been known[6] that the carbon atoms in saturated long chain hydrocarbon molecules lie in the same plane and in two parallel rows, that is; the CH_2 groups in the chains form zigzag configurations. Molecules of this kind have the approximate form of a flattened cylinder as indicated in Fig. 5.

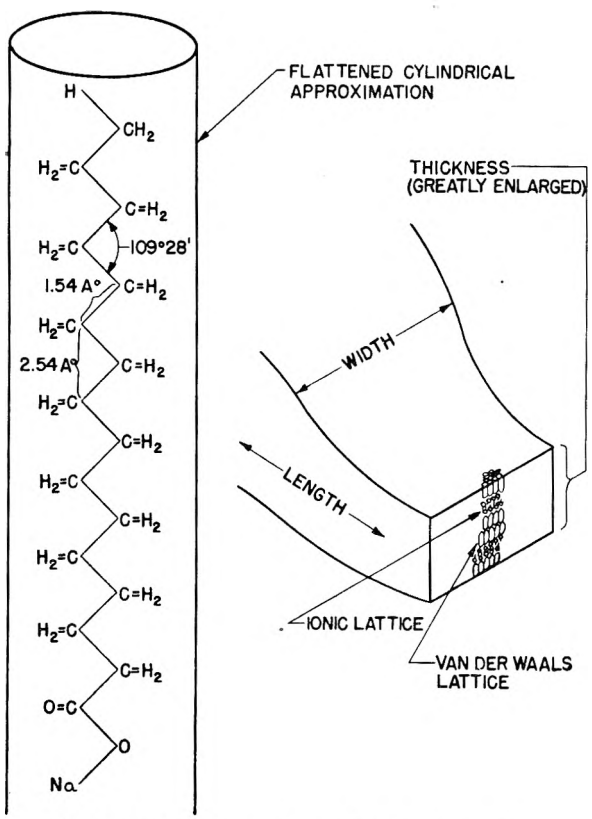

Fig. 5.—Molecular structure of sodium soap fiber.

The next point to be considered is the type of crystalline lattice which would be formed by long chain molecules such as those of the paraffinic sodium soaps. Mere consideration of the rod-like shape of these molecules leads to the proposal that any lattice, other than the layer lattice, with the long axis of the hydrocarbon chains parallel to each other, would be highly improbable. In view of the fact that the long X-ray spacings of the sodium soaps are directly associated with twice the hydrocarbon chain lengths it is logical to assume that the elemental layer consists of a central ionic lamella from both sides of which the hydrocarbon chains protrude. This lattice model is well grounded on the basis of diffraction investigations[7-9] of similar long chain organic materials and is supported by diffraction studies on the specific materials considered here which will be reported at a later date.

The question now arises as to the relationship between the above crystalline lattice and the elemental fibrous structure, characteristic of the sodium soaps, demonstrated electron microscopically. A model consistent with these is proposed in which the long axes of the hydrocarbon chains lie essentially perpendicular to or at least make steep angles with the length–width planes of the fibers.

The above is in accordance with the model of soaps as layer lattice materials. Such materials usually grow in thin sheets or flakes with the long axes of the molecules essentially perpendicular to the planes of the sheets or flakes. The sodium soaps grow in thin fibers[10] and the long axes of their molecules make steep angles with the "planes" of these fibers or, more specifically, the long axes of the soap molecules are directed along the thickness of the fibers as defined previously. Indeed, it is noted that the electron micrographs of the lower molecular weight sodium soap fibers constitute vivid representations of these fibers as sections or strips of layer lattice sheets.

Finally, it is concluded from the preceding discussion that the molecular arrangements in the typical sodium soap fibers are essentially as illustrated in Fig. 5 and a consideration of the intermolecular forces prevailing in this model is now in order.

The attractive forces operating between adjacent soap molecules are of two kinds. Along the paraffinic chains van der Waals forces prevail and the total attractive force here consists of the sum of the van der Waals forces operating between adjacent CH_2 groups. In the ionic layer, of course, coulombic forces prevail. In both regions repulsive forces arise due to the interpenetration of electronic shells.

Vand and de Boer[11] have considered these forces in detail in deriving a theory of the intermolecular forces present in soap crystals. The following is based on their theory.

The total energy of interaction of two soap-like molecules in a layer lattice structure as proposed is given by

(4) M. J. Buerger, *Am. Mineral*, **30**, 551 (1945).

(5) J. E. Miner and E. C. Lingafelter, *J. Am. Chem. Soc.*, **71**, 1145 (1949).

(6) A. Muller, *Proc. Roy. Soc. (London)*, **A120**, 437 (1938).

(7) C. A. Murison, *Phil. Mag.*, Ser. 7, **17**, 111, 201 (1934).

(8) K. H. Storks and L. H. Germer, *J. Chem. Phys.*, **5**, 131 (1937).

(9) L. H. Germer and K. H. Storks, *ibid.*, **6**, 280 (1938).

(10) A few plate-like structures were also observed in the soaps. These did not occur with sufficient frequency to be considered characteristic and analyzed here.

(11) V. Vand and J. H. de Boer, *Koninkl. Akad. Wetenschap. Amsterdam*, **50**, 9, 991 (1947).

$$E = -\frac{e^2}{r}\left\{1 - \frac{1}{n}\left(\frac{r_0}{r}\right)^{n-1}\right\} - KD\left[\left(\frac{r_m}{r}\right)^6 + \frac{1}{2}\left(\frac{r_m}{r}\right)^8 - \frac{1}{2}\left(\frac{r_m}{r}\right)^{20}\right] - (2K-2)D\left[\left(\frac{r_m}{b}\right)^6 + \frac{1}{2}\left(\frac{r_m}{b}\right)^8 - \frac{1}{2}\left(\frac{r_m}{b}\right)^{20}\right]$$

where the first bracketed term and its coefficient on the right side of the expression represent the resultant binding energy at the ionic ends of the molecules and the remaining terms, the van der Waals binding energy between the hydrocarbon chains. In this expression e is the electronic charge, n the exponent of the Born repulsive term, r_0 the equilibrium distance in the ionic lattice, r_m the intermolecular equilibrium distance along the hydrocarbon chains where van der Waals forces prevail, b the distance between next nearest neighboring CH_2 groups of adjacent molecules, K the number of CH_2 groups present in the soap under consideration, D the energy of dissociation of two CH_2 groups and r the actual intermolecular distance.

Analysis of the above expression demonstrates the binding energies associated with the ionic portion of the lattice to be at least 350 times greater than those present along the hydrocarbon chains where van der Waals forces prevail. The ionic radii of sodium and oxygen are given[12] as 0.95 and 1.4 Å., respectively; and therefore it would be expected that the equilibrium distance (r_0) between the ionic ends of adjacent soap molecules would be approximately 2.35 Å. But even if it is assumed that r_0 is as great as 3.6 Å. the ionic interaction energy is found to be 84 kcal. per gram molecular weight. On the other hand evaluation of the van der Waals interaction energy for two CH_2 groups at an equilibrium distance of 4.0 Å. gives 0.25 kcal. per gram molecular weight. This shows the elemental layer lattice to be much more tightly bound throughout its central ionic lamella than throughout the region formed by the hydrocarbon chains.

This distribution of forces has the effect of increasing the intermolecular spacings in the soap crystalline lattices with increasing molecular weight. This is demonstrated in Fig. 6 where the binding energy is plotted for different values of K. Vand and de Boer[11] have shown that X-ray studies verify this theoretical prediction.

Further consideration of the expression for the total binding energy of two soap molecules indicates that while the total binding energy between adjacent soap molecules increases with increasing molecular weight or length of molecule, the binding energy per unit length of molecular chain (per adjacent pair of CH_2 groups) decreases with increasing molecular weight. This becomes apparent when the expression given for the binding energy is divided by K.

The structures and structural changes, revealed in the sodium soap fibers by the electron microscope may now be explained on the basis of the above. The observed phenomenon of the decrease of soap fiber width with increasing molecular weight will be considered first. The theory predicts that adjacent molecules of the higher molecular weight soaps would separate more easily (because their corresponding CH_2 groups are less tightly bound) than those of the lower molecular weight soaps. It would therefore be expected that the higher molecular weight soaps would exhibit narrower fibrous structures than the lower molecular weight soaps. Perhaps this might be stated better, in that cracks, originating randomly as the separation of CH_2 groups of adjacent sodium soap molecules develop more readily in the higher molecular weight sodium soaps leading to finer shredding of a basically sheet-like material.

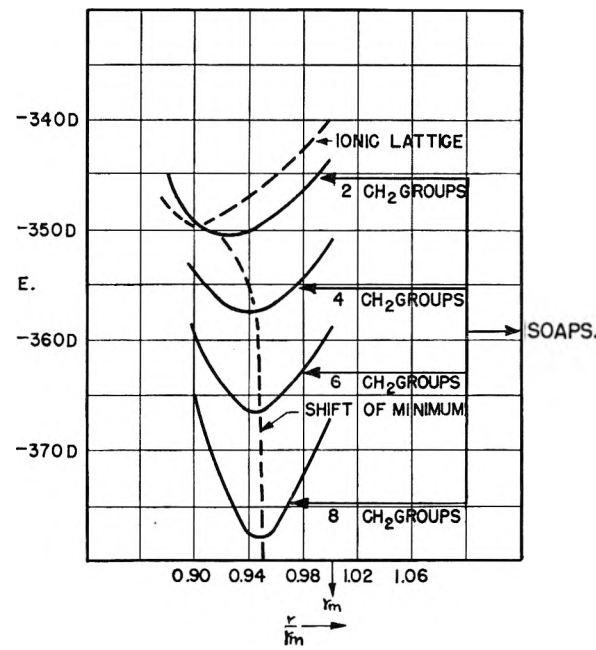

Fig. 6.—Potential functions: two soap molecule chains of 2, 4, 6 and 8 CH_2 groups, according to Vand and De Boer. D = energy of dissociation of adjacent CH_2 groups.

A somewhat more quantitative explanation of this phenomenon of the decrease of fiber width with increase of molecular weight is also offered by the theory developed above. Examination of the electron micrographs of Figs. 1 to 4 demonstrates that the fiber widths of the lower molecular weight soaps show greater decreases in width with increasing molecular weight than do those of the higher molecular weight soaps. Indeed, the latter show only slight changes of this kind. Consideration of Fig. 6, demonstrates the theoretical prediction that the spacings between adjacent molecules of the lower molecular weight soaps increase more with increasing molecular weight, than do these between adjacent molecules of the higher molecular weight soaps. This signifies that the energy per CH_2 pair of adjacent molecules decreases more rapidly with increasing molecular weight for the lower molecular weight soaps. Applying the reasoning of the preceding paragraph the theory is also seen to explain the experimentally observed phenomenon just noted.

(12) L. Pauling, "The Nature of the Chemical Bond," Cornell University Press, Ithaca, N. Y., 1940, pp. 187 ff., pp. 343 and ff.

The actual soap fibrous structures themselves will now be considered, particularly the question of why they are fibrous or why their lengths are so much greater than their widths. Otherwise stated, why do not CH_2 separations develop, equally limiting the lengths and widths of the observed structures. The answer to the above is found in a consideration of the shapes and packing of the sodium soap molecules and their hydrocarbon chains. As has been noted previously, the carbon atoms in the hydrocarbon chain lie in the same plane but in two parallel rows and such molecular chains are most accurately approximated by flattened or elliptical cylinders. This implies that the van der Waals force fields of these molecules do not exhibit cylindrical symmetry and since such forces add algebraically it would be expected that the greatest total van der Waals forces existing between molecules are those along the greatest areas of contact. This points to association of the length of the fiber with "broadside" to "broadside" molecular packing, that is, the length of the fiber is along a line passing normally through the major axes of the flattened cylindrical molecular approximations. The width of the fibers, on the other hand, is along a line passing normally through the minor axes of the flattened cylindrical molecular approximations. This explanation of the basic nature of the fibrous structure of the sodium soaps requires that the molecules be oriented consistently the same with respect to each other throughout the soap fiber. Such a consistent molecular arrangement is substantiated by the electron reflection diffraction patterns shown by the sodium soaps.

The observed closed structures are explained merely as fibers joined at their ends. The fact that these structures occur more frequently in the higher molecular weight soaps indicates the ratio of the binding forces between molecules "packed broad side" to "broad side" to those of the same molecules "packed narrow side" to "narrow side" to be greater in the higher than in the lower molecular weight soaps.

As already noted the thickness of the soap fibers is associated with the thickness of the bimolecular lamina, or twice the long spacings of the soaps. As previously mentioned layer lattice materials form thin macro structures, as the plates characteristic of graphite or clays, because the forces between layers of the lattice are so much weaker than those between the constituents of a given layer. This is also illustrated in the soap crystalline fibers where the force between succeeding bimolecular layers is less than between the molecules of a given layer, accounting therefore for the extreme thinness of the soap fibers.

This association of the thickness of the soap fibers with the thickness of the bimolecular lamina is substantiated by the work of Marton, McBain and Vold[13] on sodium laurate. This group found that "electron microscope photographs of a curd of sodium laurate show that it consists of a mass of fibers whose widths tend to be integral multiples of approximately twice the length of the sodium laurate molecule." Now Marton, *et al.*, confined their measurements "chiefly to the narrowest fibers since the absolute error increases with width of fiber." Further, in their technique of specimen preparation (dipping a 400-mesh screen into a 5.6% solution of this soap in water and vacuum drying) the fibers were not deposited onto a supporting film and were not shadowcast. This would make the distinction between width and thickness extremely difficult. In view of the above it seems quite definite that the term width used by Marton, McBain and Vold is equivalent to the term thickness used here. This, then, gives further evidence of the association of soap fiber thickness with the bimolecular lamina as loosely bound stacks of such laminae.

With the above a complete analysis of the elemental gross structures of the paraffinic sodium soaps, as revealed by the electron microscope, has been given. The structural changes with changes in molecular weight, observed electron microscopically have also been accounted for on the basis of a theory involving the forces operating between the soap molecules as they are aligned in the characteristic fibrous structures of these materials.

Acknowledgments.—The author wishes to express his appreciation to Drs. J. Lloyd Bohn and L. Muldawer of Temple University for their stimulating discussion and review of this work.

(13) L. Marton, J. W. McBain and R. D. Vold, *J. Am. Chem Soc.*, **63**, 1990 (1941)

SURFACE TENSION AT ELEVATED TEMPERATURES. I. FURNACE AND METHOD FOR USE OF THE SESSILE DROP METHOD; SURFACE TENSION OF SILICON, IRON AND NICKEL

BY W. D. KINGERY AND M. HUMENIK, JR.

Ceramics Division,[1] Department of Metallurgy, Massachusetts Institute of Technology, Cambridge, Massachusetts

Received September 26, 1952

Difficulties in the experimental determination of surface tension at elevated temperatures have been overcome by use of the sessile drop method with precise methods of measurement. A description of the sessile drop method of surface tension determination is included with a description of an induction furnace suitable for determining the shape of sessile drops *in vacuo* or in pure atmospheres up to temperatures of at least 2000°. Methods of obtaining precise measurements capable of yielding surface tensions within ±2–3% are described. Calculations of the surface tension of water and molten silver by the sessile drop method gave values in good agreement with determinations by other methods. Surface tensions of liquid silicon, iron and nickel have been measured.

Introduction

The difficulty of experimental measurement of surface tension at elevated temperatures is demonstrated by the almost total lack of reliable values for surface tension above 1400° available in the literature. The variation in values reported and the limited number of values reported has been caused primarily by difficulties in design of equipment for high temperatures and difficulties in maintaining an uncontaminated surface at high temperatures. For various applications the contact angle or "wettability" of high temperature materials is of importance as well as the surface tension. Consequently, it was felt desirable to develop equipment that would be suitable for determination of contact angles as well as surface tension.

A number of methods of determining surface tension and contact angles were considered. Some preliminary experiments made with pure iron and sintered alumina capillaries indicated that contact angles and surface contours after solidification were extremely variable. These variations occurred at different points around the capillary and between the inside and outside surface of the capillary. These experiments seemed to confirm that measurements at temperature were required.

Methods for measuring surface tension have been summarized by Dorsey,[2] Bikerman[3] and others. A number of methods have been employed at elevated temperatures. Considerations of theoretical soundness, precision and adaptability to use at high temperatures led to the development of equipment and methods for employing the sessile drop method at temperatures up to 2000°. The sessile drop method is advantageous in that it allows the determination of contact angles coincidentally with the determination of surface tension.

Of the materials studied here, only iron has previously been investigated. Values reported by various investigations for iron and iron alloys are shown in Fig. 1. These values were obtained by a maximum bubble pressure method,[4] a sessile drop method[5] and a pendant drop method.[6] Values reported range from 820 to 1370 dyne cm.$^{-1}$

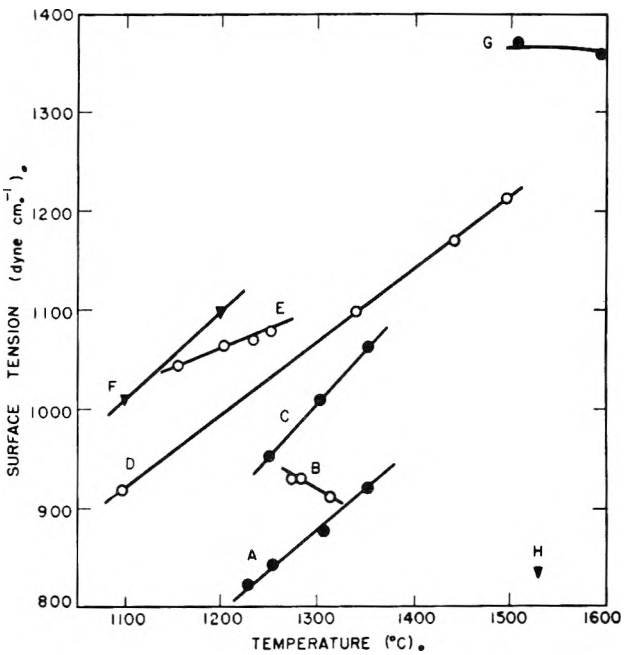

Fig. 1.—Surface tension of iron reported in literature: A[3], 3.32 C, 0.56 Mn, 2.76 Si, 0.49 P, 0.13 S; B[3], cast iron; C[3], 1.40 C, 0.29 Mn, 1.27 Si, 7.44 P; D[3], 2.0 C, 6.8 P; E[3], 3.52 C, 2.10 Mn, 0.65 Si, 0.11 S; F[4], pig iron; G[4], electrolytic iron; H[5], electrolytic iron.

TABLE OF SYMBOLS

b, drop size factor = radius of curvature at origin, cm.
β, drop shape factor = gdb^2/T
c, constant, dyne cm.$^{-2}$
d, density, g. cm.$^{-3}$
f, Dorsey factor
g, gravitational acceleration, cm. sec.$^{-2}$
P, pressure, dyne cm.$^{-2}$
ϕ, angle between ρ and z axis, deg.
R, R', principal radii of curvature, cm.
ρ, meridional radius of curvature, cm.
T, surface tension, erg cm.$^{-2}$
θ, contact angle, deg.
V, volume, cm.^{3}

Sessile Drop Method

The method employed consists of calculating surface tension from the dimensions of a sessile drop. As illustrated

(1) With funds from NEPA Division, Fairchild Engine and Airplane Corporation and the U. S. Atomic Energy Commission.

(2) N. E. Dorsey, *Natl. Bur. Standards Sci. Papers* **21**, No. **540**, 563 (1926).

(3) J. J. Bikerman, "Surface Chemistry for Industrial Research," Academic Press, Inc., New York, N. Y., pp. 4–19.

(4) F. Sauerwald, B. Schmidt and F. Pelka, *Z. anorg. Chem.*, **223**, 84 (1935).

(5) G. Becker, F. Hardus and H. Kornfeld, *Arch. Eisenhuttenw.*, **20**, 363 (1949).

(6) J. K. Davis and F. E. Bartell, *Anal. Chem.*, **20**, 1182 (1948).

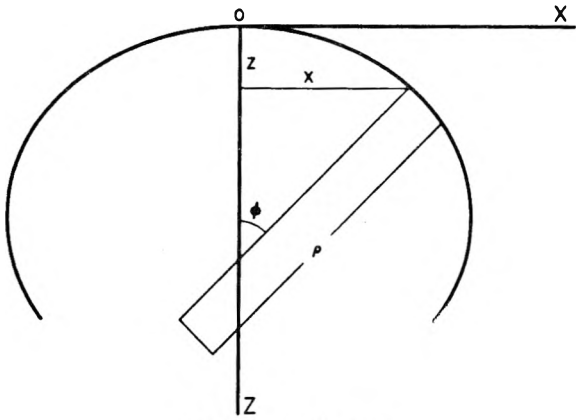

Fig. 2.—Sessile drop.

in Fig. 2, the shape of a sessile drop depends on an equilibrium between forces of surface tension and of gravity. The relations employed were developed by Bashforth and Adams[7] and calculations utilize tables prepared by them. The fundamental equation of surface tension at any point requires

$$T\left(\frac{1}{R}+\frac{1}{R^1}\right) = P = gdz + c \qquad (1)$$

If ρ is the radius of curvature of a meridional section and ϕ is the angle between ρ and the axis of revolution, z

$$R = \rho;\ R^1 = \frac{x}{\sin\phi} \qquad (2)$$

$$T\left(\frac{1}{\rho}+\frac{\sin\phi}{x}\right) = gdz + c \qquad (3)$$

If b is defined as the radius of curvature at the origin, at the origin $\rho = b$, $x/\sin\phi \rightarrow b$, and $z = 0$. From equation (3)

$$c = \frac{2T}{b} \qquad (4)$$

substituting in (3) and multiplying by b gives

$$\frac{1}{(\rho/b)} + \frac{\sin\phi}{(x/b)} = 2 + \frac{gdb^2}{T}\left(\frac{z}{b}\right) \qquad (5)$$

If we define β equal to $\frac{gdb^2}{T}$

$$\frac{1}{(\rho/b)} \frac{\sin\phi}{(x/b)} = 2 + \beta\frac{z}{b} \qquad (6)$$

Differentiation leads to a general differential relation between x and z. By developing differential increments of this relation, Bashforth and Adams[7] prepared tables of β and x/z for $\phi = 90°$, and x/b for various values of β and ϕ. Referring to Fig. 3, from a measurement of x'' and z'', β and b can be determined from tables and the surface tension calculated

$$T = \frac{gdb^2}{\beta} \qquad (7)$$

From β, x'/b, z^1/b, θ, the contact angle can be determined. Drop volume can be calculated from the relation

$$V = \frac{\pi b^2 (x^1)^2}{b}\left[\frac{2}{b} - \frac{2\sin\theta}{x''} + \frac{\beta z^1}{b^2}\right] \qquad (8)$$

Density may be calculated from drop weight and from volume.

A second method of calculation was suggested by Dorsey[8] and is based on the same fundamental relations. It depends on measurements from the top of the drop to the intersection of the axis with a 45° tangent to the drop (y in Fig. 3). The factor, f, is determined

$$f = \frac{y}{x''} - 0.4142 \qquad (9)$$

(7) F. Bashforth and S. C. Adams, "An Attempt to Test the Theories of Capillarity," Cambridge Univ. Press, 1883.

(8) N. E. Dorsey, *J. Wash. Acad. Sci.*, **18**, 505 (1928).

Then the surface tension is calculated from the empirical relation

$$T = gd(x'')^2\left[\frac{0.520}{f} - 0.1227 + 0.0481f\right] \qquad (10)$$

Since these equations all involve x'', the drop diameter at $\phi = 90°$, they must be used for drops having obtuse contact angles. In cases where the contact angle is acute, surface tension can be determined by determining x and z at any measured value of ϕ. Errors arising from estimation of the angle and the exact point of tangency make this method much less precise than the measurement with an obtuse angle.

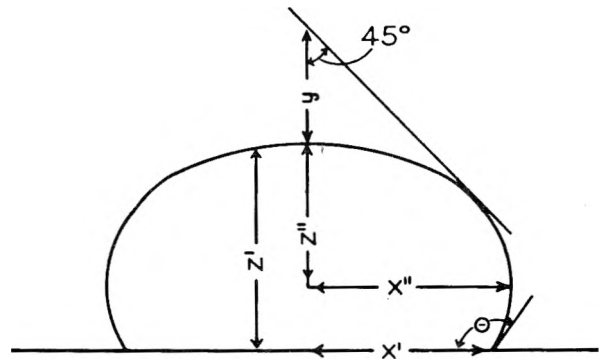

Fig. 3.—Measurements of sessile drop for surface tension calculations.

Surface tension is calculated by two methods and the contact angle is measured and calculated. Agreement of the results obtained serves as a check on drop equilibrium and on accuracy of the calculations.

Experimental

Equipment was designed to fulfill the following objectives, (a) allow the use of vacuum and purified gases so that uncontaminated surfaces could be studied; (b) allow the attainment of temperatures up to 2000°; and (c) allow measurements of sessile drops from which surface tension could be determined. Furnace design is shown in Fig. 4.

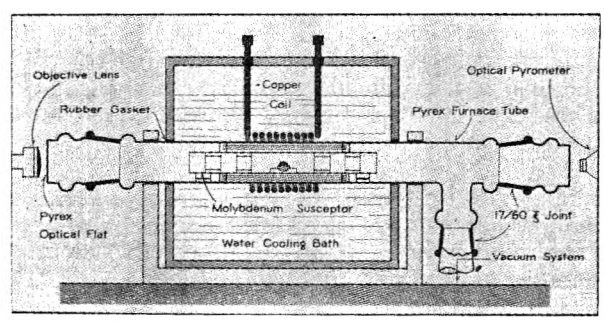

Fig. 4.—Induction furnace for sessile drop surface tension determination.

The furnace heating element consists of a 1.25″ i.d. × 12″ horizontal susceptor cylinder constructed of 0.050″ molybdenum. The susceptor is supported at each end by molybdenum supports resting directly on the Pyrex furnace tube. Open turns of 0.010″ molybdenum surround the susceptor and act as radiation shields. Radiation shield discs are inserted in the susceptor cylinder to prevent excessive heat loss from the ends. Each of these discs contains a $^1/_2$″ D sighting hole so that the four-inch heating zone may be observed from either end of the assembly. The entire molybdenum furniture is enclosed in a water-cooled Pyrex furnace tube with Pyrex optical flats sealing both ends by full-length standard taper joints. A silicone high vacuum grease has been used for sealing these ground glass joints.

Power is supplied to the susceptor by an inductor coil inserted directly in the water-bath. A high frequency motor generator set supplied 10,000 cycle power for the coil. At one end of the furnace tube a L & N optical pyrometer is

mounted to sight directly on the sample. The heating zone of the susceptor extends beyond the first radiation disc and the center of the heating zone gives an effective emissivity of about 0.99 for metal samples. A temperature correction of 23° is required for the Pyrex optical flat. At the other end of the furnace tube an optical system is mounted to obtain photographs of the sessile drop. A magnification factor of about 10 is obtained with the camera system.

The optical system consists of a Zeiss Tessar anastigmatic objective lens with focal length of 8″. The object distance is twice the focal distance; an image is formed on the photographic film with a Huggens ocular. The optical system has a fixed focus so that a constant magnification is obtained (Fig. 5). The entire furnace assembly is mounted on rubber suspension and rubber pad shock mounts to prevent vibrations. In addition the furnace supports and camera assembly are mounted with rubber pads separating them from the furnace table.

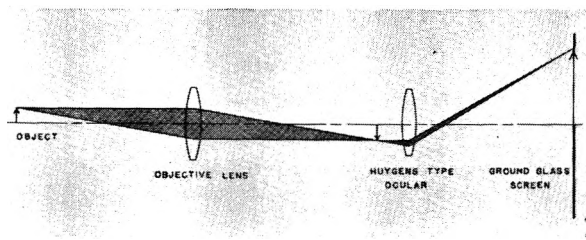

Fig. 5.—Optical system.

Provision is made for use of either vacuum or purified atmospheres. A D.P.I. Model GW 25 oil diffusion pump in conjunction with a Cenco Megavac forepump gives a working pressure of about 5×10^{-6} mm. This low pressure can be obtained since the entire furnace tube is water-cooled. Water cooling also allows the use of Pyrex rather than quartz. Purified gas atmospheres are obtained by evacuating the system and then employing bottle gas purified with an alcohol–Dry Ice trap, heated magnesium chips, $CaSO_4$ and P_2O_5. Atmospheres of hydrogen, helium and nitrogen have been employed.

In operation, furnace temperature is controlled manually by controlling the field voltage of the motor generator with both coarse and fine controls. Field voltage is measured directly for calibration of power *vs.* temperature. Control circuits are interlocked for safety purposes so that power cannot remain on if the water supply or pressure fails, if motor or generator bearings overheat, etc. Temperature limitations of the furnace with the Pyrex tube have not been determined. The maximum temperature thus far obtained is 2050°. For this temperature the power output of the motor generator is approximately 3 kilowatts.

In order to obtain data for surface tension calculation, precise measurements of sessile drop dimensions are required. Such were obtained by a photographic method. Samples to be measured are placed on a refractory plaque which is supported on a molybdenum stand. Refractory plaques were formed from various chemically pure oxide materials by dry pressing and firing to a dense condition. The plaques are leveled and carefully inserted in the furnace (illustrated in Fig. 4). In the furnace the plaque is finally leveled, radiation shields inserted and the furnace closed. After evacuation, a purified atmosphere may be admitted if desired and heating is commenced. After melting and formation of a sessile drop, the camera assembly is adjusted and photographs taken over an interval of time to ensure equilibrium being reached and to determine any effects such as interfacial changes with time. The camera system has a fixed focus and the degree of magnification obtained is constant. Therefore, a standard calibration can be employed. An entire run can be completed in about two hours. The solid sessile drop is weighed for density determination.

At temperatures greater than about 1100°, photographic negatives are obtained directly from emitted light against a dark background. At lower temperatures, shadow photographs are obtained with a light source at the opposite end of the furnace from the camera assembly. In either case the negatives are enlarged on Kodalith film. This high contrast film gives a sharp definition of the drop edges. Differential shrinkage of paper precludes its use; dimensional changes in film on processing are negligible.

Measurements of x'', x', z'', y and θ are made directly on the film enlargements (see Fig. 3). The plane of the maximum radius, x'', is determined by bisecting lines parallel to the z axis which intercept the drop surface above and below x''. A line through these points intercepts the drop surface at the plane of x''. Measurements are made to four significant figures and are consistent within ±0.5%. Surface tension and density values are calculated with the tables and formulas previously discussed. The precision obtained depends on drop size, drop density and drop surface tension. As the drop shape approaches a sphere due to small size, low density and/or high surface tension precision decreases. With metals and ionic materials and drops about 0.8 cm. in diameter, a precision of better than ±5% is obtained, with deviations generally being within ±2–3% for the Bashforth and Adams method. Deviations within ±5% are usually obtained with the Dorsey method. The same mean values are obtained by both methods.

Results

In order to check the experimental procedure employed, the surface tensions of water and of molten silver have been determined by the sessile drop method. The surface tension of water was found equal to 72.6 erg cm.$^{-2}$ at 24°. The value generally reported for the surface tension of water is 72.1 erg cm.$^{-2}$ at 24°.

The surface tension of silver was found to be 920 erg cm.$^{-2}$ at 1025° and 940 erg cm.$^{-2}$ at 975°. These values are in good agreement with values previously determined by the capillary rise method[9] and by the maximum bubble pressure method[10] as shown in Fig. 6. Surface tension values calculated from measurements on a solidified drop were variable and in general gave values from 50–70% low indicating that measurements must be made on the drop in its molten state at temperature. Equilibrium of shape for silver was established within the first minute after melting as is to be expected for metals which have high surface tension and low viscosity.

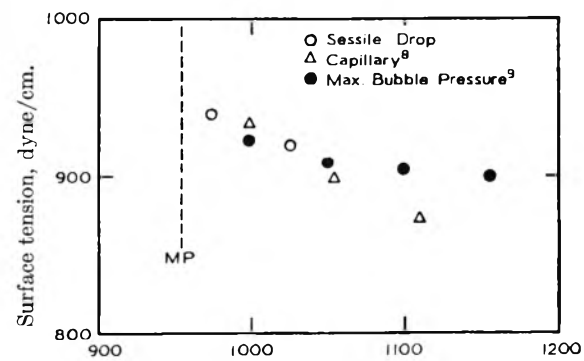

Fig. 6.—Surface tension of silver.

(a). **Nickel.**—Samples of nickel were melted on various plaque materials and surface tension values were obtained *in vacuo*, helium and hydrogen, as given in Table I. Evidence of slight reaction between metal and plaque were observed in the case of MgO and TiO_2. A discoloration at the interface of the Ni–MgO system was observed. The melting point of Ni was lowered by about 50° on the titania plaque and in the neutral and reducing atmospheres employed the titania turned the characteristic black color indicating dissociation to a lower oxygen content. The low values of surface tensions of nickel in contact with titania are ascribed to oxygen solubility.

The particularly low results on titania plaques, where oxygen is known to be available led to the use of "black" zirconia prepared by heating ZrO_2 at 2200° *in vacuo*. This black zirconia is probably a solid solution of Zr in ZrO_2[11] and should act as an oxygen "getter." The value obtained in

(9) E. E. Libman, Univ. Ill. Eng. Expt. Sta. Bull., 187 (1928).

(10) W. Krause, F. Sauerwald and M. Michalke, *Z. anorg. Chem.*, **181**, 353 (1929).

(11) D. Cubicciotti, *J. Am. Chem. Soc.*, **73**, 2032 (1951).

TABLE I

SURFACE TENSION OF NICKEL AT 1470° (dyne/cm.)

Plaque material	Atmosphere: Vacuum	Atmosphere: Hydrogen	Atmosphere: Helium
ThO_2	..	1540	1520
ZrO_2	1730	1555	1500
Al_2O_3	1760	1590	1505
BeO	1680	1595	1370
MgO	1600	1730	1625
TiO_2	1165	1320	1110
ZrO_2–Zr[a]	..	..	1615

[a] Prepared by heating ZrO_2 at 2200° *in vacuo*.

helium on "black" zirconia was considerably higher than values on other oxides. Oxygen in small amounts may be initially present in the plaque materials, original metal or atmosphere for the materials tested. In no case was any difference in the appearance of the bright metal surface observed.

Surface tension values for nickel which are believed most satisfactory are 1735 dyne cm.$^{-1}$ *in vacuo*, 1570 in hydrogen and 1615 in helium.

(b). Iron.—Samples of "armco" iron and electrolytic iron were melted on various plaque materials and surface tension values determined in hydrogen and helium atmospheres. Values obtained are given in Table II. Volatilization was rapid *in vacuo* and precluded measurements. Considerable reaction occurred on TiO_2 plaques and prevented measurement of surface tension. A discoloration of the MgO plaques at the interface was noted.

TABLE II

SURFACE TENSION OF IRON AT 1550° (DYNES/CM.)

Iron	Plaque material	Atmosphere: Hydrogen	Atmosphere: Helium
Armco	ZrO_2	1395	1395
Armco	ThO_2	1430	1320
Armco	BeO	1230	1280
Armco	MgO	..	1240
Electrolytic	ZrO_2	..	1440
Electrolytic	ZrO_2·Zr[a]	..	1560
Electrolytic (+0.1% Ti)	ZrO_2·Zr[a]	..	1565
Electrolytic	Al_2O_3	1450	1440

[a] Prepared by heating ZrO_2 at 2200° *in vacuo*.

The surface tension values obtained for armco iron were lower than those for the electrolytic iron in helium (1285 and 1440 dynes cm.$^{-1}$) and slightly lower in hydrogen (1420 and 1450 dyne cm.$^{-1}$). This is probably due to the minor constituents in the armco iron. The more nearly equal values in hydrogen may be due to removal of some impurities in that atmosphere. Low values were obtained in contact with BeO and MgO. As with nickel a higher value in helium was obtained with "black" zirconia (1560 dyne cm.$^{-1}$), and this is probably due to lower oxygen availability. A sample melted with 0.1% Ti as a de-oxidizing agent showed a value of 1565 dyne cm.$^{-1}$.

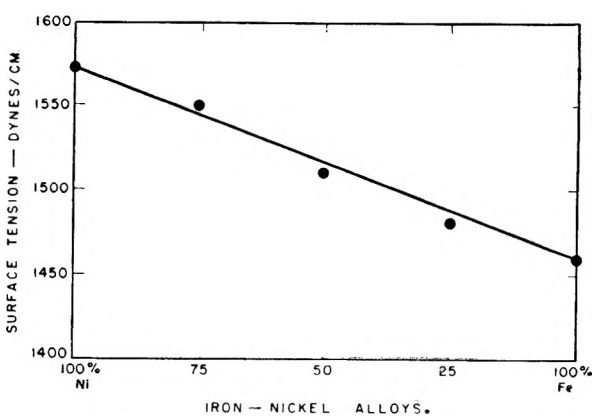

Fig. 7.—Surface tension of iron-nickel alloys.

Surface tension values for pure iron which are believed most satisfactory are 1450 dyne cm.$^{-1}$ in hydrogen and 1560 in helium.

(c) Iron–Nickel Alloys.—A series of mixtures of armco iron and nickel were prepared and melted in helium on ZrO_2 plaques. Within experimental error surface tension values varied linearly with composition as shown in Fig. 7.

(d). Silicon.—Silicon was melted on various plaque materials, and zirconia, titania and magnesia were found to give obtuse contact angles which allow the maximum precision. *In vacuo* vaporization was rapid and precluded measurements. Results in hydrogen and helium are given in Table III and Fig. 8. Uniform results of 730 ± 10 dyne cm.$^{-1}$ were obtained in helium, with the equilibrium value being established almost immediately on melting. In a hydrogen atmosphere the value of surface tension increased from an initial value of 730 to a value of 860 dyne cm.$^{-1}$ after about 15 minutes at constant temperature. The increase is probably due to the decrease in oxygen activity on melting in a hydrogen atmosphere.

TABLE III

SURFACE TENSION OF SILICON AT 1450°

Plaque material	Atmosphere	Surface tension (dyne cm.$^{-1}$)
ZrO_2	He	725
TiO_2	He	730
MgO	He	740
MgO	H_2	860

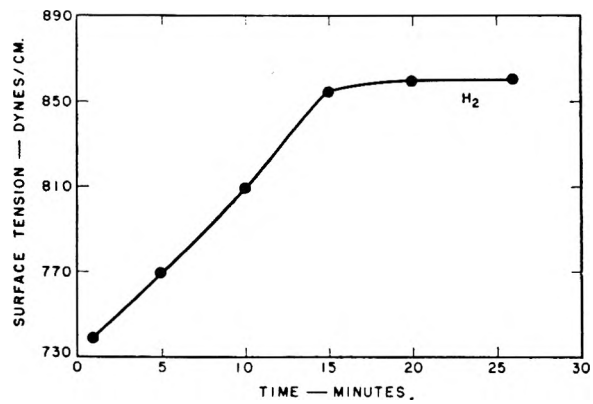

Fig. 8.—Variation of surface tension of silicon with time after melting in a hydrogen atmosphere.

Discussion of Results

The only material whose surface tension was measured here for which previous values are reported is iron. The values obtained in this investigation are universally higher than previous values for iron. This may be due to alloying constituents in previous compositions or to errors in method.

The only directly comparable values are those for electrolytic iron. The value of 1440 dyne cm.$^{-1}$ in helium found here on an Al_2O_3 plaque is in quite good agreement with the value of 1370 dyne cm.$^{-1}$ which has been reported for electrolytic iron in an argon atmosphere.[5] The value of 830 dyne cm.$^{-1}$ reported from measurements on a solidified pendant drop of electrolytic iron[6] is apparently much too low. Values obtained on solidified sessile drops in this investigation were 50–70% lower than values for liquid drops. The low value reported for a solidified pendant drop is believed due to changes in drop shape on solidification. Consequently, measurements of surface tension on solidified metals are considered unsatisfactory.

One significant result of this investigation is that

minor impurities and alloying constituents must have a considerable effect in surface tension of these metals. Values of armco iron were significantly lower than values of electrolytic iron in a neutral atmosphere. Also various plaque materials gave values more different from the mean value than can be accounted for by experimental error. Determinations of the surface tension of other metals, notably mercury,[12] at low temperatures have shown similar large effects for minor contaminants.

The largest effect noted was the effect of oxygen content which was qualitatively observed. Nickel melted on TiO_2 in helium gave a value lower by about 500 dyne cm.$^{-1}$ than nickel melted on a ZrO_2–Zr plaque having low oxygen availability. The surface tension of silicon increased from 730 dyne cm.$^{-1}$ at melting to an equilibrium value of 860 dyne cm.$^{-1}$ in hydrogen. The initial value was the equilibrium value in a non-reducing atmosphere. Both nickel and iron showed a significantly higher value of surface tension in helium when melted on a Zr–ZrO_2 plaque having low oxygen availability than when melted on a regular oxide plaque. These effects can be attributed to the oxygen contents of the molten metal, even though all samples had bright surfaces and showed no surface oxidation.

The effect of atmosphere also was found to have a significant effect on the surface tension values found. Nickel, the only metal measured *in vacuo*, had surface tension values of 1735 dyne cm.$^{-1}$ *in vacuo*, 1615 in helium and 1570 in hydrogen. Iron also showed a lower value in hydrogen than helium. These effects are not unexpected.

The large effects of minor constituents and atmosphere on the surface tension of these metals indicates the difficulty of employing accurate surface tension data for these metals unless previous measurements have been carried out under the exact conditions employed. Under various conditions and in contact with various materials values of 1110 and 1760 dyne cm.$^{-1}$ were obtained for nickel with an experimental error of less than about 50 dyne cm.$^{-1}$; that is, almost a factor of 2 difference was obtained for the same metal having the same outward appearance.

(12) C. Kemball, *Trans. Faraday Soc.*, **42**, 526 (1946).

A KINETIC STUDY OF PHOTO-OXIDATIONS ON THE SURFACE OF ZINC OXIDE IN AQUEOUS SUSPENSIONS[1]

BY MARIA C. MARKHAM AND KEITH J. LAIDLER

Department of Chemistry, The Catholic University of America, Washington, D. C.

Received September 30, 1952

The kinetics of the formation of hydrogen peroxide in aqueous suspensions of zinc oxide in near ultraviolet light have been studied under carefully controlled conditions. The initial quantum yield for hydrogen peroxide formation was found to be 0.25 in absence of organic materials and 0.4 and 0.5, respectively, when small amounts of acetanilide and phenol were added to the system. The ratio of oxygen taken up to peroxide formed has also been measured with the Warburg apparatus, and found to be 1:1 in the absence of organic compounds and 2:1 and 1:1 in the presence of acetanilide and phenol, respectively. Oxidation products of these and other organic compounds have been investigated; small activation energies of 3–4 kcal. are associated with these oxidations. Inhibition by chloride and hydroxide ions has been found in some cases. Experiments on the photopolymerization of vinyl compounds are described. The results are interpreted in the light of our present knowledge of the electrical and optical properties of zinc oxide and shown to be consistent with the theory that electron transfer to adsorbed water leads to the formation of radicals.

Introduction

It has been known for many years that a small but easily measurable concentration of hydrogen peroxide accumulates in a suspension of zinc oxide in water on exposure to sunlight or near ultraviolet light. Some investigators have asserted that oxygen was necessary for the formation[2,3] while others have claimed the contrary.[4] Rabinowitch[5] has discussed the problem of the energy changes involved. It has also been noted that very small amounts of organic materials, generally regarded as stabilizers for the hydrogen peroxide, would greatly increase the concentration of peroxide formed. However, no careful investigation of the kinetics or of the quantum yield has ever been reported in the literature.[6] Acetanilide and phenol were selected for special study: the former because Richardson[6] had used it in his determination of the quantum yield, the latter because Chari and Qureshi[3] had found it to be the most effective stabilizer. The principal objectives of the research reported in this paper were therefore as follows: (1) to determine under reproducible conditions the rate of formation of hydrogen peroxide, the effect of temperature and the quantum yield; (2) to settle definitely the question of the necessity of oxygen and to measure the rate of oxygen consumption; (3) to investigate the role of organic materials in the system; (4) to use the photopolymerization of vinyl monomers in the system to try to obtain an estimate of the initial rate of radical formation; (5) to correlate the experimental results with the present state of our

(1) Abstracted from a dissertation submitted by Sister Maria Clare Markham, C.S.M. (present address: Saint Joseph College, West Hartford, Connecticut) to the Graduate School of the Catholic University of America in partial fulfillment of the requirements for the degree of Doctor of Philosophy.

(2) E. Baur, *Helv. Chim. Acta*, **1**, 186 (1917).

(3) C. N. Chari and M. Qureshi, *J. Indian Chem. Soc.*, **21**, 97 (1944).

(4) K. Yamagudi, M. Nishioeda and H. Imagawa, *Biochem. J.*, **301**, 404 (1939).

(5) E. Rabinowitch, "Photosynthesis I," Interscience Publishers, Inc., New York, N. Y., 1945, p. 73

(6) Dr. F. D. Richardson stated in a private communication that he found the quantum yield to be 0.1 (max.) in weak light intensity. *Cf* E. Rabinowitch, ref. 5, p. 75.

knowledge of the electrical and optical properties of zinc oxide in order to formulate a probable mechanism for these oxidations.

Experimental Procedure

Materials and Arrangement of Apparatus.—The zinc oxide used was spectroscopically pure unsintered material supplied to us through the courtesy of Dr. P. H. Miller of the University of Pennsylvania. The water was triply distilled from alkaline permanganate and sulfuric acid in the last two distillations. C.P. "Dry Process" zinc oxide, Merck and Co., was also used and the results were not found to be significantly different. The specific surface areas of both zinc oxide samples were estimated by the amount of Alizarin Yellow-R adsorbed from solution, a unimolecular layer on 0.1 g. of zinc oxide corresponding to about 8×10^{17} molecules. According to similar measurements of dye adsorption on ionic crystals by Paneth[7] this can be expected to represent one-fifth to one-half of the actual surface.

The light source was a Hanovia high pressure quartz mercury arc, used in all the experiments with a Pyrex envelope to retain all radiation below about 3300 Å. A Hanovia filter #SC 5022 for the 3650 Å. line was used in the determination of the quantum yield. The apparatus for the measurement of the quantum yield was arranged as follows: the suspensions containing 0.1 g. of zinc oxide in 25 ml. of triply distilled water were placed in vertical Pyrex tubes, 30 mm. in diameter, silvered on the outside to prevent loss of light by scattering, with quartz windows sealed to the bottom; the zinc oxide was kept in uniform suspension by entraining air previously filtered through triply distilled water; the tubes were immersed in a constant temperature bath having circular quartz windows 1 cm. in diameter sealed in the base directly below the windows of the tubes containing the suspension; the light from the horizontal 4.5″ mercury arc was passed through the filter, then through collimating holes 1 cm. in diameter before entering the windows in the base of the constant temperature bath. The intensity was measured by the decomposition of uranyl oxalate[8] subsequently illuminated in the same reaction tubes.

For the effect of temperature on the rate of peroxide formation a simplified arrangement of the apparatus was used. The mercury arc was in a vertical position and placed about 8″ from the reaction vessel, which consisted in this case of a 30-ml. quartz test-tube containing 0.1 g. of zinc oxide in 25 ml. of triply distilled water as above. The tube was surrounded by a Pyrex jacket through which distilled water could be circulated at any desired temperature. Here also stirring was effected and oxygen supplied by drawing air through the suspension. In this case no filter was used but the Pyrex envelope transmitted only the visible and the 3650 Å. line in the ultraviolet. The absorption of zinc oxide has been investigated by Goodeve[9]; there is a slight tail at the end of the visible around 4000 Å.; the absorption coefficient increases sharply just below 3900 Å. and absorption is practically complete at 3800 Å., extending on back into the ultraviolet, so that zinc oxide would be "black" in practically the whole ultraviolet region.

The experiments on the uptake of oxygen were carried out by placing the suspensions in the Pyrex flasks of the Warburg apparatus. These were then shaken at constant temperature in the light of the mercury arc lamp. The system was kept at constant volume and the decrease in pressure due to the uptake of oxygen read on the attached micromanometers. Brodie solution was used as the manometric fluid, and pressure readings were converted to microliters of oxygen at S.T.P.,[10] and finally to millimoles.

All organic materials used were either C.P. or recrystallized, or in the case of liquids redistilled at constant boiling point. The acrylonitrile and the methyl methacrylate were free from stabilizers.

Analysis for Hydrogen Peroxide.—The method usually employed for analyzing the suspensions for hydrogen peroxide was the same as that used by Chari and Qureshi.[2] The reduction of the peroxide by iodide ions was carried out in approximately 1 N sulfuric acid solution and catalyzed by adding a few drops of a saturated solution of ammonium molybdate. The reaction was allowed to go to completion for 10 min. in the dark; the liberated iodine was then titrated using a microburet against a standardized solution of sodium thiosulfate, usually 5×10^{-3} N, freshly prepared from 10^{-1} N stock solution; the latter was kept on ice without decomposition for about a month at a time, the concentration being checked at intervals. Starch indicator was used to determine the end-point. Under these conditions there was no correction for a blank.

Since oxidizing agents other than hydrogen peroxide would also liberate iodine under similar conditions it was desirable to use other confirmatory tests. Titanium sulfate[11] is often used as a specific test for hydrogen peroxide, but at the low concentrations found in the absence of organic materials the yellow color developed by this reagent was too weak to use for colorimetric estimation; it was used as a check however when organic materials were present and in these cases gave identical results with the iodide determination. Catalase is an enzyme which is specific for the decomposition of hydrogen peroxide. When a trace of this was added to the irradiated suspension the peroxide was completely destroyed, no iodine being liberated on subsequent addition of iodide and acid. Further evidence that it is peroxide that is formed, and not ozone for example, is provided by the fact that it shows reducing as well as oxidizing action. When a brownish mixture of ferric chloride and potassium ferricyanide is added to the suspension after irradiation prussian blue is precipitated.

Identification of Oxidation Products of Organic Compounds.—Recent work of Weiss[12-15] on the oxidation of organic materials in very dilute aqueous solutions irradiated by ionizing radiation suggested suitable procedures for identifying possible oxidation products and estimating their concentration.

Tests for phenolic compounds were made with Folin reagent[16] using a Fisher Electrophotometer at 625 mμ. Calibration curves were made both for catechol and hydroquinone. Hydrogen peroxide does not interfere in acid solution. In alkaline solution, as used in the test for phenolic compounds from acetanilide and toluene, catalase was used to destroy the hydrogen peroxide and the zinc oxide was filtered off before adding the Folin reagent. Disappearance of salicylic acid was followed by similarly destroying peroxide and filtering off the zinc oxide, and then estimating colorimetrically at 525 mμ the purple color developed on adding dilute ferric chloride solution.

In the experiments with chlorobenzene, chloride ion was determined by turbidity measurements with silver nitrate.

Photopolymerization of Vinyl Monomers.—The zinc oxide was heated strongly for several minutes and allowed to cool under purified nitrogen. The aqueous solution of the monomer, through which the nitrogen had been bubbled for 0.5 hour, was then admitted without exposing the zinc oxide to the air again. The tube was then sealed and exposed to the light. It was shaken at 5-minute intervals. The nitrogen was Seaford grade, further purified by bubbling through pyrogallol and then passing over copper turnings at 250°. The molecular weight of the methyl methacrylate polymer was determined by intrinsic viscosity measurements in benzene solution.[17]

Results

In the Absence of Organic Matter.—Figure 1 shows the rates of formation of peroxide at different temperatures. The initial rates differ only slightly but the steady state concentrations are higher at lower temperatures. At 14°, the thermal decomposition of the peroxide is eliminated; at this tem-

(7) F. Paneth, *Ber.*, **57B**, 1221 (1924).

(8) W. G. Leighton and G. S. Forbes, *J. Am. Chem. Soc.*, **52**, 3139 (1930).

(9) C. F. Goodeve and J. A. Kitchener, *Trans. Faraday Soc.*, General discussion, 902 (1938).

(10) J. Sumner and G. F. Somers, "Laboratory Experiments in Biochemistry," Academic Press, Inc., New York, N. Y., 1949, p. 138.

(11) G. M. Eisenberg, *Ind. Eng. Chem., Anal. Ed.*, **15**, 327 (1943).

(12) J. Weiss, *Nature*, **161**, 650 (1948).

(13) J. Weiss, H. Loebl and G. Stein, *J. Chem. Soc.*, 2074 (1949).

(14) J. Weiss and G. Stein, *ibid.*, 3265 (1951).

(15) J. Weiss and G. Stein, *ibid.*, 3275 (1951).

(16) Reference 10, p. 85.

(17) H. Baxendale, S. Bywaters and M. G. Evans, *J. Polymer Sci.*, **1**, 237 (1946).

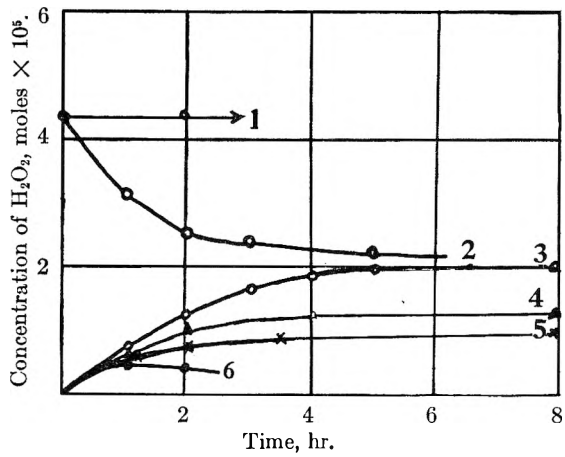

Fig. 1.—1, rate of decomposition of H_2O_2 on 0.1 g. of ZnO in 25 ml. of solution in the dark at 14°; 2, rate of decomposition of H_2O_2 at 14° (4000–3300 Å.), in absence of ZnO; 3, 4, 5 and 6, rate of formation of H_2O_2 on 0.1 g. of ZnO in 25 ml. of triply distilled water (4000–3300 Å.), at 14, 27, 33 and 45°, respectively.

perature hydrogen peroxide added initially does not decompose to a measurable extent in two hours in the dark, nor in light in absence of zinc oxide as the top curve shows. Zinc oxide in the light however catalyzes the decomposition and the same steady state concentration is approached as is found on the irradiation of a suspension without added hydrogen peroxide. The fact that under these conditions at 14° the initial rate of decomposition is about twice the initial rate of formation suggests that there are two oxidizing radicals on the surface that cause decomposition for every one that leads to its formation.

The initial quantum yield is about 0.25 at 25°. The reaction shows an "initial burst." The ratio of oxygen taken up to peroxide formed is independent of temperature from 15 to 30° and approximately 1:1. The actual experimental values vary tween 0.9:1 and 1.2:1, but not systematically with temperature.

If the zinc oxide were a true photosensitizer the over-all reaction should be

$$H_2O + {}^1/_2O_2 \longrightarrow H_2O_2$$

The fact that one molecule of oxygen disappears for each molecule of hydrogen peroxide formed indicates however that zinc oxide is being partially oxidized also, perhaps as

$$ZnO + 2H_2O + O_2 \longrightarrow H_2O_2 + Zn\begin{matrix}OH\\OOH\end{matrix}$$

The possibility that only zinc peroxide is being formed is excluded by the fact that the solid can be filtered out of the suspension after irradiation and the peroxide is found almost entirely in the solution, only a trace being associated with the solid residue.

Addition of chloride ion which might be expected to exchange electrons with free OH radicals

$$Cl^- + OH \longrightarrow Cl + OH^-$$

has no effect on the uptake of oxygen nor on the formation of peroxide. Addition of small amounts (10^{-3} M) of sodium hydroxide likewise has no measurable effect on the initial rate of formation of peroxide. 10^{-1} M, however, completely prevents the accumulation of peroxide. The pH of the initial suspension is about 7.4; after continued irradiation this drops to 6.8 or 7.0.

In the Presence of Organic Matter.—Figure 2 shows the relative rates of formation of hydrogen peroxide in suspensions containing 0.1 g. of C.P. zinc oxide in 25 ml. of 10^{-3} M solutions of various organic compounds. At the end of one hour the

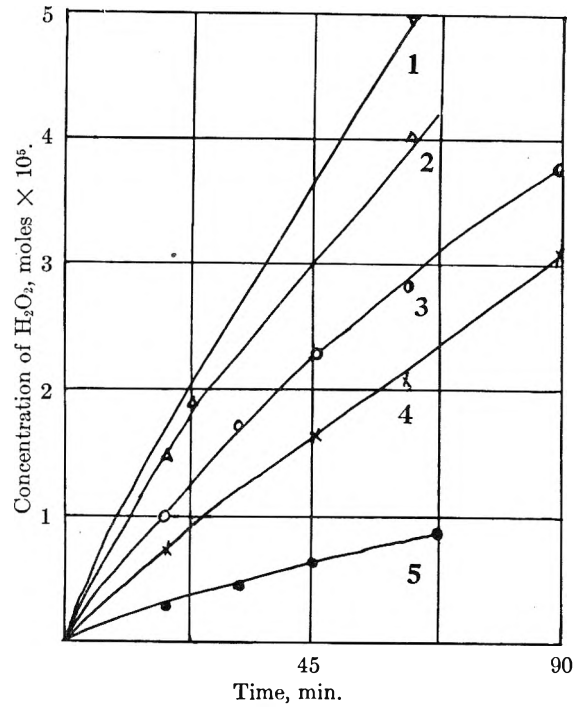

Fig. 2.—Rate of formation of H_2O_2 on 0.1 g. of ZnO in 25 ml. of solution (4000–3300 Å.) at 14° in presence of organic compounds: 1, resorcinol, phloroglucinol; 2, phenol, catechol, toluene; 3, benzene, chlorobenzene; 4, acetanilide, aniline, quinone, hydroquinone; 5, triply distilled water. All solutions of organic compounds are 10^{-3} M except benzene, chlorobenzene and toluene which are saturated.

total amounts of peroxide formed range from 5.0 × 10^{-2} mmole in the case of phloroglucinol and resorcinol to 0.62 × 10^{-2} mmole in triply distilled water. The temperature was kept at 14° where the thermal decomposition of hydrogen peroxide is negligible. Two tests were used for peroxide, since organic peroxides might react with the iodide ion, but not with titanium sulfate reagent. The results of the two analyses were identical in all cases except chlorobenzene where there was a small discrepancy probably due to the formation of some HOCl. The high efficiency of toluene is to be noted. Anderson and Taylor[18] and Richter[19] have studied the effect of organic compounds in inhibiting the photochemical decomposition of hydrogen peroxide; the results in these experiments agree fairly well with the order observed by Richter in particular. The organic compounds are generally supposed to interfere with the chain decomposition of hydrogen peroxide by reacting with free hydroxyl radicals and oxygen atoms produced in the photoly-

(18) W. T. Anderson and H. S. Taylor, THIS JOURNAL, **52**, 479 (1948).

(19) D. Richter, *J. Chem. Soc.*, 1219 (1934).

sis. The order observed in Fig. 2 does not correspond in some cases with that of Chari and Qureshi.[3]

Preliminary experiments showed that a significant difference between the kinetics in the presence of phenol and acetanilide was a marked inhibition of peroxide formation in the presence of excess phenol. Figure 3 shows the variation in the initial rates with phenol concentration. The rate with acetanilide concentration reaches a maximum and does not show inhibition before saturation is reached, about 0.05 *M*. Another significant difference is the quantity of oxygen absorbed. The results are summarized in Table I. Since Fig. 3 shows that 10^{-3} *M* phenol is near the maximum it was a convenient concentration to use in these comparisons.

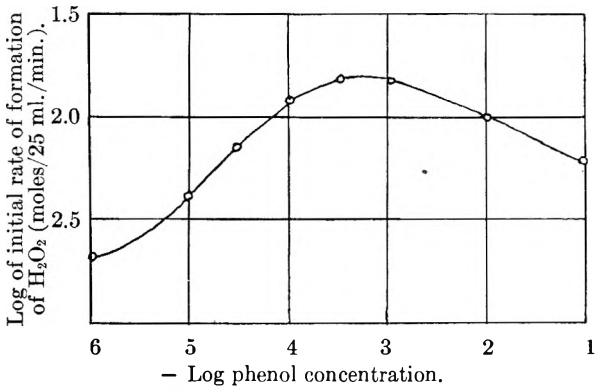

Fig. 3.—Variation in initial rate of formation of H_2O_2 with phenol concentration at 14°; 0.1 g. of ZnO in 25 ml. of solution (4000–3300 Å.).

TABLE I

	Acetanilide, 10^{-3} *M*	Phenol, 10^{-3} *M*
Quantum yield	0.4	0.5
Ratio of oxygen taken up to peroxide formed	2:1	1:1
Activation energies, kcal./mole	4.6	3.7

With 10^{-3} *M* solutions of acetanilide or phenol the rate of peroxide formation gradually falls off and under the experimental conditions reaches a limiting value after several hours. This limiting value is directly proportional to the initial concentration of the organic compound; continued irradiation beyond this point produces a slow decomposition of the peroxide.

Addition of chloride ions had no effect on the peroxide formation nor on the oxygen uptake in the case of phenol. When chloride ions, in the form of zinc chloride, were added to suspensions containing acetanilide a marked depression of both the oxygen uptake and the peroxide formation was observed. A powerful reducing agent was formed on the surface of the zinc oxide which reduced dilute sulfuric acid (about 3 *N*) to hydrogen sulfide.

Since the variation of the limiting concentration of peroxide with the initial concentration of organic material suggests the destructive oxidation of the original substance, it was desirable to try to follow the rate of formation of oxidation products. In agreement with Weiss's results it was found that irradiated suspensions containing phenol gave a positive test for catechol and/or hydroquinone with Folin reagent[14] in acid solution. That the larger part of the initial product was catechol was indicated by the fact that the green color with Folin reagent was intensified on warming. The results are shown in Fig. 4 both in the presence and absence of added hydrogen peroxide. Both curves for the formation of the dihydroxy compounds would start out more steeply if an appreciable amount could be shown to be hydroquinone, since the green color which it develops with Folin reagent is not so deep as that of catechol. Phenol in such dilute solution is not oxidized to an appreciable extent by hydrogen peroxide at 14° either on zinc oxide in the dark, or in the absence of zinc oxide in the light. The autoxidation of catechol is also negligible under similar conditions. Weiss also described as an ultimate product of the irradiation of phenol solutions in his experiments[14] a substance which condensed with 2,4-dinitrophenylhydrazine to give a product melting around 300° which "appeared to be a derivative of an aliphatic dialdehyde." The oxidation of phenol in these experiments leads also to something which condenses with 2,4-dinitrophenylhydrazine to give a product that melts around 112° with decomposition. Oxidized pyrogallol solutions, whether oxidized by air or by Fenton's reagent, give a similar derivative but of a darker color and indefinite melting point. This points to destruction of the aromatic ring. However, these solutions do not give any other tests for aldehydes such as Fehling or Schiff tests. It seems more likely that they are cyclic ketones. More concentrated solutions of phenol, and also of catechol, acetanilide and salicylic acid, show considerable yellowing on prolonged exposures with probable formation of humic acid types of compounds. After several hours no further test for any type of phenolic compound (including phenol itself) can be obtained by Folin reagent either in acid or basic solution.

The most significant feature of Fig. 4 is that the formation of the dihydroxy compound begins abruptly and rises concomitantly with the peroxide formation in the initial stages of the reaction. If the phenol were merely being oxidized by the hydrogen peroxide formed, an induction period in the catechol formation would be expected. The fact that when hydrogen peroxide is added initially it begins to decompose at first, and this period is characterized by the formation of less catechol than in the absence of initial hydrogen peroxide, indicates further that the function of the organic material is to remove from the surface active oxidizing radicals which would otherwise cause reverse reactions. The stoichiometry is less clear-cut in the presence of the organic compounds, because of the difficulty of identifying more definitely the initial oxidation products. The zinc oxide does not appear to be oxidized here, however, since the irradiated solution can be decanted and the same zinc oxide used over again with undiminished initial rate of peroxide formation. Inhibition by excess phenol suggests displacement of water from the surface.

Irradiated suspensions containing acetanilide give positive tests for phenolic compounds in the

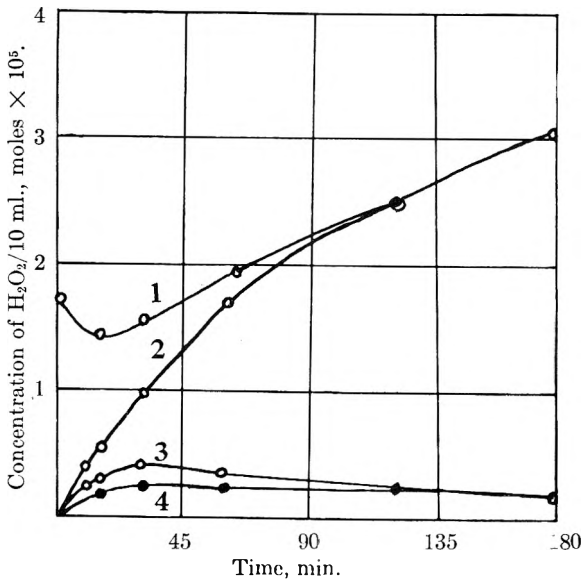

Fig. 4.—1, Rate of disappearance of H_2O_2 added initially to 0.1 g. of ZnO in 25 ml. of solution (10^{-3} *M* phenol); 2, rate of formation of H_2O_2 on 0.1 g. of ZnO in 25 ml. of 10^{-2} *M* phenol; 3, rate of formation of catechol in 2; 4, rate of formation of catechol in 1. All experiments at 14° (4000–3300 Å.).

initial stages. The course of their appearance and disappearance follows the same pattern as that of the catechol in the experiments just described on phenol.

With benzene the products are more diverse; phenols, polyphenols and diphenyl are found in only trace amounts. The main product is probably an organic peroxide. Chlorobenzene gives similar products, along with somewhat larger amounts of chloride ion. This must come from dechlorination of the ring, perhaps *via* HOCl, and it is also in agreement with observations of Weiss on chlorobenzene.[9] The products in these two cases cannot be followed very far because benzene and chlorobenzene evaporate under the experimental conditions (entraining air).

It has also been possible to follow the rate of disappearance of salicylic acid, since it is non-volatile and can conveniently be detected by means of its strongly colored chelate compound with Fe^{+-+}. The results are shown in Fig. 5. Complete disappearance of dextrose in a similar length of time can also be demonstrated by Benedict or Fehling tests.

Photopolymerization of Vinyl Monomers

In Absence of Oxygen.—Dainton[20] demonstrated that hydroxyl radicals from the photolysis of hydrogen peroxide would cause the polymerization of monomers such as acrylonitrile and methyl methacrylate which are known to polymerize by a free radical rather than ionic mechanism; these polymerizations are also induced by the free radicals formed on irradiation of water by ionizing radiation. It has proved possible in this Laboratory to initiate the polymerization of both acrylonitrile and methyl methacrylate by irradiating air-free suspensions of zinc oxide in dilute aqueous solutions of the monomers; these dilute solutions are otherwise stable over indefinitely long periods at 20° in ultraviolet light at 3650 Å. Acrylonitrile failed to polymerize on zinc oxide under these conditions in benzene or absolute alcohol, although the polymer would have been insoluble in both of these solvents. The polymers were easily separated from the zinc oxide by dissolving the latter in dilute sulfuric acid. Acrylonitrile polymer does not lend itself to mol. wt. determinations by any convenient method because it is insoluble in all common organic solvents. In case of methyl methacrylate, however, the mol. wt. as determined by intrinsic viscosity measurement in benzene was 500,000. The maximum amount was formed in a few hours and corresponded to what would be sufficient to cover about 1/10 of the surface; however the large polymer molecules probably cut off the light and prevent further action. Since there is also a short induction period, probably due to failure to eliminate all oxygen, the initial rate of polymerization cannot be taken as a reliable measure of the initial rate of formation of radicals.

(20) F. S. Dainton, THIS JOURNAL, **52**, 490 (1948).

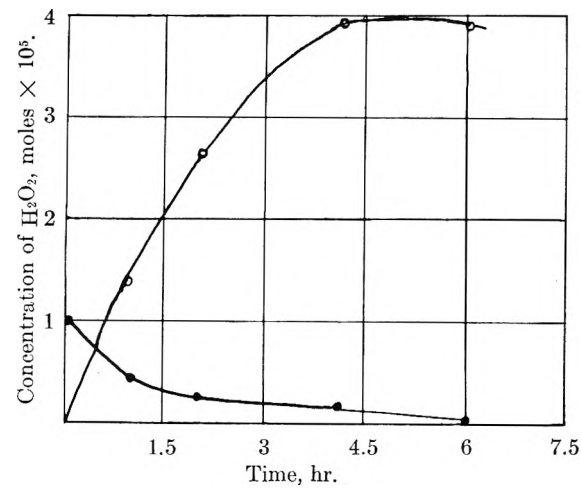

Fig. 5.—Comparison of rates of formation of H_2O_2 (upper curve) with rate of disappearance of salicylic acid (lower curve); 0.1 g. of ZnO in 25 ml. of 10^{-3} *M* salicylic acid, 14° (4000–3300 Å.). Amounts indicated are for 10 ml. of suspension analyzed.

Discussion

The Problem of the Energy Transfer.—Since neither water nor oxygen absorbs light at 3650 Å., the first question to be discussed is the mechanism of the transfer of the energy absorbed by the zinc oxide to the water or oxygen resulting in the formation of the active intermediate species. Water must either participate in the direct transfer, or provide part of the energy by solvation of intermediate radicals or ions. The first alternative seems preferable in view of the photopolymerization in absence of oxygen.

It has been suggested[5] that the energy may be transferred to adsorbed water leading to dissociation into hydrogen atoms and hydroxyl radicals on the surface of the zinc oxide. The 80 kcal. available in a quantum of light at 3650 Å. would not be sufficient since $H_2O \rightarrow H + OH$ requires 118 kcal., unless the difference in heats of adsorption of radicals and water molecules were about 35–40

kcal. This mechanism may be possible, since an activated adsorption of water on zinc oxide with an estimated heat of adsorption of 30–32 kcal. has been reported in the literature[21]; the rest could possibly be made up by the heats of solvation of the radicals. However, our qualitative finding that comparable amounts of peroxide are formed on bubbling air through irradiated suspensions of zinc sulfide and antimony trioxide,[22] makes the idea that the specific heat of adsorption of water on zinc oxide is the determining factor, seem less likely.

Careful work of several recent investigations[23–27] has done much to clarify the effect of the absorption of light by zinc oxide, which is well known as a semi-conductor whose conductivity is increased by absorption in the ultraviolet. As a result the following interpretation of its electrical and optical properties emerges. The thermal excitation of an electron from the oxide band to the conduction (Zn^+) band requires at least 2.0 e.v.; therefore it does not occur at low temperatures. In accordance with the Franck–Condon principle the energy required for optical excitation is greater than the thermal band width. Goodeve has shown[9] that a strong absorption begins at about 3850 Å. (3.1 e.v.) and this is also believed to give rise to intrinsic conduction. If excess interstitial zinc is missing the energy absorbed in the absence of an electric field is scattered with a slight shift in frequency. If the zinc oxide has been heated at 1000° for one hour in a reducing atmosphere of carbon monoxide[28] a large number of excess zinc atoms are left in the lattice. Excitation by cathode rays or ultraviolet light now produces a bright luminescence in the visible (green). We have found that a ZnO[Zn] phosphor so prepared produces one-fourth to one-fifth as much peroxide while luminescing, although surface area measurements by dye adsorption indicate that the surface has been reduced to only one-half. There are difficulties in trying to correlate conductivity data with surface reactions in a quantitative manner, since there is evidence that electrons may be trapped in surface states, hindering free passage across grain boundaries, and thus leading to spurious conductivity measurements. Surface area is extremely important.

In some oxides the absorption of energy may result in the photolysis of the crystal. This has been shown conclusively to occur in titanium dioxide[29]

$$TiO_2 \longrightarrow {}^1/_2Ti_2O_3 + {}^1/_2O_2$$

Weyl and Forland[30] have described the conditions under which this may be expected to occur; one of the most important is that the next lower valence state of the metallic element must be relatively stable. Under the conditions described in this paper no peroxide can be found in irradiated suspensions of titanium dioxide either in presence or absence of phenolic compounds.

Since Zn^+ would not be expected to be stable in water, an alternative mechanism leading to the production of radicals is suggested. In many reactions it has been demonstrated that water is capable of accepting an electron in a transfer of this type.[31–35] The resulting dissociation

$$H_2O^- \longrightarrow H + OH^- \qquad (1)$$

leads to the formation of free H atoms. If oxygen is present

$$H + O_2 \longrightarrow HO_2 \qquad (2)$$

may follow. It is then possible that OH^- will remain adsorbed on the now positively charged $(ZnO)^+$

$$(ZnO)^+ \cdot OH^- \longrightarrow ZnO \cdot OH \qquad (3)$$

The photogalvanic effect reported by Veselovski[36] has been interpreted in a similar manner.

Wagner[37] interprets the catalytic decomposition of nitrous oxide on zinc oxide as an electron transfer from catalyst to substrate.

It must also be considered possible that an electron could be transferred to oxygen adsorbed on the surface leading to the formation of O_2^-; however this ion probably would not be very stable in aqueous solution. Evans and Uri[38] have made approximate calculations of the combined electron affinity and solvation energy of some possible intermediates in reactions involving similar oxidizing species, and it appears from their calculations that equation (1) would be favored in liquid water. If the peroxide formed in our experiments resulted from $O + OH^- \rightarrow HO_2^-$, it would be hard to understand why it does not do so in irradiated suspensions of titanium dioxide buffered to *p*H 7 where oxygen atoms are known to be formed. This certainly could not be the mechanism in the case of zinc sulfide.

Mechanisms Proposed for Peroxide Formation.—On the assumption that the above evidence favors the interpretation that an electron is transferred to adsorbed water leading to dissociation and formation of free radicals, reaction mechanisms consistent with our experimental results can be formulated.

In the absence of organic matter the over-all process can be represented as

$$H_2O + O_2 + ZnO \longrightarrow H_2O_2 + ZnO{\cdot}O$$

The first two steps would probably be as given in (1) and (2) above, followed by $2HO_2 \rightarrow H_2O_2 + O_2$, which is possible in presence of a third body and so could easily occur in liquid water.

This leaves OH radicals not free, but bound to the surface. Since one O_2 yields one H_2O_2, OH + OH

(21) H. S. Taylor and D. V. Sickman, *J. Am. Chem. Soc.*, **62**, 3357 (1940).

(22) Further investigation is currently being conducted by M. C. Markham at Saint Joseph College, West Hartford, Conn.

(23) P. H. Miller, *Phys. Rev.*, **60**, 890 (1941).

(24) E. E. Hahn, "Report on Some Electrical Properties of Zinc Oxide," University of Pennsylvania, Philadelphia, Penn.,

(25) D. A. Wright, *Proc. Phys. Soc.*, **60**, 13 (1948).

(26) E. Schwarz, *ibid.*, **A62**, 530 (1949).

(27) J. M. Bevan and J. S. Anderson, *Faraday Soc. Discussions*, **8**, 238 (1950).

(28) H. W. Leverenz, "Luminescence of Solids," John Wiley and Sons, Inc., New York, N. Y., 1950, p. 67.

(29) A. E. Jacobsen, *Ind. Eng. Chem.*, **41**, 523 (1949).

(30) W. A. Weyl and T. Forland, *ibid.*, **42**, 257 (1950).

(31) M. Burton, *Ann. Rev. Phys. Chem.*, I, 113 (1950).

(32) J. L. Magee and M. Burton, *J. Am. Chem. Soc.*, **73**, 523 (1951).

(33) A. Farkas and L. Farkas, *Trans. Faraday Soc.*, **34**, 113 (1938).

(34) F. S. Dainton, THIS JOURNAL, **52**, 490 (1948).

(35) J. Weiss, *Nature*, **161**, 650 (1948).

(36) V. I. Veselovski, *Zhur. Fiz. Khim.*, **22**, 1427 (1948); *C. A.*, **52**, 2522d (1948).

(37) C. Wagner, *J. Chem. Phys.*, **18**, 69 (1950).

(38) M. G. Evans and N. Uri, *Trans. Faraday Soc.*, **45**, 224 (1949).

$\rightarrow H_2O_2$ probably contributes little to the peroxide formation. However the oxidation of the surface would bring the reaction to a stop, and the radicals on the surface may cause reverse reaction

$$OH + HO_2 \longrightarrow H_2O + O_2$$
$$OH + H \longrightarrow H_2O$$
$$OH + H_2O_2 \longrightarrow H_2O + HO_2$$

and perhaps

$$OH + OH \longrightarrow H_2O + {}^1/_2O_2$$

The maximum quantum yield in such a scheme would be 0.5; 0.2–0.3 is the observed yield. The initial rate of decomposition of added hydrogen peroxide is about twice the rate of formation (Fig. 1) suggesting again that there are two OH radicals causing the decomposition while two HO_2 radicals produce one H_2O_2.

Organic matter must not only stabilize the peroxide once it is formed, but also aid in the rate of formation by providing H atoms to the initial radicals formed on the surface. (Figure 2: the graphs start more steeply if organic matter is present.)

If the initial rate of formation of catechol (or hydroquinone) from phenol were equal to the rate of formation of peroxide, the over-all equation should be

$$RHOH + H_2O + O_2 \longrightarrow H_2O_2 + R(OH)_2;\ (R = C_6H_4)$$

The stoichiometric ratio of O_2:H_2O_2 is 1:1. But if the initial rate of formation of catechol is really half the rate of peroxide formation, as it appears from Fig. 4, and also from Fig. 3 where the rate is roughly proportional to the square root of the phenol concentration, the over-all reaction must be

$$RHOH + 2H_2O + 2O_2 \longrightarrow 2H_2O_2 + R(OH)(OOH)$$

This can only be true if R(OH)(OOH) does not react as peroxide with iodide at ordinary temperatures, and yet behaves like catechol on heating with Folin reagent. We note that the initial rate of disappearance of salicylic acid in Fig. 5 is also only half the rate of peroxide formation. The maximum concentration of catechol in Fig. 4 corresponds to the amount necessary to cover the surface, which suggests that it stays on the surface until the oxidation is far advanced. The maximum concentration of peroxide is 4–5 times the initial concentration of phenol, which indicates that each organic molecule is oxidized to a considerable degree. A sequence of reactions leading to the preceding equation might be as

$$OH + RHOH \longrightarrow H_2O + RHO\cdot \text{ (on the surface)}$$
$$RHO\cdot + OH \longrightarrow RHOOH$$
$$RHOOH + HO_2 \longrightarrow ROOH + H_2O_2$$
$$ROOH + OH \longrightarrow R\begin{matrix}OH\\OOH\end{matrix}$$

Meanwhile $2HO_2 \rightarrow H_2O_2 + O_2$, and two O_2 yield $2H_2O_2$; giving the observed 1:1 ratio. The maximum quantum yield for peroxide formation would be 0.67; the observed yield of 0.5 indicates that nearly every quantum must be effective.

In the case of acetanilide an extra molecule of O_2 is absorbed for each molecule of peroxide formed. Perhaps peracetic acid is split off, or the nitrogen may be oxidized as well as the ring. Alternatively, since the acetanilide is not adsorbed on the surface initially (excess acetanilide does not inhibit), chain reactions may occur among the organic radicals leading to the consumption of more oxygen.

$$OH + RH \longrightarrow H_2O + R\cdot$$
$$R\cdot + O_2 \longrightarrow RO_2\cdot$$
$$RO_2\cdot + RH \longrightarrow R\cdot + ROOH$$
$$R\cdot + O_2 \longrightarrow RO_2\cdot, \text{ etc.}$$

Further work is necessary to establish the proposed mechanisms with certainty, but electron transfer leading to the formation of radicals appears to be most consistent with the facts so far available.

Acknowledgments.—The authors wish to express their gratitude to Dr. Richard L. Petritz for helpful discussions and interest in the work. They also wish to thank Dr. Patricia Marshall for carrying out the molecular weight determination on the polymer, Dr. P. H. Miller of the University of Pennsylvania for supplying the spectroscopically pure zinc oxide, and Rohm and Haas Company for supplying the methyl methacrylate monomer.

ELECTROLYTIC INTERACTION OF NYLON WITH SODIUM HYDROXIDE SOLUTIONS AT DIFFERENT TEMPERATURES

BY FREDERICK T. WALL AND PATRICIA M. SAXTON

Noyes Chemical Laboratory, University of Illinois, Urbana, Illinois

Received October 13, 1952

The absorption of sodium hydroxide by nylon fibers has been measured at three different temperatures and equilibrium constants have been established for the absorption, which occurs in two stages. Using the van't Hoff equation the heats of reaction have been determined from the temperature coefficients of the equilibrium constants. A useful theoretical equation has been developed relating the values of the two equilibrium constants to the hydroxide ion concentrations at characteristic midpoints of the titration curves. Since the amount of base absorbed in the first stage can be measured much more accurately then that in the second stage of the absorption, this equation was employed to calculate values of the second equilibrium constant and to provide an estimate of the corresponding heat of reaction. An equation was also developed to connect the heat of absorption with the change in hydroxyl ion concentration necessary to keep constant the amount of absorbed base at different temperatures. Data to be used in this equation could be directly obtained from the most reliable portions of the titration curves. The values for the heats of reaction are in good agreement with those obtained from use of the equilibrium constants.

Introduction

It is generally recognized that fibrous polymeric electrolytes such as wool or nylon, which contain both carboxyl and amine groups, can absorb and react with appreciable quantities of acids and bases. If such a fiber is suspended in an aqueous environment and an acid or base is added to the solution, the cations or anions of the added electrolyte may become attached by salt linkages to definite sites on the fiber, or they may be taken up by the fiber according to the laws of a Donnan Membrane Equilibrium.[1] Although both of these points of view are useful, we shall here consider only the site hypothesis since it appears to provide the better quantitative description.

The earliest theory on this subject was developed for protein fibers by Steinhardt and Harris,[2] who based their work simply on the law of mass action. This theory was followed shortly thereafter by the more extensive work of Gilbert and Rideal,[3] who recognized the important role of the fiber potential in requiring that substantially equivalent amounts of cations and anions be absorbed by the fiber. Wool was used for these earlier absorption studies, but because of its complexity it has many disadvantages both from experimental and theoretical points of view. A much simpler problem is presented by a synthetic polyamide fiber like nylon, for which only the carboxyl and amine end groups are of prime significance.

The absorption of acids on nylon fibers was first studied by Remington and Gladding,[4] who applied a modified form of the equations of Gilbert and Rideal to their special case and found that the theoretical equations gave good agreement with their experimental data. Recently Wall and Swoboda,[5] using thermodynamic methods, have extended the theory of Gilbert and Rideal to the absorption of either acids or bases on nylons having either equal or unequal numbers of carboxyl and amine end groups. By experimentally studying the absorption of sodium hydroxide on nylon containing an excess of carboxyl groups, Wall and Swoboda were able to confirm their theory for that special case.

From an analysis of absorption data at different temperatures, the temperature coefficients, and hence the heats of reaction, can be obtained. Recently, Gilbert[6] treated the heat of interaction of acids with wool fibers, taking into account the unknown temperature coefficient of the fiber potential. His equations relate the heat of interaction of the acid with the fiber to the change in *p*H that is required to maintain at a constant value the amount of acid absorbed at different temperatures.

In the study here reported, the absorption of sodium hydroxide by nylon fiber containing an excess of carboxyl groups was measured at several temperatures. Appropriate thermodynamic equations are derived and used to interpret the data and to determine the heats of absorption of base by the fiber.

Theory

The synthetic polyamide fiber used in this work was polyhexamethylene adipamide, better known as nylon 66. This nylon fiber has a large excess of carboxyl groups so that in a neutral environment the end groups of the fiber consist of an equal number of charged carboxyl and alkyl ammonium ions, in addition to free carboxyl groups equal in number to the difference between the original numbers of carboxyl and amine groups. Since the carboxyl groups are more acidic than the alkyl ammonium ions, the first interaction between the fiber and added base will be equivalent to a titration of the carboxyl groups accompanied by the addition of an equivalent number of cations to charged carboxyl ions to keep the fiber electrically neutral. When the carboxyl groups are virtually gone, the addition of still more base will lead to reaction with the alkyl ammonium ions, an equivalent number of cations again being simultaneously adsorbed by carboxyl ions.

Graphical Determination of the Equilibrium Constants.—The theoretical development of Wall and Swoboda,[5] leading to equations from which the equilibrium constants of the two reactions mentioned above can be determined, will be summarized here for the special case of the addition of a mono-

(1) R. H. Peters and J. B. Speakman, *J. Soc. Dyers and Colourists*, **65**, 63 (1949).

(2) J. Steinhardt and M. Harris, *Bur. Standards J. Research*, **24**, 335 (1940).

(3) G. A. Gilbert and E. K. Rideal, *Proc. Roy. Soc. (London)*, **182A**, 335 (1944).

(4) W. R. Remington and E. K. Gladding, *J. Am. Chem. Soc.*, **72**, 2553 (1950).

(5) F. T. Wall and T. J. Swoboda, THIS JOURNAL, **56**, 50 (1952).

(6) G. A. Gilbert, *Proc. Roy. Soc. (London)*, **183A**, 167 (1944).

valent base, sodium hydroxide, to a nylon fiber with an excess of carboxyl end groups. The reactions which might occur between the end groups of the fiber and the ions in solution are given as

$$COOH \rightleftharpoons COO^- + H^+ \quad (1)$$

$$COONa \rightleftharpoons COO^- + Na^+ \quad (2)$$

$$NH_3^+ \rightleftharpoons NH_2 + H^+ \quad (3)$$

$$H_2O \rightleftharpoons H^+ + OH^- \quad (4)$$

The only charged ions in the fiber will be carboxyl ions and alkyl ammonium ions, so to preserve electrical neutrality of the fiber we can assert that $(COO^-) = (NH_3^+)$. Since sodium hydroxide is a strong base we can also say that at all concentrations of base, $(Na^+) = (OH^-)$. Let us define the original number of carboxyl end groups as A_0 and of amine groups as B_0, so that at all stages of the interaction of base with fiber we can write

$$A_0 = [COOH] + [COO^-] + [COONa] \quad (5)$$

$$B_0 = [NH_3^+] + [NH_2] \quad (6)$$

where A_0, B_0 and all end group symbols enclosed by parentheses represent the concentrations of these groups expressed in moles per gram of fiber.

When an aqueous solution of base is added to the fiber, the first reaction will be the titration of the free carboxyl groups. This can be represented as

$$COOH + Na^+ + OH^- \rightleftharpoons COONa + H_2O \quad (7)$$

From appropriate thermodynamic considerations, it can be shown that

$$\frac{[COONa]}{\{(A_0 - B_0) - [COONa]\}[OH^-]^2} = K_1 \quad (8)$$

where K_1 is equivalent to the equilibrium constant for the absorption of base on a fiber containing free carboxyl groups.

To test the validity of equation (8) and to determine K_1, we find it convenient to define a quantity σ as

$$\sigma = \frac{[COONa]}{[OH^-]^2} = -K_1[COONa] + (A_0 - B_0)K_1 \quad (9)$$

By plotting σ against [COONa], we should obtain a straight line with one of the intercepts equal to $(A_0 - B_0)$ and the slope equal to $-K_1$.

This initial type of absorption, involving free carboxyl groups, will continue until there are virtually no carboxyl groups left, or until [COONa] $= A_0 - B_0$. This point can be considered as a characteristic "midpoint" of the titration curve. Further addition of base will result in reaction with the alkyl ammonium ions, accompanied by addition of an equivalent number of cations to charged carboxyl ions. This second stage of the absorption can be written as

$$NH_3^+ + COO^- + Na^+ + OH^- \rightleftharpoons COONa + NH_2 + H_2O \quad (10)$$

The equilibrium constant for reaction (10) can be shown to be given by

$$\frac{\{[COONa] - (A_0 - B_0)\}[COONa]}{\{A_0 - [COONa]\}^2[OH^-]^2} = K_2 \quad (11)$$

where K_2 is equivalent to the equilibrium constant for the absorption of base on nylon fibers containing an equal number of carboxyl and amine end groups.

From equation (11) we can obtain relations for graphical testing of this development and for finding a value for K_2. To do so, we define a quantity τ such that

$$\tau = \sqrt{\frac{\{[COONa] - (A_0 - B_0)\}[COONa]}{[OH^-]^2}} = -\sqrt{K_2}[COONa] + A_0\sqrt{K_2} \quad (12)$$

By plotting τ against [COONa] we should obtain a straight line with intercept $A_0\sqrt{K_2}$ and slope $-\sqrt{K_2}$. From graphical analyses of equations (9) and (12) we obtain the end group constants, A_0 and B_0, as well as the equilibrium constants for the two stages of absorption, K_1 and K_2.

Alternative Calculation of K_2.—It sometimes happens that the experimental measurements involved in the second part of the titration, namely, that part necessary for determining K_2, are difficult to carry out accurately, especially at elevated temperatures. Assuming that at least one accurate determination can be made at some convenient temperature to establish values for A_0 and B_0, it then becomes possible to determine K_2 at other temperatures by an alternative method. This method requires, in addition to a knowledge of A_0 and B_0, values for K_1 and for $[H^+]_m$, the hydrogen ion concentration at the "midpoint" of the titration, namely, when [COONa] $= A_0 - B_0$. Although the derivation is a little long, it can be shown by direct means that

$$[H^+]^2_m = \frac{B_0K_w^2\sqrt{K_1K_2}}{(A_0 - B_0)(1 + \sqrt{K_2/K_1})} \quad (13)$$

Using this equation, we can calculate K_2, the equilibrium constant for the second stage of the absorption, from a knowledge of K_1, A_0, B_0 and $[H^+]_m$.

Determination of Heats of Absorption Reactions.—The heats of reaction (ΔH_1 and ΔH_2) associated with the interaction of nylon fiber with a monovalent base in each of the two stages of absorption, can be determined from absorption measurements at different temperatures. If the values of K_1 and K_2 at different temperatures are known, the heats of reaction can be directly determined by means of the van't Hoff equation. Moreover, assuming the heats to be constant, it is seen that $\log K_1$ and $\log K_2$ should be linear functions of $1/T$ with slopes equal to $-\Delta H_1/(2.3R)$ and $-\Delta H_2/(2.3R)$.

If the absorption data do not cover a wide enough range to permit the accurate determination of K_1 and K_2, the heats of absorption can still be determined from the changes in (OH^-) necessary to maintain at constant values the total amount of base absorbed at different temperatures. Rewriting equation (8) in logarithmic form and differentiating partially with respect to T (holding the amount of absorbed sodium constant), we obtain upon rearrangement

$$2\left(\frac{\partial pOH}{\partial T}\right)_{[COONa]} = \frac{d\log K_1}{dT} = \frac{\Delta H_1}{2.3RT^2} \quad (14)$$

Working similarly with equation (11), we obtain another equation identical in form with (14) except that ΔH_2 replaces ΔH_1. Assuming the ΔH's

to be constant, we observe that plots of pOH against $1/T$, for constant amounts of absorbed base, should give straight lines with slopes equal to $-\Delta H_1/4.6R$ and $-\Delta H_2/4.6R$, depending upon whether the amount of base absorbed is in the first or in the second stage of the absorption reaction.

Furthermore, the arithmetic mean of ΔH_1 and ΔH_2 can be obtained independently by the use of equation (13) developed for the calculation of K_2 from K_1 and midpoint data. It will be shown from the experimental data that $\sqrt{K_2/K_1}$ is of a lower order of magnitude than unity, and therefore as an excellent approximation to equation (13) we can write

$$\frac{1}{[OH^-]^2_m} = \frac{B_0\sqrt{K_1K_2}}{(A_0 - B_0)} \qquad (15)$$

Taking logarithms of both sides and differentiating we obtain

$$\frac{d[pOH]_m}{dT} = \frac{1}{4}\left(\frac{d \log K_1}{dT} + \frac{d \log K_2}{dT}\right) = \frac{1}{4.6RT^2}\left(\frac{\Delta H_1 + \Delta H_2}{2}\right) \qquad (16)$$

Thus from values of $[OH^-]_m$ at different temperatures we can obtain the mean of ΔH_1 and ΔH_2, or either quantity separately if the other is known.

Experimental

The absorption of sodium hydroxide by nylon fibers was measured at three different temperatures at a number of different concentrations of base. The nylon used for these measurements was furnished by E. I. du Pont de Nemours and Company. The fiber was an undrawn, 127 denier, 13 filament thread. An estimate of the end group constants, presumably determined by the method of Waltz and Taylor,[7] was given as $A_0 = 75 \times 10^{-6}$ and $B_0 = 43 \times 10^{-6}$ moles per gram of fiber.

As a result of extensive trials at 25°, it was found best to prepare the nylon for the experiments by cutting it into pieces about two to three inches long, and then washing thoroughly with redistilled water without subsequent drying. Unwashed nylon gave erratic and consistently low results when small amounts of absorption were measured, probably because of the interference of a film of material found to be on the nylon. On the other hand, washed and dried nylon gave erratic and consistently high results when larger amounts of absorption were measured, possibly due to breaking up of the nylon fibers during the drying process.

Two general procedures, one dynamic and one static, were used for determining the amount of absorption at different concentrations of base. The static method consisted of measuring the change in concentration of a sodium hydroxide solution that had been allowed to come to equilibrium with a known weight of nylon. The dynamic method, on the other hand, consisted of measuring, by means of radiotracer techniques, the amount of base absorbed from a large quantity of solution of known concentration which was slowly passed through a known weight of nylon until equilibrium was established. In this case, the solution in contact with the fiber after attainment of equilibrium would be at the original concentration. The principle of the dynamic method of absorption measurements was originated by Swoboda,[8] but had not actually been carried out prior to this work.

Static Method.—All of the absorption measurements at higher temperatures and most of those at 25° were made by the static method according to the following procedure. Two to three grams of unwashed nylon in equilibrium with the atmosphere was weighed into 100-ml. weighing bottles. Samples of nylon were also dried at 90° for 12 hours to determine the weight of water absorbed by nylon in equilibrium with the atmosphere. The nylon in the bottles was then washed several times with redistilled water and finally weighed again to determine the weight of water retained. An atmosphere of nitrogen was introduced into the bottles, and 75 ml. of sodium hydroxide solutions of known concentrations were pipetted over the nylon. The bottles were tightly capped and placed in constant temperature baths, which maintained the temperature within a range of 0.1°.

The weighing bottles were shaken every 12 to 24 hours and after seven days were removed from the constant temperature baths. The concentrated solutions were titrated with potassium biphthalate, but radiotracer techniques were used for analyzing the more dilute solutions.

The radiotracer used was Na^{22}, which was obtained from Washington University in St. Louis as a carrier-free salt solution. A few drops of this radioactive material were added to the dilute sodium hydroxide solutions as they were made up. From these original solutions and from the final solutions in the reactors, 25-ml. samples were pipetted into an annular glass cell and counted by Geiger-Mueller tubes. The initial and final counts of the solutions were between 1,000 and 3,000 counts per minute. Background corrections of 40 to 60 counts per minute were applied to each sample, but coincidence corrections were found unnecessary. The statistical error was less than 1% in each case since a total of 10,000 counts or more were taken for each sample.

Dynamic Method.—The dynamic method was used to obtain several points on the titration curve for the lower stage of absorption at 25°. Because the data it yields are more reliable than those from the static method, the procedure used will be explained in detail.

The cell used for the dynamic method was constructed of two concentric glass tubes held rigidly in place between brass end plates, thus enclosing an annular space of known volume. Solution entered this space through two inlet tubes at the bottom of the cell, flowed upwards through the firmly packed nylon fiber, and left through two outlet tubes sealed into the end plates. The cell could be placed over a Geiger-Mueller tube in the same manner as an annular glass sample cell and a radioactive count of its contents readily obtained. Before starting a measurement of the absorption of sodium hydroxide by the nylon, the cell was filled with redistilled water and the nylon degassed by attaching the cell to a vacuum pump. This procedure removed small air bubbles surrounding the nylon fibers and thus markedly increased the rate of attainment of equilibrium within the cell.

Approximately 200 ml. of a radioactive sodium hydroxide solution was then allowed to siphon through the cell which was immersed in a constant temperature bath. As the radioactive solution slowly passed through the nylon, a certain amount of base was absorbed, thus giving to the cell contents a larger radioactive count than that of the solution alone. After 200 ml. of the solution had passed through the cell, the flow of the solution was stopped for several hours while the nylon came to equilibrium with this solution. The cell was then disconnected from the flow system and counted, replaced and another portion of the same solution was run through the cell. The radioactive count of the cell slowly increased until it reached a constant value, at which point the nylon was presumed to be in equilibrium with this particular solution. From this final count, the normality of the solution, the count of a sample of the solution and certain constants of the apparatus, the amount of base absorbed at that concentration of sodium hydroxide could be calculated. A new solution was then made up, and likewise siphoned slowly through the cell.

The greater accuracy of the dynamic method can be attributed to the fact that the concentration of the sodium hydroxide is held constant for each absorption measurement, whereas in the static method a small change in concentration of base is used to determine the amount of absorption. The dynamic method has the added advantage of being carried on in a closed system, so that contamination with carbonate can be avoided more easily than in the static method, which involves much more handling of the solution. It has, however, the disadvantage of making possible only one absorption measurement at a time with one cell, and with a cell as large as the one used in these experiments it takes several days for each solution to come to equilibrium with the nylon. This disadvantage is partially compensated for by the possibility of degassing the nylon in the dynamic method, which increases considerably the rate of attainment of equilibrium.

(7) J. E. Waltz and G. B. Taylor, *Anal. Chem.*, **19**, 448 (1947).

(8) T. J. Swoboda, private communication.

The static method was used for most of this study only because of its rapidity; it is felt that the dynamic procedure is the more accurate.

Results and Conclusions

A series of absorption measurements were carried out at three temperatures, 25.0, 36.4 and 49.7°, and the data for each of these temperatures were subjected to graphical analysis using equations (9) and (12). The experimental and calculated data necessary for this graphical analysis are collected in Tables I, II and III. The first column gives the concentration of [COONa] groups in moles per gram of fiber, calculated directly from the data obtained as described in the experimental section. The second column gives the hydroxyl ion concentration of the solution in equilibrium with the fiber and the third column indicates the *p*OH calculated from these normalities. The *p*OH will be used instead of *p*H throughout this treatment to avoid the complication which would be introduced by the large temperature coefficient of the ionization constant for water. The fourth column gives the values of σ calculated by equation (9) and the fifth column the values of τ calculated by equation (12).

TABLE I

ABSORPTION OF NaOH AT 25°

[COONa] × 10⁶	[OH⁻] × 10³	*p*OH	σ	τ × 10³
7.62[a]	0.3934	3.405	49.4	
10.3	.4719	3.33	46.1	
16.5[a]	.6533	3.185	38.8	
17.7	.7154	3.145	34.6	
22.9	1.018	2.99	22.1	
23.65	1.111	2.95	19.15	
24.7[a]	1.375	2.86	13.1	
30.0	2.103	2.68	6.78	
31.5	2.368	2.63	5.61	
33.1	2.486	2.605	5.35	
34.1[a]	2.430	2.61	5.78	
36.5	4.165	2.34	2.10	2.68
38.2	4.201	2.38		3.29
38.8	4.607	2.34		3.20
44.8	7.572	2.12		3.01
45.4	7.774	2.11		3.03
47.0	7.90	2.11		3.23
47.4	6.929	2.16		3.74
62.5	16.93	1.77		2.52
64.4	22.38	1.65		2.01
76.2	36.37	1.44		1.58
80.7	55.33	1.26		1.12
80.9	56.12	1.25		1.10
81.0	50.01	1.30		1.24

[a] Measured by dynamic method.

TABLE II

ABSORPTION OF NaOH AT 36.4°

[COONa] × 10⁶	[OH⁻] × 10³	*p*OH	σ	τ × 10³
3.7	0.4004	3.40	23.1	
5.82	.5071	3.29	22.7	
10.80	.7562	3.12	18.9	
17.4	1.121	2.95	13.8	
20.5	1.452	2.84	9.70	
28.2	2.526	2.60	4.42	
33.5	3.366	2.47	2.95	
35.4	5.345	2.27	1.24	
39.8	7.545	2.12	0.70	2.03
42.8	10.34	1.99		1.87
62.0	22.20	1.65		1.88
71.1	53.29	1.27		0.96
82.9	66.70	1.18		.96
84.5	93.38	1.03		.70
85.5	93.08	1.03		.71

TABLE III

ABSORPTION OF NaOH AT 49.7°

[COONa] × 10⁶	[OH⁻] × 10³	*p*OH	σ	τ × 10³
2.8	0.4305	3.36	15.05	
4.95	.5643	3.25	15.6	
8.0	.8108	3.09	12.1	
14.4	1.353	2.87	7.85	
16.4	1.648	2.78	6.04	
22.8	2.442	2.61	3.82	
28.1	3.565	2.45	2.21	
30.0	3.474	2.46	2.49	
31.9	5.440	2.26	1.08	
36.8	7.522	2.12	0.65	1.25
38.7	7.608	2.12	0.67	1.88
43.9	10.69	1.97		2.01
61.8	21.04	1.68		1.99
76.4	76.99	1.11		0.745
77.4	93.06	1.03		0.63

The titration curves for the three sets of data are plotted in Fig. 1, which shows the characteristic break between the two stages of absorption at approximately [COONa] = 34 × 10^{-6}. The qualitative effect of temperature is seen to be a lowering of the amount of absorption of base at a given *p*OH as the temperature is increased. Plots of the three sets of data according to equation (9) deter-

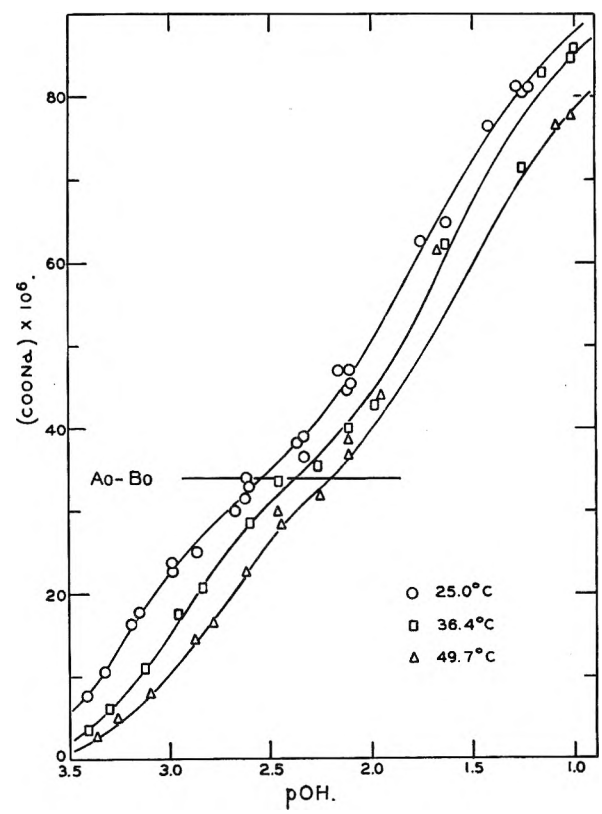

Fig. 1.—Amount of absorbed sodium ions plotted against *p*OH of solution.

mine straight lines, each having the same abscissa intercept at [COONa] = 33.9×10^{-6}. According to equation (9) this should be the value of $(A_0 - B_0)$ and it is to be compared with the analytical estimate of 33×10^{-6} which was furnished by the manufacturer. The slope of each straight line should be $-K_1$, and the values so obtained are given as

T, °C.	25.0	36.4	49.7
$K_1 \times 10^{-6}$	1.96	0.80	0.40

The data for the second stage of the absorption were similarly plotted according to equation (12). The normalities of the solutions for these measurements were obtained by analytical titration and were found to be less accurate than the corresponding values for the first stage of the absorption, which were obtained by radiotracer measurements. The points proved to be quite scattered, especially at the higher temperatures, but those at 25° did determine a definite straight line. The straight lines assumed for the higher temperatures were the best ones that could be drawn with the same abscissa intercept, which according to equation (12) should be equal to A_0. The value of 102×10^{-6} obtained from the graphical analysis differs markedly from the estimate of 75×10^{-6} from the manufacturer's analysis. As will be shown later, however, the computed values of ΔH_1 and ΔH_2 are relatively insensitive to the values assumed for A_0 or B_0, so the above discrepancy will not be investigated further. The slope of the straight lines should be $-\sqrt{K_2}$, and the values of K_2 so obtained are

T, °C.	25.0	36.4	49.7
$K_2 \times 10^{-2}$	35.4	16.0	9.9

From a comparison of K_2 with K_1, it is obvious that the first stage of the absorption should indeed proceed virtually to completion before the second stage begins, as assumed in the theoretical development.

Since these values of K_2 are quite uncertain by reason of the erratic nature of the experimental data for the second stage of the absorption, K_2 has also been calculated from K_1 and the midpoint data according to equation (13), slightly modified

$$\sqrt{K_2} = \frac{(A_0 - B_0)\sqrt{K_1}}{B_0 K_1 [OH^-]_m^2 - (A_0 - B_0)} \qquad (17)$$

The necessary data and the calculated values are given in Table IV. The values of $[OH^-]_m$ were determined graphically from an enlarged plot of the titration curves and K_1 was determined as described above. The first values of K_2 are those calculated using $B_0 = 43 \times 10^{-6}$ as estimated by end group analysis, and the second values of K_2 are those calculated using $B_0 = 68.5 \times 10^{-6}$, as obtained from our graphical method. These latter calculated values of K_2 are quite close to those estimated directly from plots made according to equation (12).

By plotting log K_1 and log K_2 against $1/T$, we can determine values of ΔH_1 and ΔH_2. By this method we find that $\Delta H_1 = -12{,}900$ cal. Since we have three different sets of values for K_2, it might be assumed that three different values for ΔH_2 would be obtained. Fortunately each of the three log K_2 plots had the same slope, within experimental error, and from that common slope we find that $\Delta H_2 = -9{,}900$ cal.

The values of ΔH_1, ΔH_2 and their mean $(\Delta H_1 + \Delta H_2)/2$, can also be computed directly from the titration curves of Fig. 1 by use of equations (14) and (16). Table V gives the pOH at different temperatures for three different values of [COONa] for each of the two stages of the absorption, as well as for the midpoint, where [COONa] = 33.9×10^{-6}. The values chosen for the second stage of the absorption were taken from the most reliable portions of the curves.

TABLE IV

VALUES OF K_2 CALCULATED USING EQUATION (17)

T, °C.	$[OH^-]_m \times 10^2$	$K_2 \times 10^{-4}$[a]	$K_2 \times 10^{-4}$[b]
25.0	2.69	0.70	0.26
36.4	3.80	.43	.16
49.7	5.50	.19	.07

[a] Assuming $B_0 = 43 \times 10^{-6}$. [b] Assuming $B_0 = 68.5 \times 10^{-6}$.

TABLE V

CHANGE IN pOH WITH TEMPERATURE

T, °C.	[COONa] $\times 10^6$	pOH
First stage of the absorption		
25.0	10.0	3.34
36.4	10.0	3.14
49.7	10.0	3.01
25.0	20.0	3.07
36.4	20.0	2.87
49.7	20.0	2.72
25.0	30.0	2.70
36.4	30.0	2.52
49.7	30.0	2.37
Second stage of the absorption		
25.0	40.0	2.28
36.4	40.0	2.13
49.7	40.0	2.04
25.0	50.0	2.01
36.4	50.0	1.85
49.7	50.0	1.76
25.0	60.0	1.80
36.4	60.0	1.63
49.7	60.0	1.55
Midpoint of the absorption		
25.0	33.9	2.57
36.4	33.9	2.42
49.7	33.9	2.26

The data of Table V have been plotted as suggested by equations (14) and (16). From the average slopes, it is found that ΔH_1 and ΔH_2 are equal, respectively, to $-12{,}600$ and $-9{,}400$ cal., which figures are in good agreement with those obtained from the temperature coefficients of K_1 and K_2. From the straight line obtained from the midpoint data, it is found that the mean $(\Delta H_1 + \Delta H_2)/2$, equals $-11{,}000$ cal., in perfect agreement with the individual figures given above.

The analysis of the data by means of equation (14) has the advantage that only a small portion of the titration curve in each absorption stage need be

known to determine ΔH_1 and ΔH_2. This very fact makes it less accurate, however, than an analysis by the van't Hoff equation, which requires a knowledge of K_1 or K_2 determined from the whole titration curve. The agreement between the values of ΔH_1 and ΔH_2 obtained by these two different approaches gives good evidence for the general validity of the theoretical presentation.

THE EFFECT OF DIPOLAR IONS UPON THE ACTIVITY COEFFICIENTS OF NEUTRAL MOLECULES

BY A. P. ALTSHULLER[1]

Contribution from the Department of Chemistry of the University of Cincinnati, Cincinnati, Ohio

Received October 13, 1952

The Kirkwood treatment of dipolar ions is extended to cover the effects of dipolar ions upon the activity coefficients of neutral molecules. Non-electrostatic deviations from ideality are discussed. Justification is given for the assumption of spherical shape for the simpler amino acids. The comparison of theory and experiment indicates that the theory as developed may serve as a satisfactory approximate treatment.

The effect of simple ions upon the activity coefficients of neutral molecules has received considerable theoretical and experimental attention.[2] The effects of dipolar ions upon the activity coefficients of neutral molecules do not seem to have been considered. A mathematical treatment is readily available through an extension of Kirkwood's treatment of dipolar ions.[3,4]

Kirkwood[3] has shown that the work of charging a spherical molecule with an arbitrary charge distribution in the absence of simple ions is given by the expression

$$W_0 = 1/2 \sum_{m=0}^{\infty} \frac{(m+1)Q_m(D_i - D)}{D_i b^{2m+1}[(m+1)D + D_i m]} \quad (1)$$

where

$$Q_m = \sum_{k=1}^{M}\sum_{l=1}^{N} e_k e_l r_k^m r_l^m P_m(\cos\theta_{kl})$$

D_i is the dielectric constant within the complex molecule; D is the dielectric constant of the medium, b is the radius of the spherical molecule; e_k and e_l are the kth and the lth charges, and r_k and r_l are the distances from the kth and lth charges to the center of the spherical molecule.

The reversible work involved in the transfer of a complex molecule from a medium of dielectric constant D_0 to one of dielectric constant D, where D_i is assumed to equal one, is given by the equation

$$\Delta F = \frac{1}{2}\sum_{m=0}^{\infty} \frac{(m+1)(2m+1)Q_m(D_0 - D)}{b^{2m+1}[(m+1)D + m)][(m+1)D_0 + m]} \quad (2)$$

The free energy of a solution containing n' molecules of complex molecules per milliliter, since $c = 1000n'/N$, is given by

$$\Delta F_t = \frac{Nc}{2000}\sum_{m=0}^{\infty} \frac{(m+1)(2m+1)Q_m(D_0 - D)}{b^{2m+1}[(m+1)D + m)][(m+1)D_0 + m]} \quad (3)$$

The dielectric constant of a solution containing a solvent of dielectric constant D_0, non-electrolyte and complex molecules may be written as

$$D = D_0(1 \pm qn + rn') \quad (4)$$

where q and r are positive constants at a given temperature, n is the number of molecules of simple non-electrolyte (neutral molecule) and n' is the number of complex molecules per milliliter. If we differentiate D with respect to n we have from equation (4)

$$\partial D/\partial n = \pm qD_0 \quad (5)$$

we then have

$$\partial \Delta F_t/\partial n = \frac{\pm Nc}{2000}\sum_{m=0}^{\infty} \frac{(m+1)(2m+1)Q_m}{b^{2m+1}} \frac{qD_0}{[(m+1)D + m]^2} \quad (6)$$

since $\partial \Delta F/\partial n = kT \ln f$, where f is the activity coefficient of the simple non-electrolyte (neutral molecule)

$$\ln f = \frac{\pm qD_0 Nc}{2000kT}\sum_{m=0}^{\infty} \frac{(m+1)(2m+1)Qm}{b^{2m+1}[(m+1)D + m]^2} \quad (7)$$

expanding in series,

$$\ln f = \frac{\pm qD_0 Nc}{2000kT}\left[\frac{e^2}{D^2 b} + \frac{6\mu^2\cos\theta}{(2D+1)^2 b^3} + \frac{15Q_2}{(3D+2)b^5}\cdots\right] \quad (8)$$

If the complex molecule is a dipolar ion the first term in the series disappears and for the simpler α-amino acids such as glycine, we may employ only the second term in the series, so we have

$$\ln f = \frac{\pm 3qD_0\mu^2 Nc}{1000kT(2D+1)^2 b^3} \quad (9)$$

If the dielectric constant of the neutral molecule is less than that of the solvent, then $\ln f$ is positive and the solubility of the neutral molecule will be decreased by the addition of the dipolar ion. On the other hand, if the dielectric constant of the neutral molecule is greater than that of the solvent, $\ln f$ will be negative and the solubility of the neutral molecule will be increased by the addition of the dipolar ion.

The assumptions and approximations underlying the theory have already been discussed by Kirkwood.[3] Two of these approximations which are

(1) National Advisory Committee for Aeronautics, Lewis Flight Propulsion Laboratory, Cleveland, Ohio.

(2) F. A. Long and W. F. McDevit, *Chem. Revs.*, **51**, 119 (1952).

(3) J. G. Kirkwood, *J. Chem. Phys.* **2**, 351 (1934).

(4) E. J. Cohn and J. T. Edsall, "Proteins, Amino Acids and Peptides," Reinhold Publ. Corp., New York, N. Y., 1943, chapter 12.

most pertinent to the present investigation need further discussion.

The first of these assumptions concerns the deviation of the solutions from ideality. The mathematical treatment given only considers purely electrostatic deviations from ideal behavior. Non-electrostatic deviations are also of importance, especially with increasing length of the hydrocarbon chain. It may be hoped that for glycine and perhaps some of the other short chain amino acids neglect of these non-electrostatic deviations will not be too serious an approximation.

The second assumption has to do with the shape of the dipolar ion. Kirkwood[3,4] has assumed that glycine may be represented by a sphere, but for the other α-amino acids he has assumed an ellipsoidal shape. In the process of treating the ellipsoidal case mathematically, the ion size was ignored to render the problem more susceptible to solution. In Table I below the dipole moments of dipolar ions are computed for several amino acids and peptides by three different procedures. In the first method, all of the dipolar ions are considered as being representable as spheres. The values of K_R,[4,5] the solubility coefficient, and a,[4,5] the sum of the radii of the dipolar ion and the real ion, are used to calculate μ, the dipole moment, from the equation $\mu = [183K_R a)^{1/2}$. The second method considers the dipolar ions, excepting glycine, as ellipsoids, but ignores the electrolyte ion size. The values used are those calculated by Kirkwood.[4] Both of these methods use equations arising from a consideration of the effect of real ions upon the solubility of dipolar ions. The third method makes use of a derived relationship[4] between the dielectric increment, δ_0, and the dipole moment, namely, $\mu = 3.30\ \delta_0^{1/2}$. The dielectric increments are those given by Wyman.[6] The dipole moments are in Debye units.

TABLE I

Dipolar ion	Solubility method: Spherical model	Solubility method: Ellipsoidal model	Dielectric model
Glycine	15.1	13	15.7
α-Alanine	15.6	13	15.9
β-Alanine	19.4	..	19.4
α-Aminobutyric acid	16.0	13	15.9
α-Aminocaproic acid	17.1	13	16.5
Diglycine	25.0	..	27.7
Triglycine	33.4	..	35.0

The agreement between the moments calculated by the solubility method for a spherical model and the dielectric polarization method is quite good. The agreement between the two methods for the two peptides is perhaps somewhat fortuitous. The reasonable increases in magnitude of the dipole moments with changes in structure along with this agreement between the results calculated by two different methods would lend some support to the belief that the assumption of spherical shape for at least the simpler amino acids is not too unsatisfactory an approximation. Furthermore, the assumption of spherical shape for amino acids would appear to be less severe a restriction than is the approximation disregarding the ion size in the more detailed consideration of dipolar ion shape.

On the basis of the above discussion one would be led to believe that the extension of the theory to the interaction of dipolar ions with neutral molecules may possibly be applicable to the simpler amino acids and especially glycine.

The author was unable to find pertinent experimental data in the monograph cited above[4-6] or in Seidell's solubility tables.[7]

The author has measured the effect of the addition of 0.100 M glycine upon the solubility of ethyl acetate in water at 25°. The solubility of ethyl acetate in water at 25° is 8.01 g./100 g. of water.[8] Upon the addition of the 0.100 M glycine the solubility of the ethyl acetate in water is reduced to 7.78 g./100 g. of water. Thus the experimental log f equals 0.0126 and the decrease in solubility is 2.9%. Employing a $\mu = 15.1 \times 10^{-18}$ e.s.u.,[4] a $b = 2.7 \times 10^{-8}$ cm.,[4] a $q = 1.26 \times 10^{-22}$ and a $D = 75.8$ units,[8,9] the log f calculated from equation (9) equals 0.0094 and the decrease in solubility predicted is 2.1%. If a $\mu = 15.7 \times 10^{-18}$ e.s.u.[3,6] is used, log $f = 0.0102$ and the reduction in solubility amounts to 2.3%.

The agreement between the experimental and theoretical results is fairly good, since even for a crude model agreement in sign and magnitude is achieved. The discrepancy between experimental and theoretical results may in large part be due to the ignoring of higher terms in the series expansion of equation (8). The experimental result given is certainly insufficient to fully substantiate the theory. Experimental work would be advisable using several different amino acids such as glycine, β-alanine, γ-aminobutyric acid and δ-aminocaproic acid, since in this series μ^2 varies by a factor of three. The use of non-polar neutral molecules would also probably be a desirable approach.

A more rigid mathematical approach to the problem discussed in this paper would no doubt be desirable. This would necessitate a new attack on the whole problem of the interactions of dipolar ions with electrolytes and non-electrolytes. It would appear that the present attack on the specialized problem treated is likely to be a fairly satisfactory first approximation.

(5) Reference 4, chapter 11.

(6) Reference 4, chapter 6.

(7) A. Seidell, "Solubilities of Organic Compounds," Third Edition (and supplement), D. Van Nostrand Co., New York, N. Y., 1941 (and 1952).

(8) A. P. Altshuller and H. E. Everson, *J. Am. Chem. Soc.*, **75**, in press (1953).

(9) A. P. Altshuller, *J. Chem. Phys.*, March (1953).

THE EFFECTS OF IONIC STRENGTH ON THE INTERACTION OF BOVINE FIBRINOGEN AND THROMBIN[1]

BY DAVID F. WAUGH AND MARY JANE PATCH

Department of Biology, Massachusetts Institute of Technology, Cambridge, Mass.

Received October 16, 1952

The kinetics of the interaction of fibrinogen and thrombin have been examined in systems in which the ionic strength is varied from 0.05 to 0.6. From the straight line plot of reciprocal rate *versus* reciprocal fibrinogen concentration may be calculated the rate constant (k) of the bimolecular activation reaction and an equilibrium constant (K) which describes the dissociation of an inactive complex between thrombin and fibrinogen plus fibrin. Both k and K are affected by ionic strength ($\Gamma/2$) changes: k having a maximum at $\Gamma/2 \approx 0.15$ and K having a minimum at $\Gamma/2 \approx 0.12$. Below these critical ionic strengths inactive and active complex formation are retarded probably due to repulsion effects; above the critical ionic strengths the ion atmospheres are assumed to shield the molecules from close approach. As the ionic strength increases there is an increasing tendency for the activated fibrinogen to appear as non-compactable fibrin: *i.e.*, fibrin which is free in suspension and not a part of the structural framework. Dilution to lower ionic strengths causes a rapid shift of non-compactable to compactable fibrin, which is the basis for the analytical procedure used. At ionic strengths of 0.3 or above there is a retention of non-compactable fibrin under circumstances which suggest that micelles of limited size are being formed. This phenomenon is attributed to imperfections in packing which lead to inactive micelle ends.

There can be little doubt that thrombin catalyzes the transformation of fibrinogen into a product which can undergo a series of aggregation reactions (see 2–4 for example). The process of gelation in a solution of fibrinogen and thrombin may therefore be divided into steps such as: the activation of fibrinogen by thrombin; the polymerization of activated fibrinogen molecules into micelles more asymmetric than the fibrinogen molecules themselves; and the cross-linking of such thread-like aggregates to establish a continuous network throughout the solution. The latter is responsible for rigidity. The physical structure of the final clot will depend upon the interrelationships between all of the preceding steps.

An examination of the kinetics of activation of fibrinogen by thrombin (the first step) at *p*H 6.85 and added ionic strength 0.15 has been made.[4] Ferry and Morrison[3] have outlined the effects which changes in ionic strength produce on the physical structure (for example, coarseness or fineness) of the clot. A direct examination of the effects of ionic strength on the clotting system has recently been made by Edsall and Lever,[5] who find that under standard conditions and at constant ionic strength, the nature of the ions (calcium *vs.* sodium) is of definitive importance in determining the course of the development of fibrin and of turbidity. Boyles, Ferguson and Muehlke[6] have examined the effects of ionic strength on clotting time and the yield of fibrin, and have re-examined the salt inhibition of clotting.

A quantitative analysis of the effects of ionic strength on the various steps in the over-all clotting reaction has not previously been made. A technique has been described[4] by which the clotting reaction may be stopped quantitatively during its course and the resulting complex of non-clottable protein, fibrinogen and fibrin analyzed. In the present analysis this technique has been modified where necessary so that the relatively large changes in clot structure which take place on materially increasing the ionic strength could be accommodated and kinetic data obtained. This paper considers the effects of ionic strength upon the kinetics of the interaction of thrombin and fibrinogen and, in preliminary form, the effects of ionic strength on the polymerization of activated fibrinogen into fibrin strands and a cross-linked network.

The General Reaction Curve.—Ultimately it is desired that we determine the conversion of fibrinogen into the various forms of fibrin at any time, t. A complete analysis of the distribution of fibrin amongst its polymers was felt to be beyond a general technical procedure.[4] It was decided therefore to follow only that fibrin which appeared as compactable fibrin. The individual points on a reaction curve were obtained as follows. Appropriate aliquots of thrombin and fibrinogen are mixed in a series of paraffined 12-ml. celluloid tubes and held at constant temperature (22.3°). At a chosen time, t, the clot is compacted in one of the tubes by forcing the contents through the annular clearance between a plunger and the wall of the reaction tube. At the same time the entire reaction was stopped by adding sufficient 20% formaldehyde to give a final concentration of 1.7%. The compacted clot was removed by centrifuging for 2 minutes at 400 × g. The ultraviolet absorptions of supernatants at λ 2800 Å. were used to calculate the residual fibrinogen and non-compactable fibrin.

At a *p*H of 6.85 and an ionic strength of 0.15 all of the reaction curves previously obtained fit into a single type. This is shown as a solid line OABC in Fig. 1. The reaction is treated as though it were first order and the natural logarithm of the ratio of the initial concentration of fibrinogen to the residual fibrinogen and non-compactable fibrin is plotted as ordinate against time as abscissa. The general curve has a non-linear portion OAB and linear portion BC. The extent of the non-linear portion depends upon *p*H and ionic strength and the relative concentrations of fibrinogen and thrombin. The linear portions (B-C) of all curves obtained at a *p*H of 6.85 and an ionic strength of 0.15 extrapolate through the origin. These reaction curves were interpreted as follows. Linearity is established when the compactable fibrin represents a structural framework whose individual strands are sufficiently close together to make negligible the diffusion time elapsing between the appearance of an activated fibrinogen molecule and its incorporation into the structural framework. Thus, over the linear portion the concentration of activated fibrinogen and intermediate polymers (non-compactable fibrin) is negligible and the curve actually measures the rate of appearance of activated fibrinogen. On this basis an extrapolation of the linear portion indicates the appearance of activated fibrino-

(1) For supporting this research, the authors are indebted to the Medical Research and Development Board, Office of the Surgeon General, Department of the Army, Washington, D. C. (Contract No. DA-49-007-MD-198) and to the Armour Laboratories, Chicago, Illinois.

(2) (a) K. Laki and W. F. H. M. Mommaerts, *Nature*, **156**, 664 (1945); (b) K. Laki, *Arch. Biochem. Biophys.*, **32**, 317 (1951).

(3) J. D. Ferry and P. R. Morrison, *J. Am. Chem. Soc.*, **69**, 388 (1947).

(4) D. F. Waugh and B. J. Livingstone, THIS JOURNAL, **55**, 1206 (1951).

(5) J. T. Edsall and W. F. Lever, *J. Biol. Chem.*, **191**, 735 (1951).

(6) P. W. Boyles, J. H. Ferguson and P. Muehlke, *J. Gen. Phys.*, **34**, 493 (1951).

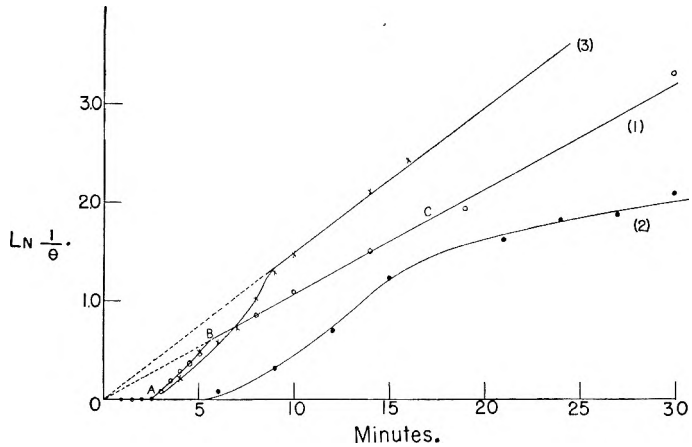

Fig. 1.—Reaction curves representative of the types observed: curve 1, at $\Gamma/2 = 0.15$, $\phi_0 = 0.176$, $Th_0 = 0.046$; curve 2, at $\Gamma/2 = 0.3$, without the dilution technique, $\phi_0 = 0.134$ and $Th_0 = 0.091$; and curve 3, at $\Gamma/2 = 0.3$, using the dilution technique, and $\phi_0 = 0.141$, and $Th_0 = 0.091$.

gen during the non-linear phase. From the difference between corresponding points on the non-linear portion of the reaction curve (OAB) and the linear extrapolation (OB) can be calculated the quantity of non-compactable fibrin. An analysis of clotting time and reaction velocity[7] has shown that, at the moment of clotting, only a small portion of the total quantity of activated fibrinogen has found its way into the structural (compactable) framework. This is corroborated by the fact that clotting occurs when the ln $1/\theta$ curve just leaves the time axis.

The same type of curve as OABC is obtained when the ionic strength is decreased below 0.15 at *p*H 6.85 except that the non-linear phase may be somewhat shortened. As the ionic strength is increased above 0.15 the non-linear phase is attenuated and the reaction curve may lack completely a linear portion. Such a curve is shown as curve 2 in Fig. 1 which is similar to curve 1 but at an ionic strength of 0.30. The gradual decrease in slope of curve 2 beyond the non-linear phase could be attributed to several sources the most obvious being first, a gradual decrease in fibrinogen or thrombin potency during the course of the reaction or, second, a failure of the activated fibrinogen to polymerize and/or the non-compactable fibrin strands to enter the compactable clot structure (*i.e.*, a failure of polymerization and cross-linking). The first alternative was checked; thrombin and fibrinogen were found to be stable at an ionic strength of 0.3 and at considerably higher ionic strengths. The ionic strength used by Seegers to activate prothrombin is much in excess of 1.0.[8] It had been found by Laki and Mommaerts[2] and Boyles, *et al.*,[6] that at very low *p*H values and high ionic strengths thrombin will not clot fibrinogen but that instantaneous clotting is obtained if the *p*H is increased to normal values or if the system is diluted. Thus the alternative that higher ionic strengths block the activation of fibrinogen was unlikely. The second alternative was accepted. By dilution it was readily shown that systems which were greatly retarded at higher ionic strengths could be made to clot within a few seconds if the ionic strength was returned to 0.15.

The following technique by which the rate of activation of fibrinogen at the higher ionic strengths could be quantitatively determined was devised. The thrombin–fibrinogen aliquot was reduced from the usual 7.7 to 4.4 ml. for ionic strength experiments between $\Gamma/2 = 0.22$ and $\Gamma/2 = 0.3$. It was 3.3 ml. for $\Gamma/2 = 0.45$ and 2.2 ml. for $\Gamma/2 = 0.6$. At the time when a sample was to be compacted the end result was arrived at in two stages. First, a 4.4-ml. or 6.6-ml. volume of salt solution, adjusted to return the ionic strength to 0.15, was dispersed through the aliquot volume. Second, after the lapse of a 40-second time interval during which clot structure was allowed to develop, compaction was performed in the customary way by plunger action and the addition of formaldehyde (see above).

In all cases it was found that the dilution technique returned the reaction curves obtained at high ionic strengths to the type shown as curve 1 of Fig. 1, *i.e.*, a non-linear lag period followed by a linear rise. Such a curve is shown as curve 3 of Fig. 1 which is identical with curve 2 except for the dilution step. In almost all cases extrapolations passed through the origin within the experimental error. A set of representative curves covering most of the ionic strength range used is shown in Fig. 2. As in previous work the linear portion of the reaction curves and linear extrapolations were taken to represent the appearance of activated fibrinogen.

The 40-second time interval was arrived at as follows. The clot structure compactable directly at the higher ionic strengths does not give rise to a linear reaction curve and therefore cannot be used. Dilution allows the rapid development of compactable clot, but during the time interval between dilution and compaction additional activated fibrinogen appears at some new rate which is difficult to predict. It was felt that a time interval after dilution could be chosen at the end of which the compactable fibrin present would approximate the potential compactable fibrin occurring just before dilution. The correct time interval was determined as follows. Dilutions were made at selected times during the course of a reaction. Thereafter the appearance of compactable fibrin in the diluted samples was determined in the usual way by compacting by plunger action and addition of formaldehyde. The results of one experiment are shown in Fig. 3 for a reaction at $\Gamma/2 = 0.3$, $Th_0 = 0.091$ μ per ml., and $\phi_0 = 0.137$ mg. clottable nitrogen per ml. Dilutions were made at 6, 9, 12 and 15 minutes after the start of the reaction. Zero time in Fig. 3 corresponds to the moment of dilution for each set of samples. After dilution there is a rapid appearance of compactable fibrin followed by a slow linear rise thereafter, the reaction being plotted as first order.

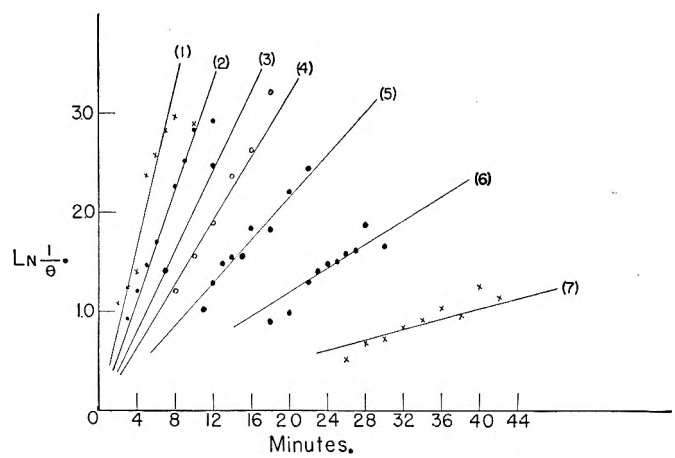

Fig. 2.—Representative reaction curves at various ionic strengths using the dilution technique described.

Curve	$\Gamma/2$	ϕ_0	Th_0
1	0.25	0.139	0.182
2	.10	.136	.136
3	.22	.138	.091
4	.3	.279	.091
5	.20	.139	.091
6	.45	.141	.091
7	.60	.279	.091

Each point on curve 3 is an average of four determinations.

When dilution is performed after the lag period of the final reaction curve (curve 3, Fig. 1) the initial rise shown in any selected curve of Fig. 3 is considered to represent the rapid conversion of non-compactable to compactable fibrin and the slow linear rise thereafter to the incorporation of activated fibrinogen as it appears in solution. On this basis, extrapolation of the linear portions of the curves of Fig. 3

(7) D. F. Waugh and B. J. Livingstone, *Science*, **113**, 121 (1951).
(8) W. H. Seegers, *Proc. Soc. Exptl. Biol. and Med.*, **72**, 677 (1949).

to zero time gives the logarithmic value corresponding to the time of dilution. This same logarithmic value is found on the reaction curves uniformly at a time near 40 seconds after dilution.

Materials and Methods.—*Fibrinogen.*—Armour Fraction-I lot 128–163 contained approximately 65% protein of which 71.5% was clottable. The non-protein material was mainly sodium citrate. Fraction-I was used without further purification since it had been found that non-clottable protein did not materially affect the reaction.[4]

Thrombin.—Parke-Davis, topical, contained 25 units per milligram.

Formaldehyde.—Merck U.S.P. was diluted to 20% formaldehyde with appropriate buffer and used as such. For the varied effects of formaldehyde see (9) and (10).

Buffer Solutions.—In all buffer solutions the phosphate contribution was kept at ionic strength 0.05 and changes in ionic strength ($\Gamma/2$) were produced by varying the content of sodium chloride. Runs were made at 22.3°.

Edsall and Lever[5] find that at constant $\Gamma/2$ the nature of the cation is of considerable importance. We have found that at *p*H 6.85 and $\Gamma/2 = 0.15$, the same reaction curve is obtained when the contribution of phosphate to the total ionic strength is varied from 0.025 to 0.15.

Symbols.—As in a previous publication[4] ϕ will refer to the fibrinogen concentration in mg. clottable nitrogen per ml.; Th the thrombin concentration in N.I.H. units per ml., and ϕ' will refer to activated fibrinogen. Th_0 and ϕ_0 refer to total initial values.

Spectrophotometry.—Residual fibrinogen and non-compactable fibrin were determined as previously by ultraviolet absorption analysis at λ 2800 Å. Non-clottable protein was determined in each run after clotting a control for 1.5 hours.

Reaction Kinetics.—In a previous analysis[4] at $\Gamma/2 = 0.15$ and *p*H 6.85 it was found that the activation reaction

$$\phi + \mathrm{Th} \rightleftharpoons \mathrm{Th}\phi^* \longrightarrow \mathrm{Th} + \phi'$$

in which $\mathrm{Th}\phi^*$ is an active complex, behaves as a bimolecular reaction described by eq. (1)

$$-\frac{d\phi}{dt} = k(\mathrm{Th})(\phi) \qquad (1)$$

where k is a rate constant and Th is the free thrombin concentration. Fibrinogen and fibrin were found to combine equally with thrombin to form an inactive complex according to

$$\mathrm{Th}\phi \rightleftharpoons \mathrm{Th} + \phi$$

Applying the law of mass action led to

$$\mathrm{Th} = K\mathrm{Th}_0/K + \phi_0 \qquad (2)$$

The symbol ϕ_0 appears in the denominator because, at any time during the reaction, it represents the sum of fibrinogen plus fibrin. Inactive combination of thrombin with fibrinogen and fibrin reduces the amount of thrombin free in solution. Substituting in eq. (1) gives

$$-\frac{d\phi}{dt} = k\frac{(K\mathrm{Th}_0)}{(K + \phi_0)}\phi \qquad (3)$$

the integrated form of which is

$$\ln\frac{\phi_0}{\phi} = \ln 1/\phi = \frac{(kK)}{(K + \phi_0)}\mathrm{Th}_0 t \qquad (3a)$$

The initial rate of a reaction is given by

$$R = -d\phi_0/dt = S\phi_0 \qquad (4)$$

where S is the slope of the linear portion of the reaction curve when plotted as $\ln 1/\theta$ *vs.* t in minutes. On inverting eq. (3) according to Lineweaver and Burk[11] we obtain

$$1/R = \frac{1}{k\mathrm{Th}_0} \times \frac{1}{\phi_0} + \frac{1}{kK\mathrm{Th}_0}$$

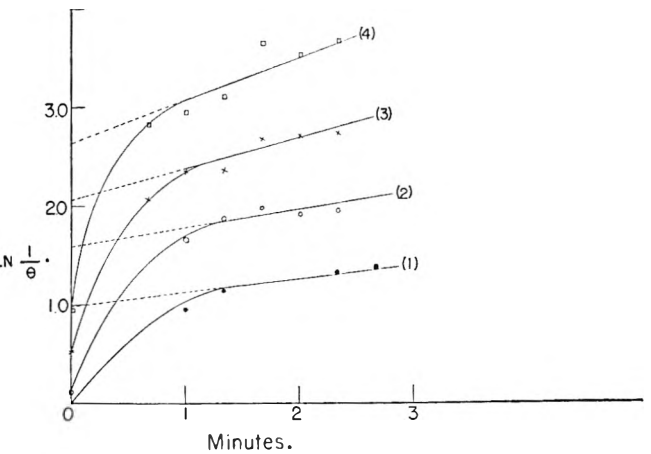

Fig. 3.—Determination of the appropriate time after dilution at which compaction will yield a logarithmic reaction curve value consistent with the extent to which the activation reaction has progressed at the time of dilution. Dilutions (0 time) were made at 6 minutes (curve 1), 9 minutes (curve 2), 12 minutes (curve 3), and 15 minutes (curve 4). The reaction was carried out at $\Gamma/2 = 0.3$, $\phi_0 = 0.137$, and $\mathrm{Th}_0 = 0.091$.

According to eq. (5) a plot of R^{-1} *vs.* ϕ_0^{-1} will yield a straight line of slope $(k\mathrm{Th}_0)^{-1}$ and intercept $(kK\mathrm{Th}_0)^{-1}$. Knowing the thrombin concentration, values of k and K may be obtained. At $\Gamma/2 = 0.15$ and *p*H 6.85, $k = 9.5$ and $K = 0.051$.[4]

The data for reaction curves obtained at *p*H 6.85 and varying ionic strength are shown in Table I. The data of Table I have been analyzed using eq. (5). Table II gives the results of such an analysis. In Table II the first column gives the ionic strength. The second and third headed Int. and slope refer to the values for the plot of eq. (5). The fourth column gives k, the rate constant and the fifth K, the equilibrium constant of the inactive complex. When the thrombin concentration alone is varied at constant ϕ_0 a plot of S *vs.* Th_0 will be a line having a slope predicted by $kK/(K + \phi_0)$ as indicated by eq. (3a) and (4). The predicted slope is given in column 6 of Table II and the experimentally determined slope in column 7, the comparison being made at $\phi_0 = 0.13$ to 0.14. The deviations between columns 6 and 7 are shown in column 8. The data for $\Gamma/2 = 0.15$ and higher represent average values. The fraction of thrombin free in solution, $f = \mathrm{Th}/\mathrm{Th}_0$, is sensitive to ϕ_0 as well as K (see eq. (2)). For illustration purposes the values of f corresponding to $\phi_0 = 0.15$ are given in the last column of Table II.

Discussion

A more detailed analysis must await determinations of (a) the effects of *p*H on the interaction of thrombin and fibrinogen and (b) the effects of *p*H and further analysis of the effects of ionic strength on the polymerization of activated fibrinogen. These are under current investigation. The discussion which follows is therefore preliminary in nature.

The maximum in k *vs.* $\Gamma/2$ and the minimum in f *vs.* $\Gamma/2$ (Table II) are in the same sense and may be interpreted in the same way. At approximately the same critical ionic strength the thrombin molecules are able to combine most effectively to produce activation and are adsorbed most strongly in inactive complex formation. Below each critical ionic strength active and inactive combinations are probably retarded due to charge effects. Above each critical ionic strength the ion atmospheres may be shielding the molecules and preventing sufficiently close approach to give either active-complex or inactive-complex formation. The critical ionic strength for active-complex formation is

(9) D. F. Waugh and B. J. Livingstone, THIS JOURNAL, **55**, 464 (1951).

(10) E. Mihalyi and L. Lorand, *Hung. Acta Physiol.*, **1**, 218 (1948).

(11) H. Lineweaver and D. Burk, *J. Am. Chem. Soc.*, **56**, 658 (1934).

TABLE I

REACTION CURVE DATA

The reaction curve data for $\Gamma/2 = 0.15$ are in good agreement with those previously reported.[4] The ionic strengths given are "added" ionic strength. The average increment due to the presence of citrate in Fraction - 1 is $\Gamma/2 = 0.016$.

$\Gamma/2$	ϕ_0, mg. C.N/ml.	Th_0, μ/ml.	Slope	$\Gamma/2$	ϕ_0, mg. C.N/ml.	Th_0, μ/ml.	Slope	$\Gamma/2$	ϕ_0, mg. C.N/ml.	Th_0, μ/ml.	Slope
0.05	0.134	0.182	0.279	0.20	0.139	0.182	0.437	0.30	0.138	0.182	0.327
	.134	.136	.208		.139	.136	.346		.138	.136	.245
	134	.091	.159		.139	.091	.205		.138	.091	.178
	.134	.0455	.089		.139	.0455	.108		.138	.0455	.089
	.272	.091	.092		.279	.091	.148		.279	.091	.160
	.207	.091	.117		.209	.091	.179		.205	.091	.155
	170	.091	.133		.174	.091	.197		.172	.091	.158
	.134	.091	.150		.139	.091	.221		.141	.091	.168
	.099	.091	.174		.105	.091	.243		.107	.091	.163
0.10	.136	.182	.369	0.22	.138	.182	.426	0.45	.137	.182	.114
	.136	.136	.278		.138	.136	.345		.137	.136	.085
	.136	.091	.182		.138	.091	.202		.137	.091	.059
	.136	.0455	.092		.138	.0455	.103		.137	.0455	.022
	.279	.091	.107		.279	.091	.145		.281	.091	.057
	.213	.091	.141		.174	.091	.181		.209	.091	.058
	.170	.091	.160		.105	.091	.213		.174	.091	.060
	.138	.091	.188						.141	.091	.061
	.1007	.091	.244								
0.15	.138	.364	.880	0.25	.139	.182	.412	0.60	.139	.182	.055
	.138	.182	.452		.139	.136	302		.139	.136	.038
	.138	.136	.358		.139	.091	.205		.139	.091	.008
	.138	.091	.242		.139	.0455	.099				
	.138	.0455	.124		.281	.091	.209		.279	.091	.027
	.276	.091	.374		.212	.091	.207		.174	.091	.029
	.207	.091	.225		.174	.091	.214		.105	.091	.032
	.170	.091	.197		.139	.091	.231				
	.137	.091	.180		.070	.091	.237				
	.068	.091	.137								

TABLE II

CONSTANTS FROM REACTION CURVE DATA

For details see text.

					Slope thrombin curve			
$\Gamma/2$	Int.	Slope	k	K	Calcd.	Measured	Difference, %	
0.05	25.0	3.05	3.6	0.122	1.72	1.57	8.7	0.45
.10	28.5	1.36	7.95	.049	2.09	2.01	3.8	.244
.15	45.7	2.32	9.52	.051	2.56	2.50	2.3	.254
.20	14.6	2.62	4.19	.179	2.42	2.42	0	.544
.22	13.1	3.22	3.41	.260	2.37	2.23	6.2	.634
.25	6.07	3.54	3.10	.584	2.51	2.28	9.2	.895
.30	2.74	5.75	1.91	2.09	1.79	1.63	8.9	.934
.45	6.5	15.26	0.72	2.35	0.68	0.63	7.4	.940
.60	38.0	27.2	0.404	7.15	0.39	0.29	25.6	.980

$\Gamma/2 = 0.15$ and for inactive-complex formation it is $\Gamma/2 = 0.12$.

An empirical analysis of the data suggests that, over the ionic strength limits specified, the rate constant and added ionic strength are related by the equations

$$k = 63(\Gamma/2)^{0.92};\ \Gamma/2 < 0.15 \qquad (6)$$

and

$$k = 0.126(\Gamma/2)^{-2.24};\ \Gamma/2 \geq 0.15 \qquad (7)$$

Below the $\Gamma/2$ corresponding to the maximum in k (rate constant), k increases linearly with the ionic strength but above this maximum it drops off with the 2.24 power of the ionic strength.

The equilibrium constant K bears no simple relationship to the ionic strength. For this reason a discussion of K will be given at the time when the effects of pH are also discussed.

Consideration of the Polymerization Reactions.— We assume the reactions

$$\phi + \mathrm{Th} \rightleftarrows \mathrm{Th}\phi^* \longrightarrow \mathrm{Th} + \phi' \text{ (activated fibrinogen)} \qquad (8)$$

and

$$n\phi' \longrightarrow \phi'_n \longrightarrow (\phi'_n)_m \text{ (structural network)} \qquad (9)$$

In eq. (8) and (9) and similar equations the symbols represent the molecular species themselves. In other equations the symbols represent abbreviations for C_ϕ, etc. (concentrations).

The analysis so far has been concerned with eq. (8). Certain complexities of the second, eq. (9), have been indicated in a study of the relationships between reaction velocity and clotting time.[7] In this analysis it became clear that, at the moment of clotting, much of the fibrin present was non-compactable, therefore free in suspension (ϕ'_n).

The relationships between the total fibrin production (activated fibrinogen, polymers and structural framework) and the other fractions is shown in Fig. 4. Here for convenience the distributions are plotted as percentage values of the initial fibrinogen (ϕ_0) *versus* time. Curve 1b of Fig. 4 has been calculated from the linear portion and linear extrapolation of curve 1 of Fig. 1. Since the total activated fibrinogen is also equal to the total fibrin, curve 1b of Fig. 4 represents total fibrin production. Curve 2 of Fig. 4 represents the appearance and disappearance of non-compactable fibrin at $\Gamma/2 = 0.15$. Curve 2 has been obtained from curve 1

of Fig. 1 by using ordinate differences between the linear extrapolation and the reaction curve as measured. Curve 2, Fig. 4, returns to the abscissa at 6 minutes, the time when the reaction curve on which it is based achieves linearity. At any given time subtraction of curve 2 from curve 1b will give, as per cent. of ϕ_0, the amount of compactable fibrin present. At 6 minutes reaction time, approximately 45% of the initial fibrinogen is present in the structural framework. Thus, an extensive structural framework is necessary before the non-compactable fibrin is reduced to negligible values.

Curve 1a of Fig. 4 represents the appearance of activated fibrinogen (total fibrin) at $\Gamma/2 = 0.3$, $Th_0 = 0.091$ and $\phi_0 = 0.136$. It is calculated from the linear portion and linear extrapolation of curve 3 of Fig. 1 which, in turn, was obtained using the dilution technique described. Curve 3 of Fig. 4 shows the formation and disappearance of non-compactable fibrin at $\Gamma/2 = 0.3$ using the dilution technique. It is calculated from ordinate differences between the linear extrapolation of curve 3, Fig. 1, and the reaction curve as measured. Curves 3 and 2 of Fig. 4 are not strictly comparable. However, the increased persistence of non-compactable fibrin indicated by curve 3 certainly is due to the incompleteness of the aggregation reactions taking place just after dilution. Incompleteness, in turn, may be related to the persistence of non-compactable fibrin at higher ionic strengths discussed below.

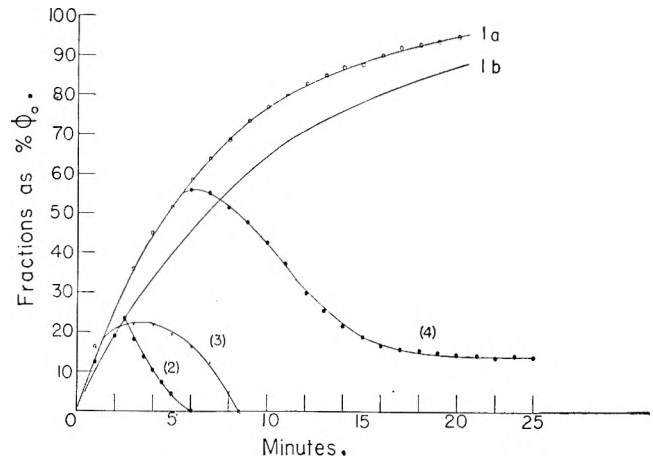

Fig. 4.—The appearance of various fibrin fractions plotted as per cent. of initial fibrinogen *vs.* time. Curve 1b represents total fibrin for $\Gamma/2 = 0.15$, $\phi_0 = 0.176$, $Th_0 = 0.045$. Curve 2 represents non-compactable fibrin for the same reaction. Curve 1a represents total fibrin for $\Gamma/2 = 0.3$, $\phi_0 = 0.138$, and $Th_0 = 0.091$. Curve 3 represents non-compactable fibrin for the same reaction using the dilution step. Curve 4 represents the non-compactable fibrin for the same reaction without the dilution step. For details see text.

Curve 4, Fig. 4, shows the build-up and retention of non-compactable fibrin at $\Gamma/2 = 0.3$ which, in conjunction with the decrease in the rate of appearance of activated fibrinogen, is responsible for the increase in clotting time obtained with increasing ionic strength. Curve 4 was calculated from ordinate differences between (a) the linear portion and linear extrapolation of curve 3 of Fig. 1 (total fibrin) and (b) curve 2 of Fig. 1 which, since the dilution technique was not used, represents the appearance of compactable fibrin at the ionic strength of 0.3. The difference between curves 4 and 3 of Fig. 4 represents the effect of the dilution step in converting non-compactable into compactable fibrin.

The persistence of non-compactable fibrin at $\Gamma/2 = 0.3$ long after (a) the majority of the fibrinogen has been activated and (b) the appearance of an extensive compactable network (Fig. 4, curve 1a minus curve 4) merits consideration. At the lower ionic strength of 0.15 and at 6 minutes the compactable framework represents 45% of the initial fibrinogen. Thereafter activated fibrinogen will be incorporated as rapidly as it is formed. The situation at $\Gamma/2 = 0.3$ is in clear distinction. After 17 minutes the compactable structure represents about 75% of the initial fibrinogen, but at this time and for at least 7 minutes thereafter the non-compactable fibrin (curve 4) remains near the equivalent of 15% of the initial fibrinogen. Eventually the non-compactable fibrin will disappear (Boyles, *et al.*,[6] also found that their reactions would go to completion). The slope of curve 4 between 7 and 14 minutes indicates that a compactable structure can develop rapidly and extensively at $\Gamma/2 = 0.3$. As the ionic strength is increased above 0.3 non-compactable fibrin persists in increasing amounts. At the same time the reaction tubes, after compaction, are increasingly transparent indicating a decrease in the micelle size of the non-compactable fibrin.

Ehrlich, Shulman and Ferry[12] have recently described the formation of stable micelles of $S = 25$ in clotting systems inhibited by urea at $\Gamma/2 = 0.15$. Similar micelles of limited size were observed in clotting systems inhibited by hexamethylene glycol at $\Gamma/2 = 0.45$. Micelles of twice the cross sectional area of fibrinogen and six- to tenfold the length of fibrinogen are cited as being consistent with the data.

Ferry[13] has recently examined the events presumed to take place in the over-all transformation of fibrinogen to fibrin. He proposes that a structure is built up in which the lateral association of the ends of activated fibrinogen molecules with the centers of neighboring molecules is the basic pattern of fibrin formation. The molecules are oriented in the same direction. The association is attributed to the asymmetric distribution of charged groups on the fibrinogen molecules which allows the positive groups of one to interact with the negative groups of a neighbor. Ferry suggests that the relatively uniform intermediate polymers, found in systems inhibited as described, may be the result of the increasing electrostatic work which must be done to enlarge a polymer all of whose units carry a net negative charge. As in the soap micelle[14] cessation of growth will occur when, on the association of a monomer, the free energy changes due to local attractive forces and long-range electrostatic repulsive forces are comparable.

(12) P. Ehrlich, S. Shulman and J. D. Ferry, *J. Am. Chem. Soc.*, **74**, 2258 (1952).

(13) J. D. Ferry, *Proc. Nat. Acad. Sci.*, **38**, 566 (1952).

(14) P. Debye, THIS JOURNAL, **53**, 1 (1949).

In the experiments described here, the persistence of non-compactable fibrin at higher ionic strength should not be attributed to the integrated repulsion effects due to charges for (a) an extensive compactable structure does develop (in the presence of which non-compactable fibrin persists) and (b) eventually the non-compactable fibrin is incorporated.

It is suggested that imperfections of packing during monomer association may be in part responsible both for limited micelle growth and for the persistence of non-compactable fibrin in our experiments. It is assumed that the bonding regions, attributed to the interactions of many charges, are diffuse and constructed so that center to center distances between activated fibrinogen molecules in the micelle may be made variable by increasing ionic strength. It is possible also that the lengths of the fibrinogen molecules are variable (Hall[15]). Under such circumstances the random association of ϕ' will lead to the formation of micelle ends whose molecules cannot accommodate an additional molecule in stable linkage. The polymer will then be of limited growth. The imperfections of structure would also tend to decrease the probability that such a micelle will be incorporated in the structural framework, eventual incorporation possibly requiring a rearrangement of molecules within the micelle or a transfer of molecules from the micelle. Such an effect would account for the persistence shown in curve 4, Fig. 4, and might, in addition, be a part of the basis for the slow phase of clot development observed by Edsall and Lever[5] as a gradual increase in clot opacity.

A more detailed analysis of the polymers present during and after the lag periods of selected reactions is under investigation.

(15) C. E. Hall, *J. Biol. Chem.*, **179**, 857 (1949). See also K. Porter and C. V. Hawn, *J. Exptl. Med.*, **90**, 225 (1949).

THE EQUILIBRIUM EXCHANGE RATES OF ADSORBED SPECIES WITH UNADSORBED SPECIES IN SOLUTION[1]

BY R. NELSON SMITH, C. F. GEIGER AND CONWAY PIERCE

Chemistry Department, Pomona College, Claremont, California

Received December 12, 1952

The rate of exchange, at equilibrium, of adsorbed radioactive benzoic acid with non-radioactive benzoic acid in solution has been studied for a variety of adsorbents. As a charcoal is steam-activated it permits a more ready exchange of benzoic acid, thus indicating that the capillary pores have been enlarged on activation. Exchange is almost immediate with a carbon black or a very wide-pore decolorizing charcoal. The exchange results are discussed in connection with isotherms on the same samples.

Introduction

There are some who believe that when charcoals are steam-activated the existing capillaries are made larger by the reaction with steam, while others believe that activation merely creates more small capillaries similar to those existing before activation. In this paper we present new evidence to support the view that activation enlarges existing capillaries.

We demonstrate this by determination of the rate, at equilibrium, at which adsorbed radioactive benzoic acid exchanges with non-radioactive benzoic acid in solution. In principle, the radioactive benzoic acid molecules in very small capillaries should have much greater difficulty exchanging with non-radioactive species than would those in large capillaries. Hence, if activation enlarges the capillaries then exchange should be easier the greater the activation. If activation creates more capillaries of the same size there should be no change in the rate of exchange after activation. We find that the rate is greatly increased by activation.

In 1934, Lindau and Salomon[2] tried to determine the equilibrium "exchange number" for tartaric acid on blood charcoal using the *d* and *l* optical forms of tartaric acid, but they were unsuccessful because complete exchange (racemization) took place in less than 20 seconds. We have applied the same principle to systems which exchange more slowly and have used the more sensitive tracer methods not available to Lindau and Salomon.

Experimental

Radioactive benzoic acid containing C-14 in the ring was prepared by oxidation of radioactive toluene (Tracerlab, L6-2) by the method of Ullmann and Uzbachian.[3] Recrystallization from water gave a product with m.p. 122°. Enough of this was added to non-radioactive benzoic acid to give a 0.0208 *M* stock solution with about 3,000 counts per ml. per min. This stock solution is designated as HBz*. A stock solution of non-radioactive benzoic acid of identical strength was prepared, which is designated as HBz.

For a given run equal weights of dried carbon sample were placed in 100-ml. glass-stoppered volumetric flasks and 50.0 ml. of HBz* added to one and 50.0 ml. of HBz added to the other. These were mechanically shaken for 24 hours in a constant temperature bath at 25.0°. The solutions were then withdrawn as completely as possible from the carbons with clean, dry filter sticks, and 25.0 ml. of the HBz equilibrium solution was added to the carbon sample that had been equilibrated with HBz*. Shaking at 25.0° was then continued and 1.2-ml. samples were withdrawn with a hypodermic syringe at various time intervals. Time of contact was reckoned from the moment of adding the non-radioactive solution to the radioactive carbon sample.

0.5-ml. aliquot portions of the 1.2-ml. samples were transferred by pipet to the center of copper disks and neutralized with an excess of NaOH solution (1 drop). The liquid was kept on the disk by means of a thin coating of silicone grease applied at the edge of the disk. The solution was evaporated to dryness under an infrared lamp and the dried so-

(1) This is a report of work under Contract N8 onr 54700 with the Office of Naval Research.

(2) G. Lindau and G. Salomon, *Ber.*, **67**, 1296 (1934).

(3) F. Ullmann and J. B. Uzbachian, *ibid.*, **36**, 1797 (1903).

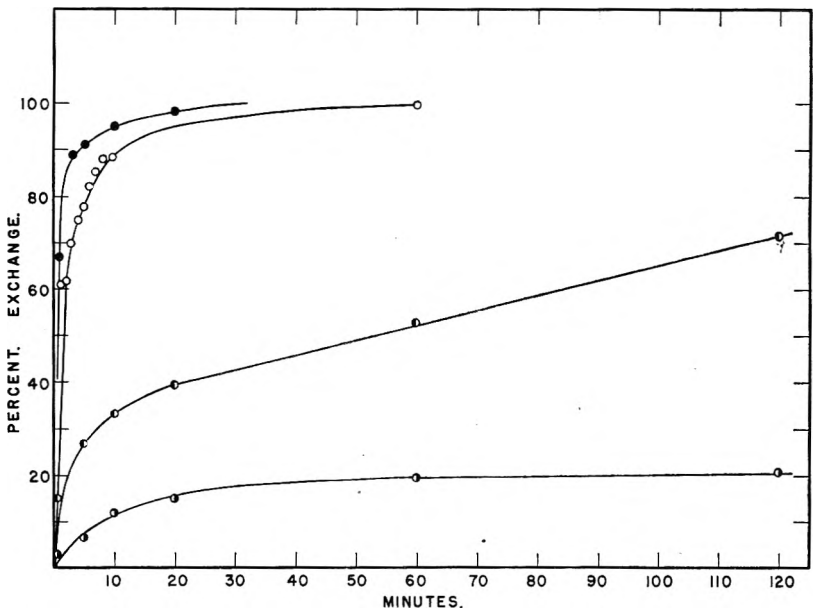

Fig. 1.—Per cent. exchange of benzoic acid at equilibrium at 25°: ●, S-94; ○, S-87; ◐, B; ◑, S-600.

dium benzoate film used for counting. Counts were made over 5-minute periods with a Tracerlab "100" Scaler and a thin-window counting tube, #TGC-2. Reproducible geometry was maintained with Tracerlab sample changer #SC-9. All counts were corrected for background and computed as counts per ml. per min.

The rate of adsorption–desorption exchange at equilibrium was studied for the following samples whose properties are described in a previous publication.[4] S-600: Chips of sheet Saran were slowly carbonized in a muffle furnace with gradual increase in temperature to a final temperature of 600°. The carbon was ground and heated *in vacuo* in a quartz tube at 1000° for removal of volatile matter. S-87: Saran charcoal carbonized at 600° was steam-activated at 900° to 87% weight loss. Sample was cooled in a nitrogen atmosphere. S-94: Saran charcoal carbonized at 600° was steam-activated at 900° to 94% weight loss. Sample was cooled in a nitrogen atmosphere. Darco G-60: A commercial decolorizing charcoal from the Darco Corporation, New York. The method and temperature of activation are not known. Graphon: A carbon black, partially graphitized at a temperature of 3200°, obtained from the Godfrey L. Cabot Co., Boston, Mass. Charcoal B: A steam-activated nut charcoal for gas masks. The sample was deashed with HCl in a Soxhlet extractor, dried, and then heated *in vacuo* at 1000°. The residual ash content is about 0.25%. The temperature of activation is not known.

Results and Discussion

To facilitate comparison of the results obtained for the various adsorbents, the observed rates of appearance of radioactivity into the non-radioactive equilibrium solutions were calculated as "per cent. exchange." When exchange is complete there will be the same number of counts per minute per milliequivalent of benzoic acid, whether the benzoic acid is adsorbed or in solution. Thus, from the known number of adsorbed counts per minute and the known amount of adsorbed and unadsorbed benzoic acid it is possible to compute the number of counts per ml. per min. expected for complete exchange. "Per cent. exchange" is then defined as

$$\frac{\text{(observed counts per ml. per min.)} \times 100}{\text{counts per ml. per min. expected for complete exchange}}$$

All computations of per cent. exchange take account of the amount of HBz* and HBz removed from the system with each sample taken for counting. The results for S-600, S-84, S-94 and B are summarized by representative curves in Fig. 1. Sample B actually reaches a state of complete exchange in about two days, but in the case of S-600 only 40% exchange occurs by the end of eight days. In the case of Graphon and Darco G-60, exchange is complete in about two minutes. Accurate measurements at a shorter time were not practical. Benzoic acid solution isotherms for all of the samples except S-84 are shown in Fig. 2. The equilibrium concentrations of Table I show the region of the isotherm at which the exchange measurements were made. It will be noted that for all samples this concentration is at or above "point B" or the region at which small capillaries are filled and a monolayer formed on exposed surfaces not in small capillaries.

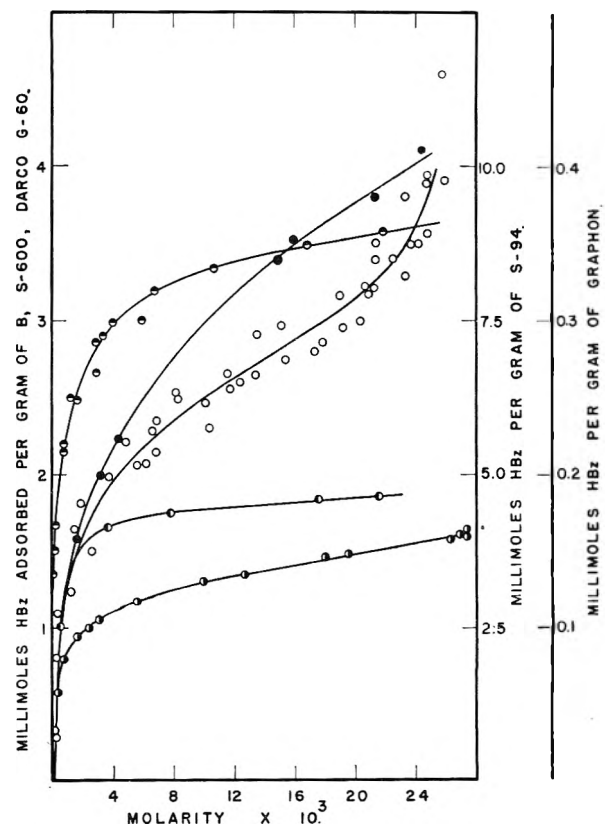

Fig. 2.—Adsorption of benzoic acid from solution at 25°: ○, Graphon; ◓, B; ●, S-94; ◐, S-600; ◑, Darco G-60.

Only near saturation will non-porous Graphon adsorb as much as two statistical layers of HBz. And as might be expected for a film whose molecules

(4) C. Pierce, R. N. Smith, J. W. Wiley and H. Cordes, *J. Am. Chem. Soc.*, **73**, 4551 (1951).

are nearly all in contact with the liquid, we find that Graphon gives almost instantaneous exchange. Darco G-60 likewise gives very rapid exchange. This, too, is to be expected for the ethyl chloride isotherm shows that much of the surface in this sample is in large capillaries. These are not filled by benzoic acid but rather there is a layer on the walls with free access to the solution.

TABLE I

EQUILIBRIUM CONCENTRATIONS AT WHICH EXCHANGE OCCURS

Sample	Equil. concn., M	Sample	Equil. concn., M
S-94	5.7×10^{-3}	B	5.1×10^{-3}
S-87	4.8×10^{-3}	Graphon	1.75×10^{-2}
S-600	8.0×10^{-3}	Darco G-60	1.1×10^{-2}

The Saran series is strong evidence that the capillaries widen with activation. Ethyl chloride isotherms for S-600 and a steam-activated sample S-84 show that the capillary volume increases threefold during activation. The isotherms show that a much higher pressure is required to fill the capillaries of the activated sample, which we take as indication that the capillaries are made wider by activation. This is further supported by the adsorption and desorption water isotherms[4] obtained for H_2-treated samples of S-600 and S-84. Unless the ash content and oxygen complexes are eliminated, water isotherms cannot be used for such interpretation. The exchange rate, Fig. 1, increases with the degree of activation. S-94 exchanges almost as rapidly as Graphon, S-87 somewhat more slowly, while S-600 exchanges very slowly. Our interpretation is that when pores are very narrow the HBz* is very strongly held by the capillary walls and diffusion through the adsorbed material to the solution where exchange may take place is difficult. As pores widen the molecules are less strongly held and the amount of material through which HBz* must diffuse to reach solution is much less.

Commercial charcoal B shows pores intermediate in size between S-600 and highly-activated samples. Some of its adsorbed molecules exchange rapidly, others slowly. The result is a slow attainment of exchange equilibrium which requires two days for completion.

Acknowledgment.—The benzoic acid isotherms of Fig. 2 were determined by Mr. John C. Godfrey.

"75 EVENTFUL YEARS"

By CHARLES ALBERT BROWNE
and MARY ELVIRA WEEKS

A History of the
AMERICAN CHEMICAL SOCIETY

526 pages . . . cloth bound
illustrated with portraits.
Price, $5.00. Order from:
American Chemical Society
1155 Sixteenth St., N.W.
Washington 6, D. C.

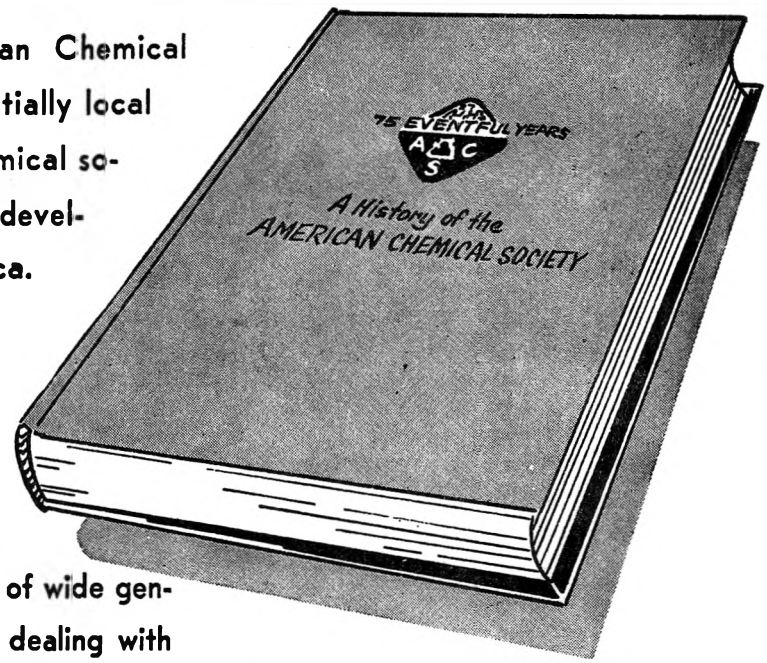

The evolution of the American Chemical Society from a small and essentially local organization to the largest chemical society in the world parallels the development of chemistry in America. Therefore the record of events described in this book is of value to all concerned with the science, the profession and the industry.

Topics treated in detail which are of wide general interest include the chapters dealing with the beginning and subsequent development of industrial chemistry as exemplified by the stories of the ACS Divisions: the activities of the Society in both World Wars, treating of the increasingly important role of the scientist in wartime: the account of the outstanding contributions of the Society toward better standards of training and the campaigns for professional recognition.

The student of ACS history also will be interested in the accounts of the various reorganizations, in the story of the granting of the Federal Charter and in the growth of the publications. A detailed chronology provides a compact record of the notable events of the 75 eventful years.

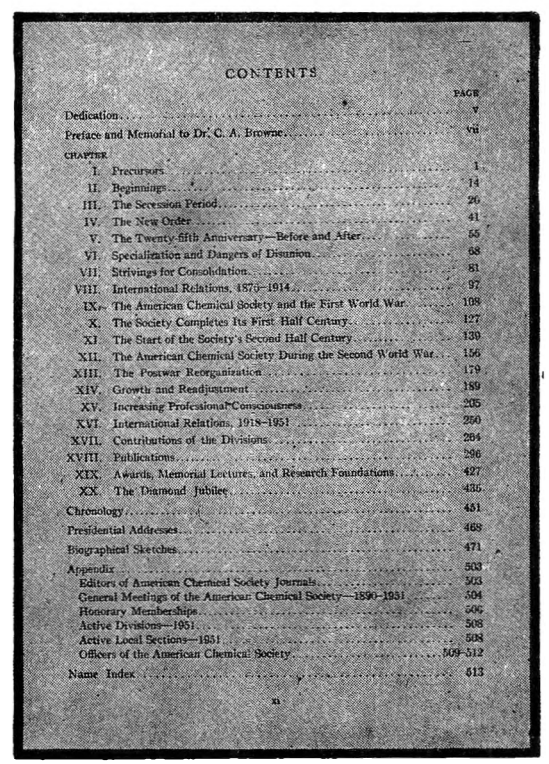

CONTENTS

The most complete treatment to date—
how to use kinetics to determine
the mechanism of chemical reactions

KINETICS and MECHANISM

A Study of Homogeneous Chemical Reactions

By ARTHUR A. FROST *and* RALPH G. PEARSON, *Associate Professors of Chemistry, Northwestern University.* This treatment of chemical kinetics differs from all other books on the subject by emphasizing the complexities of chemical reaction and the close relationship of kinetics to mechanism, particularly the mechanism of organic reactions. For physical and organic chemists who are using, or want to use kinetics to investigate reaction mechanism—this book provides a mine of tested information.

In order to show most clearly how kinetics is used to determine how reactions are proceeding, the authors present detailed stereochemical discussions of reaction steps. In addition, the theories of kinetics, mathematical and experimental details, and the calculation of energies receive the attention merited by their importance in a study of this kind.

Here are fundamental physical principles with theories (such as the collision theory and the transition state theory) used to aid in understanding. *Note*—An unusually complete mathematical treatment of complex reactions is provided and flow methods are treated in detail. Numerous practical examples of mechanism deduced from kinetics illustrate the theory.

1953 **343 pages** **$6.00**

The only book in English to explore non-aqueous solvent chemistry—
key to countless untapped industrial and research possibilities

NON-AQUEOUS SOLVENTS

Applications as Media for Chemical Reactions

By L. F. AUDRIETH, *University of Illinois; and* JACOB KLEINBERG, *University of Kansas.* Written by two of the pioneers in the use of non-aqueous solvents, this concise, well-organized book brings you pertinent theoretical and physicochemical aspects of selected reactions with non-water solvents. The book answers two important questions:

1) what can be done in organic, inorganic, and analytical chemistry by employing non-water solvents?

2) what solvents may be used advantageously to effect specific reactions?

1953 **284 pages** **$6.75**

Copies available on approval

JOHN WILEY & SONS, Inc. 440—4th Ave., New York 16, N. Y.